Neurophysiological characterisation of neurons in the rostral nucleus reuniens in health and disease.

Submitted by **Darren Walsh**, to the University of Exeter as a thesis for the degree of Doctor of Philosophy in Medical Studies, September 2017.

I certify that all material in this thesis which is not my own work has been identified and that no material has previously been submitted and approved for the award of a degree by this or any other University.

(Signature) ……

Word Count = 44,836

Abstract

Evidence is mounting for a role of the nucleus reuniens (Re) in higher cognitive function. Despite growing interest, very little is known about the intrinsic neurophysiological properties of Re neurons and, to date, no studies have examined if alterations to Re neurons may contribute to cognitive deficits associated with normal aging or dementia.

Work presented chapter 3 provides the first detailed description of the intrinsic electrophysiological properties of rostral Re neurons in young adult (~5 months) C57-Bl/6J mice. This includes a number of findings which are highly atypical for thalamic relay neurons including tonic firing in the theta frequency at rest, a paucity of hyperpolarisation-activated cyclic nucleotide–gated (HCN) mediated currents, and a diversity of responses observed in response to depolarising current injections. Additionally this chapter includes a description of a novel form of intrinsic plasticity which alters the functional output of Re neurons.

Chapter 4 investigates whether the intrinsic properties of Re neurons are altered in aged (~15 month) C57-Bl/6J mice as compared to a younger control group (~5 months). The intrinsic properties were remarkably similar across age ranges suggesting that alterations to the intrinsic properties of Re neurons do not contribute to age-related cognitive deficits.

Chapter 5 investigates whether alterations to the intrinsic properties of Re neurons occur in the J20 model of amyloidopathy. Alterations to the resting membrane potential (RMP), propensity to rebound fire, and a reduction in action potential (AP) width were observed. This suggests that alterations to the intrinsic properties of Re neurons may contribute to cognitive deficits observed in Alzheimer's disease (AD).

Chapter 6 investigates whether alterations to the intrinsic properties of Re neurons occur in a mouse model ($CHMP2B_{intron5}$) of frontotemporal dementia (FTD). Only subtle changes were observed suggesting that alterations to the intrinsic properties of Re neurons does not contribute to cognitive deficits observed in FTD linked to chromosome 3 (FTD-3).

Acknowledgements

First and foremost, I would like to thank my supervisors Prof. Andy Randall and Dr. Jon Brown for all their help and support over the last 4 years. Needless to say without their input none of this would have been possible.

I would also like to thank all of the Hatherly crew, past and present, for their warmth, friendship and making this Irish country bumpkin feel at home in the metropolis that is Devon. Particular thanks go to Hannah Smithers (who prepared some of the slices used in chapter 3) and Tom Ridler, who have been there all the way. To quote Drizzy Drake, “Started from the bottom now we’re here”.

Next a special thanks goes to the Fabreeze Brothers (Ben H, Myles J, Tom H, and Jeff L) for the stimulating quasi-intellectual pub talk, both scientific and otherwise, and for not losing faith when I wandered.

To Soraya, for believing in me when I didn’t and your unwavering ability to make me smile, I am more grateful than you could ever know.

Finally to my family at home. I did this for you guys. I hope ye are proud.

*This work is dedicated to the memory of my late grandfather Tommy Kelly. A victim of Alzheimer’s disease; I couldn’t have done it without him***.**

Table of Contents

List of figures

List of tables

Abbreviations

αEPSC	Mock EPSC
3V	Third ventricle
aCSF	Artificial cerebrospinal fluid
ACC	Anterior cingulate cortex
AD	Alzheimer's disease
ADP	Afterdepolarisation
AHP	Afterhyperpolarisation
ALS	Amyotrophic lateral sclerosis
AMPA	α-amino-3-hydroxy-5-methyl-4-isoxazolepropionic acid
ANOVA	Analysis of variance
AP	Action potential
APP	Amyloid precursor protein
ATP	Adenosine triphosphate
Aβ	beta-Amyloid
bvFTD	behavioural variant frontotemporal dementia
c-AMP	3',5'-cyclic adenosine monophosphate
Ca_v	Voltage-gated Ca^{2+} channels
CB	Calbindin
CHMP2B	Charged multivesicular body protein 2b
CNS	Central nervous system
CR	Calretinin
dV/dt	First derivative of V_m
EPSC	Excitatory postsynaptic current
EPSP	Excitatory postsynaptic potential
FAD	Familial Alzheimer’s disease
fMRI	Functional magnetic resonance imaging
FTD	Frontotemporal dementia
FTD-3	Frontotemporal dementia linked to chromosome 3
GABA	Gamma-Aminobutyric acid
Gabazine	2-(3-Carboxypropyl)-3-amino-6-(4 methoxyphenyl)pyridazinium bromide
HCN	Hyperpolarisation-activated cyclic nucleotide–gated
HF	Hippocampal formation
HPC	Hippocampus
HVA	High voltage activated
I_h	HCN current
IL	Infralimbic cortex
IPSC	Inhibitory postsynaptic current

IPSP	Inhibitory postsynaptic potential
L-689,560	trans-2-Carboxy-5,7-dichloro-4-phenylaminocarbonylamino-1,2,3,4-tetrahydroquinoline
LTP	Long-term potentiation
LVA	Low voltage activated
MAPT	Microtubule-associated protein tau
Max dV/dt	Maximal rate of rise
mGluR	Metabotropic glutamate receptor
Mi-124	microRNA-124
ML-218	3,5-Dichloro-N-[[(1α,5α,6-exo,6α)-3-(3,3-dimethylbutyl)-3-azabicyclo[3.1.0]hex-6-yl]methyl]-benzamide hydrochloride
mPFC	Medial prefrontal cortex
mRNA	Messenger RNA
MWM	Morris water maze
NBQX	2,3-Dioxo-6-nitro-1,2,3,4-tetrahydrobenzo[f]quinoxaline-7-sulfonamide
NFT	Neurofibrillary tangles
NMDA	N-Methyl-D-aspartate
PBS	Phosphate buffered saline
PCP	Phencyclidine
PFA	Paraformaldehyde
PL	Prelimbic cortex
PPA	Primary progressive aphasia
PS1/2	Presenilin 1/2
PV	Parvalbumin
Re	Nucleus reuniens
REM	Rapid eye movement
R_i	Input resistance
RM-ANOVA	Repeated measures analysis of variance
RMP	Resting membrane potential
Rt	Reticular nucleus of the thalamus
SK	Ca^{2+} activated potassium
SWS	Slow wave sleep
SZ	Schizophrenia
τ	Membrane time constant
TC	Thalamocortical
TG	Transgenic
TTX	Tetrodotoxin
UV	Ultraviolet
VC-DNM	Varying choice – delayed-non-match-to-paces
V_m	Membrane potential
WT	Wild-type
X_i	Xiphoid nucleus

1 Introduction

1.1 General electrophysiological properties of neurons.

Neurons are the primary electrically active signalling unit of the nervous system. Neuronal morphology is incredibly diverse and complex however certain morphological commonalities are shared across neuron type and brain region. The metabolic and protein synthesis centre of a neuron is the cell soma, containing the nucleus. Arising from the soma are two functionally distinct processes, namely dendrites and axons. Dendrites receive and integrate incoming signals from other neurons whilst axons conduct signals generated by a neuron to a site called the pre-synaptic terminal. (Kandel *et al.*, 2000).

The intrinsic electrophysiological properties of individual neurons govern the quintessential action of the nervous system, that is, to integrate incoming signals and generate an appropriate output response. This section will highlight the major intrinsic properties of neurons, both passive and active, and the ion channels and ionic gradients which give rise to these properties.

1.1.1 Resting membrane potential.

There is a separation of charge between the inside and outside of a neuron as a result of the unequal distribution of charged ions (Na^+, K^+, and Cl^-) and intracellular large organic anions (negatively charges proteins and amino acids). This separation of charge across the neuronal plasma membrane gives rise to a difference in the electrical potential between the inside and the outside of a neuron and this difference is referred to as the membrane potential (V_m; where $V_m = V_{inside} - V_{outside}$ and $V_{outside} = 0$). Na^+ and Cl^- ions are more concentrated on the outside of neurons than on the inside, while K^+ ions are more concentrated on the inside of neurons than the outside. The intra and extracellular concentrations of these ions for a “typical” neuron are listed in table 1.1.

Table 1.1. The ionic concentrations inside and outside a "typical" neuron and resultant equilibrium potential. From Wright, (2004).

Ion	Intracellular concentration (mM)	Extracellular concentration (mM)	Equilibrium potential (mV)
K^+	135	4	-92
Na^+	12	140	+64
Cl^-	4	116	-88

This concentration gradient is vital to normal cellular functioning. It is primarily a product of the Na^+-K^+-ATPase pump, necessitated by the ability of Na^+, K^+, and Cl^- to move across the plasma membrane due to a diverse array of selectively permeable ion channels. When ion channels are permeable, their associated ion will cross the membrane under the driving force of the concentration gradient of the ion, and the electrical force resultant of the difference in electrical potential between the inside and the outside of the neuron.

The RMP is the V_m at rest. To best describe the processes underpinning the generation of the RMP it is useful to consider a simplified system, for example a glial cell. Glial cells have similar relative concentrations Na^+, K^+, Cl^-, and large organic anions to neurons, however at rest they are almost exclusively permeable to K^+. Because of the concentration gradient described above, K^+ diffuses from the inside to the outside of the cell. This creates a negative charge on the inside of the cell relative to the outside, creating a difference in electrical potential across the membrane which counterbalances the diffusion of positive charged K^+ across the membrane. There will continue to be a net diffusion of K^+ out of the cell until the difference in electrical potential grows large enough that inward K^+ flow, resultant of the electrical potential, and the outward K^+ flow, resultant of the concentration gradient, are equal. This difference in electrical potential between the inside and the outside of the cell is known as the potassium equilibrium potential (E_K). As glial cells are almost only permeable to K^+ at rest, the RMP of glia is very close to E_K. The balance of electrical and chemical forces underpinning the equilibrium potential of an ion can be described using the Nernst equation:

$$E_x = \frac{RT}{zF} \ln \frac{[X]_o}{[X]_i}$$

where E_X is the equilibrium constant of the ion X, R is the gas constant (8.31 J/(K)(mol)), T is the temperature in °K (37°C = 310°K), z is the ionic valence, F is the Faraday constant (96,500 coulombs/mol), and $[X]_o$ and $[X]_i$ are the ionic concentrations outside and inside the cell respectively.

Although neurons are also highly permeable to K^+ at rest, the RMP is always more depolarised than E_k. This is because at rest neurons are also somewhat permeable to Na^+ and Cl^- ions. Unlike glial cells, where the RMP is a product of the intra and extracellular concentrations of K^+, the RMP of neurons is a product of the concentration gradients of Na^+, K^+, and Cl^- as well as the permeability (in units of velocity) of the membrane to each ion. This can be described by the Goldman equation:

$$V_m = \frac{RT}{F} \ln \frac{P_K[K^+]_o + P_{Na}[Na^+]_o + P_{Cl}[Cl^-]_i}{P_K[K^+]_i + P_{Na}[Na^+]_i + P_{Cl}[Cl^-]_o}$$

where P is the ionic permeability (Kandel *et al.*, 2000; Wright, 2004).

1.1.2 Passive membrane properties

Although the Goldman equation provides a solid theoretical grounding on how the neuronal RMP is generated, it only applies when V_m has reached a steady state. However *in vivo* the V_m of neurons is constantly changing, for example in response to a synaptic potential or during the generation of an AP. The amplitude and time course of V_m alterations in response to a stimulus is controlled by the passive neuronal membrane properties. These passive membrane properties include the membrane resistance, the membrane capacitance and the axial resistance of the dendrites and axons.

The neuronal membrane functions as a variable resistor within an electrical circuit. The resistance of a neuron can be measured by injecting a hyperpolarising or a subthreshold depolarising current injection and measuring the resultant voltage deflection. Using Ohms law, the input resistance (R_i) is calculated by dividing the

amplitude of the voltage deflection once it has reached steady state by the amplitude of the current injection (R = V/I). Thus the greater the R_i of a neuron, the larger the voltage deflection following an input (e.g. a synaptic potential). In simple terms R_i is a measure of how easily current can pass the neuronal membrane and as such is dependent on both the density of open ion channels and the size of a neuron (a bigger surface area means more ion channels).

As well as a resistor, the neuronal membrane acts as a capacitor (i.e. can store charge). The capacitance of the membrane is a result of the insulating properties of the membrane phospholipid bilayer, which retards the change in V_m in response to a current injection. Notably since the membrane acts as a resistor and capacitor in parallel, it does not act as a true resistor (e.g. V_m does not respond in a step-wise manner in response to a step change in current because of the membrane's ability to store charge) or a true capacitor (V_m does not continue to increase over time during a step wise current injection because of the membrane resistance). Instead the initial response to a step wise hyperpolarising current injection reflects the capacitive element of the membrane while the steady state reached towards the end of the current step reflects the resistive element. The membrane time constant (τ) defines the rate of change of V_m towards steady state during a hyperpolarising or subthreshold depolarising current injection. It is defined as the product of the capacitance and the input resistance ($\tau = R_i \times C$) (Kandel *et al.*, 2000).

1.1.3 Voltage-gated ion channels.

The RMP and passive membrane properties of neurons (which govern the amplitude of changes in V_m in response to stimuli) are of vital importance because of the existence of neuronal Na^+, K^+ or Ca^{2+} permeable ion channels which undergo conformational changes in a voltage dependant manner. A vast array of different voltage-gated ion channels have been described, each sharing a similar architecture. Voltage-gated ion channels consist of 4 repeats of a large integral-membrane α subunit, each composed of 6 α-helical transmembrane segments (S1-S6). Notably voltage-gated K^+ channels consist of 4 α subunits which assemble post-translationally into a tetramer while voltage-gated Na^+ and Ca^{2+} channels consist of one α subunit (which is the equivalent of 4 concatenated K^+ α subunits). Each voltage-gated ion

channel has a charged transmembrane component (containing positively charged basic amino acid at every third residue) of the channel protein, called the voltage sensor, which confers the channels voltage sensitivity. Voltage-gated ion channels also have a large extracellular loop between S5-S6 (which lines the channel pore) which forms the selectivity filter for the channel. A schematic diagram showing the general structural features of voltage-gated ion channel α subunits is displayed in Figure 1.1 (Kandel *et al.*, 2000).

There is considerable diversity in the regional and cell type specific expression of α subunits of individual sub-types of voltage-gated ion channels, specific for a particular ion, which confers specific cell type specific aspects of neuronal function (Vacher *et al.*, 2008). A specific example of this with regards to the regional expression of T-type Ca^{2+} channels will be discussed in section 1.2.3.1. Voltage-gated ion channel complexes also contain auxiliary subunits which can profoundly influence the function, expression and localisation of α subunits (Kandel *et al.*, 2000; Vacher *et al.*, 2008).

Voltage-gated ion channels can exist in two or more relatively stable conformational states which they can transition between in a process termed gating. The majority of voltage-gated ion channels can exist in three functional conformational states, namely closed (but available to open in response to changes in V_m), open (allowing charged ions to diffuse across the neuronal membrane) and inactivated (closed and not available to open in response to changes in V_m). The transition from the closed to open state requires energy which is provided by the movement of the voltage-sensor, through the electrical field of the ion channel. Most, but not all, voltage-gated ion channels can inactivate, resulting in a block at the intracellular side of the channel pore. Voltage-gated Na^+ and K^+ channels inactivate in a voltage dependant manner independent of the spatial region governing channel opening, while voltage-gated Ca^{2+} channel inactivation requires Ca^{2+} entry through the channel pore (Kandel *et al.*, 2000).

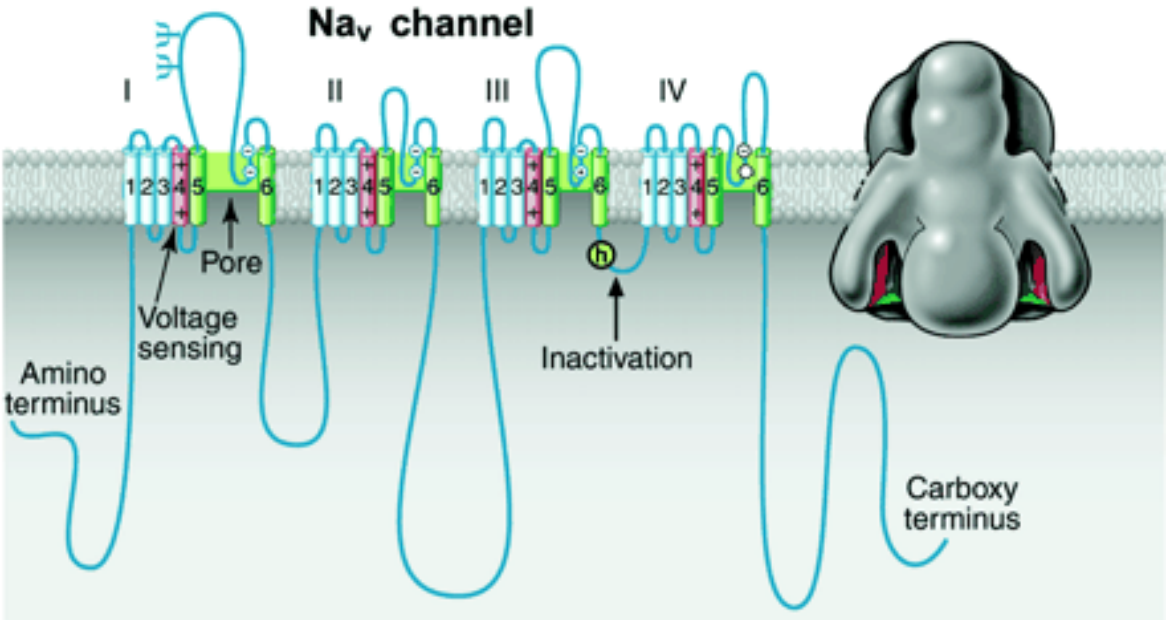

Figure 1.1. The structure of the voltage-gated Na^+ channel. Schematic figure highlighting the 4 transmembrane domains, the voltage sensor, the channel pore and inactivation gate of the voltage-gated Na^+ channel. Taken from (Yu *et al.*, 2005).

1.1.4 The neuronal action potential.

The neuronal AP, a self-propagating electrical signal, allows neurons to carry signals over long axonal distances. APs are generated when V_m becomes depolarised (e.g. in response to synaptic input) to a voltage sufficient to activate a percentage of available voltage-gated Na^+ channels (AP threshold). Na^+ flows through open channels which causes further depolarisation, invariably other voltage-gated Na^+ channels open and consequently greater Na^+ diffusion into the neuron occurs. This positive feedback cycle rapidly increases the membrane's permeability to Na^+ and drives V_m rapidly towards E_{Na} (the rising phase of the AP). However V_m never reaches E_{Na} because during the rising phase of the AP, voltage-gated Na^+ channels gradually inactivate and voltage-gated potassium channels, following a delay, begin to open increasing the permeability of the membrane to K^+. The resultant outward diffusion of K^+ repolarises the membrane towards resting V_m (the descending phase of the AP) (Kandel *et al.*, 2000). Figure 1.2 illustrates the contribution of Na^+ and K^+ to an AP observed in a squid axon as described by Hodgkin-Huxley (Hodgkin & Huxley, 1952).

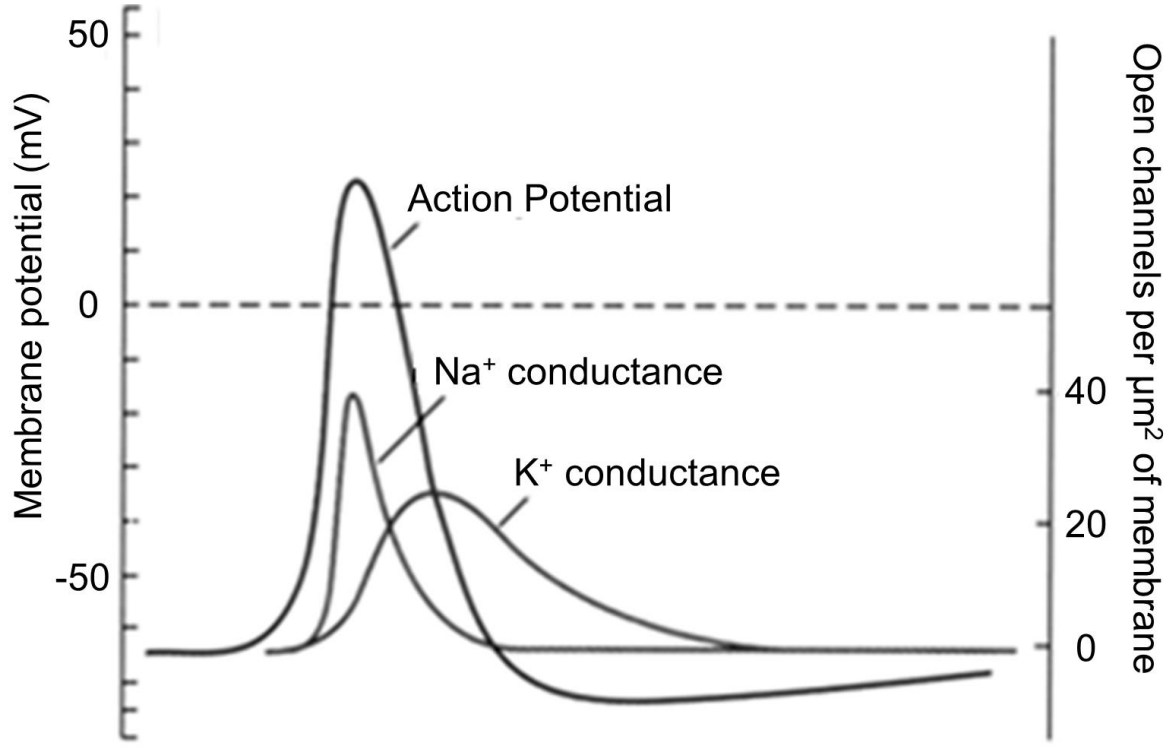

Figure 1.2. Voltage-gated Na^+ and K^+ channels generate the neuronal action potential in a squid axon. Adapted from Kandel (2000).

Because of the sheer diversity of voltage-gated ion channels described in the mammalian central nervous system (CNS), the AP waveform can vary wildly from the simplified model described above leading to a much larger range of observed firing behaviours (Bean, 2007). After-spike potentials, which are a result of such voltage-gated conductances, can significantly contribute to the functional output of a neuron (Brown & Randall, 2009; Springer *et al.*, 2015). After-spike potentials can be either hyperpolarising (Afterhyperpolarisation; AHP) or depolarising (Afterdepolarisation; ADP). AHPs plays a very important role in shaping the pattern of AP generation by providing negative feedback in proportion to AP output (a refractory period) (Kandel *et al.*, 2000). Voltage-gated K^+ currents, involved in the repolarisation of the AP (Fig 1.2), terminate subsequent to V_m returning to its resting value, resulting in a fast AHP (<10 ms). Medium (<100 ms) and long (~1 – 2 s) AHPs are also observed following prolonged activity in CA1 pyramidal neurons (Alger & Nicoll, 1980; Gu *et al.*, 2005). ADPs also have a profound influence on the functional output of neurons. If an ADP is large enough it will bring V_m towards AP threshold and one or more APs can arise

in quick succession. Such an effect has been observed in CA1 pyramidal neurons as a result of a non-inactivating Na^+ current (Azouz *et al.*, 1996) or thalamic relay neurons where T-type Ca^{2+} channels become activated and drive a neurons to burst from hyperpolarised potentials (Zhan *et al.*, 1999).

1.1.5 Synaptic transmission.

How neurons integrate incoming information to generate an appropriate response was discussed in previous sections. In this section, the mechanism through which neurons transmit these output responses to other neurons will be discussed. The structure through which one neuron communicates to another is called a synapse. The pre-synaptic terminal contains clusters of vesicles, each containing thousands of molecules of a specific neurotransmitter. Following AP induced Ca^{2+} entry at the pre-synaptic terminal, theses vesicles interact with the neuronal membrane through a complex machinery of proteins called SNARE proteins, resulting in the release of neurotransmitter into the synaptic cleft. This release in quantal in nature, i.e. each vesicle released results in a post-synaptic potential of the same size, and is dependent on the influx of Ca^{2+} through voltage-gated Ca^{2+} channels (Südhof, 2013).

Once released, neurotransmitters diffuse across the synaptic cleft and bind to receptors on the post synaptic neuron. In response the target neuron can display a range of responses based on the receptor subtype bound to and the neurotransmitter released. There are two main classes of receptors, ionotropic and metabotropic. Ionotropic receptors gate ion fluxes directly, i.e. the binding of a specific neurotransmitter causes conformational change to the receptor which allow the diffusion of ions across the membrane. The prerequisite for ligand binding is a notable difference between ionotropic receptors and the voltage-gated ion channels described in section 1.1.3. Another important difference is that many ionotropic receptors are not specific for a particular ion, ionotropic glutamate receptors being the best example of this (discussed below) (Kandel *et al.*, 2000).

Metabotropic receptors, the other main class of synaptic receptor, act indirectly on ion channel function, and other cellular processes, by altering intracellular metabolic processes. These receptors are made of two components, a receptor component and an effector component. Activation of these receptors usually leads to changes in the

levels of intracellular second messengers which alter channel activity through action on the intracellular biochemical makeup of the neuron (e.g. protein kinase mediated phosphorylation) (Kandel *et al.*, 2000).

Glutamate is widely accepted as the primary excitatory neurotransmitter in the brain (Watkins & Jane, 2009). When released it can bind to both ionotropic and G-protein coupled metabotropic glutamate receptors (mGluR). Ionotropic glutamate receptors can be subdivided into 3 classes based on their pharmacological profile. α-amino-3-hydroxy-5-methyl-4-isoxazolepropionic acid (AMPA) and kainate receptors are almost equally permeable to both Na^+ and K^+. N-Methyl-D-aspartate (NMDA) receptors meanwhile are permeable to Na^+, K^+, and Ca^{2+}. All 3 subtypes of ionotropic glutamate receptors have a reversal potential close to 0 mV and hence only produce excitatory postsynaptic potentials (EPSPs). Originally these receptors were subdivided into NMDA and non-NMDA glutamate receptors based on the unique properties of the NMDA receptor (Watkins & Jane, 2009). NMDA receptors while ligand gated ion channels, are also voltage dependant. This is largely due to Mg^{2+} ions which block the channel pore in a voltage dependant manner, preventing the flow of ions through the channel following ligand binding at a relatively hyperpolarised V_m. Thus for current to flow through these channels V_m must be depolarised in order to relieve the Mg^{2+} block (e.g. following a depolarising flow of ions through AMPA/Kainate receptors). NMDA receptors also require co-activation by glycine or D-Serine to facilitate the flow of ions (Kandel *et al.*, 2000; Watkins & Jane, 2009). Notably the grouping described above is a gross oversimplification, as the glutamate receptor groupings described above can be further subdivided based on the subunit composition of each receptor. 18 genes encode for glutamate receptor subunits (Traynelis *et al.*, 2010) and differing subunit compositions can have substantial functional consequences, i.e. NMDA receptors containing the NR2C or NR2D subunit are relatively poorly blocked by Mg^{2+} (Kuner & Schoepfer, 1996) and thus can mediate tonic currents at rest in response to sufficient levels of ambient glutamate. There are 8 different genes which encode for subtypes of mGluR (mGluR 1-8), which are subdivided into three groups based on sequence homology, G-protein coupling and ligand selectivity (Niswender & Conn, 2010).

Gamma-Aminobutyric acid (GABA) is the main inhibitory neurotransmitter in the CNS (Kandel *et al.*, 2000; Bowery & Smart, 2009). The ionotropic receptors activated by GABA are Cl^- specific $GABA_A$ and $GABA_C$ receptors. Because of the relative

concentration gradients of Cl^- in a “typical” adult neuron, and the difference in electrical potential between the inside and the outside of a neuron discussed above, the inward diffusion of Cl^- through these channels usually results in an inhibitory post-synaptic potential (IPSP). However in certain situations, i.e. early in development (Ben-Ari, 2002) or following excessive excitation of GABAergic interneurons during epileptic network activity (Ellender *et al.*, 2014), E_{Cl} can be such that the binding of GABA to these receptors results in the depolarisation of V_m. $GABA_B$ receptors are G-protein coupled receptors and indirectly activate G-protein coupled K^+ channels. This leads to a relatively slow and long lasting hyperpolarisation compared to IPSPs produced by ionotropic GABA receptors (Bowery & Smart, 2009). Notably the activation of $GABA_B$ receptors also regulates adenylyl cyclase activity, an enzyme which converts adenosine triphosphate (ATP) to 3’,5’-cyclic AMP (c-AMP) in important cellular signalling cascades and also inhibits voltage dependant Ca^{2+} currents (Padgett & Slesinger, 2010).

1.1.6 Neuronal oscillations

Complex tasks, such as memory, require the synchronisation of neuronal activity within and between brain regions, often over long distances. Such synchronous activity manifests as neuronal oscillations, an emergent property of large populations of neurons firing synchronously (Buzsaki & Draguhn, 2004). The emergence of oscillations is dependent on both a complex network of inter-connected neuronal populations and the intrinsic oscillatory properties characteristic to specific neuronal sub-types which confer rhythmic patterns of AP firing (e.g. as a result of specific voltage-gated ion channels; see Figure 1.5). The temporal coherence of oscillatory activity provides a theoretical framework for the processing, transfer and storage of information across discrete networks of neurons (Engel *et al.*, 2001).

Within the context of animal research, oscillations are typically recorded via the use of an implanted electrode which records the extracellular voltage resultant of the summative activity of large population of neurons, termed the local field potential (LFP). Such recording are typically classified within discrete frequency bands based on associations with the cognitive state of the subject (Engel *et al.*, 2001). Memory centres of the brain (e.g, HF, mPFC) primarily display neuronal oscillations in the theta

(5-12 Hz) and gamma (30-120 Hz) frequencies in awake behaving mice (Buzsáki, 2002; Onslow *et al.*, 2011). Theta oscillations facilitate synchronisation of neuronal activity across brain areas (discussed below, section 1.3.2), and gamma oscillations are associated with numerous forms of memory. Notably gamma oscillations appear in a manner dependant on the relative stage of the theta oscillatory cycle (Fig 1.3.) and the degree of coupling of these frequencies strongly correlates to cognitive ability in both humans and rodents (Colgin, 2015). Although theta and gamma oscillations are tightly linked in both temporal and functional domains, each is independently generated through complex interactions between characteristic inhibitory interneuron sub-classes and excitatory pyramidal neurons (Pelkey *et al.*, 2017). The neuronal oscillation most associated with the thalamus are delta oscillations which are observable during slow-wave sleep. The physiological relevance and cellular basis of this oscillatory activity will be discussed in section 1.2.3.

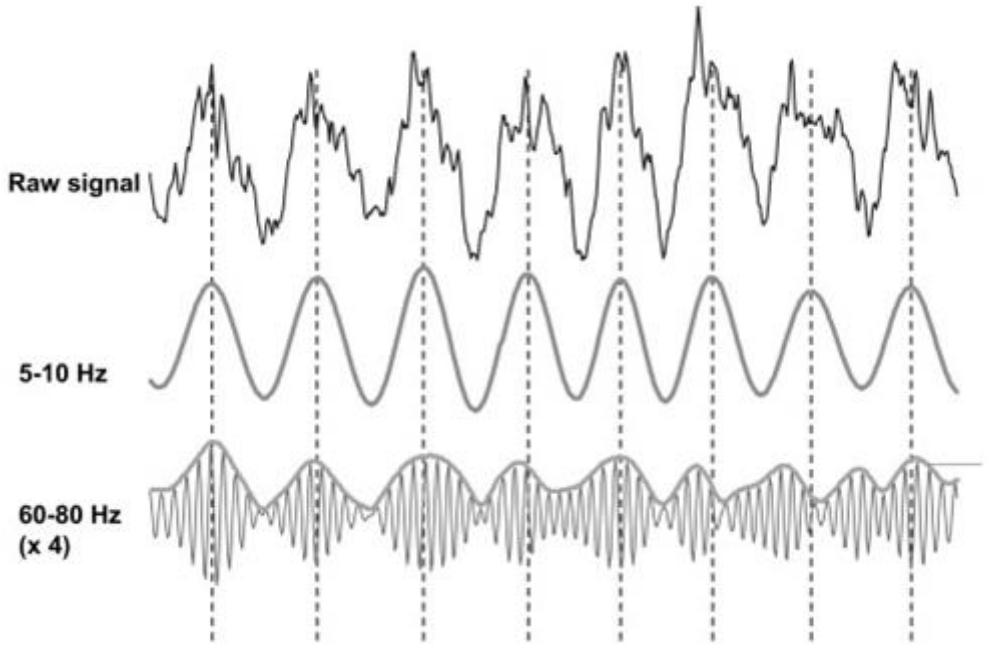

Figure 1.3. Neuronal oscillations in the rodent hippocampus. Raw data from a 1 s window, displaying the raw LFP recorded from a rodent hippocampus. Filtered races with the theta and gamma frequency display the dependence of gamma activity on the relative stage of the theta cycle (grey lines). Adapted from (Onslow *et al.*, 2011).

1.2 The thalamus

The thalamus is a large mass of grey matter in the diencephalon. It has classically been thought to act primarily as a relay centre in the brain, transmitting motor and sensory input from the periphery to the cortex. The word thalamus is derived from the Greek word *thalamos*, referring to a bridal chamber or bridal couch (Jones, 1985) and in the past decades there is a growing appreciation that the thalamus may indeed live up to its name. That is to say, with the somewhat recent appreciation that a population of thalamic nuclei are intricately involved in higher level cortical processing, the characteristic intrinsic neuronal profile of thalamic neurons may facilitate a certain degree of magic happening. This section will review the neuroanatomy of the thalamus, how first and higher order thalamic relays contribute to cortical function and the characteristic intrinsic properties of a "typical" thalamic relay neuron.

1.2.1 Neuroanatomy of the thalamus.

The thalamus was first anatomically categorised into individual nuclei around the turn of the 20th century, based on the cortical targets of fibres arising from specific thalamic regions. The first comprehensive description of the internal structure of the thalamus was made by Franz Nissl in the late 19th century, using his newly developed Nissl stain. These experiments utilised retrograde atrophy, the observation that experimentally lesioning a cortical structure results in significant atrophy of neurons of the thalamus which target the lesioned cortex. These studies were later refined by an increase in the specificity of cortical lesions during the 1950's, and the advent of more sensitive neuroanatomical techniques in the 1970's which have refined the classification of thalamic relay nuclei to the ones still in use today. These include:

- Anterior nucleus of the thalamus
- Dorsomedial nucleus
- Paratenial nucleus, paraventricular nucleus, reuniens nucleus and rhomboid nucleus (midline nuclear group)
- Rostral and caudal intralmainar nuclei
- Pulvinar
- Ventral nuclear group
- Medial and lateral geniculate nucleus

Notably every thalamic relay nucleus projects to the ipsilateral cortex. The reticular nucleus of the thalamus (Rt), a thin band of grey matter circumventing the extent of the thalamus which receives extensive input from the cortex and provides GABAergic input onto thalamic relay neurons, does not (Jones, 1985).

1.2.2 First and higher order relays influence on cortical function.

The classical view of the thalamic role in cortical function is to relay information from the subcortical areas of the brain to functionally linked cortical areas. Indeed each major neocortical area has a specific well defined thalamocortical (TC) driving input. For example all visual information that arrives at the visual cortex first passes through the lateral geniculate nucleus. Thalamic nuclei which exclusively fulfil this role are termed first order thalamic nuclei (Sherman & Guillery, 2006).

While the evidence for the transfer of such information is overwhelming, it does not occlude the potential for specific thalamic nuclei to functionally engage the cortex in alternate contexts. Anatomical evidence has been provided for a transthalamic corticothalamocortical pathway which was proposed to play a role in corticocortical communication (Guillery, 1995). These inputs arise from layer V of the cortex and terminate in a specific higher order thalamic nucleus which, in turn, provides an afferent to the middle layers of a distinct area of the cortex (Theyel *et al.*, 2010). These higher order thalamic relay nuclei differ from first order nuclei in that the they convey information to cortical areas which has been previously been processed in the cortex, thus representing a higher level of processing (Sherman & Guillery, 2006). A schematic diagram of the differential actions of first and motor relays are shown in Figure 1.4.

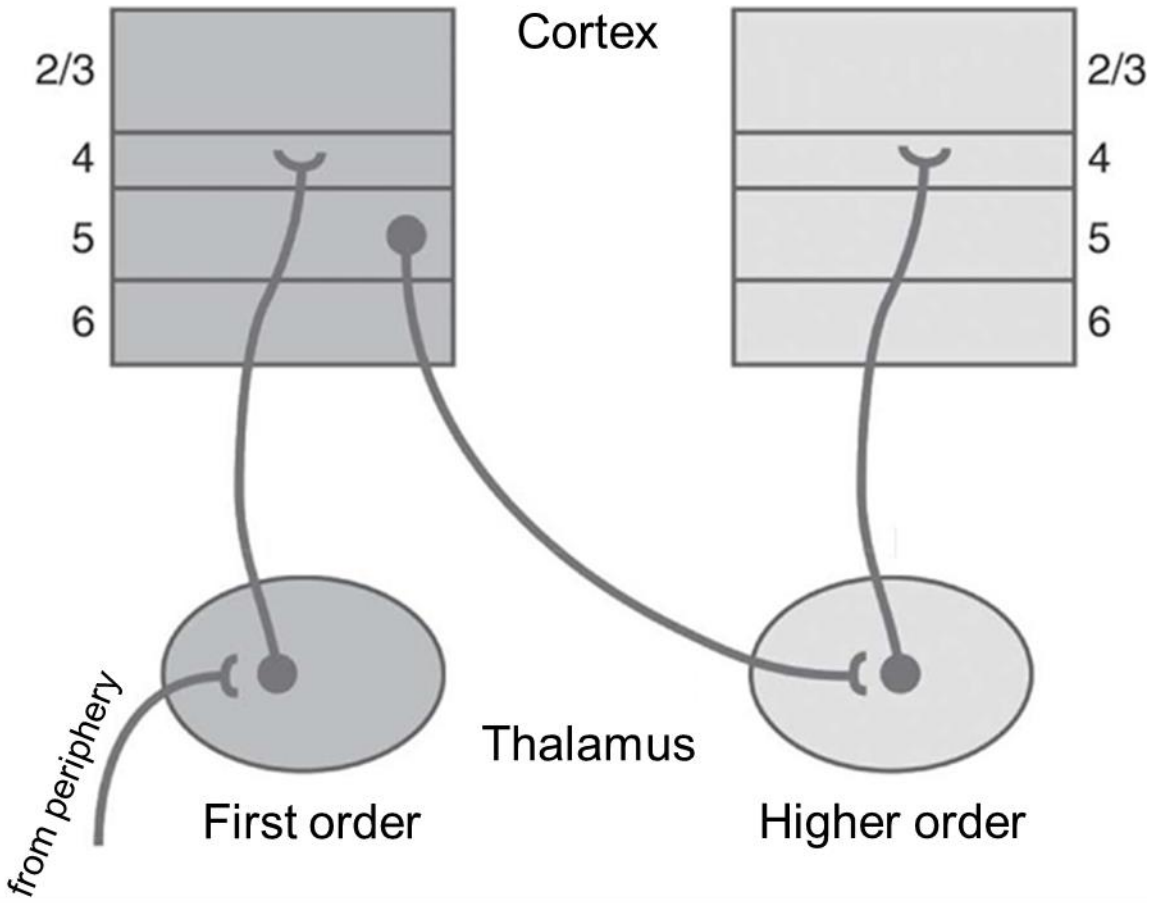

Figure 1.4. Differential actions of first and higher order thalamic relays on cortical function. First order nuclei project to layer 4 of the cortex conveying information from the periphery. This information can be subsequently processed in another cortical area through a corticothalamocortical circuit involving higher order thalamic nuclei. Adapted from (Theyel et al., 2010).

It is important to stress that all thalamic nuclei receive input from the cortex however in first order relay nuclei these inputs originate from layer 6 and exclusively target metabotropic receptors, while in higher order nuclei cortical input originates from layer 5 and largely target ionotropic receptors similar to the synaptic input to first order nuclei from the periphery illustrated in Figure 1.4 (Sherman & Guillery, 2006). Such input onto ionotropic receptors is necessary for corticothalamocortical communication, which has been demonstrated (with respect to specific higher order thalamic nuclei) both *in vivo* (Shumikhina & Molotchnikoff, 1999; Soares *et al.*, 2004), and in *in vitro* slice preparations (Theyel *et al.*, 2010).

1.2.3 Intrinsic electrophysiological properties of thalamic relay neurons

Thalamic neurons contain stereotypical voltage-gated ionic conductances which massively affect the functional output of neurons in response to a stimulus. They can display two distinct modes of firing, namely tonic and burst firing, depending on the value of V_m. This section will outline the conductances involved in stereotypical thalamic relay neuron behaviour and the significance of each mode of firing.

1.2.3.1 T-type Ca^{2+} channel current.

T-type Ca^{2+} channels provide a useful model to illustrate the functional states voltage-gated ion channels display because of the large effect these states have on the functional output of thalamic relay neurons. T-type Ca^{2+} channels, like the majority of voltage-gated ion channels, display three functional states, open, closed and inactivated. Open channels allow the diffusion of Ca^{2+} across the membrane. T-type channels were originally known as low voltage activated (LVA) Ca^{2+} channels because of the hyperpolarised V_m (~-65 mV) at which they begin to open relative to other types of high voltage activated (HVA) Ca^{2+} channels. Closed channels open in response to a depolarising stimulus, while inactivated channels will not open in response to a depolarising stimulus and require a period of time at a relatively hyperpolarised V_m to return to a closed state (Perez-Reyes, 2003).

T-type Ca^{2+} channels are encoded by a Ca_v3 gene. There are 3 subtypes of channel based on the gene which encodes the pore forming α subunit present, namely Ca_v 3.1, Ca_v 3.2, and Ca_v 3.3 (Fig 1.5A). Figure 1.5B shows normalised voltage responses and the biophysical properties of the different isoforms. Ca_v 3.1 has faster activation and inactivation kinetics than Ca_v 3.3 while the steady state activation and inactivation curves for Ca_v 3.3 is ~5-7 mV more depolarised than Ca_v 3.1 (Chemin *et al.*, 2002). Ca_v 3.1 is the primary isoform found in thalamic relay nuclei, although robust Ca_v3.3 expression is also found in specific relay nuclei. Meanwhile Ca_v 3.2 and Ca_v 3.3 are robustly expressed in the Rt (Talley *et al.*, 1999), resulting in the generation of longer bursts of Na^+/K^+ dependant APs in Rt neurons relative to relay neurons (Domich *et al.*, 1986).

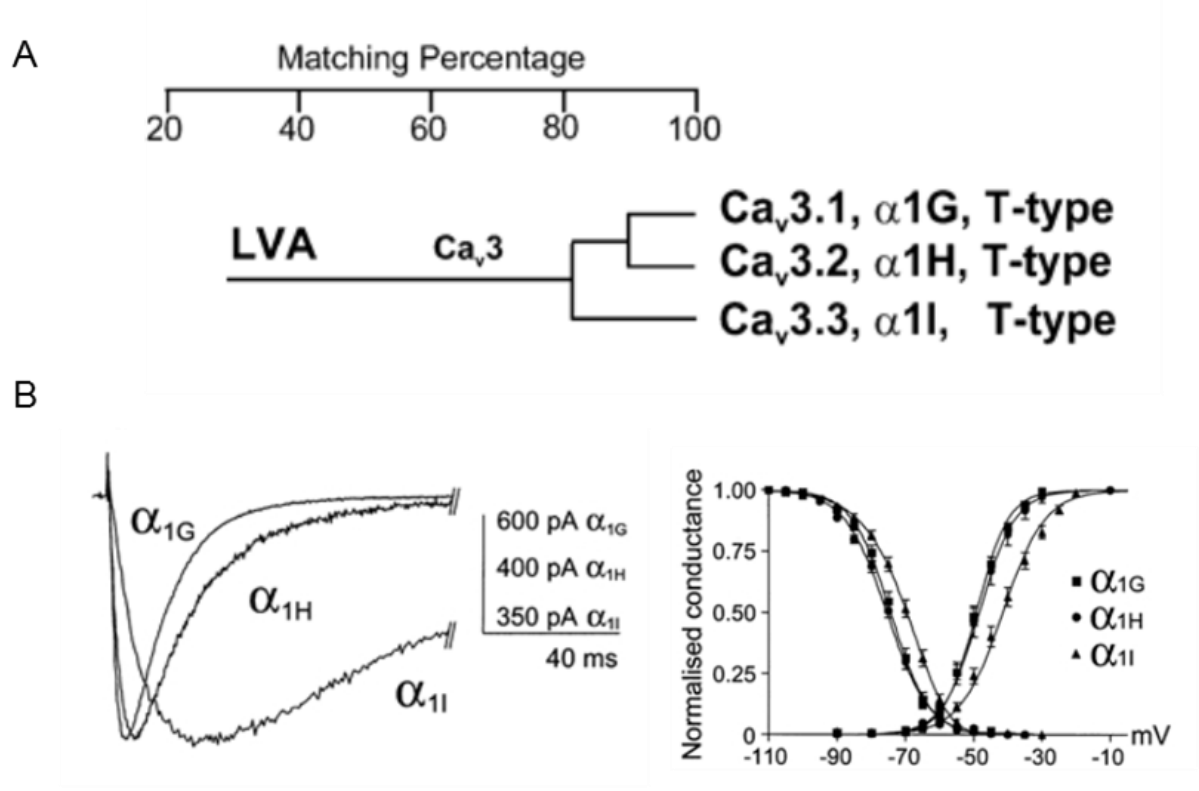

Figure 1.5. Evolutionary tree of T-type Ca^{2+} channel subunits and their biophysical properties. (A) Sequence homology of the three T-type Ca^{2+} channel isoforms. Adapted from (Perez-Reyes, 2003). (B) (Left) Normalised current response to a voltage step from a holding potential of -110 mV to -35 mV from cloned human T-type Ca^{2+} channel isoforms. (Right) Biophysical properties of T-type Ca^{2+} channels. Adapted from (Chemin et al., 2002).

Besides the Na^+ and K^+ currents underlying the AP, T-type Ca^{2+} currents are by far the most important voltage-gated conductance in thalamic relay neurons. The flow of Ca^{2+} through open T-type channels leads to the generation of low threshold Ca^{2+} spikes and subsequent bursting and oscillatory behaviour (Steriade & Llinás, 1988; Huguenard & Prince, 1992; Steriade *et al.*, 1993; Huguenard, 1996). This can occur in response to a depolarising input from a hyperpolarised V_m (where T-type channels are available to open) or from a prolonged hyperpolarising input from a relatively depolarised potential (during which T-type channels recover from inactivation).

1.2.3.2 I_h current.

One of the most striking features of features of thalamic relay neuron neurophysiology is the robust, depolarising change in V_m observed in response to a hyperpolarising current injection, commonly known as “sag” (Steriade & Deschenes, 1984; Steriade & Llinás, 1988). The flow of Na^+ and K^+ through non-specific cation channel, i.e. HCN

channels, is responsible for this depolarisation and is designated I_h. Four genes encode for HCN channels (HCN 1-4) with HCN 2 being the most prominent isoform expressed in the thalamus (Santoro *et al.*, 2000).

I_h has a large effect on the response mode of thalamic relay neurons through its role in modulating the RMP (Meuth *et al.*, 2006; Amarillo *et al.*, 2014). It is also vital to the emergence of oscillatory activity within the defined V_m range where both burst firing and "sag" can occur. This oscillatory activity presents as the production of rhythmic bursts of APs as displayed in Figure 1.6. During the hyperpolarisation following a burst of APs, a result of the opening of Ca^{2+} activated K^+ channels, T-type Ca^{2+} channels recover from inactivation. I_h then activates and pushes V_m towards the threshold for the activation of T-type Ca^{2+} channels resulting another burst of APs (McCormick & Pape, 1990; Pape, 1996). The physiological relevance of this oscillatory activity will be discussed in detail below.

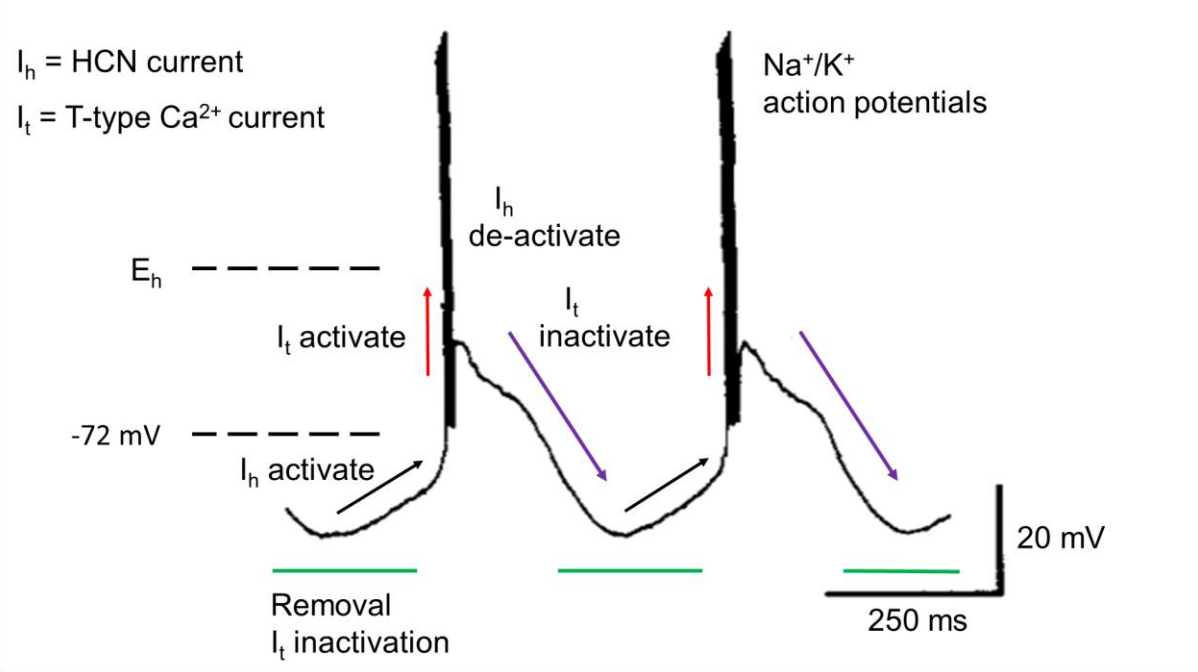

Figure 1.6. Interplay between T-type Ca^{2+} current (I_t) and I_h in the generation of rhythmic burst firing in a "typical" thalamic neuron. From a relatively hyperpolarised potential, the inactivation of I_t is removed (green line) and I_h activates (black arrow) pushing V_m towards E_h. Upon sufficient depolarisation I_t activates producing a burst of Na^+/K^+ mediated APs. During this burst of APs, V_m is such that I_h no longer passes current. Meanwhile following the burst I_t has inactivated (purple arrow) ceasing depolarising conductances while Ca^{2+} influx during the burst causes in membrane hyperpolarisation through Ca^{2+} activated K^+ channels resulting in removal of I_t inactivation, activation of I_h and rhythmic burst firing. Adapted from (Pape, 1996).

1.2.3.3 Burst and tonic firing mode.

The rhythmic burst firing described above (synchronised across large populations of thalamic relay neurons) was originally described during slow wave sleep (SWS) (Steriade *et al.*, 1993). During this rhythmic firing, the thalamus cannot faithfully relay incoming information to cortical targets. Conversely, when T-type Ca^{2+} channels are inactivated, the thalamus can function effectively as a relay, i.e. there is a linear relationship between the size of the stimulus and the number of APs produced (Sherman & Guillery, 2006). In contrast, arrhythmic burst firing has been observed in both awake animals (Nicolelis *et al.*, 1995; Albrecht *et al.*, 1998) and humans (Radhakrishnan *et al.*, 1999), indicating that arrhythmic burst firing can relay useful information in an awake state. Notably these arrhythmic bursts are observed at greater frequencies in higher order relay nuclei (Ramcharan *et al.*, 2005).

This form of transmission is non-linear, and step-wise in nature, due to the all or nothing nature of the T-type Ca^{2+} current which underlies bursting activity (Zhan *et al.*, 1999). A similar level of information is transmitted to the cortex by tonic and burst firing modes (Reinagel *et al.*, 1999) and indeed, arrhythmic bursting has several advantages over tonic firing in terms of relaying information including increased detectability and a larger signal to noise ratio (Sherman, 2001).

The main advantage of two relay modes is that neuronal output can be modulated easily through modulatory inputs onto relay neurons. These modulatory inputs, which account for the majority of input onto thalamic relay neurons (Sherman & Guillery, 1998, 2006), can modulate V_m and thus ensure the appropriate output mode of relay neurons.

1.3 The nucleus reuniens.

The Re is a large ventral higher order nucleus of the midline thalamus located atop the dorsal tip of the third ventricle. It is part of what is classically considered the limbic thalamus, a group of thalamic nuclei that have intimate interconnections with those cortical and subcortical structures that comprise the limbic system (Taber *et al.*, 2004). This section will summarise the current literature on the connectivity of the Re, its cellular diversity at a neurochemical level, and its role in behaviour and disease.

1.3.1 Connectivity of the nucleus reuniens.

As described in section 1.2, a thalamic nucleus largely derives its designation from the specific set of cortical regions which it projects to (Jones, 1985). To understand the role of the Re within the context of a complex neuronal network such as the mammalian brain it is vital to intimately understand such connections. This section will provide an overview of the findings of anterograde and retrograde tracing studies which have teased out in great detail the connectivity of the Re.

1.3.1.1 Efferent projections of the nucleus reuniens.

The Re, as part of the midline thalamus nuclear group, was once thought to project to widespread areas of the cerebrocortex in a “non-specific” manner (Groenewegen & Berendse, 1994), in a fashion atypical for sensory/motor thalamic relay neurons which usually project with high degrees of specificity to defined cortical targets (Jones, 1998). This was based largely on a study conducted by Dempsey & Morison (1942) which showed that low frequency electrical stimulation of the midline thalamus produced widespread slow synchronous activity throughout large spans of the cortex. This notion was later revised when studies showed each nuclear constituent of the midline nuclear group projects specifically to well-defined cortical targets (Berendse & Groenewegen, 1991). The Re primarily innervates limbic structures (Vertes *et al.*, 2015). There are some projections to specific subcortical targets, including the basolateral amygdala and, as is typical for thalamic relay neurons, the Rt (Vertes *et al.*, 2006). The Re projects to all 4 units of the medial prefrontal cortex (mPFC) (medial agranular cortex, anterior cingulate cortex (ACC), prelimbic cortex (PL), infralimbic cortex (IL)) with innervation of the PL and IL being particularly dense (Wouterlood *et al.*, 1990; Vertes *et al.*, 2006). The Re also projects strongly to parahippocampal

structures and the hippocampal formation (HF). Areas innervated include the stratum lacosum-moleculare of the CA1 region of the hippocampus (HPC), the molecular layer of the subiculum, as well as the perihinal and entorhinal cortices (Wouterlood *et al.*, 1990; Vertes *et al.*, 2006). Interestingly ~8% all neurons projecting to either the HF or the mPFC project to both structures (discussed below).

1.3.1.2 Afferents to the nucleus reuniens.

The Re receives diverse afferents from the cortex, HPC, basal forebrain, amygdala, and brainstem. This section will specify these inputs based on their region of origin and group these inputs based on the putative concomitant neurotransmitter.

Glutamatergic input.

The Re receives extensive putative excitatory input from all 4 subdivisions of the mPFC (medial angular cortex, ACC, PL, and IL (Vertes, 2002; McKenna & Vertes, 2004)). Projections to the Re also arise from the diverse cortical structures including the medial orbital, insular, ectorhinal, perihinal, and retrosplenial cortices (McKenna & Vertes, 2004). Notably the Re also receives projections from the subiculum, the main output centre of the HPC (Witter *et al.*, 1990; McKenna & Vertes, 2004). Finally the Re is one of the few thalamic nuclei to receive Zn^{2+}-positive input (Mengual *et al.*, 2001) from a proportion of its glutamatergic input (Frederickson & Bush, 2001), although the origin of this input is currently unknown.

GABAergic input.

In rodent brains, interneurons account for <1% of neurons in thalamic relay nuclei outside of the visual thalamus (Arcelli *et al.*, 1997). As is typical for other thalamic relay nuclei in mice, the Re receives its primary inhibitory input from the Rt (McKenna & Vertes, 2004), although it is likely that extrathalamic inhibitory input contributes somewhat. For example the Re receives input from the zona incerta which is known to specifically provide GABAergic input to higher order thalamic nuclei (Bokor *et al.*, 2005).

Neuromodulatory input.

The Re receives extensive putative neuromodulatory input from the brainstem. The Re receives dopaminergic input from the ventral tegmental area, noradrenergic input from the locus coeruleus, serotinergic input from the raphe nuclei (McKenna & Vertes, 2004). The Re also receives cholinergic input from the basal forebrain (Kolmac &

Mitrofanis, 1999). Interestingly first and higher order thalamic nuclei display differential responses following application of acetylcholine and serotonergic agonists. Neurons in first order nuclei do not exhibit hyperpolarisation in response to acetylcholine or serotonergic receptor activation, while between 5–25% of neurons in higher order nuclei are hyperpolarised in response to such input (Varela, 2014). Notably the response of Re neurons was not directly measured in this study. As a higher order nucleus with abundant neuromodulatory input, the response of the Re to such input seems a fertile area of research for those interested in the role the thalamus plays in cortical arousal.

1.3.2 The role of the nucleus reuniens in hippocampal prefrontal interactions

Profound working memory deficits are produced following the selective lesioning of either the HPC or the mPFC (Kesner *et al.*, 1996; Floresco *et al.*, 1997) and mounting evidence suggests that the functional interaction between these brain structures is critical for the process. This section will review this evidence and examine the functional and anatomical basis for HPC-mPFC interactions, with a particular focus on the role of the Re in mediating communication between these structures.

1.3.2.1 Hippocampal-prefrontal interactions in working memory

One metric of functional interactions between two brain structures is the emergence of synchronised neural activity. In 2005, Jones & Wilson provided the first evidence that HPC-mPFC synchrony is required for working memory. While simultaneously recording in both areas, they showed that units (extracellularly recorded APs) recorded in the principle cells of the mPFC were phase-locked to HPC theta rhythm (4-10 Hz), an oscillation believed to be important in learning and memory (Buzsáki, 2002), during choice epochs of a spatial working memory task. This result has since been reproduced using different behavioural paradigms (Hyman *et al.*, 2010; Benchenane *et al.*, 2010). Meanwhile experimental manipulations designed to attenuate HPC-mPFC functional connectivity produce working memory deficits (Floresco *et al.*, 1997; Churchwell & Kesner, 2011; Spellman *et al.*, 2015).

The precise anatomy underlying functional interactions between the HPC and mPFC during working memory tasks is still unclear. A projection from the HPC to the mPFC exists that is both monosynaptic (Ferino *et al.*, 1987; Jay *et al.*, 1989; Jay & Witter,

1991) and excitatory (Jay *et al.*, 1995; Ishikawa & Nakamura, 2003) but no reciprocal pathway exists (Beckstead, 1979; Room *et al.*, 1985; Hurley *et al.*, 1991). In order for the mPFC to reciprocally communicate with the HPC, a relay must exist through which the mPFC sends signals to the HPC. The Re has been proposed to serve this role (discussed below).

1.3.2.2 The role of the nucleus reuniens in mediating hippocampal-prefrontal synchrony

As mentioned above the Re has strong reciprocal connections with both the HPC and mPFC (McKenna & Vertes, 2004; Vertes *et al.*, 2006) and exerts a strong excitatory influence on both structures (Dolleman-Van der Weel *et al.*, 1997; Bertram & Zhang, 1999; Hur & Zaborszky, 2005; Di Prisco & Vertes, 2006). Evidence for the role of Re in facilitating HPC-mPFC interactions is mounting. Using a combination of retrograde and anterograde viral tracers, Vertes *et al.*, (2007) showed for the first time a direct interaction between the post synaptic terminal of mPFC afferents to Re and the dendrites of Re neurons which project to the HPC providing anatomical evidence for a disynaptic pathway through which the mPFC can influence hippocampal function. Additionally when retrograde tracers are injected into the HPC and mPFC, approximately 8% of labelled Re neurons projected to both sites defining a distinct population of neurons in the Re which are particularly well positioned to influence interactions between these structures (Hoover & Vertes, 2012). A schematic diagram showing the connections within the HPC-Re-mPFC network is displayed in Figure 1.7.

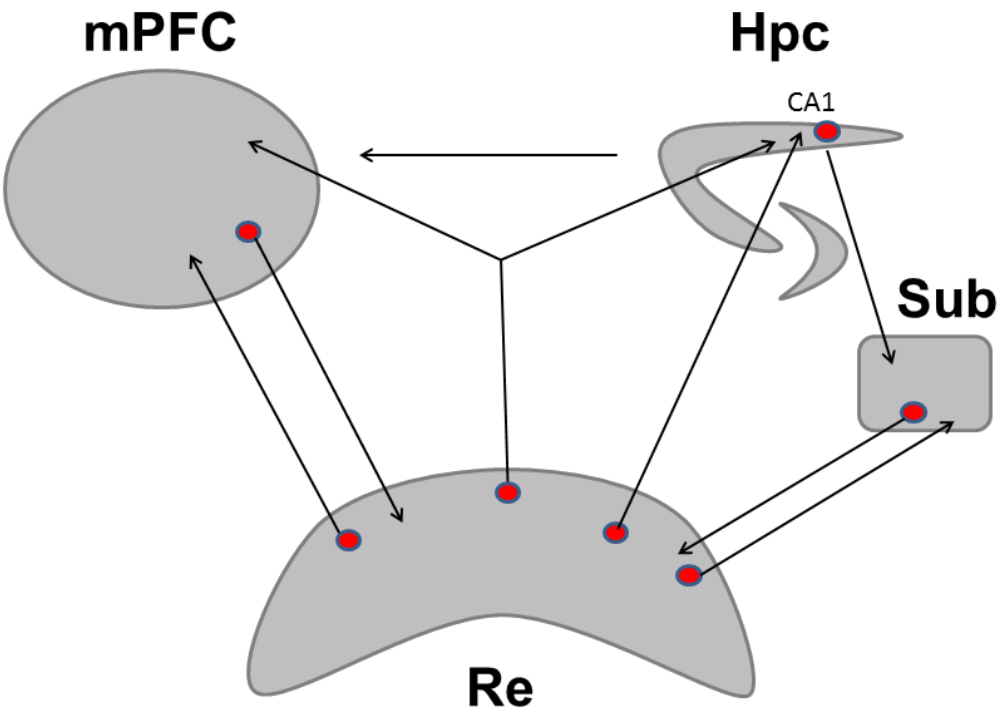

Figure 1.7. Pathways connecting the medial prefrontal cortex, hippocampal formation, and nucleus reuniens. The HPC projects to the mPFC but there is no reciprocal connection. The Re is connected to both the HPC and mPFC with strong bidirectional projections. There is a population of Re neurons which project to both the HPC and mPFC (Each red dot represents a population of neurons).

The first direct evidence of Re involvement in HPC-mPFC synchrony was published recently from Amy Griffin's lab. Here the authors demonstrated that the HPC-mPFC synchrony observed during a spatial working memory was abolished following pharmacological inactivation of the Re with $GABA_A$ receptor agonist muscimol (Hallock *et al.*, 2016). Recently a functional magnetic resonance imaging (fMRI) study in humans provided evidence that the HPC is functionally connected to the mPFC in a Re-dependant manner, in a task designed to test object recognition and discrimination (Reagh *et al.*, 2017).

1.3.3 Cellular diversity in the nucleus reuniens.

Diversity in the neuronal expression of calcium binding proteins calbindin (CB), calretinin (CR) and parvalbumin (PV) is observed across thalamic relay nuclei (Arai *et al.*, 1994). This allows the identification of distinct neuronal populations at a histochemical level. Following staining for the Ca^{2+} binding proteins the Re displays immunoreactivity for CB and CR but not for PV (Arai *et al.*, 1994). Further studies into the cellular architecture of the Re has identified 4 distinct neuronal populations, including CB-positive neurons, CR-positive neurons, neurons which are positive for both CB and CR, and neurons which have are not positive for either CB or CR (Bokor *et al.*, 2002). Interestingly the CR expression profile corresponds to both the functional output of neurons as well as the extent to which their function is modulated by hippocampal activity. Recently Lara-Vásquez *et al* (2016) reported that neurons which no not express CR display higher AP firing rates compared to CR-positive neurons and increased their firing rate during hippocampal theta activity, while hippocampal sharp wave ripples, a form of hippocampal activity thought to be vital to the consolidation of memory during SWS (Girardeau *et al.*, 2009; Ego-Stengel & Wilson, 2010), inhibited the activity of CR-positive neurons. Notably the Re neurons which project to CA1 are almost exclusively neurons expressing CB, irrespective of CR immunoreactivity (Bokor *et al.*, 2002). These differences suggest asymmetric hippocampal connections of neurochemically-defined Re neuronal populations.

1.3.4 The effect of experimental manipulation of the nucleus reuniens on cognitive function.

Within the past 10 years, these insights into the role of the Re on HPC and mPFC function has led researchers to study how experimental manipulation of the Re effects behaviours known to be associated with HPC function, mPFC function or both. This section will review this literature in an attempt to outline the specific role of the Re in normal cognitive functioning.

1.3.4.1 The role of the nucleus reuniens on hippocampal dependant memory.

Due to its strong excitatory influence on the HPC, a number of authors have examined the role of Re function on tasks designed to test hippocampal-dependant memory. A study by Davoodi *et al.* (2009) reported that inactivation of the Re using tetracaine

injections resulted in deficits in memory acquisition on a Morris water maze (MWM). Notably the canula used to deliver tetracaine created large unilateral lesions throughout the dorsal HPC and thalamus, complicating interpretation of this study (control group does not perform significantly above chance level). Contradicting this, a number of studies have reported that excitotoxic lesions of the Re did not induce deficits in the acquisition or recent retention of reference memory using the same behavioural paradigm (Dolleman-van der Weel *et al.*, 2009; Loureiro *et al.*, 2012) and these studies were reproduced using muscimol (a potent $GABA_A$ receptor agonist) inactivation of the Re (Cholvin *et al.*, 2013). These studies do not suffer from confounding damage to the HPC and hence appear much more convincing. Similarly muscimol inactivation of the Re has no effect on a varying choice delayed-non-match-to-place task (VC-DNM) (Hembrook *et al.*, 2012). Both the MWM (de Bruin *et al.*, 1994; Granon & Poucet, 1995; Silva *et al.*, 1998) and VC-DNM (Porter *et al.*, 2000) are sensitive to hippocampal but not prefrontal function. Together these studies suggest that Re inactivation/destruction has no significant effect on HPC-dependant cognitive tasks.

1.3.4.2 Role of the nucleus reuniens on prefrontal dominated behaviours.

While animals do not show a deficit in memory acquisition during a MWM trial, there have been reports that there is a change in behavioural flexibility following Re lesion/inactivation (Dolleman-van der Weel et al., 2009; Loureiro et al., 2012; Cholvin et al., 2013). All three studies reported that following removal of the underwater platform, Re compromised animals swam directly towards to the former platform location before adopting an atypical search pattern compared to control mice. Control mice focused their subsequent search in the target quadrant while Re compromised animals searched the whole pool or spent less time searching the target quadrant (i.e. they gave up searching for the platform faster). These results were interpreted by the authors as a consequence of altered strategy shifting or behavioural flexibility, (i.e. the ability to switch to a correct strategy in response to a changing environment). Such behaviours are dependent on the mPFC (Ragozzino et al., 1999; Dias & Aggleton, 2000). Re lesions also reduce the control of impulsive responses on a 5-choice reaction time test (Prasad *et al.*, 2013), similar to what is seen following lesions of the IL (Chudasama *et al.*, 2003). This suggests that the Re influences prefrontal dominated cognitive tasks through its excitatory projections. A recent paper from the

same lab reputes this view however, demonstrating that Re lesions lead to increased attention and reduced impulsivity in a combined visual memory-attention task (Prasad *et al.*, 2017). Since visual attention is increased upon dopaminergic stimulation of the mPFC (Chudasama & Robbins, 2004), remarkably mPFC activity may have be enhanced by lesioning Re in this study implying that the Re exerts an inhibitory role on the mPFC. Two conflicting reports on the role of Re on impulsivity originating from the same lab is puzzling and may be a result of different portions of the Re being lesioned across cohorts. Alternatively since different subsections of the mPFC are thought to be involved in different aspects of executive function (Goldman-Rakic *et al.*, 1996), this may suggest that Re projections terminate primarily onto populations of inhibitory interneurons in defined subregions of the mPFC. A detailed study into the specific subtype of neuron the Re projects to in the mPFC has not yet been carried out, thus this is speculative. However, this result if reproducible will undoubtedly alter and refine the way we view how the Re interacts with the mPFC.

1.3.4.3 Role of reuniens in behavioural tasks requiring both, HPC and mPFC.

A number of authors have examined the role of the Re in working memory tasks. Hembrook & Mair, (2011) showed that Re lesions caused deficits on the radial arm maze task which is both HPC and mPFC dependant (McDonald & White, 1993; Mair *et al.*, 1998; Porter *et al.*, 2000). The same lab followed this study up with a report that Re inactivation with muscimol produced deficits in a delayed-non-match-to place lever pressing task which is dependent both on HPC and mPFC while showing no deficit in a hippocampal-dependant memory task (Hembrook *et al.*, 2012)(see section 1.3.4.1). Loureiro *et al*, (2012), who reported no deficit in the MWM (see above), reported deficits in a double H maze task (see (Pol-Bodetto *et al.*, 2011)) which is dependant both on spatial memory and behavioural flexibility. Finally Re inactivation with musicomol produces deficits in a modified T-maze designed to test working memory (Hallock *et al.*, 2013). Together these studies suggest that the Re is functionally required for behavioural tasks which require interactions between the HPC and mPFC, supporting anatomical evidence suggesting that the Re is a vital relay hub between HPC and mPFC.

1.3.4.4 The role of the nucleus reuniens in memory consolidation.

The dominant view of declarative memory consolidation is an initial labile memory representation is transferred from the HPC, where it is formed, to neocortical areas (in

particular the mPFC (Takashima *et al.*, 2006; Gais *et al.*, 2007)) where it is integrated into a network of pre-existing long term memories. This is thought to occur during sleep, with SWS underlying the reorganisation of engrams and rapid eye movement (REM) sleep acting to stabilise memories at the level of the synapse (Diekelmann & Born, 2010). During SWS, neocortical slow oscillations (<1Hz), TC spindles (7-14 Hz) and hippocampal sharp wave ripples (140-200 Hz) are thought to provide the temporal frame-work for information transfer between the HPC and neocortical areas (Sirota *et al.*, 2003; Marshall & Born, 2007). Sharp wave ripples provide the temporal frame-work for the re-activation of the hippocampal neuronal populations which were active during the acquisition of a memory while awake (Wilson & McNaughton, 1994; Nádasdy *et al.*, 1999). Both TC spindles and sharp wave ripples increase during the up-state and decrease during the down-state of the neocortical slow oscillation (Mölle *et al.*, 2002; Isomura *et al.*, 2006), suggesting that the neocortex controls transfer of information from the HPC to neocortex in a feed-forward manner. For full review see Diekelmann & Born, (2010).

Given the hippo-thalamo-cortical circuits involved in memory consolidation, it has been suggested that the Re may play a role in memory consolidation on the basis of its connectivity (Pereira de Vasconcelos & Cassel, 2015). In support of this Loureiro *et al*, (2012) described a complete lack of recall following 25 days post-acquisition in a MWM task with no initial deficit in memory acquisition following excitotoxic lesions of the Re. To my knowledge, this is the only study which has endeavoured to test the effect of Re inactivation/lesion on memory consolidation. Interestingly, however, a study has implicated the HPC-Re-mPFC circuit in memory specificity and generalisation. Xu & Südhof (2013) trained mice to respond to a tone/footshock pairing in a conditioning chamber before testing in a similar but slightly altered chamber to measure fear memory generalisation. They found that inactivation of mPFC input to Re, suppression of the activity of Re neurons using tetanus toxin, or phasic 30 Hz optogenetic stimulation of Re neurons significantly increased freezing in a slightly altered context suggesting an upregulation of fear memory generalisation. Conversely, upregulation of Re activity using neuroligin-2 knockdown or tonic optogenetic stimulation of Re neurons at 4 Hz increased memory specificity. Although not directly measuring memory consolidation, if the Re plays a role in the specificity of an encoded memory engram resultant of its input from the mPFC, it would follow that the Re plays

a role in the consolidation of memories at a systems level. This seems especially likely when considered alongside the strong evidence for a role of a hippothalamocortical network in memory consolidation (Sirota *et al.*, 2003; Marshall & Born, 2007).

1.3.5 The role of the nucleus reuniens in disease.

The previous section highlighted experimental interventions to alter the integrity/function of the Re to address its function in physiologically "normal" animals. Although providing useful information, these experiments are best considered within the context of neurological disorders in which the Re is implicated. For self-explanatory reasons conducting experiments involving experimental manipulation of the Re in humans to evaluate its role in disease is considered unethical. Thus to tease out the role the Re plays in human neurological disorders, one must first look to clinical presentations in which the Re, as a matter of happenstance, is selectively compromised. Alternatively one looks to animal models designed to imitate human neurological disorders (the efficacy of which will be discussed in chapter 7). This section reviews the growing evidence implicating the Re in a number of neurological disorders.

1.3.5.1 Role of the nucleus reuniens in dementia.

The Re area is selectively compromised in Korsakoff's syndrome (amnesic-confabulatory syndrome), a form of dementia resulting from thiamine (vitamin B1) deficiency, usually arising from alcoholism or malnutrition (Mair *et al.*, 1979), resulting in anterograde and retrograde amnesia similar to that seen following HPC lesion. Infarcts which result in damage to the anterior or medial thalamus cause similar deficits (von Cramon *et al.*, 1985; Graff-Radford *et al.*, 1990). Notably small infarcts affecting the Re can lead to deficits in declarative memory and executive function (Carlesimo *et al.*, 2011), supporting studies carried out in animal models (see section 1.3.4). A caveat to studies involving thalamic infarcts is that they very rarely affect just one specific thalamic nucleus which complicates interpretation of results.

The Re exhibits pathological changes in late stages of AD (Braak stage V-VI). The study of post-mortem AD brains reveals that, although amyloid plaques do not develop in the Re, it does exhibit a robust neurofibrillary pathology (Braak & Braak, 1991). There is also evidence for a regionally specific atrophy in the medial thalamus, which

includes the Re, in AD patients (Zarei *et al.*, 2010). The integrity of the fornix is also compromised in AD while lesions of the anterior thalamic radiation have been observed in MCI patients (Torso *et al.*, 2015). Thus the extent to which the Re can communicate within the context of a HPC-Re-mPFC may contribute to cognitive dysfunction in dementia.

1.3.5.2 Role of the nucleus reuniens in schizophrenia

There is some evidence that the Re may be involved in the neural network dysfunction in schizophrenia (SZ). Working memory deficits are observed in SZ patients, while HPC-PFC interactions and synchrony are altered in SZ patients (Henseler *et al.*, 2010; Rasetti *et al.*, 2011) and mouse models of SZ (Sigurdsson *et al.*, 2010) respectively. Delta oscillations are elevated in SZ patients (Clementz *et al.*, 1994) while administration of ketamine and phencyclidine (PCP), which produce symptoms which model both positive and negative symptoms of SZ (Javitt, 2007), also produce TC delta oscillations (Miyasaka & Domino, 1968; Buzsáki, 1991). Interestingly local infusion of ketamine into the Re produces local delta oscillations (Zhang *et al.*, 2012; Duan *et al.*, 2015) and these oscillations are subsequently transposed onto the HPC (Zhang *et al.*, 2012). Interestingly, using optogenetic methods to mimic delta bursts in Re neurons causes deficits in working memory (Duan *et al.*, 2015) suggesting abnormal delta activity in the Re may play a causative role in working memory deficits observed in SZ patients.

1.3.5.3 Role of the nucleus reuniens in epilepsy

Several mouse models of epilepsy indicate that the Re is involved in facilitating seizure activity. Following initiation of seizure activity with hippocampal stimulation, the midline thalamus is activated from the first stimulation and mirrors hippocampal fast spike activity throughout ictal events, ultimately resulting in significant levels of neuronal death in the Re (Bertram *et al.*, 2001). Similarly in a kainic acid induced model of temporal lobe epilepsy, the number of CR-positive Re afferents projecting to the HF and entorhinal cortex is reduced (Drexel *et al.*, 2011). In a pilocarpine model of epilepsy, the inactivation curve of the $Ca_V3.2$ channels in the Re shifts 10 mV more depolarised leading to increased rates of burst firing (Graef *et al.*, 2009) and is mirrored by a reduction in zincergic terminals (Zn^{2+} being a endogenous modulator of Ca_v 3.2 activity (Traboulsie *et al.*, 2007)) terminating in the Re (Hamani *et al.*, 2005). It is well documented that patients who suffer unprovoked seizures are more likely to

experience subsequent seizures (Hauser *et al.*, 1990, 1998). The changes to Re inputs and cellular function following chronic seizure activity may contribute to a reduction in the seizure threshold. In support of this, excess excitation of the Re, through local injection of either NMDA (Hirayasu & Wada, 1992) or KCl (Luna-Munguia *et al.*, 2017), reduces seizure threshold in hippocampal kindling or pilocarpine models of epilepsy, respectively.

1.4 The effects of physiological aging on the brain.

The decline of cognitive abilities with normal physiological aging is well documented in the scientific literature (Harada *et al.*, 2013). As aging is also the primary risk factor in disorders characterised by cognitive decline (e.g. major neurocognitive disorders, discussed below), understanding "normal" cognitive changes associated with physiological aging is very important to aid in differentiating such changes from those observed in disease. This section will focus on two key changes in the CNS observed with physiological aging, namely changes in the volume and connectivity of brain regions important in memory formation and intrinsic electrophysiological changes observed in such structures.

1.4.1 Regional decline in brain volume with physiological aging

Declines in both grey and white matter are observed along the human lifespan from early adulthood (Svennerholm *et al.*, 1997), with the rate of decline increasing over the age of 70 (Scahill *et al.*, 2003). Longitudinal studies suggest that this shrinking of the brain is not uniform (Scahill *et al.*, 2003), however, for logistical reasons cross-sectional studies have been the primary source of information on differential rates of atrophy across brain regions. A review of five such studies identified the prefrontal cortex as the area most atrophied with physiological aging (Raz, 2004) while other studies identify the HPC as the most affected site (Jernigan *et al.*, 2001). Declines in prefrontal white matter volume have been consistently reported with physiological aging (Gunning-Dixon *et al.*, 2009) along with a loss of integrity of the fornix (the main output of the HPC, (Douet & Chang, 2014)). Disruptions are observed with HPC-mPFC synchrony suggesting that the disconnection of these brain regions may underpin cognitive decline (Mander *et al.*, 2013). Notably in support of this, specific age-related changes in the volume and connectivity of the medial thalamus (which contains the Re) have been observed (Ota *et al.*, 2007; Hughes *et al.*, 2012).

1.4.2 Changes in intrinsic excitability with physiological aging

In essence, "the calcium hypothesis of brain aging" states that the homeostasis of cytosolic free Ca^{2+} is changed with physiological aging, be that though changes in volume transmission across the neuronal membrane (Ca^{2+} ion channels), changes to

intracellular buffering of Ca^{2+} or indeed the mechanisms of Ca^{2+} release from intracellular stores (Gibson & Peterson, 1987; Landfield, 1987; Disterhoft *et al.*, 1994; Khachaturian, 1994). This hypothesis was largely based on evidence suggesting that CA1 pyramidal neurons were hypoexcitable as a result of an increase the post-burst refractory period, stemming from an increase in the amplitude of post-burst medium and long AHPs (Landfield & Pitler, 1984; Kumar & Foster, 2007; Matthews *et al.*, 2009; Gant & Thibault, 2009).

Post-burst AHPs are a result of Ca^{2+} influx into neurons, which in turn acts either through Ca^{2+} activated K^+ channels (mAHP, (Maylie *et al.*, 2004)) or via Ca^{2+}-dependant signalling cascades (sAHP, (Andrade *et al.*, 2012)). The amplitude of a post-burst AHP depends on the number of APs in a burst (Landfield & Pitler, 1984), and as such the amount of Ca^{2+} influx across the neuronal membrane. This increase in Ca^{2+} is thought to arise from an increase in Ca^{2+} flux through L-type Ca^{2+} channels during the AP in aged animals (Thibault & Landfield, 1996; Thibault *et al.*, 2001) along with an increase in the Ca^{2+}-mediated Ca^{2+} release from intracellular stores (Gant *et al.*, 2006).

Notably the post-burst AHP and resultant accommodation of subsequent APs in CA1 pyramidal neurons is reduced following learning in an eye blink conditioning paradigm (Moyer *et al.*, 1996). Meanwhile pharmacological interventions which rescue age-related cognitive deficits in rabbits also reliably reduce the size of the post-burst AHP and increase the excitability of CA1 pyramidal neurons suggesting that the hypoexcitability described above represents a single cell correlate of aging related cognitive deficits (Disterhoft & Oh, 2006). Supporting this the AP threshold of CA1 pyramidal neurons is more depolarised in aged rodents (Randall *et al.*, 2012).

However the intrinsic changes in neuronal excitability following aging appear to be regionally specific. CA3 pyramidal neurons are hyperexcitable in aged rats, a result of an increase in the repolarisation phase of single APs (Simkin *et al.*, 2015). Hyperexcitability is also observed in layer 2/3 mPFC pyramidal neurons in aged rhesus monkeys, with these changes correlating to performance on cognitive tasks (Chang *et al.*, 2005).

1.5 Major Neurocognitive Disorders.

Major neurocognitive disorders, more commonly known as dementia, refers to a clinical syndrome which most commonly presents in elderly patients. It involves loss of function in one or more cognitive domains of sufficient severity to interfere with social or occupational functioning (Kandel *et al.*, 2000; American Psychiatric Association, 2013). This section will review the two most common forms of dementia with a focus on associated symptoms, disease pathology, current treatments and underlying genetic underpinnings of familial forms of the disease. Finally we will review genetically engineered mouse models which seek to mimic aspects of pathology for use in basic scientific research.

1.5.1 Alzheimer's Disease.

AD is the most common form of dementia in the elderly. Globally it affects ~3% of people between the ages of 70-74 years old and ~25% of people over the age of 85 years old (Ferri *et al.*, 2005) with an estimated prevalence of ~40 million people worldwide (Selkoe & Hardy, 2016). Late onset AD is idiopathic and accounts for the majority of AD cases, with typical age of symptomatic onset between 65-70 years old. Early onset (<65 years old) or familial AD (FAD) account for a small percentage (~4-8 %) of cases and is caused by genetic mutations.

AD is a prototypical neurodegenerative disease, selectively compromising the viability of neurons in particular brain regions including the neocortex, the entorhinal area, the HPC, and nuclei of the limbic thalamus (Kandel *et al.*, 2000). The most prominent clinical outcome of this widespread neuronal death is the progressive dissolution of cognitive function which is associated with two main pathological features, namely the build-up of extracellular plaques comprised of beta-amyloid (Aβ) peptides and intracellular neurofibrillary tangles (NFT) comprised of hyperphosphorylated microtubule associated tau protein (MAPT) (Querfurth & LaFerla, 2010). Notably synaptic loss observed in AD patients correlates better with functional impairments than either plaques or tangles (Perl, 2010), while neuroinflammatory responses, long thought to arise secondary to neurodegeneration, may contribute significantly to AD pathology (for review see (Heneka *et al.*, 2010)).

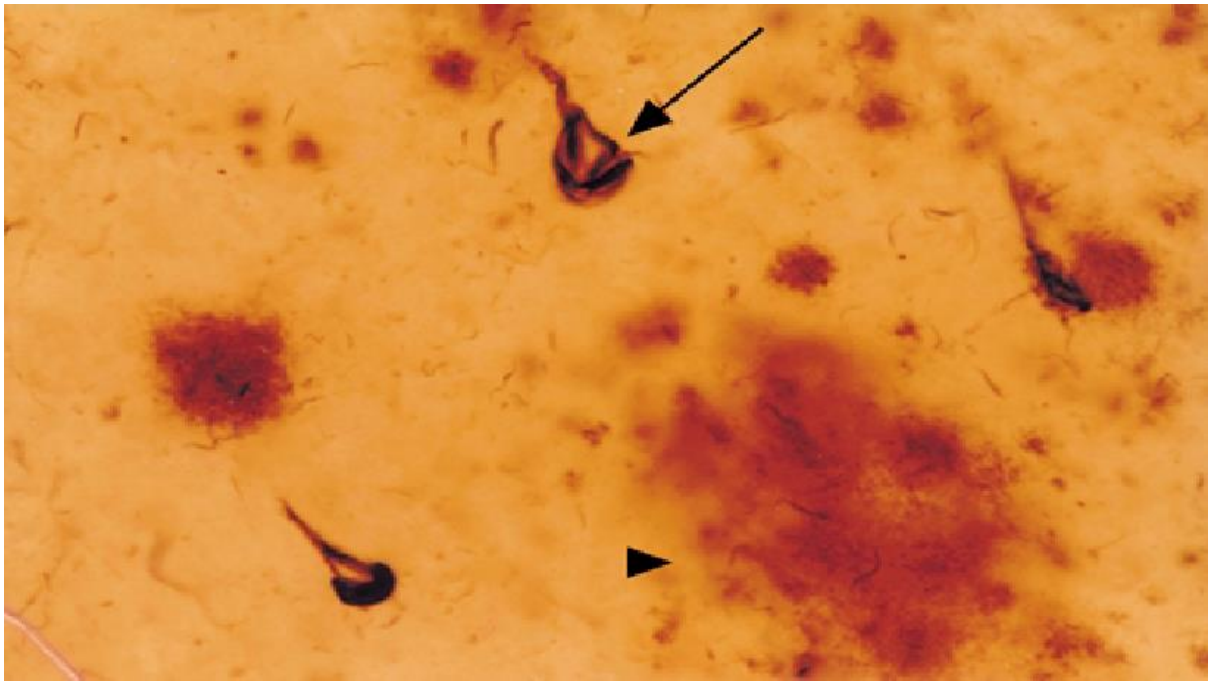

Figure 1.8. Alzheimer's disease neuropathology. Photomicrograph of a cortical section from an AD patient showing plaques and tangles. Plaques (arrowhead) are stained with an antibody specifically targeting β-amyloid. Tangles (arrow) are stained with an antibody specifically targeting helical filaments. (Nowotny et al., 2001).

1.5.1.1 Amyloid hypothesis of Alzheimer's disease

Aβ is the main constituent of amyloid plaques. It is formed following the proteolytic cleavage of amyloid precursor protein (APP) by β-secretase and γ-secretase as displayed in Figure 1.9 (LaFerla & Oddo, 2005). The two main species of Aβ produced by this sequential cleavage are $A\beta_{40}$ and $A\beta_{42}$, with $A\beta_{42}$ considered the more toxic as a result of its higher hydrophobicity which underlies a proclivity to aggregate (Walsh & Selkoe, 2004). Evidence has shown that this aggregation underpins Aβ toxicity, with soluble Aβ oligomers being the most toxic species (Walsh & Selkoe, 2004). Notably several longer species of Aβ including $A\beta_{43}$, $A\beta_{45}$, $A\beta_{48}$ and $A\beta_{49}$, which are precursors to $A\beta_{40}$ ($A\beta_{49} \rightarrow A\beta_{46} \rightarrow A\beta_{43} \rightarrow A\beta_{40}$) and $A\beta_{42}$ ($A\beta_{48} \rightarrow A\beta_{45} \rightarrow A\beta_{42}$) during sequential cleavage of C99 by γ-secretase (Takami *et al.*, 2009), have been described in the brains of AD patients (Miravalle *et al.*, 2005). These longer species of Aβ are often ignored despite research revealing that $A\beta_{43}$ (and potentially others) can confer AD like pathology in mice (Saito *et al.*, 2011).

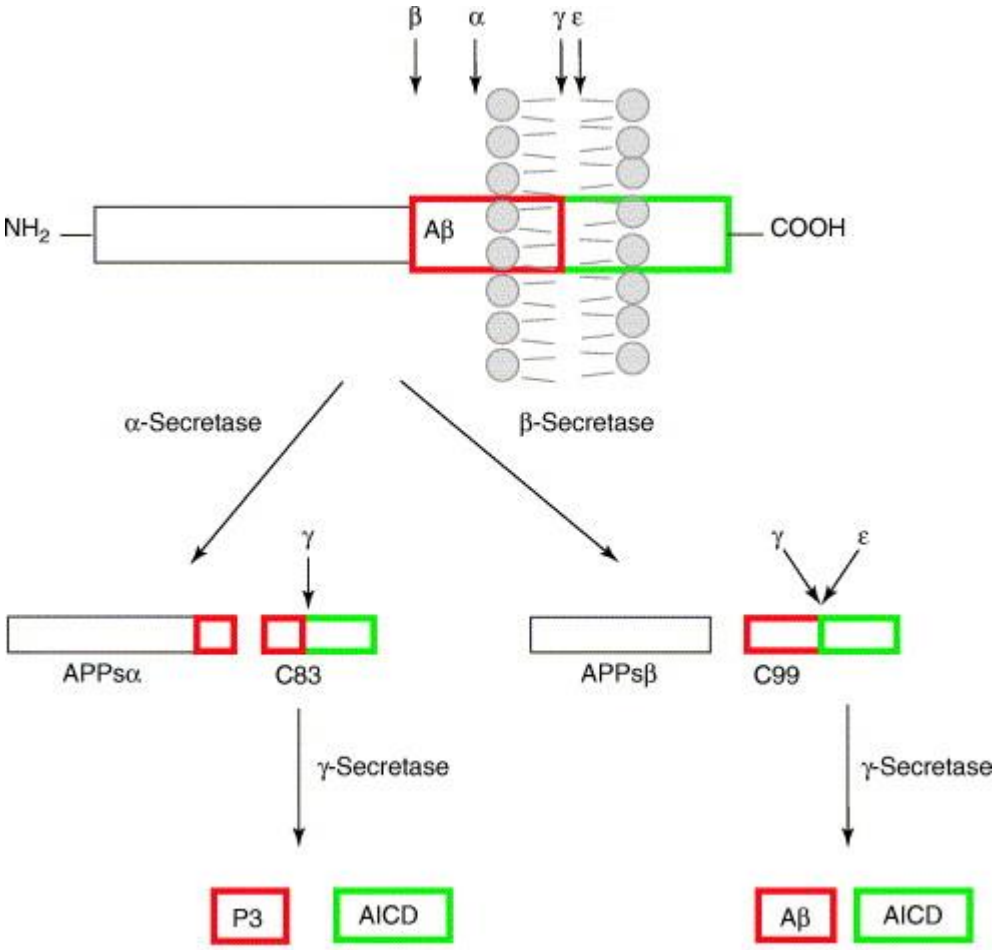

Figure 1.9. The APP processing pathway. Transmembrane protein APP undergoes initial cleavage by either α-secretase (non-amyloidogenic pathway) or β-secretase (amyloidogenic pathway). Cleavage of APP by α-secretase occurs within the Aβ domain (red), releasing a large intracellular N-terminal portion of APP (APPsα) and an 83 amino acid C-terminal fragment (C83). C83 undergoes subsequent cleavage by γ-secretase protease to produce a P3 fragment and a C-terminal fragment of APP known as the APP intracellular domain (AICD, green). Cleavage of APP by β-secretase occurs at the N-terminal region of the Aβ sequence releasing a shorter N-terminus APPsβ fragment and a longer C-terminal fragment (C99). Subsequent cleavage of C99 by γ-secretase produces AICD and Aβ. Taken from (LaFerla & Oddo, 2005).

Suggestions that Aβ dyshomeostatis plays a key role in the initiation of AD (the amyloid hypothesis) has been around for over 25 years (Selkoe & Hardy, 2016). Since then substantial evidence has accumulated supporting the hypothesis: 1) All AD patients undergo progressive Aβ accumulation in key memory centres of the brain; 2) Mutations in and around the Aβ region of the APP gene, and mutation in presenilin 1 or 2 (the catalytic subunit of γ-secretase) cause familial AD; 3) Humans with trisomy

21 invariably develop AD like pathology (APP is located on chromosome 21); 4) ApoE4 the main genetic risk factor for sporadic AD decreases the clearance of Aβ resulting in increased aggregation; 5) $A\beta_{42}$ oligomers isolated from AD brains impair long-term potentiation (LTP), cause synaptic loss in the rodent HPC and cause memory deficits when injected intraventricularly; 6) $A\beta_{42}$ oligomers isolated from AD brains induce tau hyperphosphorylation in cultured rodent neurons; 7) Synapse loss is greatest in the proximity of amyloid plaques; 8) CSF $A\beta_{42}$ is detectable years before other AD-related changes including increased CSF tau, decreased cerebral glucose metabolism, brain atrophy and dementia; and 9) mice expressing mutated forms of both human APP and human tau increases tau deposition without altering Aβ deposition (Selkoe & Hardy, 2016).

Despite this the significant body of evidence supporting the amyloid hypothesis, there is still considerable controversy regarding its legitimacy based on findings which appear to contradict the hypothesis. One such contradiction is that transgenic mice overexpressing human APP do not subsequently develop tau pathology, however recent evidence suggests that human Aβ overexpression requires the simultaneous expression of all 6 human tau isoforms to induce tau pathology in rodents (Cohen *et al.*, 2013). Another contradiction, the supposed “Achilles heel” of the amyloid hypothesis, is the significant plaque pathology often observed with normal physiological aging in the absence of dementia (Selkoe & Hardy, 2016). However amyloid plaques in AD patients appear to contain a much higher concentration of soluble oligomers than in non-demented pathological controls (Esparza *et al.*, 2013). Finally none of the phase 3 clinical trials targeting Aβ in AD patients have reached statistical significance on pre-specified clinical endpoints although the Aβ human monoclonal antibody Aducanumab has had promising results in a phase 1b clinical trial and is currently undergoing phase 3 studies (Selkoe & Hardy, 2016).

1.5.1.2 Microtubule associated tau protein

As discussed NFTs are one of main pathological features of AD, however, they are also observed in other forms of dementia in the absence of a robust amyloid pathology. These disorders are collectively termed tauopathies, and include frontotemporal dementia, Pick’s disease, corticobasal degeneration and progressive supranuclear palsy (Iqbal *et al.*, 2005).

Microtubules form part of the neuronal cytoskeleton, functioning as a scaffold protein that plays key roles in developing and maintaining neuronal processes (Kandel *et al.*, 2000), while also providing a "track" on which molecular motors (dyneins) can transport vital cargo through the cytoplasm (Vale, 2003).

MAPT promotes the assembly and stability of axonal microtubules (Avila *et al.*, 2004). Due to biological redundancy, MAPT gene knock-out does not affect viability (Harada *et al.*, 1994), however hyperphosphorylation of MAPT, as seen in AD and other associated tauopathies, causes disassociation of MAPT from microtubules preventing their stable assembly (Lindwall & Cole, 1984; Alonso *et al.*, 1994). Subsequent to this MAPT appears available to accumulate to form NFTs or helical filaments (Avila *et al.*, 2004). These accumulations of abnormally hyperphosphorylated MAPT correlate with the duration and severity of dementia (Arriagada *et al.*, 1992; Gómez-Isla *et al.*, 1997) and with synaptic dysfunction and neuronal degeneration (Lasagna-Reeves *et al.*, 2011). While the mechanism through which MAPT contributes to pathology is still unclear, given the vital cellular functions microtubules play within a neuron, it is not hard to imagine any loss of function/toxic gain of function producing a reduction in cellular viability. Conversely it has been suggested that NFT-bearing neurons can survive for up to 20 years in AD patients (Morsch *et al.*, 1999) while the majority of degenerating neurons in AD do not present with tangle pathology (Gómez-Isla *et al.*, 1997; Andorfer *et al.*, 2005). Evidence has suggested that soluble forms of hyperphosphorylated MAPT, rather than NFTs themselves are the primary contributor to pathology (SantaCruz *et al.*, 2005; Spires *et al.*, 2006) suggesting that NFTs may even play a neuroprotective role. Whatever the mechanism through which MAPT contributes to AD pathology, the fact Aβ toxicity depends on physiological levels of endogenous tau (Roberson *et al.*, 2007) and the wide range of dementias which exhibit tau pathology clearly suggest it plays a significant role in AD pathology.

1.5.2 Frontotemporal Dementia.

FTD is a grouping term for a clinically and pathologically diverse group of non-AD dementias characterised by relatively selective atrophy of the frontal and anterior temporal lobes. After AD, it is the second most common variant of dementia, affecting 10 – 30 people per 100,000 between the ages of 45 – 60 years old (Sieben *et al.*,

2012). FTD can be subdivided based on the primary clinical symptom patients present with. Behavioural variant FTD (bvFTD) accounts for up to two thirds of cases and patients present with profound changes to behaviour and personality including disinhibition, apathy, and loss of empathy (Neary *et al.*, 1998). Primary progressive aphasia (PPA), where patients present with language difficulties, accounts for the remaining FTD population. PPA can be further subdivided into nonfluent/agrammatic PPA, semantic variant PPA and logopenic variant PPA based on the specific speech and language features characteristic of each subtype (Gorno-Tempini *et al.*, 2011). Notably there is a large clinical overlap between sufferers of FTD and amyotrophic lateral sclerosis (ALS). Up to 50% of patients suffering with ALS exhibit mild cognitive decline (in particular executive function) with up to 12.5% meeting the criteria for concurrent FTD diagnosis (Ringholz *et al.*, 2005) while up to 40% of FTD patients display some degree of motor dysfunction with 15% also meeting the diagnostic criteria for ALS (Burrell *et al.*, 2011).

A significant proportion of FTD patients have a contributory family history including 45% of bvFTD patients, increasing to 59% with concurrent diagnoses of FTD and ALS (Goldman *et al.*, 2005). MAPT was the first reported genetic cause of FTD (Hutton *et al.*, 1998). Subsequently 6 other genes have been identified that, when mutated, cause FTD. These include *C9orf72*, CHMP2B, FUS, GRN, TARDBP, and VCP (Cruts *et al.*, 2012). The relative frequencies reported in FTD populations varies significantly between studies however, in general, MAPT, GRN and *C9orf72* are considered most common while TARDBP, VCP, FUS and CHMP2B are considered rare (Sieben *et al.*, 2012).

FTD populations can also be subcategorised based on the pathology present. One such category is FTD exhibiting NFT pathology in neurons and glial cells, resultant of the abnormal accumulation of MAPT. The second, most common, form of FTD is associated with ubiquitin-positive inclusions (McKhann *et al.*, 2001). The pathological protein constituting these inclusions has been identified as either TDP-43 (Neumann *et al.*, 2006) or FUS (Neumann *et al.*, 2009). Virtually all cases of FTD can be categorised based on inclusions exhibiting immunoreactivity for MAPT (FTD-tau), TDP-43 (FTD-TDP), or FUS (FTD-FUS) however in rare cases where the disorder is caused by CHMP2B mutations, ubiquitin positive inclusions which are not

immunoreactive for either TDP-43 or FUS are present leading to a classification of FTD-UPS (Mackenzie *et al.*, 2010).

1.5.3 Mouse models of dementia.

One use of transgenic models of dementia is to model specific aspects of disease pathology. This is necessitated by certain limitations which are inherent to human studies for a number of ethical and pragmatic reasons. These include a limited spatial and temporal resolution possible while ethically recording human brain activity and the difficulty in recruiting subjects for well powered studies. Working in mouse models in diseases of aging is an attractive alternative because of the large overlap (>99%) between the human and mouse genome (Chinwalla *et al.*, 2002) along with their short relatively short lifespan (2-3 years) and possibilities of genetically manipulating their genomes (Vanhooren & Libert, 2013).

Transgenic models of AD can be generally categorised into two groups based on the aspect of AD pathology they model. Models of amyloidopathy generally overexpress mutated versions of genes associated with FAD, namely APP, Presenilin 1 or 2 (PS1/2). Far too many models have been produced to name, with many of these expressing more than one mutation found in FAD in an attempt to hasten the increase of $A\beta^{42}$ load in the brain. The extent to which these models have contributed to our understanding of amyloid pathology is comprehensively reviewed at (McGowan *et al.*, 2006; Randall *et al.*, 2010). Widely used strains of such models display a robust plaque pathology and associated cognitive deficits, however, NFT pathology or the widespread neurodegeneration associated with AD are not observed (McGowan *et al.*, 2006). Notably recent evidence from mutated stem cell lines suggests that the lack of MAPT pathology observed in such models is a consequence of mice lacking two isoforms of the human MAPT protein (Muratore *et al.*, 2014; Moore *et al.*, 2015).

Conversely models of tauopathy (a form of FTD), which express mutated forms of MAPT, model the robust NFT pathology and progressive neurodegeneration associated with both AD and FTD. Due to the historic interest in the role of MAPT in neurodegenerative diseases, far more transgenic models expressing MAPT encoding gene mutations have been generated than other familial FTD associated mutations. These models have displayed great utility in helping us understand the pathophysiology of tauopathies, as discussed in (Götz *et al.*, 2007; Roberson, 2012).

In recent years mouse models expressing mutations in TARDBP (Wils *et al.*, 2010; Xu *et al.*, 2010), VCP (Custer *et al.*, 2010), and CHMP2B (Ghazi-Noori *et al.*, 2012; Gascon *et al.*, 2014; Vernay *et al.*, 2016) have been developed which appear to mimic important pathological and behavioural features of their relative FTD presentation.

1.5.3.1 Alterations in the intrinsic neurophysiological properties in mouse models of amyloidopathy.

Over the past 15 years, many studies have reported changes in synaptic and neural network neurophysiology in mouse models of amyloidopathy (Randall *et al.*, 2010). More recently there has been an increase in the interest in alterations of the intrinsic electrophysiological properties in HPC and cerebrocortical neurons. Some such studies have reported no changes to these properties (e.g. no changes to excitability in HPC interneurons in 7 month TASTPM mice (Spencer *et al.*, 2006) or in layer 2/3 pyramidal neurons in the frontal cortex (Rocher *et al.*, 2008)). However the majority of studies have found differences in important cellular neurophysiology following a more in-depth analysis of the multitude of intrinsic neuronal parameters across different age ranges, brain region and model of amyloidopathy. There have been reports that the RMP is more depolarised in layer 2/3 pyramidal cortical neurons in 3.5 month APdE9 mice (Minkeviciene *et al.*, 2009) and layer 2/3 PV positive interneurons in the parietal cortex in 4-7 month old J20 mice (Verret *et al.*, 2012), however no changes to RMP is observed in CA1 pyramidal neurons in 8-10 month old PSAPP or PDAPP (9-10 or 20-23 month old) mice (Brown *et al.*, 2011; Kerrigan *et al.*, 2014; Tamagnini *et al.*, 2015). Notably alterations to the afterspike potential, spike frequency output in response to prolonged depolarising current injections and AP waveform properties have been reported in CA1 pyramidal neurons in these same studies. AP width in particular seems to be reliably decreased by approximately 10-15% in response to depolarising current injections in CA1 pyramidal neurons (Brown *et al.*, 2011; Kerrigan *et al.*, 2014; Tamagnini *et al.*, 2015), even before a significant plaque pathology is present (CRND8 mice, 1-2 months old) (Wykes *et al.*, 2012).

1.6 Aims

The Re plays a key role in cognitive processes as a relay in a memory circuit involving the HPC and mPFC. However, very little is understood about cellular level neurophysiological properties of Re neurons. This study seeks to characterise, for the first time, the intrinsic properties of rostral Re neurons in young adult male mice *in vitro* using the whole cell patch clamp technique.

Following the establishment of this baseline condition, this study will seek to characterise these properties following physiological aging, where memory and HPC-mPFC synchrony is disrupted. Finally this study will characterise these properties in mouse models of dementia, where measurable deficits are observed in cognition and executive function. Models studied include a model of amyloidopathy (J20 mice) and FTD ($CHMP2B_{intron5}$ mice).

Overall this study seeks to significantly contribute to the field of thalamic cellular neurophysiology as well as potentially identifying novel cellular level dysfunctions underlying cognitive deficits in mice.

2 Materials and Methods

2.1 Ethical approval and animals

All studies detailed in this work were approved by the University of Exeter Animal Welfare Ethical Review board. Animals were sacrificed by cervical dislocation in accordance with schedule 1 of the Animals (Scientific Procedures) Act 1986 and its subsequent amendment to align with European Directive 2010/63/EU on the protection of animals used for scientific purposes. All studies described utilise tissue obtained from adult male mice, kept on a 12:12 light/dark cycle and granted *ab libitum* access to food and water. All experiments and analysis described throughout this work were performed with no blinding. Details of the strain and age of mice will be described in individual methods summaries.

2.2 Slice preparation

Cervical dislocation of mice was typically performed approximately 4 hours into the light cycle of the animal. The animal's brain was rapidly excised and transferred to an ice cold oxygenated sucrose solution consisting of (in mM): 189 Sucrose, 10 D-Glucose, 26 $NaHCO_3$, 3 KCl, 5 $Mg_2SO_4(7H_2O)$, 0.1 $CaCl_2$, 1.25 NaH_2PO_4. The brain was promptly sliced into 300 µm coronal sections using a Leica VT1200 vibratome. Only a single 300 µm section containing the rostral Re could be obtained per mouse, a result of the Re's relatively small size in comparison to more widely studied brain structures. This section was subsequently transferred to a holding chamber containing artificial cerebrospinal fluid (aCSF) perfused with a continuous flow of carbogen (95% 0_2, 5% CO_2). The composition of the aCSF was (in mM): 124 NaCl, 3 KCl, 26 $NaHCO_3$, 2 $CaCl_2$, 1.25 NaH_2PO_4, 1 $MgSO_4$, 10 D-glucose. Prior to all experiments the slice was allowed to recover at room temperature for at least 1 hour prior. Following recovery it was transferred to a recording chamber secured on the stage of an Olympus BX51 upright microscope.

2.3 Visual identification of neurons in the rostral nucleus reuniens

As discussed in section 1.2, individual thalamic nuclei cannot be readily distinguished visually. Thus the Paxinos and Franklin brain atlas (Paxinos & Franklin, 2001) was used to identify the location of the rostral Re, ~Bregma - (0.5 – 0.8 mm). Several brain structures whose shape and location are dependent on their position along the rostral-caudal axis in a coronal brain slice preparation were used to facilitate identification of an appropriate coronal section. The fornix, a dense tract of white matter, is easily identifiable on a coronal brain slice and within a slice containing the rostral Re it is at the same level or slightly ventral (~0.1 mm) to the dorsal tip of the 3rd ventricle along the dorsal-ventral axis. The 3rd ventricle itself also has a specific morphological signature within brain slices containing rostral Re. It appears ~0.15 mm dorsal to the ventral edge of the slice and extends ~1-1.3 mm dorsally (Figure 2.1).

Neurons in the rostral Re were visualised using infra-red differential interference contrast optics using a CMOS USB 2.0 camera (Thor labs) with a 40X objective lens. Neurons were identified as laying within the rostral Re based on their X,Y coordinates versus the dorsal tip of the 3rd ventricle. In order for these X,Y coordinates to accurately represent their position in the brain slice, care was taken to align the ventral end of the brain slice parallel to the edge of the recording chamber. The coordinates used relative to the tip of the 3rd ventricle were ±0.075-0.375 mm on the X axis and 0.1-0.6 mm on the Y axis (Figure 2.1). As the rostral Re has varying levels of lateral expansion within a 300 µm section (Figure 2.1), these coordinates were selected to ensure that selected neurons would be located within the confines of the rostral Re regardless of their position on the Z axis of the coronal section. In practice this means that neurons on the lateral edge of the rostral Re at the point of its greatest lateral expansion (~Bregma -0.58 mm) were not included in any studies. Neurons along the midline were also avoided as the xiphoid nucleus of the thalamus extends dorsally from the tip of the 3rd ventricle through the midline of the rostral Re in certain Z planes (Figure 2.1).

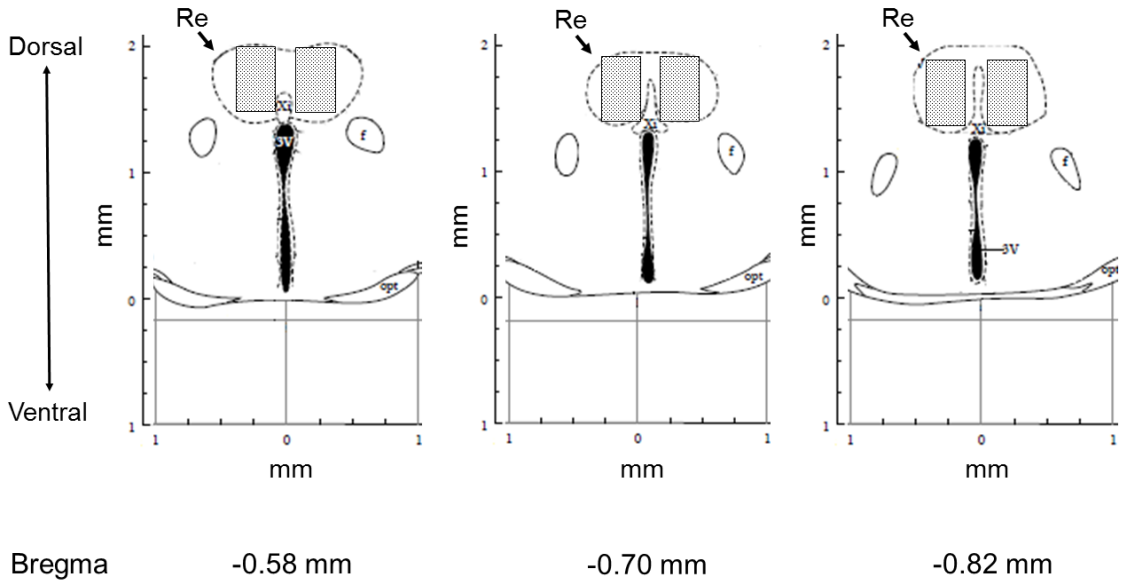

Figure 2.1. Recording position within the rostral Re. Each shaded box (0.3 x 0.5 mm) indicates the region of the rostral Re in which cells were selected to record from. Re, Nucleus Reuniens; f, fornix; opt, optic tract; Xi, Xiphoid nucleus of the thalamus; 3V, 3rd ventricle. Modified from (Paxinos & Franklin, 2001).

2.4 Electrophysiological recordings

2.4.1 Whole cell patch clamp

The recording chamber was continuously perfused with oxygenated aCSF (flow rate ~2 ml/min) and maintained at a temperature of 32-33 °C. All pharmacological agents mentioned in this work were introduced to the recording chamber via the perfusion system. With the express exception of pharmacological agents that were present in the recording chamber throughout the experimental day in order to form a background condition (highlighted in the relevant results section), we endeavoured to never perform experiments on a slice which had previously been treated with a pharmacological agent. The small size of the Re, meant that we could only obtain one brain slice per animal, thus limiting the number of pharmacology experiments to one per mouse.

Borosilicate glass microelectrodes (3-5 MΩ) were fabricated using a P-97 Flaming Brown micropipette puller (Sutter Instrument Co., CA, US) and on occasion fire polished using a Narishige microforge. The resultant microelectrodes were filled with one of the internal solutions detailed in table 2.1. Following entry intro whole cell

configuration, a liquid junction potential arose resultant of the pairing of external and internal solutions. This error was corrected for arithmetically during analysis. The recorded signal was amplified using a Multiclamp 700B amplifier, digitised with a Digidata 1440 and stored for future analysis using pClamp 10 software.

Table 2.1. Composition of internal solutions. Solutions were adjusted to have a pH of 7.3, using KOH or CsOH as appropriate, and to have an osmolarity between 285-290 mOsm.

	Concentration (in mM)		
	K-gluconate solution #1	K-gluconate solution #2	$CsMeSO_4$ solution
K-gluconate	130	140	-
$CsMeSO_4$	-	-	130
KCl	20	10	-
NaCl	-	-	20
HEPES	10	10	10
EGTA	0.2	0.2	0.2
Na-GTP	0.3	0.3	0.3
Mg-ATP	4	4	4
Liquid junction potential	15 mV	15 mV	17 mV

2.4.1.1 Current clamp recordings

Measures of passive membrane properties, excitability, AP waveform properties, and spike afterpotentials were made in the whole cell current clamp configuration by transiently injecting current waveforms of varying shape, amplitude and polarity. The bridge circuit of the amplifier was used to compensate for the access resistance,

allowing for faithful recording of the membrane voltage. All data were lowpass filtered at 10 kHz and digitised at 100 kHz.

Spontaneous activity at rest

V_m and mean spontaneous firing frequency were measured during a 1 minute long recording performed immediately following entry into current clamp mode. This recording was made without the injection of any bias current (Fig 2.2A).

Passive membrane properties

Other passive properties, i.e. R_i and τ, were measured using -20 pA, 500ms square-wave hyperpolarising current injection from a pre-set fixed membrane potential of -80 mV unless otherwise stated (Fig 2.2B). This fixed membrane potential was achieved via the injection of a suitable amount of bias current. Recording such passive membrane properties (which are necessarily voltage dependant) from a set membrane potential is vital given cell to cell variability in V_m.

Neuronal Excitability

Excitability was tested using a thorough battery of current injections from a set pre stimulus potential (either -80mV or -72 mV). This was necessary as a large proportion of Re neurons exhibit spontaneous tonic AP firing across age and genotype (See chapters 3-6). One such "standard" measure of excitability was to measure the number of APs generated in response to a series of incremental 500 ms depolarising square current injections, ranging from 10 – 60 pA (Fig 2.2B). The first AP generated by a Re neuron to the largest of this incremental series of current injections was used to quantify the waveform properties of the AP.

Another standard measure of excitability is the rheobase of a neuron, or the minimum amount of depolarising current required to elicit generation of an AP. Formally rheobase is measured from RMP however because of the significant proportion of Re neurons which generate spontaneous APs (see chapter 3), we measured an alternative form of rheobase by employing a series of 100 ms square depolarising current injections from a set membrane potential. These injections were increased in increments of 2 pA at a rate of 1 Hz until an AP was generated (Fig 2.2C).

These square wave current injections, although informative, are not particularly representative of how neurons are pushed towards AP generation *in vivo* and as such it can be useful to use current injections which more closely model synaptic inputs. Thus we employed protocols using a series of mock excitatory postsynaptic current (αEPSC) injections from a set pre-stimulus membrane potential to measure how physiological inputs may drive the generation of APs *in vivo*. Specifically a series of 4 αEPSC's of incrementally increasing amplitude and a decay time of 5ms (Fig 2.2D) and a series of three αEPSC's where the amplitude of the injected αEPSC remained constant but the decay time was varied in a 4 fold manner from 5-20 ms (Fig 2.2E).

AP Afterpotentials

In order to measure the amplitude of the afterpotential following a single evoked AP we injected a short, strong square current injection (1.3 ms, 2 nA) from a set prestimulus potential. To correlate the size of this afterpotential with AP firing patterns, we applied a longer 500 ms depolarising current step 1.5 s subsequent to the aforementioned short current pulse. To study the effect of pharmacological or electrophysiological stimuli on the amplitude of this afterpotential we employed an almost identical protocol, but alternated the longer pulse between a 500 ms depolarising step and a 500 ms hyperpolarising step at a rate of 0.1 Hz to allow measurement of the effect of the experimental variable on passive membrane properties as well as excitability (Fig 2.2F). For pharmacology experiments the drug was added to the aCSF after a stable 5 minute baseline of the dependant variable was recorded and the recording was followed for a further 15 minutes. To test if intrinsic firing patterns could alter the size of the ADP we employed a theta paced burst stimulus. This consisted of 75 bursts of five AP, elicited at an intraburst rate of 150 Hz, delivered with an interburst interval of 200 ms (Fig 2.2G). Again a 5 minute baseline was obtained and the recording was followed up for 15 minutes post conditioning stimulus.

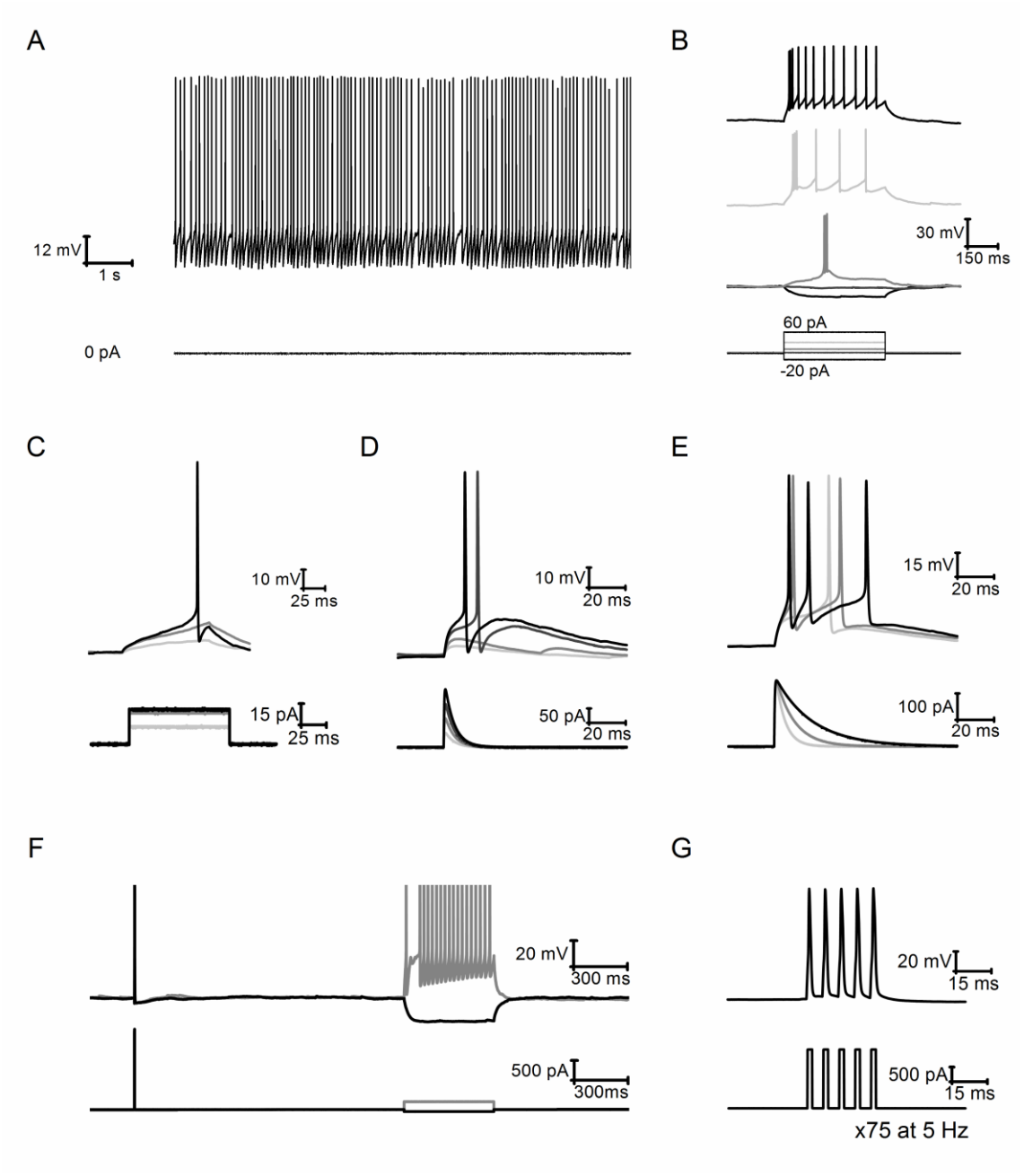

Figure 2.2. Example traces of current clamp protocols used in this work. (A) Excerpt from a 60 s long current clamp recording with no bias current injected. (B) 500 ms square depolarising current injections ranging from -20 pA to 60 pA in 10 pA increments as a measure of excitability. Example traces in response to -20, 0, 10, 30, and 60 pA current injections are displayed. (C) 100 ms square depolarising current injections increasing in 2 pA increments as a measure of rheobase. Example traces in response to half rheobase, rheobase – 2 pA, and rheobase current injections are displayed. (D) αEPSC current injections of incrementally increasing amplitude and a decay time of 5 ms as a measure of excitability.(E) αEPSC current injections of equal amplitude and an increasing decay time over a four-fold range of 5-20 ms as a measure of excitability. (F) Single spike protocol elicited by a short, large (1.3 ms, 2 nA) square current injection used to measure the AP afterpotential. This primary spike was followed 1.5 s later by alternating a 500 ms hyperpolarising and depolarising square current injection to record passive and excitability properties concurrently.

These sweeps were applied at a rate of 0.1 Hz. (G) Theta burst protocol consisting of 75 bursts of five AP, elicited at a rate of 150 Hz, delivered at 5Hz.

2.4.1.2 Voltage clamp recordings

The voltage clamp configuration was used to measure spontaneous synaptic currents, probe the existence of a hyperpolarisation activated current I_h, and measure t-type calcium channel currents. A neuron was considered suitable to record from if it had an access resistance of < 20 MΩ. All data were lowpass filtered at 3 kHz and digitised at 10 kHz.

Spontaneous synaptic currents

Spontaneous synaptic currents were recorded immediately following entry into whole cell configuration. The cell was held at a membrane potential of -85 mV and the current crossing the membrane was monitored for 1 minute.

I_h current

In order to probe for the existence of a hyperpolarisation activated current I_h we employed a series of incrementally growing 5 s hyperpolarising steps applied at a holding potential of -55 mV. The test potential varied from -60 to -125 mV in 5 mV increments. This was carried out in the absence of any voltage gated sodium or potassium channel blockers. No leak subtraction was used during this recording.

T-type Ca^{2+} channel currents.

To measure the current amplitude and activation kinetics of t-type calcium channels we employed a series of 100 ms depolarising steps from a holding potential of -85 mV. These steps ranged from -75 mV to -47 mV in 2 mV increments. To gather data on the steady state inactivation profile of these currents we employed a series of invariant 100 ms steps to -65 mV from a variety of holding potentials (-105 mV to -63 mV). Finally we profiled the recovery from steady state inactivation with a standard two pulse protocol. Each pulse consisted of a 100 ms step to -65 mV from a holding potential of -95 mV and the interpulse interval was varied from 51 ms to 1.7 s, increasing in a quarter log fashion. Leak currents were compensated for through the use of pre-pulses of opposing polarity to isolate the t-type calcium channel current.

2.5 Data analysis

Data were analysed using custom written MATLAB scripts unless otherwise stated. The data was extracted and subsequently processed using Microsoft Excel and Origin 9.0.

Statistical significance was ascertained using paired student's t test, linear regression analysis, Chi-Square test, unpaired student t test, independent sample Mann-Whitney U test, Kolmogorov-Smirnov test, Kruskal-Wallis one-way analysis of variance (ANOVA) and repeated measure two-way ANOVA using SPSS, as appropriate. All comparisons of means/medians of cellular populations utilised each Re cell recorded from as a discrete data point. To ensure that the variability observed within populations of cells accurately reflected variation within the Re, as opposed to inter-animal variability, the mean intra-animal and inter-animal coefficient of variance (CV) were calculated for the largest population of recordings in this thesis (Chapter 3). Across a range of intrinsic properties the intra-animal CV was consistently higher than the inter-animal CV (table 2.2) supporting the use of individual neurons versus individual animals as data points.

Table 2.2. Comparison of intra-animal and inter-animal coefficient of variance.

	Coefficient of Variance	
	Intra-animal	Inter-animal
Average V_m	9.7	8.2
R_i	30.2	18.3
τ	30.9	21.3
Capacitance	29.2	22.2
AP height	62.7	35.5
AP width	13.0	10.8
AP threshold	8.7	5.6
AP maximal dV/dt	22.4	12.9

Passive membrane properties

V_m was measured as the mean membrane voltage of a continuous 60 s current clamp recording. R_i was calculated utilising Ohm's law, measured as the mean voltage deflection calculated during the last 50 ms of the -20 pA hyperpolarising sweep divided by the amplitude of the negative current injection. τ was calculated using a single exponential curve fitted to the charging curve of the membrane between 20 and 80% of the peak amplitude of the voltage deflection. An approximation of capacitance was measured as the ratio of these two values, namely τ/R_i

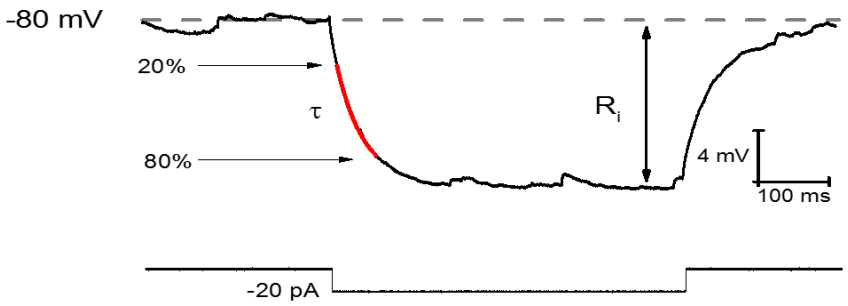

Figure 2.3. Calculation of passive membrane properties. Voltage trace in response to a 500 ms square hyperpolarising current injection. Highlighted is the voltage deflection used to calculate R_i and the charging curve of the membrane used to calculate τ.

Excitability and AP waveform

Excitability was measured as the total number of APs generated by a given depolarising current stimulus. For the standard 500 ms current step (Fig 2.2B) this was limited to APs falling within the time window of the given current stimulus. For rheobase and αEPSC current injections (Fig 2.2C-E), which are considerably shorter, excitability was defined as any AP which was generated prior to the membrane voltage returning back to baseline. This distinction is important given the ability of T-type calcium currents to activate and drive AP firing subsequent to the cessation of a given stimulus (will be discussed in greater detail in chapter 3). This was not a concern in the longer 500 ms measures of excitability given how readily T-type Ca^{2+} channels inactivate over a period of 100 ms. Spike latency was measured as the time taken to generate an AP subsequent to the onset of the current stimulus. Instantaneous frequency was measured on a spike by spike basis as the reciprocal of the inter spike interval.

As mentioned, the first AP generated in response to the 60 pA square current injection (Fig 2.2B) was used to measure AP waveform properties. AP peak was measured as the absolute voltage peak of the AP. AP threshold was defined as the voltage at which the first derivative of the membrane voltage (dV/dt) during the AP waveform exceeded 15 mV/ms. Maximal rate of rise (max dV/dt) was defined as the peak value of the first derivative during the AP waveform. AP width was measured as the width at half height of the AP, where height was defined as AP peak minus AP threshold.

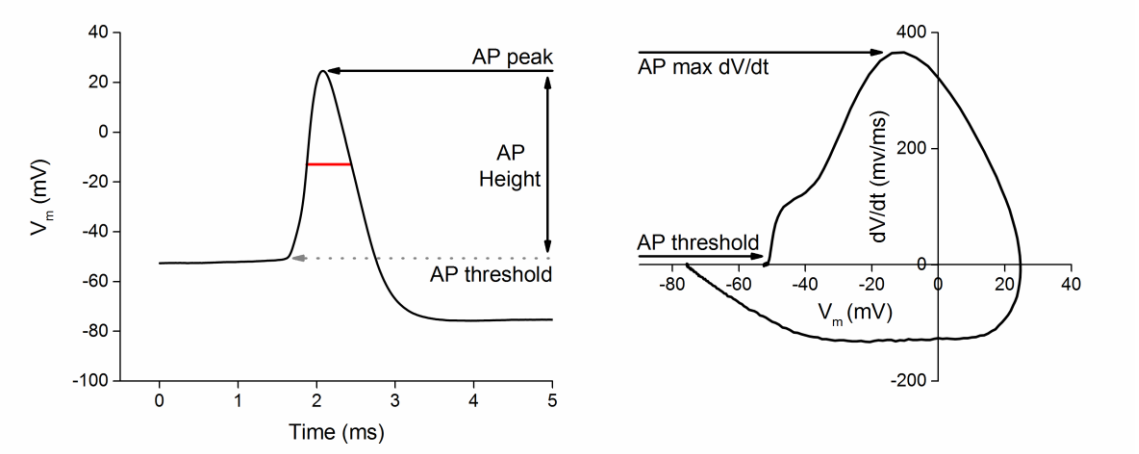

Figure 2.4. Measurement of AP properties. Sample voltage trace (left) and corresponding phase plane plot (right) of the 1st AP elicited in response to a 60 pA

depolarising current step. Highlighted is the AP peak, AP threshold and max dV/dt (identified by a solid black line) and the AP width measured at half height (red line).

Spike Afterpotential

The ADP was measured as the peak amplitude of the depolarising deflection, within a window of 5 to 60 ms following the peak of the primary AP, relative to the pre stimulus baseline (Fig 2.6A). In any neuron without a clear depolarising phase the ADP amplitude was interpreted to be zero (Fig 2.6B). Conversely when the ADP is sufficiently large it can cross the AP threshold and elicit voltage gated sodium channel dependant AP firing (Fig 2.6C). Although it is theoretically possible to mimic the voltage curve of an AP in the presence of a voltage gated sodium channel blocker such as tetrodotoxin (TTX) to measure the amplitude of the underlying ADP, this is unfeasible given the relatively long τ observed in Re neurons (as compared to CA1 pyramidal neurons) and the limitation of one slice per animal. As such we only included sub threshold ADP's in our analysis and considered the number of ADP spikes to be an indirect measure of the underlying ADP amplitude in neurons displaying ADP spikes.

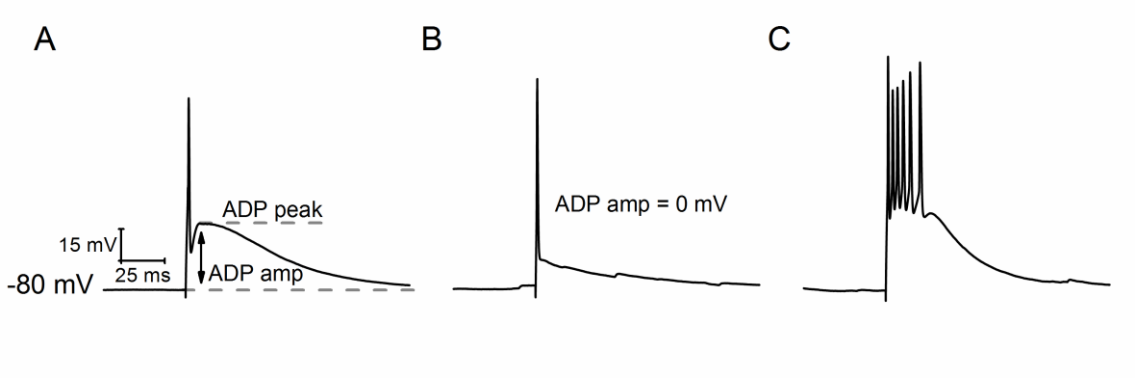

Figure 2.5. Measurement of the ADP peak. (A) Voltage trace showing an ADP following generation of a single AP. ADP amplitude (ADP amp) is measured as the voltage differential between the peak of the ADP and baseline. (B) Voltage trace showing a single spike with no clear evident depolarising phase of an ADP. The ADP amplitude is designated as 0 mV. (C) Voltage trace following elicitation of a single spike showing an ADP which elicits voltage gated sodium channel dependant APs. The number of ADP spikes was taken as an indirect measure of ADP amplitude in the neurons.

Measurement of the AHP following a primary AP is considerably simpler. In Re neurons where the membrane voltage went >0.5 mV below pre stimulus baseline

levels on the descending stage of the AP, the AHP amplitude was measured as the voltage differential between baseline and the most negative point 0-100 ms post AP peak.

Voltage clamp recordings

Spontaneous excitatory postsynaptic currents (EPSCs) were detected using custom templates in PClamp Clampfit software. Individual templates were constructed for each neuron.

To test for the presence of I_h current we compared the first and last 60 ms of the largest hyperpolarising step to -125 mV. The presence of HCN channel dependant current would lead to a clear current differential between the first 60 ms (before the channels have opened) and the last 60 ms (when HCN channel opening probability is higher).

The amplitude of T-type calcium channel currents was measured as the negative peak of the observed current within the time window of the voltage step. During the paired pulse protocol to measure the recovery from inactivation of these channels the amplitude of the second pulse was divided by the first to give a paired pulse ratio. A ratio of 1 represents full recovery from inactivation of the T-type calcium channels.

2.6 Staining for amyloid plaques

Amyloid plaques were identified in coronal brain slices using fluorescent histochemical probe Amylo-Glo (Schmued et al., 2012). Following the experimental day, slices were fixed overnight in 4% paraformaldehyde (PFA) before subsequent storage in a phosphate buffered saline (PBS) solution. Prior to staining, slices were transferred into to a 70% ethanol solution for 5 minutes and then rinsed in distilled water for 2 minutes without shaking. Slices were then transferred to and incubated for 15 minutes in 1X Biosensis Amylo-Glo staining solution. The slices were rinsed in 0.9% saline solution for 5 minutes without shaking before being washed in PBS for 30 minutes. Slices were briefly rinsed in distilled water for 15 seconds. Slices were transferred onto a slide and a coverslip was mounted using aqueous mounting fluid fluoromount (pH 5.0 - 7.0). Amyloid stained plaques were then visualised using ultraviolet (UV) epifluorescent illumination.

3 Intrinsic electrophysiological properties of neurons of the rostral nucleus reuniens

Disclaimer: A significant portion of the work presented in this chapter has been previously published at (Walsh *et al.*, 2017).

3.1 Introduction

The roles of the Re has been the subject of growing interest in recent years (Cassel *et al.*, 2013; Aggleton, 2014). Despite the significant body of data that address the connectivity of the Re (Vertes, 2006; Vertes *et al.*, 2007, 2015; Prasad & Chudasama, 2013; Varela *et al.*, 2014), its roles in behaviour (Prasad *et al.*, 2013; Xu & Südhof, 2013; Cholvin *et al.*, 2013; Hallock *et al.*, 2013), and its pathology in disease (Mair *et al.*, 1979; Braak & Braak, 1991; Graef *et al.*, 2009; Duan *et al.*, 2015), a cellular levell understanding of this cognitively important thalamic structure is far from comprehensive. Interestingly, *in vivo* awake tetrode recording has recently revealed that Re has “head direction” cells (Jankowski *et al.*, 2014), a neural activity more commonly associated with neurons in the entorhinal cortex and HPC/subiculum (Taube *et al.*, 1990; Sargolini *et al.*, 2006). This finding prompted further investigation of spatially responsive cells in the Re which revealed evidence of both place cells and border cells, providing further evidence for the importance of the Re in spatial navigation (Jankowski *et al.*, 2015). *In vivo* recordings have also demonstrated the presence of Re neurons which exhibit trajectory-dependant firing during a T-maze based continuous alteration task, similar to neural activity observed in the CA1 region of the HPC and the mPFC (Ito *et al.*, 2015). Notably, practically all published Re neurophysiology to date has been performed with *in vivo* extracellular recording methods either in anesthetized (Dolleman-van der Well 1997, Bertram and Zhang 1999) or, more recently, awake behaving rats (Jankowski et al., 2014; Ito et al., 2015; Hallock et al., 2016).

Neurochemically, 4 distinct neuronal populations of Re neurons have been described including CB-positive neurons, CR-positive neurons, neurons which are positive for both CB and CR, and neurons which have are not positive for either CB or CR (Bokor *et al.*, 2002). As the expression profile of Ca^{2+}-binding proteins has been used previously to isolate neurophysiologically distinct cellular populations in the HPC and cortex (Pelkey *et al.*, 2017), it might be expected that

up at least 4 distinct neurophysiological classes of Re neurons could be characterised.

However there have been few detailed cell-level electrophysiological studies of Re neurons. Working in the mid-line thalamus, which likely included Re, Graef and colleagues examined changes to bursting and T-type Ca^{2+} channels produced in a pilocarpine-induced epilepsy model (Graef et al., 2009). The same group subsequently made a similar study, in this case specifically working within Re, examining consequences of ethanol exposure and withdrawal (Graef et al., 2011). To my knowledge the only other intracellular data from Re neurons is a single panel in a supplementary figure in Xu and Sudhof (2013)- which presents miniature inhibitory postsynaptic currents (IPSCs) recorded from 6 mice at 26ºC.

Given the growing interest in the neural functionality of Re a series of *in vitro* brain slices studies were carried out, designed to better characterize the cellular neurophysiology of Re. The intrinsic excitability properties of neurons in the rostral Re are described from studies entirely performed using coronal brain slices prepared from adult male mice.

3.2 Methods

All procedures were carried out in accordance with the Animals (Scientific Procedures) Act 1986. Male C57-Bl/6J mice aged 14-18 weeks old were bred in house at the University of Exeter. They were subsequently housed on a 12:12 light/dark cycle and granted *ab libitum* access to food and water. Coronal slices were prepared and neurons were recorded from as described in Materials and Methods. K-gluconate solution #1 (table 2.1) was used as the internal solution throughout recordings.

3.3 Results

3.3.1 Cellular properties at in the absence of injected current

Data collected from intact Re neurons using loose patch/cell-attached recording indicated that the majority of cells exhibited a significant degree of spontaneous AP firing. Figure 3.1A(a) illustrates a segment of such activity from a typical recording of this nature. The timecourse of the instantaneous frequency of AP firing for this cell recorded over 60 s is presented in Figure 3.1A(b).

Commensurate with observations made in loose-patch or cell-attached mode (Fig 3.1A), robust spontaneous AP firing was also observed in the majority of Re neurons following entry into the whole cell recording mode and immediate collection of a 60 s period of current clamp data with zero injected current . In 135 of 154 (~88%) whole cell recordings of this nature, the neuron fired one or more spontaneous APs during the 60 s epoch immediately following entry into the whole cell configuration (Fig 3.1B). For all cells (i.e. both spontaneously firing and silent) the average membrane potential observed over the entire 1 minute period is presented in Figure 3.1C. The 19 cells exhibiting no spontaneous spiking were characterized by a membrane potential (-70.6 ± 3.2 mV) somewhat more negative than the overall population mean (-63.7 ± 0.6 mV). The vast majority (107) of the 135 cells that exhibited AP firing maintained their spiking activity throughout the entire 60 s period, with no single interspike interval longer than 5 s (and in most cells no longer than 300 ms). These cells had a mean membrane potential of -61.4 ± 0.4 mV (n=107). For these recordings a histogram presenting the distribution of mean AP frequency is shown in Figure 3.1D. This was compiled by calculating the average of the reciprocal of all inter-spike intervals for each cell. The mean of these mean instantaneous frequencies was 9.2 ± 0.5 Hz.

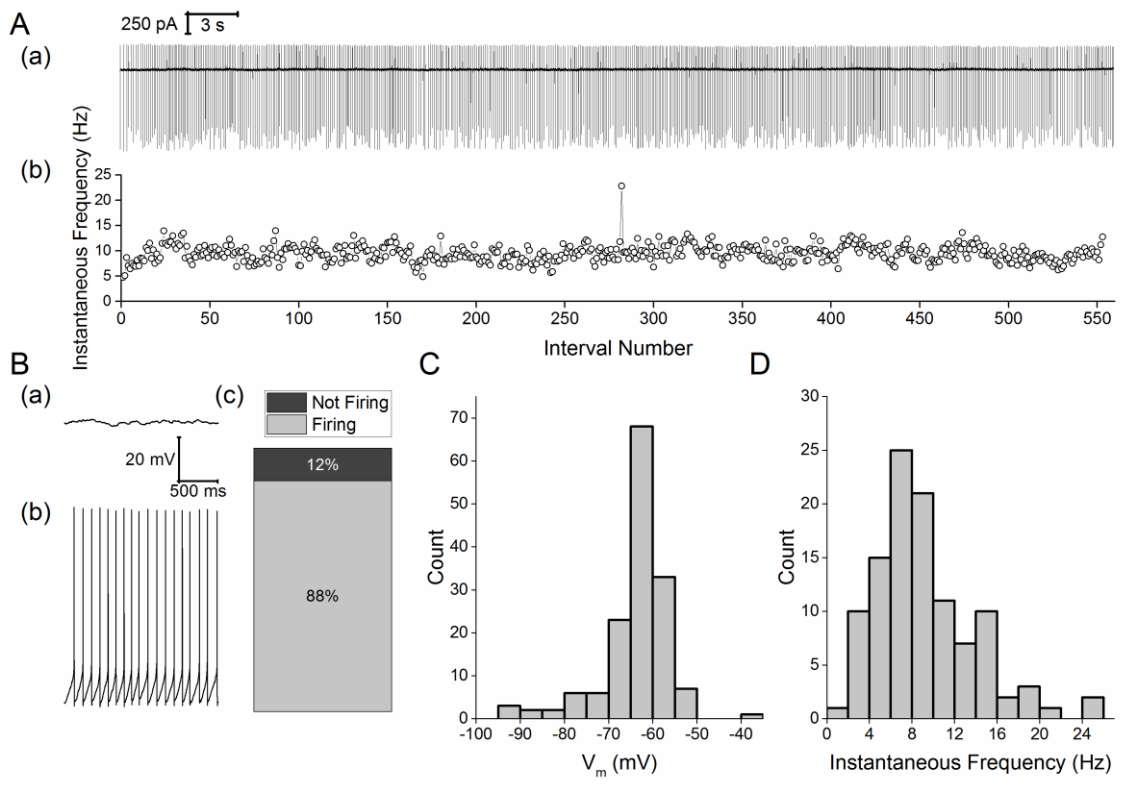

Figure 3.1. Firing properties of tonically firing Re neurons. (A) (a) Sample trace of spontaneous AP firing recorded in cell-attached mode over a 60 s period. (b) A plot showing the Instantaneous frequency vs spike interval number for this cell-attached recording. (B) Sample traces from whole cell current clamp recordings illustrating (a) a neuron which showed no spontaneous activity and (b) a neuron that fired regularly at rest. (c) A cumulative column representation of the percentage of silent and spontaneously firing neurons in the Re population. (C) Histogram presenting the mean membrane potential recorded during a 60 s epoch soon after gaining whole cell access (D) Histogram showing, for firing cells, the mean instantaneous AP frequency during this 60 s epoch.

In the remaining 27 cells that fired any AP during the 60 s recording epoch a range of spiking behaviours was observed. In 9 of the cells APs initially fired regularly at 3-10 Hz, essentially in a fashion mirroring the majority group illustrated in Figures 3.1B+D, but at some stage this activity first slowed and then ceased, seemingly as a consequence of modest and progressive (2-4 mV) hyperpolarizing shift in membrane potential (Fig 3.2A). In the remaining 18 cells in which any spontaneous AP generation was seen, prolonged spike-free periods (at least 5 s) were interrupted by brief periods of spiking. These cells fell into two clear groups. The first comprised 12 cells in which the intermittent spiking only comprised low frequency (<15 Hz) activity (Fig 3.2B), essentially similar to the spiking seen in the cells that maintained their firing for the whole 60 s (Fig 3.1). The second group comprised only 6 cells (Fig 3.2C), in these occasional brief bouts of spontaneous firing were observed which included very much briefer inter-spike intervals (as short as 3.2 ms), and thus considerably higher maximum instantaneous frequencies of spiking (75-310 Hz). A noticeable difference between the 11 cells with low frequency intermittent firing and the 6 cells with occasional high frequency bursting was in membrane potential. In the latter group this was always more negative than -75 mV (mean -82.2 ± 2.9 mV), whereas in the 11 cells in which the intermittent AP firing comprised only of low frequency spiking the membrane potential was significantly more depolarized (-66.0 ± 1.9 mV, $p<0.005$ unpaired, two tailed student's t-test). This latter value lies between the average membrane potential of the 17 cells that fired no AP in 60 s (circa -70 mV) and the largest group of cells, those exhibiting maintained regular firing (circa -61 mV). The very negative membrane potential of the 6 cells in high frequency spiking group, meant that the observed bursts rode atop a substantial transient depolarizing shift which brought the cells to threshold, the nature of which will be discussed below.

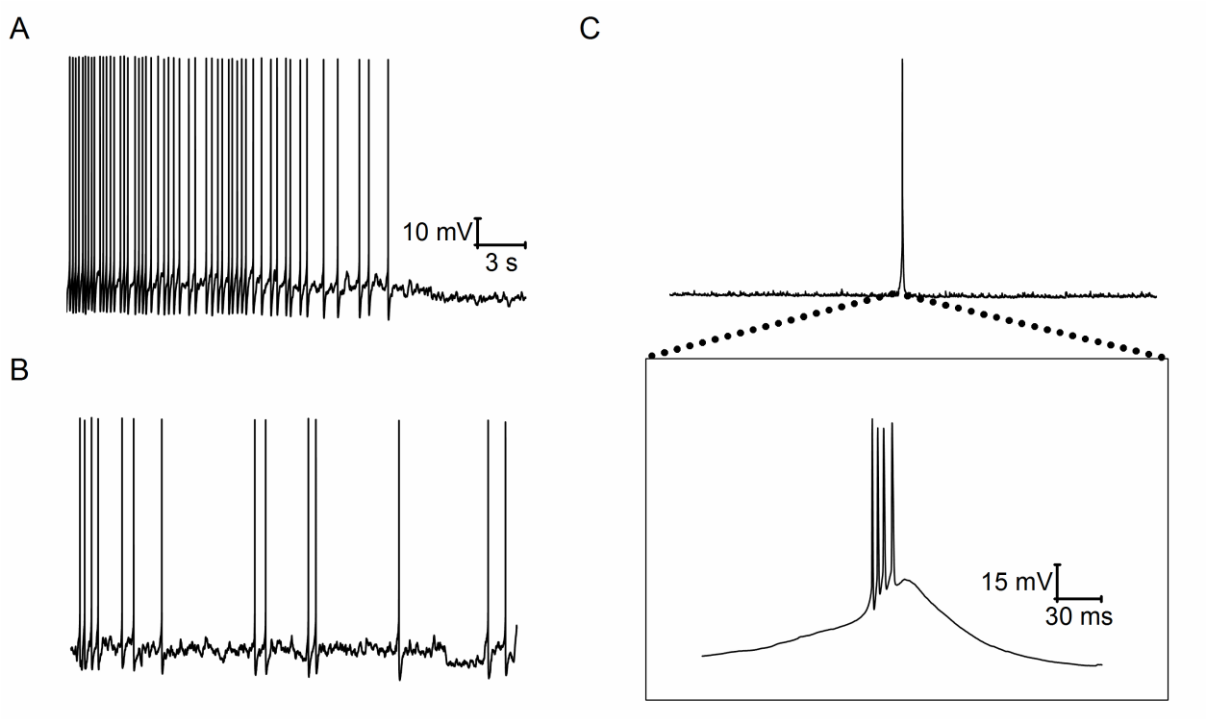

Figure 3.2. Heterogeneous firing patterns of Re neurons. Sample current clamp trace of (A) an initially regularly firing neuron in which cessation of firing was accompanied by a hyperpolarising shift in membrane potential, (B) a neuron exhibiting irregular firing at a low frequency and (C) a neuron which fired irregularly in short high frequency bursts. The inset shows the very high frequency spiking present in such a burst with 4 AP arising in under 30 ms.

As described above, ~70% of Re neurons fired constantly at rest with a frequency of 2-20 Hz (Fig 3.1D). Inspection of the voltage traces revealed that this firing appeared to be predominantly paced by a robust AHP that followed each AP. On average this AHP peaked 13.7 ms after the AP peak and took the membrane potential to -20.1 mV below the previous spike threshold (Fig 3.3A). As the AHP decayed and the cell depolarized again it was able to initiate another spike; consequently the rate of the AHP decay was appeared to be a key determinant of spontaneous firing frequency.

In the 135 cells firing spontaneously at rest, all of the spikes were detected and core waveform properties were examined. For the 120 cells firing a total of 20 or more AP histograms plotting the distribution of mean AP threshold, max rate of rise, zenith and width at half height (defined as the voltage halfway between AP threshold and zenith) are presented in Figure 3.3B-E. When the distribution of AP thresholds (Fig 3B) is compared with the membrane potential distribution (Fig 3.1C) it is apparent why most Re neurons exhibit spontaneous firing. As expected, bath application of TTX (500 nM) first slowed and then eliminated spontaneous AP firing in Re neurons (data not shown).

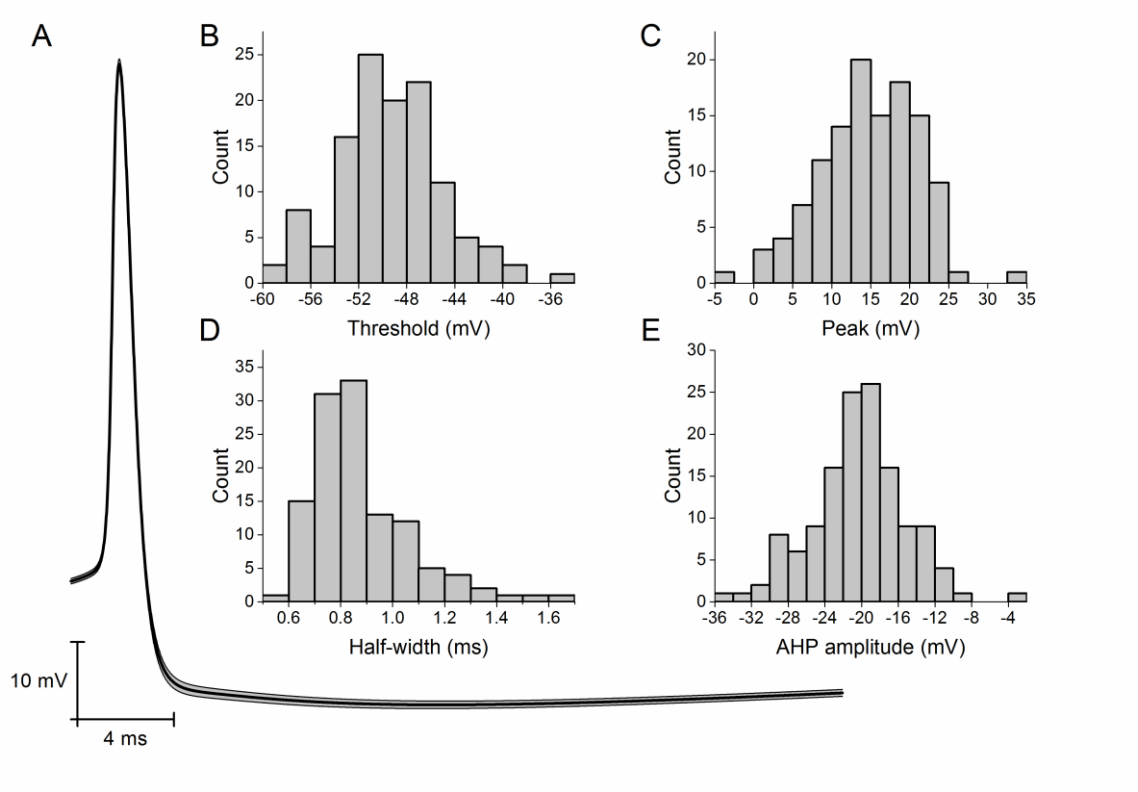

Figure 3.3. Action potential properties of Re neurons at V_m. (A) Average trace of a spontaneous action potential measured in the absence of injected current. SEM is highlighted in grey. (B-E) Histograms showing the average spike properties of spontaneously fired APs, specifically (B) AP threshold, (C) AP peak value (i.e. zenith), (D) AP width measured at half height and (E) AHP amplitude.

3.3.2 Spontaneous synaptic input

It was clear from close examination of current clamp recordings at rest that Re cells *in vitro* received a significant degree of spontaneous synaptic input (Fig 3.4A). Classical fast spontaneous synaptic activity was also apparent in recordings made in voltage clamp mode at a holding potential of -85 mV (Fig 3.4B). Indeed, spontaneous IPSCs recorded *in vitro* in voltage clamped Re cells at 26°C have been presented in one previous publication (Xu & Südhof, 2013).

When, during voltage clamp recordings, TTX (500 nM) was added to the perfusing aCSF to isolate miniature inward-going synaptic events (i.e. post-synaptic responses arising from presynaptic release of single quanta), a spread of response amplitudes with a median peak of typically around 10-15 pA was observed. Most of these events rose very fast and decayed rapidly and exponentially with a time constant of around 1 ms (Fig 3.4C mPSCs).

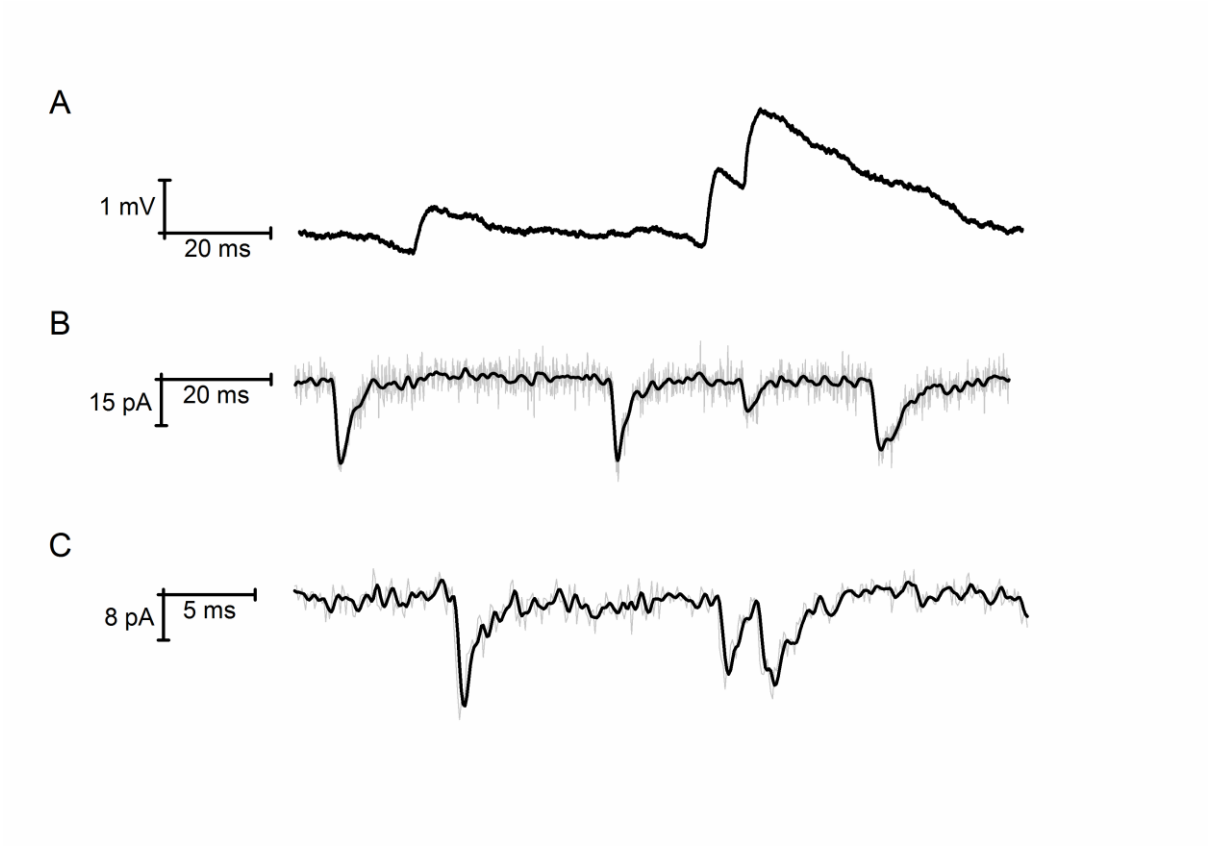

Figure 3.4. Spontaneous synaptic input to Re neurons. (A) Sample post-synaptic potentials measured at V_m. (B) Sample inward going post-synaptic currents measured at a holding potential of -85 mV. (C) Sample trace of miniature post-synaptic currents measured at a holding potential of -85 mV in the presence of 500 nM TTX. Black current traces in (B&C) are Gaussian filtered versions of the raw grey traces.

To establish if the spontaneous synaptic drive to Re cells could be a major factor in their spontaneous AP firing, a series of recordings were made in the maintained presence of NBQX (5 µM), L689560 (5 µM) and gabazine (5 µM) to block AMPA/Kainate, NMDA and $GABA_A$ receptors, respectively. Under these conditions spontaneous post-synaptic potentials were absent but the mean V_m remained relatively depolarized (-66.7 ± 2.1 mV, n=29, Fig 3.5A). Furthermore, spontaneous AP electrogenisis was still apparent in the majority (20/29, 69%) of cells (Fig 3.5B). This spontaneous activity occurred with a mean frequency (8.0 ± 1.0 Hz) very similar to that observed in the absence of pharmacological block of amino-acid mediated synaptic transmission (Fig 3.1D). The various waveform properties of spontaneous APs also appeared unaffected by synaptic blockade (data not shown). This indicates that the relatively depolarized membrane potentials and consequent tonic spontaneous AP firing in Re neurons *in vitro* arises largely from cell-intrinsic properties, rather than synaptic drive, although the latter will no doubt shape this activity to some extent.

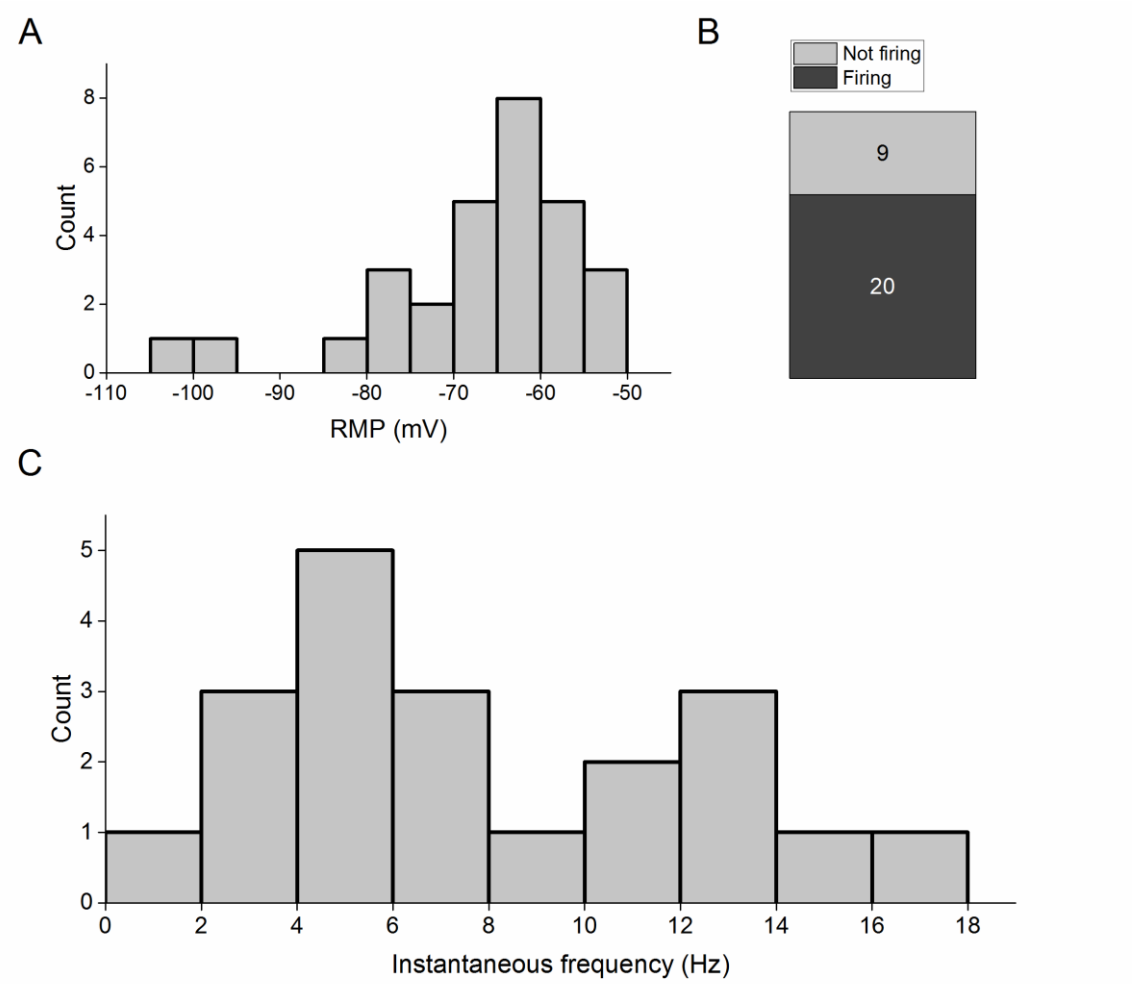

Figure 3.5. Firing properties of Re neurons in the presence of synaptic blockers. (A) A plot illustrating the distribution of membrane potentials in Re cells recorded in the combined presence of blockers of AMPA/Kainate, NMDA and $GABA_A$ receptors. (B) An illustration of the relative proportions of spontaneously firing and silent cells under these conditions (C) The distribution of mean instantaneous AP frequency in the absence of injected current during a 60 s epoch recorded in whole cell configuration. All recordings were made in the presence of NBQX (5 µM), Gabazine (5 µM) and L-689560 (5 µM).

3.3.3 Passive and active membrane properties

For a variety of underpinning biophysical reasons, the passive membrane and intrinsic excitability properties of all neurons depends on their V_m. Consequently, to make comparisons across neurons within a population it is helpful to set the pre-stimulus membrane potential of each cell to constant defined level. Furthermore, it is helpful to choose a pre-stimulus potential at which spontaneous firing is absent, because the presence of ongoing background firing complicates interpretation of any subsequent stimulus-evoked activity. Thus, to gain a detailed insight into the passive membrane and intrinsic excitability of Re neurons, measurements were initially made from a pre-stimulus membrane potential of -80 mV. This pre-stimulus potential was set by applying a suitable amount of bias current via the recording amplifier; this varied in amplitude from +46.8 to -153.7 pA, averaging -45.4 pA (n=154).

Having set the pre-stimulus membrane potential to -80 mV, we then applied a range of defined current stimuli to probe the sub- and supra-threshold intrinsic properties. Firstly, to determine an approximation of “rheobase” for cells at -80 mV we applied an incremental series of 100 ms duration, depolarizing current injections. These were increased stepwise in amplitude in small increments at 1 Hz until AP firing was observed. As illustrated in Figure 3.6A, cells could be divided into those which fired just one AP at rheobase and those which produce a burst of between 2 and 6 AP. The mean AP count in latter group was 2.9 ± 0.2 AP. Data summarizing the amount of current required to produce at least one AP across 107 cells is shown on the left of Figure 3.6B. Alongside this are data from a series of similar recordings made in the synaptic blocker cocktail described above. These exhibited an almost identical mean rheobase of 25.3 ± 5.1 pA (n=25, Fig 3.6B). For the larger drug free experimental group Figure 3.6C compares the mean rheobases for those cells firing just one AP and those producing a burst of 2-6 AP. The latter group had a 18% lower rheobase (Single spike, median = 22 pA, n = 77; Burst, median = 18 pA, n = 30; P = 0.01, Mann Whitney U test), and consequently were both easier to bring to AP threshold and once there produced a greater spike output.

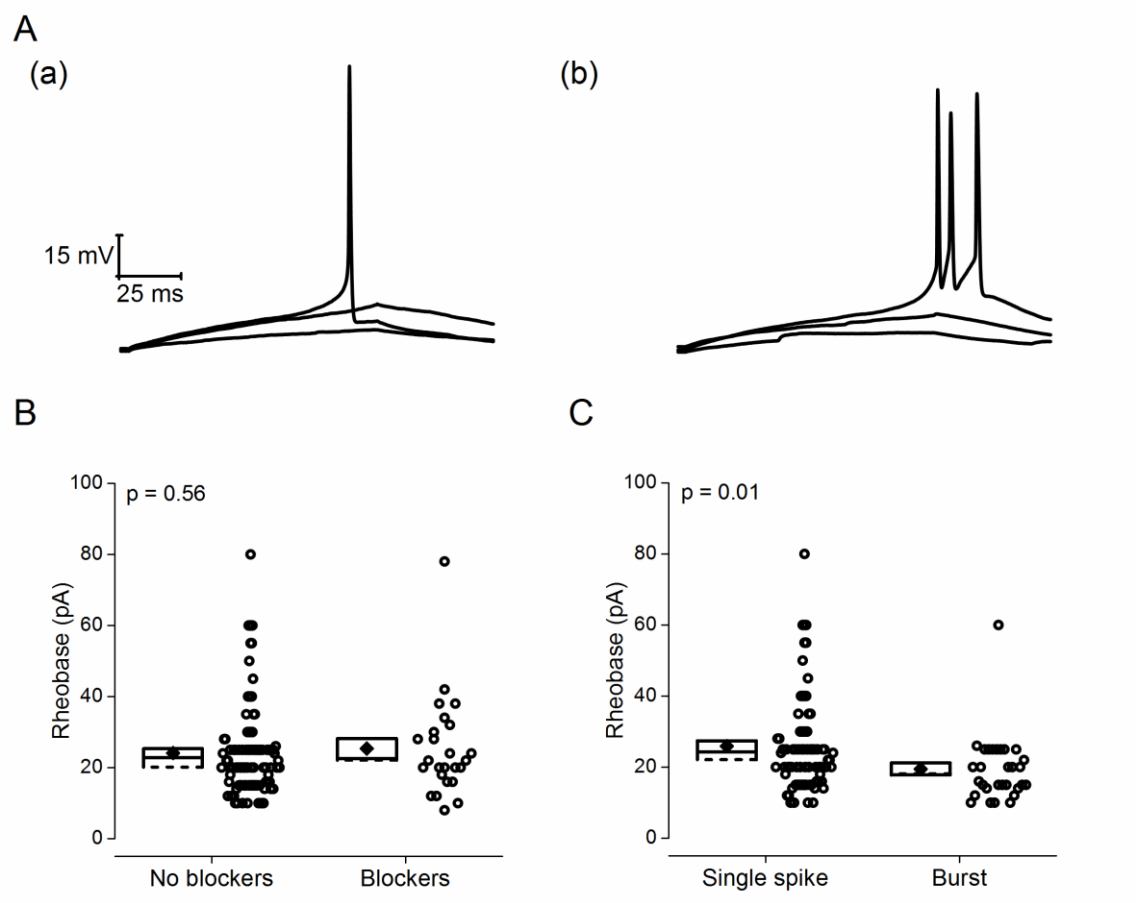

Figure 3.6. Approximation of rheobase in Re neurons from a pre-stimulus potential of -80 mV. (A) Sample voltage traces extracted from a series of incrementally growing 100 ms current injections used to approximate the rheobase from -80 mV. Data are shown are from 2 cells, (a) one with a single spike and (b) one with a burst. The traces shown in each are responses to the minimal current injections which elicited an AP (rheobase), rheobase – 2 pA and rheobase/2. (B) A plot comparing rheobase distributions recorded both in the absence and presence of NBQX (5 µM), Gabazine (5 µM) and L-689560 (5 µM). (C) The "no blocker" data from (B) broken down by cells which fired only one AP at rheobase and cells which generated a burst of 2-6 AP. In (B) and (C) each round symbol is a separate recording. The diamonds plot the mean, the boxes the standard error and the line crossing the box the median.

We next employed a standard incremental current injection protocol in which a series of 9 consecutive 500 ms current stimuli were delivered with an inter-stimulus interval of 10 s. The amplitude of the first current pulse was -20 pA and each subsequent pulse was +10 pA larger such that the final pulse had an amplitude of +60 pA (Fig 3.7A). The first (i.e.-20 pA stimulus) sweep was used to determine the subthreshold intrinsic properties of Re neurons including R_i, τ, and capacitance. Approximately 12% of Re cells exhibited a significant rebound depolarization following cessation of hyperpolarizing current injections from a prestimulus potential of -80 mV. As reported previously by others (Graef *et al.*, 2011), these rebound depolarizations were capable of driving spiking in some cells (Fig 3.7C), and when spiking was seen multiple AP were typically produced within a short time window. The basis of this rebound potential will be described later.

Mean R_i was 615 ± 17 MΩ (Fig 3.7D), and mean τ was 38.5 ± 1.1 ms (Fig 3.7E). The capacitance estimated by τ by R_i averaged 66.6 pF, indicating that, for CNS neurons, these cells were modest in size.

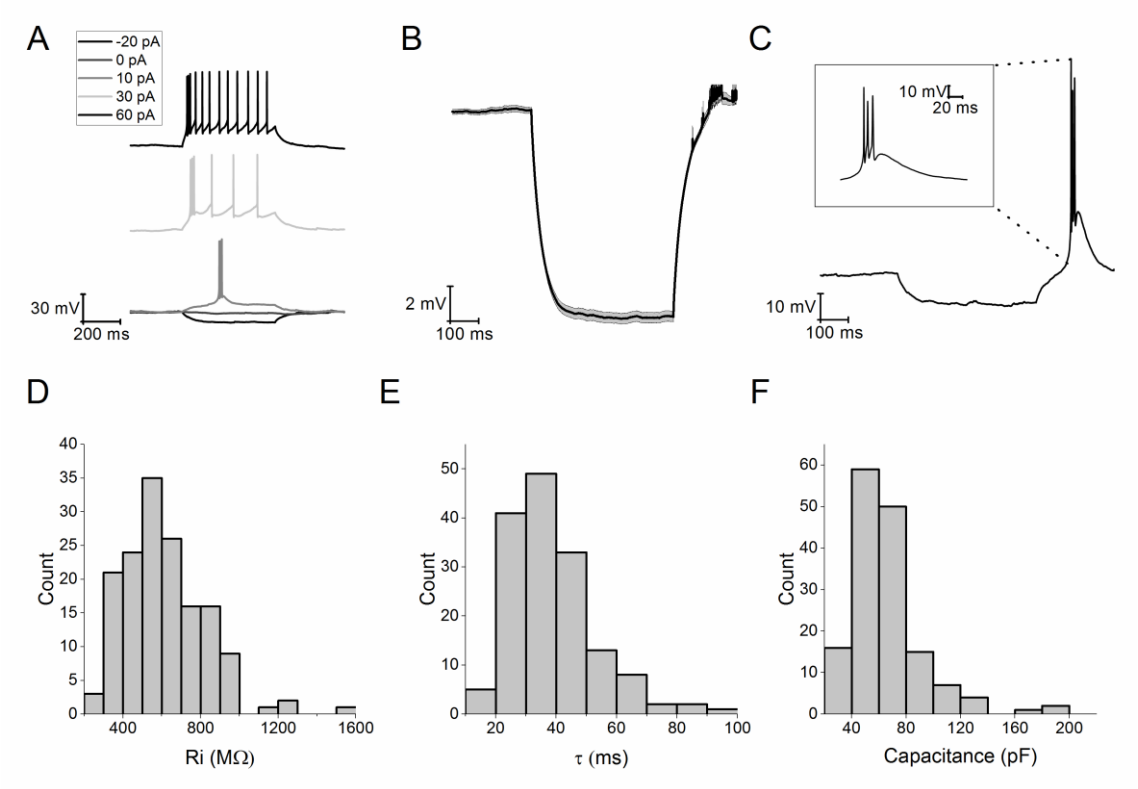

Figure 3.7. Passive membrane properties of Re neurons. (A) Sample voltage traces a series of current injections (-20 – 60 pA) from a set pre-stimulus potential of -80 mV. For clarity the responses to 30 and 60 pA stimuli have been offset. (B) Average voltage response to a -20 pA, 500 ms hyperpolarising current injection from a set pre-stimulus potential of -80 mV. SEM is highlighted in grey. Highlighted in (C) is the high frequency rebound spiking behaviour observed from some cells following termination of negative current injections. (D-F) Histograms showing (D) input resistance, (E) time constant and (F) an approximation of capacitance.

Describing the mean passive properties of Re neurons is useful when comparing these to neuronal passive properties reported in other structures of the CNS. Notably however there is considerable variation in the R_i, τ, and capacitance of Re neurons. I wondered whether this variation was symptomatic of the existence of several distinct cellular populations of Re neurons. Initially hierarchical cluster analysis was used to attempt to separate neurons based on their passive membrane properties however this analysis proved ineffective in separating distinct populations based on these properties. In absence of a reliable clustering method of separating neuronal populations based on these passive properties, we decided to test whether these properties differ based on a quantitatively defined set of neuronal populations, namely those separated based on their basal firing patterns as described in figure 3.2. The firing properties of neurons has previously been used in other areas of the brain has previously been used to classify useful populations of neurons, for example stellate neurons in the entorhinal cortex (Pastoll *et al.*, 2012). Grouped based on firing properties, the R_i of Re populations displayed no differences (Fig 3.8A, $F = 4.1$, $p = 0.39$, Kruskal-Wallis one-way ANOVA). The τ of Re neurons differed based on their firing properties (Fig 3.8B, $F = 12.17$, $p = 0.02$, Kruskal-Wallis one-way ANOVA), with differences between regularly firing neurons and neurons which do not fire displaying significance during post-hoc analysis ($p < 0.05$, Bonferroni correction). The capacitance of Re neurons differed based on their firing properties (Fig 3.8C, $F = 22.6$, $p < 0.001$, Kruskal-Wallis one-way ANOVA), with differences between regular firing neurons and neurons which do not fire displaying significance during post-hoc analysis ($p < 0.01$, Bonferroni correction).

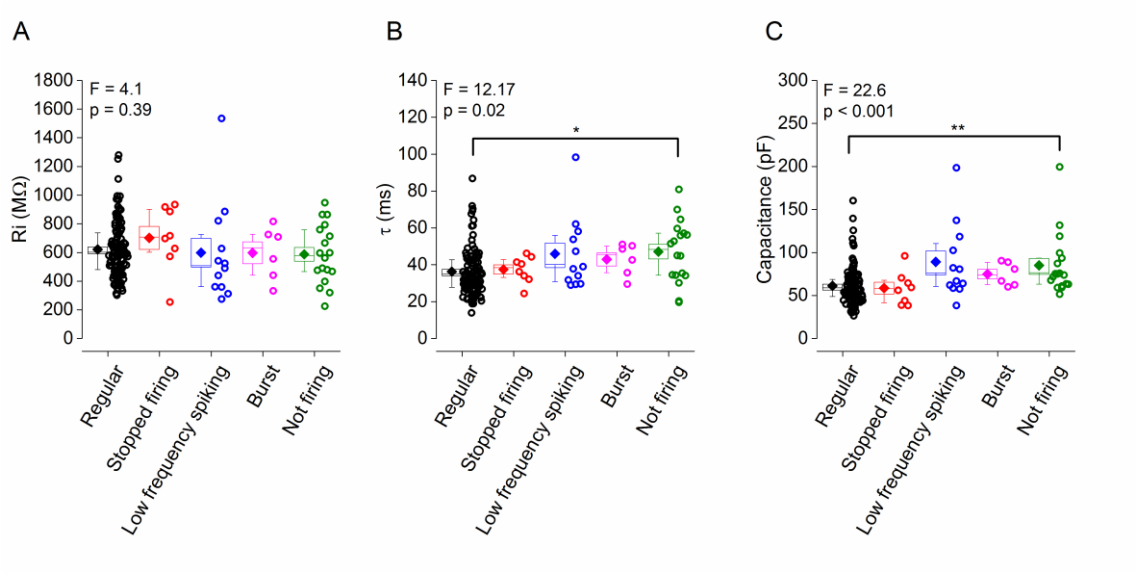

Figure 3.8. Passive membrane properties of Re neurons differs based on firing properties in the absence of external current stimuli. (A) Plot showing the mean R_i based on firing properties at V_m. Diamond represents mean, dashed line represents median, and box represents SEM. (B) Plot showing the mean τ based on firing properties at V_m. Diamond represents mean, dashed line represents median, and box represents SEM. (C) Plot showing the mean capacitance based on firing properties at V_m. Diamond represents mean, dashed line represents median, and box represents SEM. All F and p values were calculated using a Kruskal-Wallis one-way ANOVA.

3.3.4 Apparent absence of HCN like current

A slow depolarizing relaxation of the membrane potential and accompanying decrease in membrane resistance during application of a hyperpolarizing current injection is commonly known as “sag”. It is a prominent and important subthreshold feature of a number of CNS neurons, and arises from activation of HCN channels. The majority of Re neurons exhibited little or no sag in response to a 500 ms, 20 pA hyperpolarising current injection, as exemplified by the average voltage traces shown in Figure 3.7B. The extent to which HCN2 channels, the predominantly expressed HCN channel in the thalamus (Santoro *et al.*, 2000), would activate in response to a relatively short hyperpolarising current injection is questionable given this channels long activation time constant (in the order of seconds). However when a five-fold longer 20 pA hyperpolarising step (2.5 s) was employed, no appreciable sag was observed as exemplified by the average trace in Figure 3.9A. In case HCN channels were already largely activated at -80 mV, 2.5 s 20 pA current injections at -72 mV and 500 ms current injections at -64 mV were also examined, neither of which exhibited any significant sag.

To finally confirm this apparent paucity of HCN current, and to look for any potential activation from even more depolarized prestimulus potentials, a series of voltage-clamp recordings were carried out to look for any sign of HCN-like conductance. Here a series of 5 s duration hyperpolarising steps were applied to Re cells at a holding potential of -55 mV. The test potential varied from -60 to -125 mV in 5 mV increments (Fig 3.9B). In such protocols HCN channel activity is revealed by a slowly growing inward current that takes 10s or 100s of milliseconds to come to steady state level. The cross-cell average current response from 6 Re neurons can be seen in Figure 3.9B. In this average there is no sign of any slow gating HCN-like current. The presence of HCN currents can be readily revealed by looking for difference between the current level in the first few milliseconds following hyperpolarization (before the slowly gating HCN channels have opened) and that seen at the end of the voltage pulse (when the HCN channel opening probability has had time grow). Such an analysis in presented in Figure 3.9C. This compares of the inward current level recorded in the first and last 60 ms of the voltage step to -125 mV relative to the holding

current. This revealed that 5 of the 6 neurons recorded exhibited no slow gating inward current whatsoever. The remaining neuron exhibited a small (~50 pA) growth in inward current although on average, across the 6 cells, there was no significant difference in current level at the start and end of the pulse (Fig 3.9C, Trace start, mean = -383 ± 52 pA; Trace end, mean = -396 ± 50 pA; n = 6, p = 0.2, paired, two tailed student's t-test). Upon inspection of the average voltage trace (Fig 3.9B) it became clear that the amplitude grew in a non-linear fashion across sequential voltage steps. This is also evident from Figure 3.9D, an I-V plot of the current amplitude at the end of the 5 s step versus voltage. This form of this curve is suggestive of the presence of inwardly rectifying potassium channels as the membrane conductance increases at potentials negative to the potassium equilibrium potential.

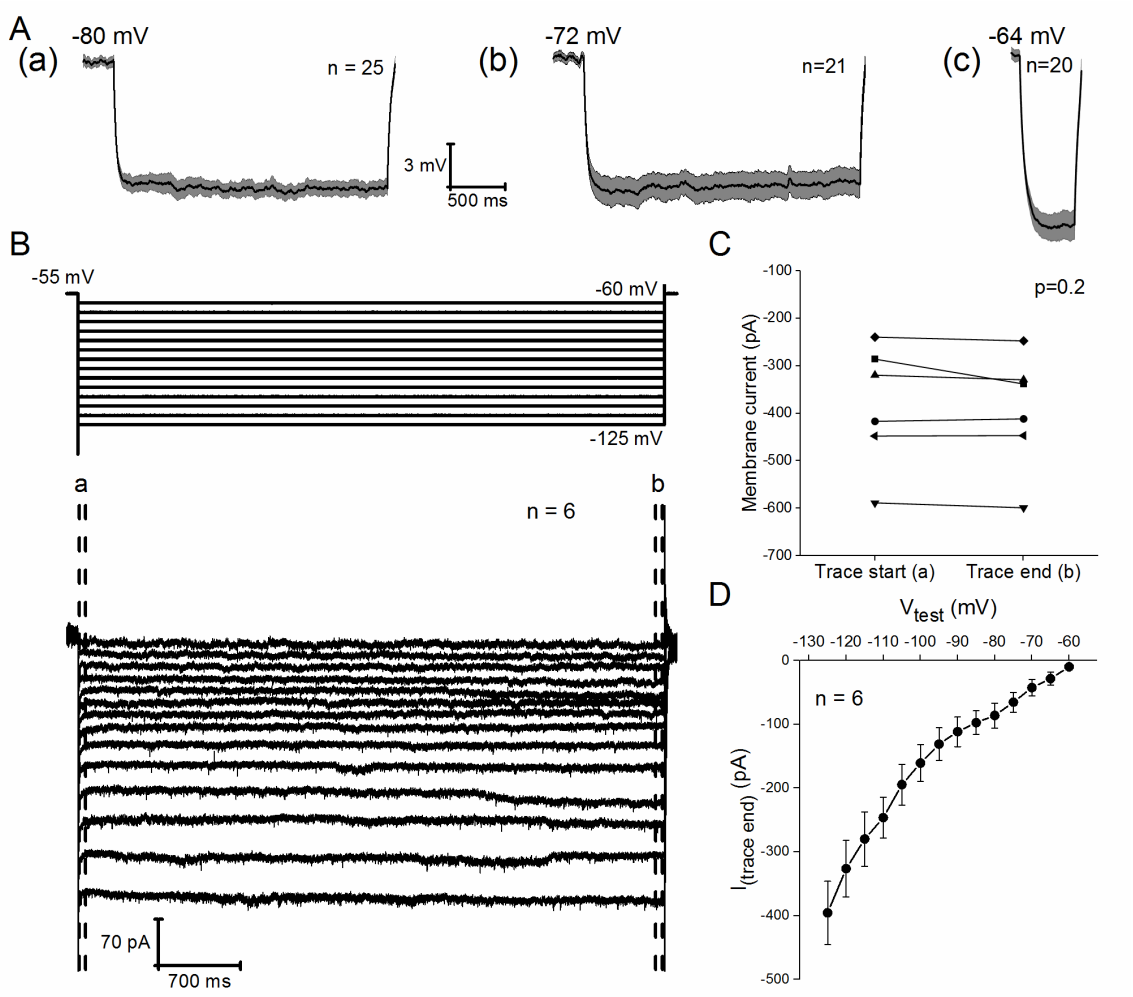

Figure 3.9. Apparent absence of HCN channel-like current in Re neurons. (A) (a+b) Average current clamp trace showing the response to a 2.5 s, 20 pA hyperpolarising current injection applied to cells at a prestimulus potential of (a) -80 mV and (b) -72 mV. (c) Average current clamp trace showing the response to a 500 ms, 20 pA hyperpolarising current injection applied to cells at a prestimulus potential of -64 mV. (B) Voltage clamp protocol (top) and resultant average traces (bottom) of a series of 5 mV hyperpolarising steps from a holding potential of -55 mV. (C) Plot showing the change in membrane current between the first 60 ms (a) and the final 60 ms (b) of a voltage step to -125 mV. (D) Average I-V plot of the current response during the final 60 ms of a 5 s test pulse for a series of 5 mV hyperpolarising voltage steps applied to 6 neurons held at -55 mV.

The incrementally growing depolarizing 500 ms current stimuli (Fig 3.7A) lead to AP firing in all Re neurons. A graph plotting the fraction of cells firing 1 AP or more versus the amplitude of the depolarizing stimulus is shown in Figure 3.10A, whereas Figure 3.10B summarizes the relationship between number of spikes elicited and current stimulus applied. The graph in Figure 3.10B does not provide any information about the temporal dynamics of AP production during the 500 ms current stimulus. This feature of excitability is illustrated in Figure 3.10C which plots the mean instantaneous frequency versus spike interval for applied current stimuli ranging from 10 to 60 pA. An additional dataset from a smaller group (n=25) of Re neurons using 2.5 second long current stimuli was also gathered. An example recording and pooled data from the 30 and 60 pA stimuli are shown in Figure 3.10D. These recordings show that maintained lower frequency (8-20 Hz) firing following post-burst accommodation could continue for at least 2.5 seconds. In reality this activity seems ostensibly similar to the maintained firing observed in the absence of injected current in most Re neurons (Fig 3.1).

It is clear from Figures 3.10C+D that, on average, when Re neurons receive current injections sufficient to inducing fire they tend to generate an initial burst of AP around 115-145 Hz followed by accommodation to maintained spiking rates around 10-30 Hz. Although providing a useful and standard summary, data averaged in the way shown in Figure 3.10C do not reflect the full diversity of firing behaviours that were observed in our population of Re recordings. In particular the full spectrum of behaviours featured both highly bursty and regular spiking cellular responses to the same stimulus (Fig 3.11A). This diversity of firing patterns is illustrated in an alternative manner by the cell by cell data presented in Figure 3.11B. Here there relative timing of APs (relative to the first = black symbols) is shown for a 60 pA depolarizing stimulus. This plot confirms that many cells fire a prominent and very high frequency initial AP burst, whereas other cells lack this initial strong burst and fire more regularly throughout the applied stimulus (e.g Fig 11A(b)).

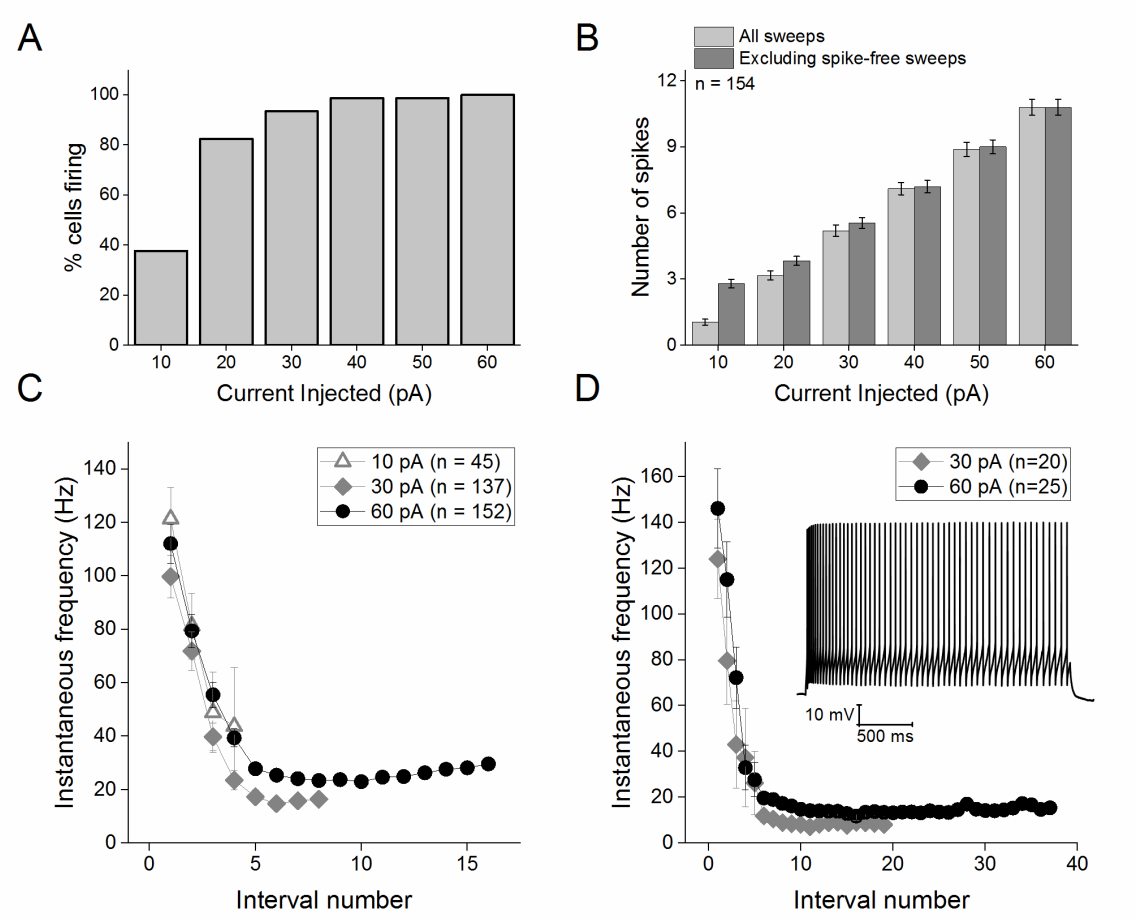

Figure 3.10. AP production of Re neurons in response to depolarising 500 ms "square-wave" current injections. (A) The fraction of cells generating at least one AP and (B) the mean number of AP produced in response to a series of 6 incremental 500 ms depolarising current injections (10 – 60 pA) from a set pre-stimulus potential of -80 mV. (C) A plot of instantaneous AP frequency vs interval number for a 10, 30 and 60 pA 500 ms current stimuli. (D) A plot of instantaneous AP frequency vs interval number and inset a sample voltage response, for a 30 and 60 pA 2.5 s current stimuli. All error bars represent SEM. All cells were set at -80 mV prior to current application.

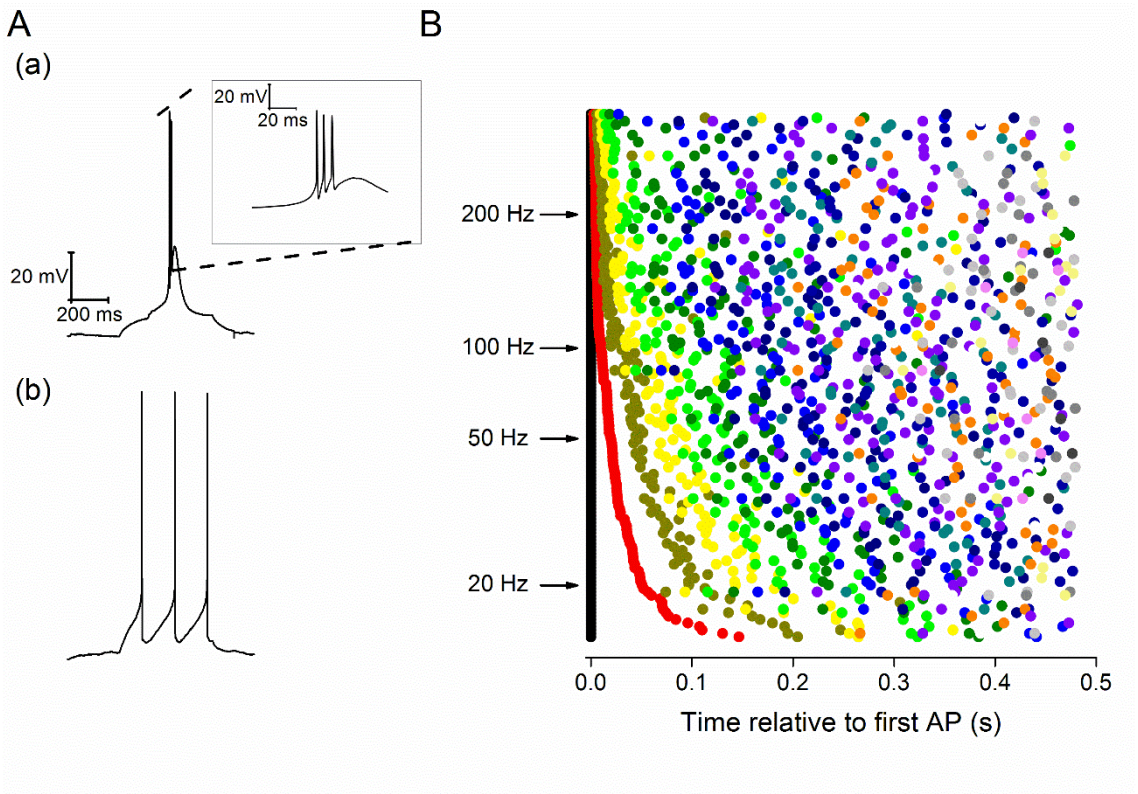

Figure 3.11. Diversity of firing observed in Re neurons following a depolarising current injection. (A) Sample voltage traces in response to a 10 pA, 500 ms depolarising current injection from a set pre-stimulus membrane potential of -80 mV. Different neurons display diverse firing outcomes for this stimulus including (a) high frequency bursting and (b) regular firing. (B) Scatter plot displaying the heterogeneity of firing behaviour in response to a 60 pA depolarising current step. Each row represents a different neuron and the time at which the first AP is generated for each neuron is represented on the graph by a black point at 0 ms. The timing of all subsequent APs generated is plotted relative to the first spike. The second spike is represented by a red point, the third by dark yellow, the fourth by yellow and the fifth by green etc. Representing the data in this form illustrates the diverse array of different firing patterns present in the neuronal population.

The diversity of cell by cell data represented in figure 3.11 suggests demonstrates that Re neurons can display a wide array of firing properties in response to depolarising current injections. To ascertain whether the diversity of firing patterning was resultant of distinct cell groupings based on their basal firing properties (Fig 3.2, Fig 3.8), we examined whether such Re populations differed in their response to depolarising current. The number of action potentials produced in response to current injections differed broadly across groups ($F = 19.67$, $p = 0.05$, RM two-way ANOVA) however post-hoc analysis did not identify differences between specific groups. The patterning of AP generation in response to current injections also differed broadly across groups when as demonstrated by differences in the instantaneous frequency of the 1^{st} two APs produced ($F = 19.67$, $p = 0.05$, Kruskal-Wallis one-way ANOVA) however post-hoc analysis did not identify differences between specific groups.

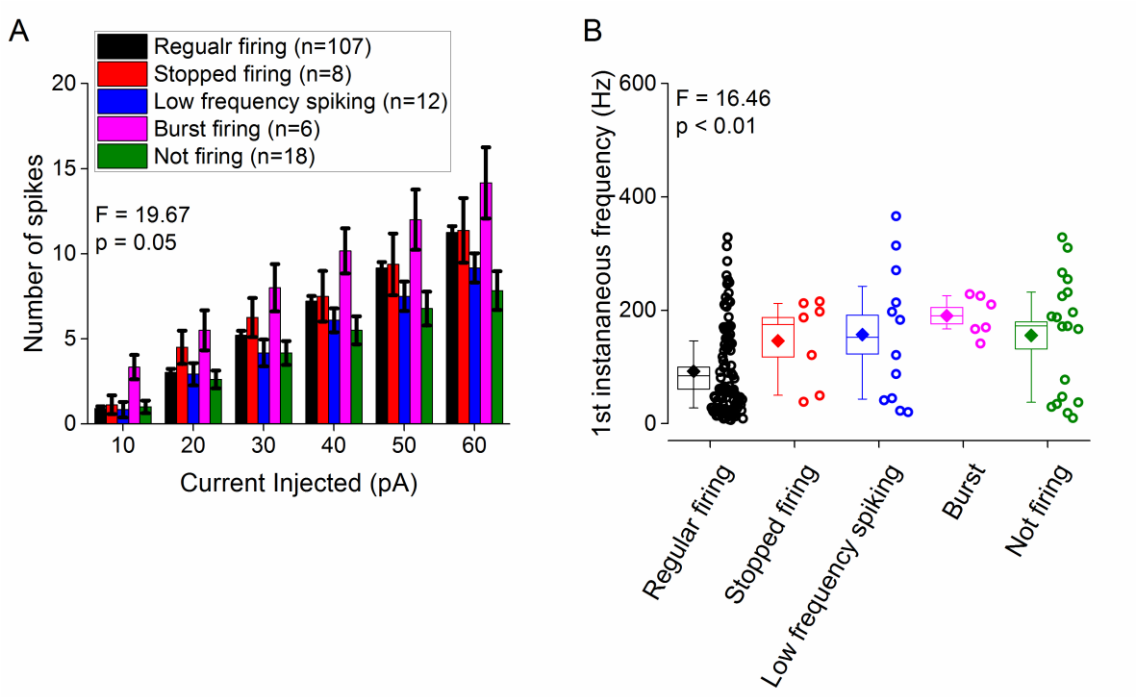

Figure 3.12 Differences in AP generation based on firing properties at V_m. (A) The mean number of APs produced, grouped by basal firing properties in response to a series of 500 ms depolarising current injections from a prestimulus potential of -80 mV. F and p values calculated using a 2 way RM-ANOVA. (B) Plot showing the mean first instantaneous frequency of Re neurons, grouped based on basal firing properties. Diamond represents mean, dashed line represents median, and box represents SEM. F and p values were calculated using a Kruskal-Wallis one-way ANOVA.

3.3.5 Afterpotential following elicitation of a single spike.

In hippocampal pyramidal cells (Jensen *et al.*, 1996; Yue & Yaari, 2004; Brown & Randall, 2009) and some other "bursty" neurons, the presence of bursting correlates with the presence of a fast spike ADP. This afterpotential is best observed when very short (1-2 ms), strong current (1-2 nA) stimuli are used to elicit a single (primary) AP. In the period after the very brief current stimulus is removed the primary AP is followed by an ADP, which can, when sufficiently large, result in production of one or more secondary APs. An ADP of this nature was present in many (67%) Re neurons. Examples of a subthreshold and a suprathreshold ADP are show in Figure 3.13, note the intense short burst of firing produced by the latter.

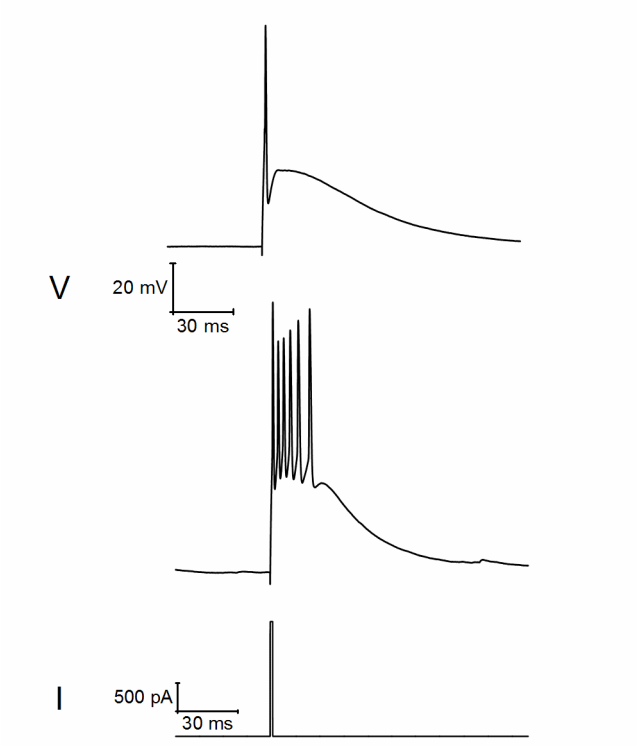

Figure 3.13. After-depolarising potential in Re neurons following a single spike. Two sample traces (top) of the voltage response following generation of a single spike elicited by a short (2 ms), strong (2 nA) square current injection (bottom). (V = Voltage, I = Current).

3.3.6 Action potential production in response to αEPSC current injections.

Although “square-wave” current injections in current-clamp recordings are a very useful and standard means to characterise the excitability of neurons, they are not particularly representative of how cells are activated *in vivo*. To examine how physiological synaptic inputs might drive firing in Re neurons *in vivo*, an approach was used in which current stimuli with EPSC-like waveforms (αEPSCs) were applied to Re neurons during current clamp recordings, an approach previously employed to study the basis of high frequency bursting in hippocampal CA3 pyramidal cells (Brown & Randall, 2009). To facilitate interpretation, and to parallel the datasets described above for conventional “rectangular” current stimuli (Fig 3.6, 3.7, 3.10, 3.11, 3.13), these stimuli were applied from a defined pre-stimulus membrane potential of -80 mV, at which spontaneous firing is absent. Stimuli were examined in which the decay rate of the injected current was varied across a 4-fold range (Fig 3.14), and also examined different stimulus peak amplitudes between 50 and 250 pA (Fig 3.15).

When sufficiently large (e.g 250 pA), αEPSC stimuli produced AP generation in 100% of Re neurons maintained at a pre-stimulus potential of -80 mV. In contrast, 50 pA stimuli almost always failed to produce APs (Fig 3.15B) and instead produced a subthreshold EPSP like waveform. With sufficiently large stimuli the αEPSC typically produced a high frequency (100-250 Hz) burst of 2 or more AP, as exemplified by Figure 3.14A. Furthermore as the decay of the αEPSC was slowed the mean spike output increased, approximately doubling as the decay time constant was lengthened from 5 to 20 ms.

A feature of the spiking response to αEPSC stimuli was that the AP firing often occurred considerably after the peak of the injected current. Indeed, with just suprathreshold αEPSCs (i.e. 150 pA peak amplitude) and a 5 ms decay time constant the first AP occurred after the αEPSC waveform had decayed practically to baseline (Fig 3.15A+C). Even with the strongest αEPSC stimuli examined (250 pA) the first AP occurred some 5-12 ms after the peak of the current injection. In either case it was generally apparent that the αEPSC activated another subthreshold depolarizing current that in turn drove the cells towards their AP threshold.

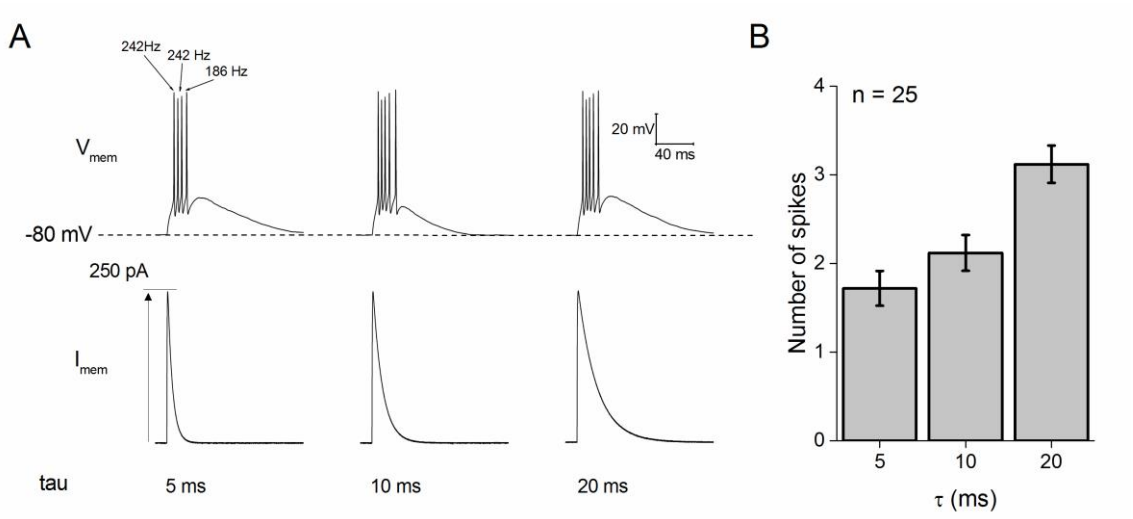

Figure 3.14. αEPSC current injections can elicit high frequency burst firing in Re neurons. (A) Sample voltage responses to 250 pA αEPSC current injections with time constants of 5, 10 and 20 pA, respectively. Note the resultant high frequency bursting observed in many cells. (B) A graph plotting the number of AP elicited versus the time constant of the αEPSC injected. As the time constant of the current injection increases so does the number of evoked APs.

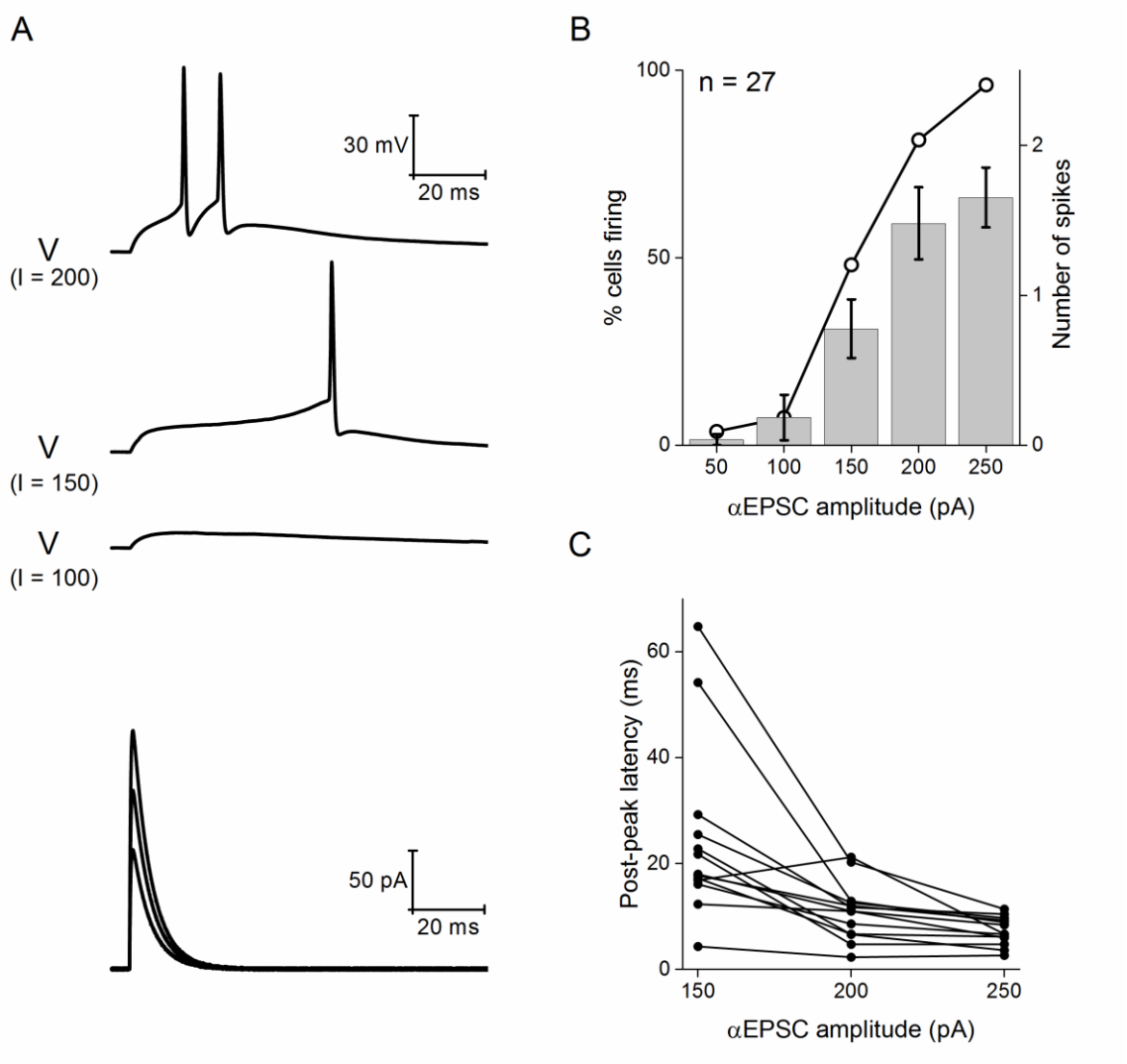

Figure 3.15. AP production of Re neurons in response to αEPSC current injections of varying sizes. (A) Sample voltage responses (top) to incrementally large αEPSC injections (decay tau = 5 ms) ranging from 50-200 pA (bottom). (B) Graph plotting the mean number of spikes (column) and the percentage of neurons firing any spikes (line and symbol) in response to an αEPSC current injection with decay tau = 5 ms. (C) A plot of the post-peak latency (i.e. the time after the peak of αEPSC the 1st AP fires) vs αEPSC amplitude (tau decay = 5 ms).

3.3.7 Firing behaviour in response to square current potentials are voltage dependant

The excitability data described above were collected from neurons placed at a set prestimulus membrane potential of -80 mV prior to delivery of a current stimulus. This level lies in the negative tail of the range of membrane potentials seen in the Re population *in vitro* (Figure 3.1C). In a subset of cells, additional datasets were collected from a somewhat more depolarized pre-stimulus potential of -72 mV, although still one at which spontaneous spiking at rest was absent (Fig 3.16A). These recordings demonstrated that quite substantial changes in aspects of the excitability profile of Re neurons arose when their membrane potentials were changed by just a few mV. Perhaps somewhat surprisingly, depolarizing the pre-stimulus membrane potential by 8 mV had no effect on the total AP output observed during the 500 ms depolarizing current pulses of various amplitudes. Thus, very similar spike numbers were observed for each level of stimulus (Fig 3.16B) and the relationship between percentage of cells firing at least 1 AP and injected current was almost identical (Fig 3.16C). However, on visual examination of the voltage traces it was clear that the original high frequency AP burst seen in the majority of cells at -80 mV (Fig 3.10 & 3.11) was almost always absent in cells resting at -72 mV, as exemplified in Figure 3.16A. This is also reflected in the pooled data plotted in Figure 3.16D which present the mean instantaneous frequency for the first interspike interval elicited by each level of current injection. The initial spiking rate is around 5 to 8 times faster in the cells resting at -80 mV. In a similar vein, whereas 50-60% of cells at -80 mV produced a first spike pair with instantaneous frequency of 100-330 Hz, this was only around 5% for cells at -72 mV, and in this small population spiking did not exceed 155 Hz. The reason for the very similar total AP counts during the entirety of the 500 ms stimulus (Fig 3.16B) was that the average rate of steady state spiking in the latter part of the current stimulus was approximately 10% higher in the cells starting from -72 mV.

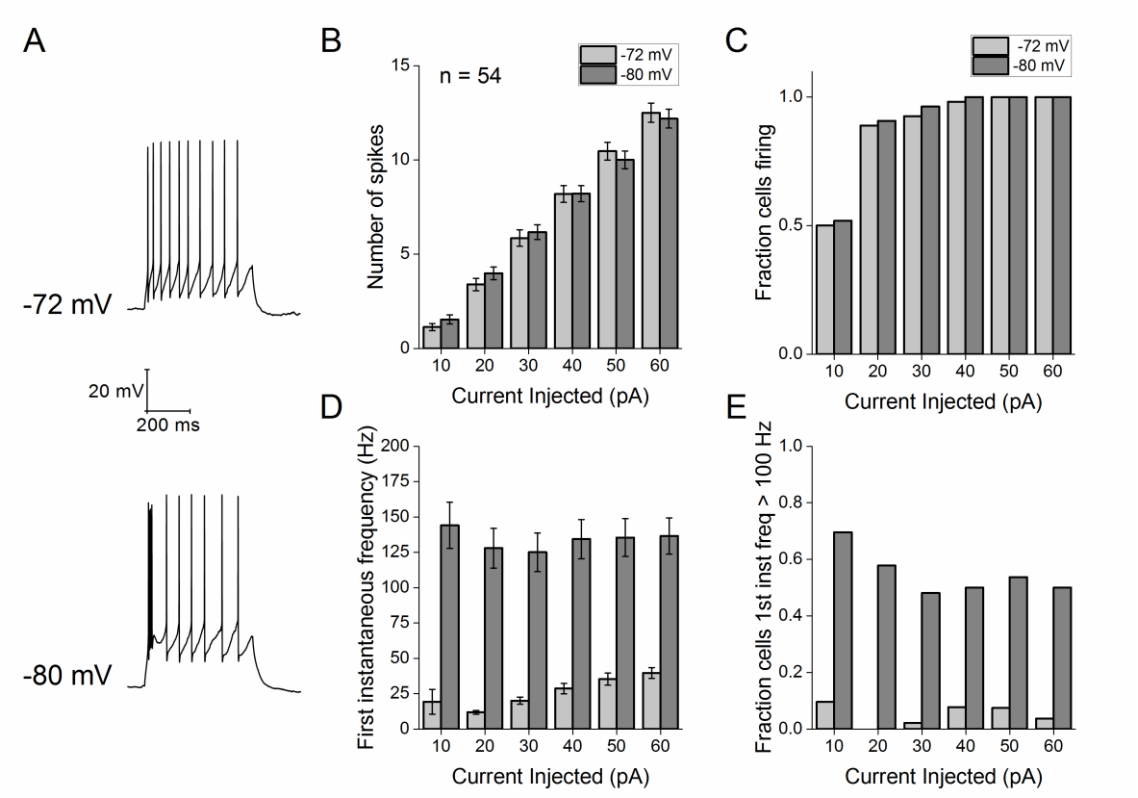

Figure 3.16. Firing behaviour of Re neurons in response to square current injections are dependent on membrane holding potential. (A) Sample voltage responses to a 60 pA square current injection applied from pre-stimulus membrane potentials of -72 and -80 mV. (B) Graph showing the average number of spikes fired in response to 6 depolarising current injections (10-60 pA) from a V_m of -72 or -80 mV. Error bars represent SEM. (C) Graph showing the fraction of cells firing one or more AP for each current injection. Number of spikes fired or the fraction of cells firing in response to current injections were unaffected by V_m. (D) An illustration of the average instantaneous frequency between the first two spikes fired in response to a depolarizing stimulus of the indicated amplitude. (E) A graph showing the fraction of cells firing two action potentials at a frequency greater than 100 Hz. Both the average first instantaneous frequency and fraction of cells firing with a first instantaneous frequency >100 Hz were significant decreased by depolarising the membrane by 8 mV.

3.3.8 Electrophysiological and pharmacological evidence for a T-type Ca^{2+} conductance

The presence of both hyperpolarization-induced rebound firing in the absence of significant sag (Fig 3.7, 3.9), and the sub-threshold depolarizing potentials that trigger subsequent high frequency firing when Re neurons are depolarized from more negative potentials (Fig 3.10, 3.11, 3.14) are suggestive of the presence of T-type (Ca_V 3 family) Ca^{2+} channels. Classically these channels have a low threshold for activation (more negative than AP threshold), and are readily inactivated when the resting potential becomes slightly depolarized (Perez-Reyes, 2003). Commensurate with this, the Allen Brain Atlas (http://mouse.brain-map.org) (Lein *et al.*, 2007) indicates robust expression of the Ca_V 3.1 isoform of low threshold Ca^{2+} channel in Re. Furthermore, two previous studies (Graef *et al.*, 2009, 2011) have demonstrated expression of T-type Ca^{2+} channel messenger RNA (mRNA) and classical low threshold currents in the midline thalamus.

The size and geometrical complexity of CNS neurons in brain slices or *in vivo*, combined with their typically very large current densities can greatly hinder high fidelity voltage-clamp analysis of voltage-gated ionic conductances. However, with sufficient care and suitable protocols it is possible to gather some useful information particularly with regards to modest sized, slower-gating conductances, which suffer less from space-clamp associated issues. Voltage-clamp recordings were made pairing our standard pipette solution and our standard aCSF supplemented with 500 nM TTX (to eliminate voltage-gated sodium currents). Initially an incremental series of voltage steps from a holding potential of -85 mV were applied, producing mixed currents like those presented in Figure 3.17A. Notably with modest depolarizations, for example to -63 mV, only inward currents were observed, whereas once the test potential became depolarized beyond about -45 mV large outward-going, partially inactivating currents began to dominate the response. These outward currents, which are carried by K^+ ions, rapidly increased in size to many nanoamps if depolarization was increased further. The voltage-dependence and waveform kinetics of the inward current elicited with modest depolarizations was highly suggestive of a classical low threshold, T-type current. A series of small voltage steps separated by 2 mV increments was used to further profile the inward current within the

narrow voltage range where it was the predominate current (Fig 3.17B). The current activated at the negative voltages expected for a T-type current and largely inactivated over around 60 ms of depolarization. The steady state inactivation data for these channels was also gathered by varying the holding potential prior to an invariant step to -65 mV (Fig 3.17D) and profiled the rate of recovery from inactivation with a standard variable interval two step protocol (Fig 3.17E).

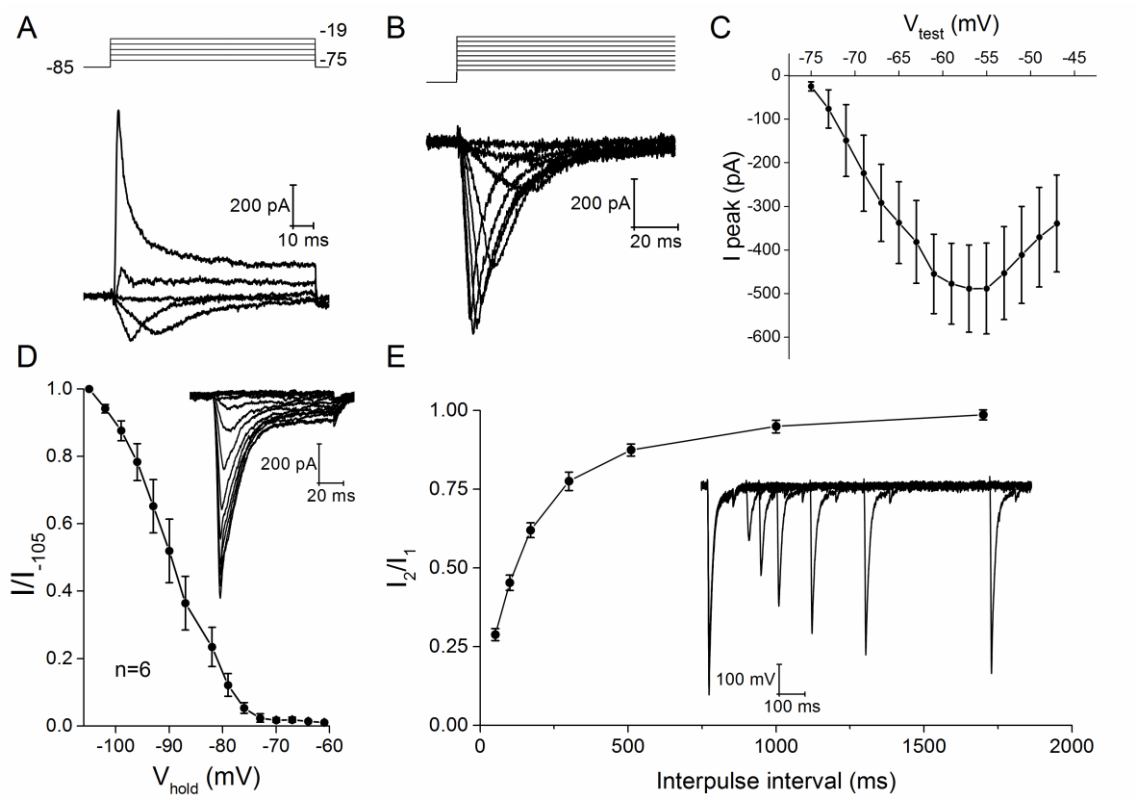

Figure 3.17. Gating properties of low-threshold inward currents in Re neurons. (A) Voltage-clamp protocol (top) and resultant current responses for a series of 8 mV incremental depolarising voltage steps applied from a holding potential of -85 mV. (B) Sample voltage trace and the subsequent current response to a series of 2 mV incremental depolarising voltage steps (from -75 – -47 mV) from a pre-stimulus holding potential of -85 mV. (C) Average I-V plot of the observed peak inward current in response to this series of 2 mV voltage steps. (D) Inactivation curve showing the average voltage at which the T-type calcium current inactivates in Re neurons. (E) Line and symbol plot showing the rate of recovery from inactivation of T-type Ca^{2+} current determined with a standard variable interval two pulse protocol.

The pivotal neurophysiological roles of low threshold Ca^{2+} channels have been widely studied in other thalamic neurons for many years (Pape *et al.*, 2004), although the availability of reasonably potent and selective T-type channel blockers is a more recent advance (Xiang *et al.*, 2011). Application of one such molecule ML-218 (3 µM) caused a substantial decrease in the amplitude of the ADP elicited following a single short strong current injection (Fig 3.18A). The drug also reduced the instantaneous frequency of the first pair of spikes produced by a 500 ms depolarizing current step, without changing the total spike output from the stimulus. Finally, the drug eliminated the rebound firing produced when Re neurons resting at -70 mV (a membrane potential where 59% of neurons exhibit rebound firing following a hyperpolarising step) were hyperpolarized for 500 ms with a -50 pA current stimulus. The data in Figures 3.17 and 3.18 together indicate that T-type channels play a key role in the ability of Re neurons to produce very high frequency firing after transient sojourns at negative membrane potentials.

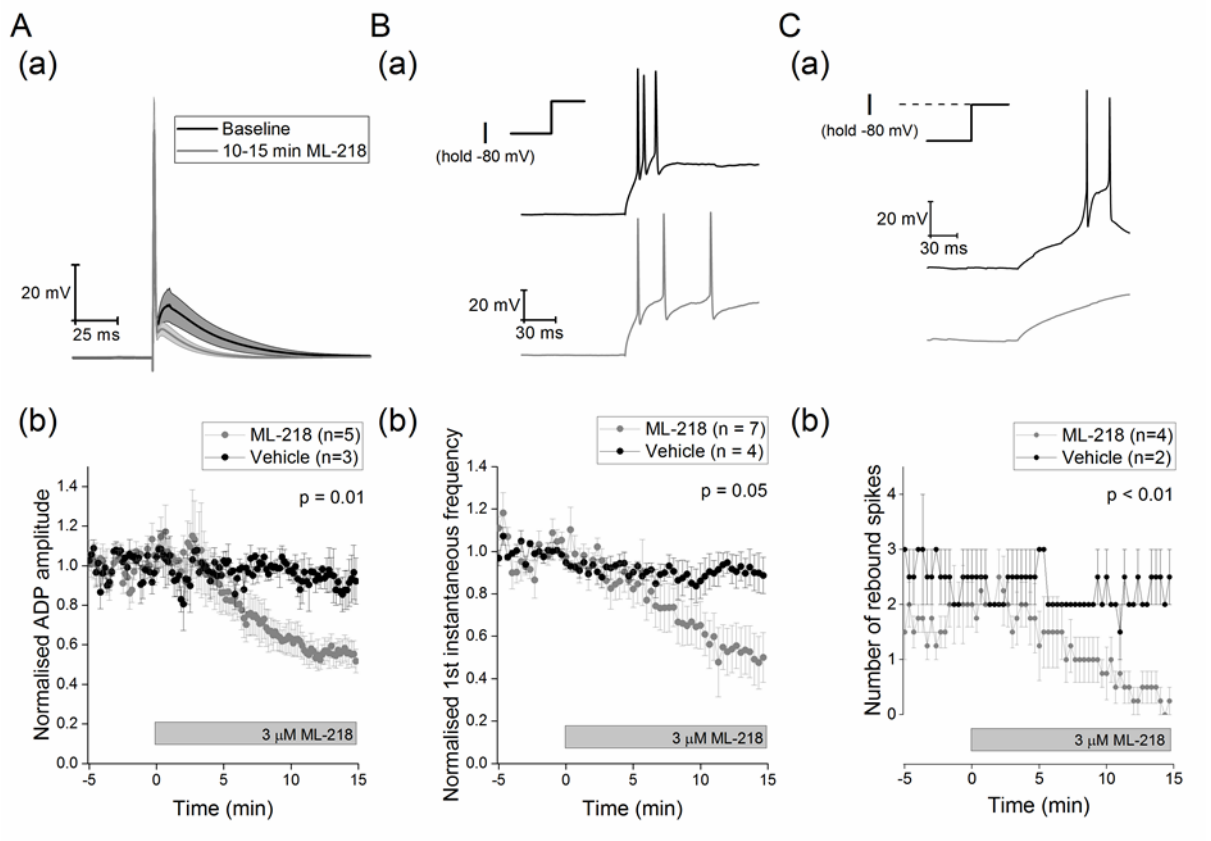

Figure 3.18. Pharmacological inhibition of T-type calcium channels alters firing properties in Re neurons. (A) Application of the T-type calcium blocker ML-218 (3 μM) reduces the amplitude of the ADP that arises following a single spike. (a) Average trace of the waveform of a single spike elicited by a short, strong current injection (2 ms, 2 nA) recorded during a 5 minute baseline (black), and during the last 5 minutes of a 15 minute exposure to 3 μM of T-type calcium channel blocker ML-218. Shaded area represents SEM. (b) A plot describing the time course of the effect of ML-218 on the average ADP amplitude normalised to the pre-drug baseline. (B) (a) Sample trace of the voltage response to a 100 pA depolarising current injection just prior to application of ML-218 (black) and following 15 minutes of exposure to ML-218 (grey). (b) A graph showing the effect of ML-218 on the first instantaneous frequency normalised to the predrug baseline. (C) (a) Sample traces showing the repolarisation driven rebound spiking following a -50 pA hyperpolarising current injection just prior to application of ML-218 (black) and following 15 minutes of exposure to ML-218 (grey). (b) A plot showing the effect of ML-218 on the average number of rebound spikes observed following repolarisation. All p values represent paired comparisons of the selected measurement between the pre-drug baseline and the final 5 minutes of the drug application.

3.3.9 Reduction in burstyness through activity-dependent intrinsic plasticity

The data in Figure 3.1 - 3.18 outline core aspects of the neurophysiology of rostral Re neurons, in particular their intrinsic excitability properties. Although often tonically firing at around 8 Hz at rest, after short periods at sufficiently negative potentials (i.e. ~-80 mV) the cells are capable of producing very high frequency burst firing, sometimes reaching instantaneous frequencies in excess of 300 Hz. The presence of an ML-218-sensitive, low threshold Ca^{2+} conductance seems central to the production of this high frequency burst firing. Intrinsic neuronal plasticity describes how the excitability properties of neurons can be modified by "experience" delivered experimentally as a conditioning stimulus of some form. For example, the burstyness of hippocampal pyramidal neurons can be persistently reduced either by brief cell-intrinsic activity patterns or via the activation of metabotropic glutamate receptors at synapses (Brown & Randall, 2009; Brown *et al.*, 2011).

In vivo, the Re exhibits a strong theta oscillation and the firing of many neurons is synchronized to this (Jankowski *et al.*, 2014, 2015; Ito *et al.*, 2015). Therefore a theta-paced burst firing protocol was employed as a candidate conditioning stimulus for induction of intrinsic plasticity in Re neurons. Notably a similar protocol has proved effective in persistently altering excitability of hippocampal neurons (Brown & Randall, 2009). In whole cell current clamp recordings the prestimulus membrane potential was maintained at -80 mV and a data sweep was collected every 10 s. In all sweeps a 2 nA, 2ms stimulus was first applied to evoke a single spike and subsequent ADP (as in Figures 3.13 and 3.18A); notably we did not use cells in which the ADP triggered AP firing as this complicates quantification of this afterpotential and consequently experimental interpretation. In every second sweep the short-strong ADP eliciting stimulus was followed 1.5 s later by a 500 ms, 50 pA hyperpolarizing current pulse which could be used to measure passive properties (as in Figure 3.7B). We ran this protocol for at least 5 minutes to collect baseline data prior to applying the conditioning stimulus. The conditioning stimulus consisted of using short (2 ms) strong (2 nA) current injections to drive the cells to spike 5 times at 150 Hz (Fig 3.19A), this was repeated continuously every 200 ms for 15 s (thus a total of 75 bursts of 5 spikes in 15 s). During application of the conditioning stimulus the membrane potential was allowed to follow its desired trajectory rather than endeavouring to keep it at

the fixed prestimulus level of -80 mV. Following application of the 15 s conditioning stimulus we returned to the stimulus protocol employed in the pre-conditioning period and followed the cell for a further 15 mins. In this post-conditioning period, as in the preconditioning period, the interstimulus membrane potential was again maintained at -80 mV.

As illustrated in Figure 3.19A+B, application of the 75 spike, theta-patterned conditioning protocol caused a progressive, acute change in the membrane potential of Re neurons. Thus, the cells on average hyperpolarized by over 6 mV, a change that followed an exponential trajectory that was largely complete after circa 9 theta burst cycles (i.e. 45 AP). Notably, this change did not stop the current stimuli from producing AP although the post-burst AHP was lost, likely as a result of the decreased driving force for K^+ ion fluxes that mediate the AHP. Notably this change was transient and cells returned to their pre-conditioning membrane potential within <1 min. In line with this the bias current used to keep the cells at -80 mV in the pre- and post-conditioning periods was not different.

More interestingly, following the conditioning stimulus a persistent change in the intrinsic excitability of Re neurons was observed. This was manifest as a decrease in the amplitude of the ADP observed following a single AP (Fig 3.19C+D). Indeed, the ADP was largely absent in most cells and the amplitude measured was just that afforded by the need for the membrane to discharge (see Brown and Randall, (2009) for a discussion of this). The conditioning protocol acutely caused a 10-15% decrease in R_i but this disappeared within 40 s and no lasting changes to R_i were observed. Thus, in the last 5 minutes on the experiment the R_i was 100 ± 3% of its baseline value ($P>0.98$).

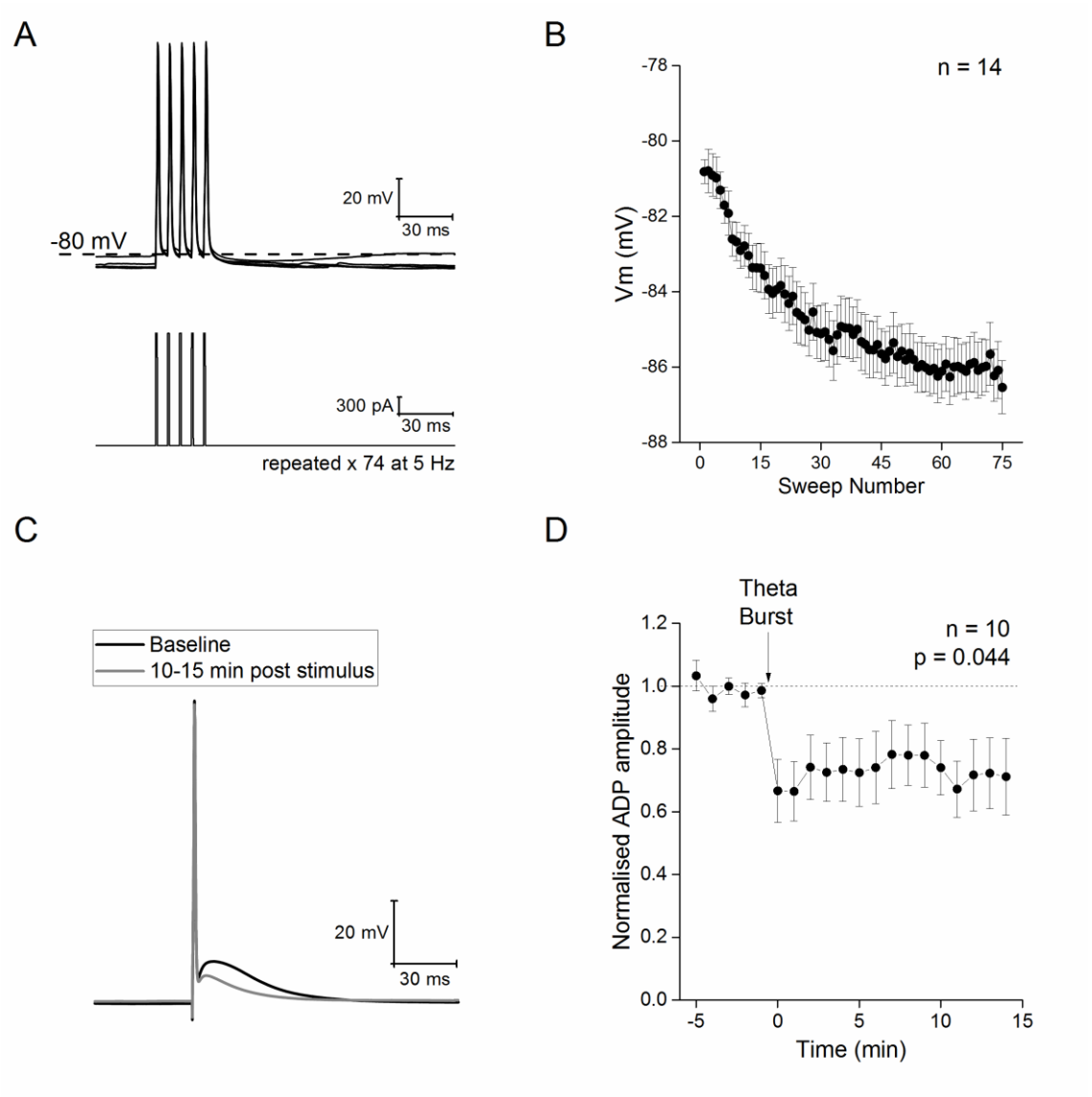

Figure 3.19. Re neurons exhibit intrinsic plasticity of the ADP. (A) Sample voltage (top) and current (bottom) traces of a theta burst induction protocol used to induce intrinsic plasticity. Briefly each burst was driven induced with 5 short, strong (2 ms, 2 nA) current injections at a frequency of 150 Hz. 75 bursts were induced at 5 Hz in order to induce plasticity. (B) A plot showing the modest hyperpolarisation in the membrane potential that developed as the induction protocol progressed. (C) Voltage trace from an example experiment showing the average response to a single spike during the baseline period (black) and 10-15 minutes after the conditioning protocol (grey). (D) A plot showing the timecourse of the baseline-normalised ADP amplitude from 10 experiments.

3.4 Discussion

TC neurons, have been the subject of substantial neurophysiological investigation over the last 40 years. Amongst the most widely studied TC neurons are those which convey sensory information within either the visual or somatosensory systems, for example those whose cell bodies reside in the lateral geniculate and ventrobasal nuclei. Such studies have produced a general view of the intrinsic electrical properties of TC and how these shape the contribution of these neurons to network activities associated with sensory processing (Jahnsen & Llinás, 1984; McCormick & Huguenard, 1992; Turner *et al.*, 1997; Williams *et al.*, 1997; Hughes *et al.*, 1999; Pape *et al.*, 2004; Llinas & Steriade, 2006; Huguenard & McCormick, 2007).

In this study the cell-level neurophysiological properties of Re neurons were characterised. Unlike classical first order TC neurons of sensory pathways, these higher order cells of the midline thalamus receive little if any direct sensory information, but still both send and receive extensive cortical connections (Vertes *et al.*, 2015). This work specifically focussed on neurons located in the rostral portion of Re because this is the predominant source of the afferent projections to the hippocampal and prefrontal circuits which have recently generated considerable interest (Varela *et al.*, 2014). Furthermore, from an anatomical perspective, rostral Re is also easy to identify unequivocally in murine brain slices. Although beyond the scope of this first study, in future it would be of interest to compare the properties of the rostral and caudal aspects of Re. Also given the diversity of intrinsic properties observed it would also be of interest to examine if there is a relationship between defined post synaptic target of these cells, established with retrograde labelling methods, and their neurophysiological properties at the cellular level. In addition, future studies should investigate whether the neurophysiological properties of Re neurons differ based on the expression of Ca^{2+}-binding proteins. This would involve post hoc immunostaining of neurons recorded from with biocytin/neurobiotin included in the recording electrode. The above experiments would aid researchers seeking to understand the role of the Re in behaviour (e.g. by allowing targeted optogenetic stimulation of specific subsets of Re neurons) and disease, for example understanding network consequences of the reduction of calretinin expressing Re neurons to the HPC in epilepsy (Drexel *et al.*, 2011).

Brain slice preparations encompassing the rostral Re are somewhat limiting for those wishing to examine the effects of pharmacological agents, especially in mice. This is because the region is both relatively small and resides on the midline, meaning each mouse provides only one slice (unlike, for example, the HPC or cerebellum where perhaps 10 unilateral slices can be obtained per animal). Efforts were taken to stringently avoid recording from cells in slices that have been previously treated with a drug during a prior recording. Consequently, this typically limits pharmacological analysis to studying effects of one acute drug exposed cell per animal. Our only exception to this is studying cells in slices chronically treated with drugs to establish a particular background condition– for example, use of synaptic blockers throughout all recordings.

In whole cell recordings the majority of Re neurons were found to be relatively depolarized at rest. A major consequence of this was the presence of robust spontaneous firing of fast rising and decaying AP in the majority of cells. This firing often, although not always, occurred in a tonic fashion with a mean frequency around 8-9 Hz. These observations of spontaneous tonic firing in the majority of neurons are in agreement with Re recordings performed from slices obtained from both younger (6 weeks, data not shown) and older mice (>1 year, see chapters 4-6).

The depolarized membrane potential and resultant spiking does not seem to arise as a consequence of entering the whole cell mode as spontaneous spiking was also clearly evident in loose patch or cell attached recordings in which the cytoplasmic contents are undisturbed. Furthermore, in our laboratory exactly the same recording solutions and conditions result in much more negative resting potentials in other neurons, for example both CA1 and CA3 pyramidal cells (Brown & Randall, 2009; Booth *et al.*, 2016*b*) as well as various cortical neurons (Tamagnini *et al.*, 2014; Dawson *et al.*, 2015; Booth *et al.*, 2016*a*). Interestingly the depolarised membrane potential also contrasts starkly with the hyperpolarised membrane potential observed in both first and other higher order thalamic nuclei (Jahnsen & Llinás, 1984; Varela & Sherman, 2007; Kolaj *et al.*, 2012). Indeed, to the best of our knowledge, in no other thalamic relay nuclei have the majority of neurons been reported to fire spontaneously when recorded during the light stage of a 12:12 day-night cycle. Although not supported by our loose patch/cell-attached observations, in which the cytoplasmic contents are

undisturbed, the depolarized membrane potential seen may have reflected the relatively depolarized Cl- equilibrium potential our intracellular solution produces combined with a significant level of tonic GABAergic drive. However blocking $GABA_A$ receptors with GABAzine produced little effect on either membrane potential or firing behaviours. Furthermore, blocking $GABA_A$ receptors did not appear to result in substantial increases in overall network activity in the Re, whereas in HPC and many areas of cortex pharmacological elimination of ongoing GABAergic inhibition generally produces huge hypersynchronous epileptiform burst events (Brown *et al.*, 2003).

Although the properties of synaptic inputs to Re neurons are not a major feature of this study, which instead focusses on intrinsic properties, it is notable that Re cells receive a significant ongoing spontaneous synaptic barrage. Indeed, even when spontaneous firing of neurons throughout the slice was eliminated with TTX, Re neurons received a substantial barrage of spontaneous miniature synaptic input. The quantal sizes of many of these events measured in voltage clamp, combined with the relatively high R_i of Re neurons would indicate that they are individually capable of transiently driving the membrane potential a few mV depolarized. A thorough study of the properties and plasticity of key defined synaptic input pathways to Re neurons is unquestionably required to better understand how this component of the higher order thalamus contributes to circuit function. Optogenetic approaches would seem highly suited to this objective. Having said this, our work reveals that blocking all spontaneous ionotropic, amino acid-mediated synaptic function had no discernible effect on the rates of spontaneous spiking or the distribution of membrane potentials within the reduced complexity of a brain slice preparation.

The predominant spontaneous firing frequencies of Re neurons corresponds well with the mean firing rates of Re neurons described *in vivo* (Ito *et al.*, 2015), as well as the robust theta rhythm that can be recorded *in vivo* with electrodes implanted into Re. Indeed, autocorrelations of *in vivo* extracellular recordings of the firing of single Re neurons also reveals a strong phase locking to theta rhythms (Jankowski *et al.*, 2014). Importantly, in brain slices, normal CNS circuit connectivity and resultant network activity is lost, consequently the observation of spontaneous firing at rates in the theta band suggest that Re could be an intrinsic theta generator and may in turn relay this activity to the limbic structures

to which it is connected. The fact that many Re neurons fired tonically at ~8 Hz in blockers of glutamatergic and GABAergic synaptic transmission lends further support this concept of a theta range oscillator intrinsic to Re neurons. Full testing of the idea that Re can act as a theta generator will require *in vivo* experiments, for example using optogenetic or pharmacogenetic manipulation of Re neurons whilst recording network behaviours in Re and defined projection targets. One initial study of this nature indicates that theta activity in hippocampal area CA1 is preserved when Re is lesioned with ibotenic acid or firing rates are optogenetically reduced (Ito *et al.*, 2015). This may be because the primary hippocampal targets of Re projections appears to be interneurons, rather than pyramidal cells (M. Craig and C McBain, personal communication).

Although seemingly able to intrinsically fire spikes tonically in the theta frequency range in the absence of synaptic drive, the spiking behaviour of Re neurons *in vivo* will unquestionably be modulated and modified by various forms of excitatory and inhibitory synaptic drive into these cells. These synaptic influences will arise from multiple sources (McKenna & Vertes, 2004), most notably various components of the limbic system. Synaptic inhibition is likely to pivotally involve input from the Rt and the zona incerta (Cassel *et al.*, 2013). As outlined above, for those wishing to understand Re contribution to CNS circuits the functional properties of these afferent inputs to Re are worthy of much more experimental consideration in the future.

Compared to the cortical and hippocampal principal cells previously recorded *in vitro* using similar solutions at similar temperatures, Re neurons have a much higher R_i. Hence, the average value in this study was over 600 MΩ, for example, adult CA1 pyramidal cells are typically circa 130 MΩ, pyramidal cells in layer 2 of perirhinal cortex average 100 MΩ (Tamagnini *et al.*, 2014) and layer 2/3 stellate cells in the dorsal end of entorhinal cortex average 40 MΩ (Booth *et al.*, 2016*a*). To some extent their high R_i likely reflects the smaller size of Re neurons (capacitance circa. 50% lower), but also points to a relative paucity of active background K^+ channels. Rodent TC neurons in other nuclei recorded with broadly similar methods (patch clamp in slices, ~32-35 C, Kgluconate pipette solution) typically have an R_i of ~200 MΩ and resting potentials around -60 to -70 mV (Brunton & Charpak, 1998; Augustinaite & Heggelund, 2007; Samios & Inoue, 2014). Notably however, I have been unable to find any methodologically

equivalent (i.e. patch clamp at circa 33°C with Kgluconate intracellular solution) studies of other thalamic nuclei at the same adult age as our mice (circa 4 months). Indeed, many TC neuron studies employ much younger rodents often <=3-4 weeks of age. Cells in such animals might be expected to have higher input resistances than those of true adults as this feature of membrane physiology generally decreases with age.

A paucity of active background K^+ channels is also is a likely contributor to the depolarized membrane potential of Re neurons compared to various cortical and hippocampal pyramidal cells studied under identical conditions. The combination of depolarized membrane potentials and high input resistances found in Re neurons mean subthreshold cells need little depolarizing current to initiate firing. For example, even when set at -80 mV, around the 95^{th} percentile of membrane potentials, only 20 pA of current is required to bring around 80% of the cells to firing threshold (Figs 3.6 and 3.10). The large input resistance of Re cells also means they have a comparatively long membrane time constant averaging almost 40 ms. This means voltage changes in either direction are relatively slow. This maybe particularly pertinent for shaping the decay of synaptic potentials and also spike after-potentials. For example, the timecourse over which the AHP declines seems to pace firing at rest and anything which reduced input resistance without causing substantial hyperpolarization could speed firing. This could potentially occur, for example, through a GABAergic shunting conductance if the chloride equilibrium potential was not too negative. Additional studies utilizing gramicidin-perforated patch or dynamic clamp could be very informative in this regard.

The I_h current and the sag it produces in voltage recordings is a cardinal feature of other TC neurons. This conductance plays a role in determination of resting potential (Meuth *et al.*, 2006; Amarillo *et al.*, 2014) and its gating has long been considered crucial to facilitate transitions between hyperpolarised potentials where burst firing predominates and more depolarised modes of tonic firing. It is also considered crucial to the emergence of rhythmic activities in the thalamus (McCormick & Pape, 1990; Pape, 1996). Notably Re neurons appear to lack hyperpolarization-activated sag and I_h-like currents (Figs 3.7B and 3.9), although these exact same recording conditions are capable of supporting robust I_h-mediated currents in other cells types (Booth *et al.*, 2016*b*, 2016*a*). The apparent

absence of I_h-like currents and sag is also in line with the relative lack of HCN channel expression in Re as reported in the Allen brain atlas (www.mouse.brain-map.org).

One important caveat is that given the relatively long τ of Re neurons (Fig 3.7), current passing through HCN isomers with faster gating kinetics (i.e. HCN1) would potentially be masked in Re neurons. Thus while one cannot say with absolute certainty that Re neurons express no functional HCN channels, the HCN2 currents typically associated with thalamic relay neurons are conspicuously absent. In contrast to other TC cells (Meuth *et al.*, 2006; Amarillo *et al.*, 2014), the lack of HCN2 mediated I_h and associated sag in Re neurons suggests other mechanisms account for their depolarised V_m. It also seems likely, the lack of functional I_h could produce telling consequences for how Re neurons contribute to their cognitive networks, and suggest substantial differences from the behaviours of other more widely studied TC neurons.

To investigate the intrinsic properties underlying the neurophysiological profile of Re neurons, the study was extended to look at how various current stimuli triggered AP production. In this work to reduce the variability that arises from cell to cell difference in resting potential the prestimulus resting potential was initially set to -80 mV, since at this negative level there is no on-going spontaneous firing which also simplifies interpretation of data. From this hyperpolarized prestimulus membrane potential sufficiently large depolarizing current injections produced firing. For over 80% of cells only 20 pA of applied current was required to produce spiking. In many cells the first 2-4 spikes arrived in the form of an initial high frequency spike burst, such that the mean instantaneous frequency of the first spike pair was around 120 Hz (Figs 3.10, 3.11 & 3.16)- although observations in excess of 200 Hz were not uncommon. This was the case with either the weakest or strongest suprathreshold stimuli (Figs 3.10 and 3.11). Indeed, with the weaker current stimuli, often only an initial high frequency burst of spiking was observed (Figs 3.7A & 3.10C), whereas with stronger stimuli, for example 30 or 60 pA, the initial burst was typically followed by more tonic spiking at 20-30 Hz (Figs 3.10 and 3.11). This behaviour is typical of TC neurons however Figure 3.11 highlights the variety of observed responses. The initial frequency of firing of a Re neuron correlates significantly with the size of its observed ADP ($r = 0.62$, $p < 0.001$) suggesting that the variable expression of T-type calcium channels in these

neurons could be responsible for the observed diversity. Neurons in the Re have been classified into 4 groups based on the differential expression of Ca^{2+} binding proteins CB and CR (Bokor *et al.*, 2002). As such it also seems plausible that differential calcium buffering capabilities between groups could contribute to the observed diversity. Given that the Re appears to be first thalamic nucleus in which such variety of responses from a fixed potential has been reported, future studies should focus on the underlying cellular mechanisms responsible.

Additionally some degree of diversity was seen in the patterns of spontaneous firing in the Re. Unquestionably most cells fired in a tonic fashion at 2-16 Hz, although more intermittent or bursty patterns of firing were seen in a minority of cells. Notably, the only cells which spontaneously fired high frequency spike bursts where those with very negative mean membrane potentials. In these cells, the occasional spontaneous bursts of spikes which could exceed instantaneous frequencies of 200 Hz, were seen atop an initiating depolarizing transient, which based on others observation here, likely reflects a burst of feedforward activation of low threshold Ca^{2+} channels. Examining the passive membrane properties of Re neurons separated based on their basal firing properties gave some insight into the diversity of firing patterns observed. Neurons which do not fire in the absence of external stimuli displayed a longer membrane time constant and an increased membrane capacitance (Fig 3.8B+C). This suggests that in the Re “silent” neurons were generally of larger size than neurons displaying regular firing at rest although a detailed morphological study would be required to confirm this. There was no statistically significant differences in firing frequency or patterning of APs generated in response to depolarising current stimuli between individual neuronal populations grouped based on their basal firing properties (Fig 3.12).

Notably the sample size of some of the populations grouped as such is extremely small (e.g. burst firing neurons, n = 6) and it is possible that such comparisons suffer from type II error associated with a lack of statistical power. It is also notable that although differences can be observed in passive and active properties of Re neurons based on basal firing properties, significant variation is observed within groups separated in this way. In light of this intra-group diversity and the difficulty generating a large sample size (imposed by the relatively low prevalence of Re neurons falling into these categories), future studies looking to categorise Re

neurons should attempt to do this with the help of viral tracing and immunohistochemistry (discussed above) methods rather than relying purely on analysis at a neurophysiological level.

High frequency burst spiking was also notable when cells at -80 mV were activated with short (2 ms) strong (1-2 nA) current stimuli that rapidly elicited a single primary AP (Fig 3.13) or αEPSC current stimuli (Figs 3.14 & 3.15). In these cases the spike burst occurred after the current stimulus was over, indicating that pro-spiking neurophysiological processes initiated during the current stimulus continued. These processes were apparent in the ADP that followed the single spike driven by short strong current injections (Fig 3.13) or the deviations from a typical EPSP waveform in the αEPSC-driven burst firing (Figs 3.14 & 3.15).

The high-frequency burst firing in response to 500 ms depolarizing stimuli was eliminated when the Re cells where placed at -72 mV prior to application of the current stimulus. At this potential, the low threshold inward current with classical T-type channel biophysics seen in voltage-clamped Re neurons is essentially completely inactivated, whereas at -80 mV some 15% of the channels appear available (Fig 3.17D). In line with this, high frequency bursting driven by depolarizing current stimuli, both short strong (Fig 3.18A) and longer and weaker (Fig 3.18B) as well as from an “anodal break” following hyperpolarization are also attenuated by the selective T-type blocker ML-218.

Thus, Re neurons exhibit radically different firing outputs to depolarizing stimuli depending on their membrane potential prior to the arrival of the stimulus. A shift of only 8 mV completely reconfigures the resultant spiking response. This appears to be predominantly due to the presence of low threshold, T-type Ca^{2+} channels. The currents arising from these voltage-gated channels have long be shown to play a prominent role in the neurophysiological profile of various thalamic neurons, in particular those of the Rt and the lateral geniculate. Furthermore, two of the very few prior papers employing cellular recordings in the midline thalamic nuclei have focussed on T-type channels and their modulation in rodent models of epilepsy and alcoholism (Graef *et al.*, 2009, 2011). T-type Ca^{2+} channels are effectively activated by EPSP-like waveforms (Warre *et al.*, 2002), and T-type currents have been shown to contribute to the depolarizing envelope of EPSPs in cerebellar Purkinje cells (Ly *et al.*, 2016).

The ability of Re neurons to fire short bursts of AP at very high frequencies either in response to depolarizing current stimuli or through “rebound” following a negative current stimulus is important when considering consequences for the synapses these cells form in the HPC, prefrontal cortex and elsewhere. Due to the effects of short-term synaptic plasticity, the glutamatergic drive generated from a Re afferent pathway exhibiting occasional bursts of spikes at 100-300 Hz will certainly be very different from that produced by tonic 8 Hz firing. Notably, nothing is known about the short-term plasticity of Re projections and related features of synaptic function such as their probability of release and post-synaptic response kinetics.

The synaptic terminations of Re projections into area CA1 of the HPC are concentrated in the stratum lacunosum moleculare, which is also where most temporoammonic inputs from the entorhinal cortex terminate. In this distal dendritic region far from the CA1 pyramidal cell layer, electrical stimulation of axons with small numbers of high frequency bursts produces robust long-term potentiation of excitatory synapses on hippocampal neurons (Remondes & Schuman, 2003; Booth *et al.*, 2014, 2016*b*). Although this long-term synaptic plasticity is frequently attributed to temporoammonic afferents, unquestionably a component of such responses arise from stimulation of Re neurons which have long been known to produce a robust synaptic response in area CA1 (Dolleman-Van der Weel *et al.*, 1997; Dolleman-Van der Weel & Witter, 2000) and also to exhibit robust LTP (Bertram & Zhang, 1999). On this basis, high frequency burst firing of presynaptic Re neurons would seem ideal to drive synaptic potentiation of their inputs to the HPC.

Importantly, our data suggest the means through which Re neurons will communicate with their downstream synaptic partners will depend strongly on their membrane potential. Cells around -65 mV may be tonically firing in the theta frequency range. Assuming these spikes generated in the perisomatic region successfully complete their journey to downstream synapses, post-synaptic responses will be produced every so often, largely dependent on probability of release. One would probably not expect much in the way of EPSP summation or short-term synaptic plasticity. Re neurons more depolarized than -72 mV but not spontaneously firing will not produce high frequency spike bursts when activated, for example by excitatory synaptic drive, and thus may only produce single spikes

or a period of low frequency regular spiking. In contrast Re cells sat at -80 mV or below will likely generate a robust multispike burst on activation that could drive a substantial summated, frequency facilitated EPSP in post-synaptic cells, a response of the sort that might induce synaptic plasticity if repeated a few times. Notably, Re cells do not need to spend long at negative potentials for T-type channels to deinactivate and the ability to generate high frequency spike bursts to emerge. For example 300 ms at -85 mV deinactivates ~80% of T-type channels (Fig 3.17E).

For the reasons described above, both gaining an understanding of the actual membrane potentials of Re neurons *in vivo* and determining key things that control membrane potential are crucial to understanding how Re contributes to the function of CNS circuits in which it sits. For example, metabotropic receptor-mediated IPSPs (produced by activation of $GABA_B$, dopamine D2 or noradrenaline α2 receptors, coupled to GIRK K^+ channels) last at least 500 ms and can often last many seconds (see North & Surprenant, 1985 for example), certainly enough time to deinactivate T-type channels and enable burst firing. Notably Re receives inputs from the ventral tegmental area and the locus coeruleus (Cassel *et al.*, 2013) and there are correlations between expression of α2 receptors in Re and behaviour (Wilmot *et al.*, 1988).

In vitro electrophysiological recordings are generally performed with the expectation, or at least hope, that the recorded neurophysiological outcomes relate to those of the corresponding cells *in vivo*. With faith in this expectation, it is possible to use the data obtained *in vitro* to consider how the neurophysiological properties of the investigated cell shape its functional contributions to the various neural circuits of which it forms part. Such interpretations can be performed at various levels, from the sorts of general ideas voiced here to utilization of the data to aid in the building of computational models. By performing the first substantial cellular level study of Re neurons, our goal here has been to obtain insights of this nature; and accordingly some of the ways the properties we have observed *in vitro* may shape the behaviour of Re neurons in CNS circuits have been discussed.

However, it is prudent to introduce a note of caution; it is certainly possible that the cellular properties documented are not facsimiles of what would be seen with cellular recordings performed *in vivo*. Indeed, the very process of preparing brain

slices would no doubt result in excess depolarisation of Re neurons and could induce significant and long-lasting changes to intrinsic and/or synaptic neurophysiological features of a neuron. However, the task of obtaining over 100 *in vivo* patch clamp (or intracellular) recordings from a deep and relatively small midline structure in the murine brain would be daunting, and if data gathered without the confounds of anaesthesia were required (for example from head-fixed recordings), the challenge might best be described as Herculean.

Consequently, in the absence of equivalent *in vivo* data, this dataset is valuable for those who wish to better understand the contribution of Re to various CNS processes, particularly so when considered hand in hand with what we have learnt from recent *in vivo* investigations of the activity of these neurons in behaving rodents (Jankowski *et al.*, 2014, 2015; Ito *et al.*, 2015) as well as studies that outline changes to Re neurons in disease models (Graef *et al.*, 2009, 2011).

4 The electrophysiological properties of neurons in the rostral nucleus reuniens are unchanged by physiological aging

4.1 Introduction

Although varying in extent between individuals, normal aging leads to a profound decline in cognitive abilities, particularly retention of episodic memories. This decline is paralleled by structural changes in the brain, particularly in cortical regions (Sowell *et al.*, 2003), as well as disruptions in SWS and HPC-mPFC synchrony (Mander *et al.*, 2013).

Alterations to the intrinsic neuronal properties of CA1 pyramidal neurons have been proposed to play a causative role in age related cognitive decline. This work formed a basis for the calcium hypothesis of physiological aging (Gibson & Peterson, 1987; Landfield, 1987; Disterhoft *et al.*, 1994; Khachaturian, 1994) and has centred around alterations to the post-burst AHP, which has been reliably reproduced in CA1 pyramidal neurons (Landfield & Pitler, 1984; Kumar & Foster, 2007; Matthews *et al.*, 2009; Gant & Thibault, 2009). This post burst AHP is dependent on Ca^{2+} entry following AP genesis and results in a reduction in the amount of APs generated in response to a prolonged depolarising stimulus (Gant & Thibault, 2009). A sodium channel dependant reduction in AP threshold has also been observed in CA1 pyramidal neurons (Randall *et al.*, 2012) suggesting that a decrease in the likelihood of AP generation is a key feature of age related neurophysiological alterations.

Recent evidence has supported a role for T-type Ca^{2+} channels in aging related neurophysiological alterations. The expression of Ca_V 3.1 channels is down-regulated across multiple brain regions including the HPC, enthorhinal cotex and frontal cortex as a result of physiological aging in humans and mice (Rice *et al.*, 2014). In chapter 3, the major role this conductance plays in the normal function of young adult Re neurons was discussed and a similar down-regulation in Re neurons would significantly alter the functional output of Re neurons.

Studies have shown an age related decline in the volume and connectivity of medial thalamic structures (Ota *et al.*, 2007; Hughes *et al.*, 2012). The Re, an important mediator in HPC-mPFC synchrony, is likely to mediate an age related reduced in the flow of information between the HPC and mPFC. In support of this, extensive atrophy in the mPFC (Mander *et al.*, 2013) and loss of integrity of the

fornix (Douet & Chang, 2014), are observed with aging. However whether the output function of Re neurons is altered in response to this reduced flow of transmitted information is still unknown. This is an important question given the diversity of responses Re neurons can feasibly exhibit in response to depolarising stimuli (see Figure 3.10B).

This study seeks to augment our understanding of how physiological aging affects the HPC-Re-PFC circuit by examining how the intrinsic properties of rostral Re neurons are altered by physiological aging. This represents the first time anyone has studied how aging affects the intrinsic neurophysiological properties of a thalamic nucleus.

4.2 Methods

All procedures were carried out in accordance with the Animals (Scientific Procedures) Act 1986. Male C57-Bl/6J mice were bred in house at the University of Exeter, housed on a 12:12 light/dark cycle and granted *ab libitum* access to food and water. This study used 2 groups of mice, a young adult population (mean 5.3 months, range 4 - 6 months, n=5) and an aged population (mean 15.58 months, range 15.4 – 15.66 months, n = 8).

Coronal slices were prepared and neurons were recorded from as described in Materials and Methods. K-gluconate solution #2 (table 2.1) was used as the internal solution throughout recordings.

Data was analysed using custom written MATLAB scripts and Microsoft Excel. SPSS was used to test for statistical significance. Details can be found in Materials and Methods.

4.3 Results

4.3.1 The effect of physiological aging on spontaneous activity and passive membrane properties of neurons in the rostral Re.

A reduction in the connectivity and/or the activity of depolarising inputs into Re neurons could affect their basal activity. The activity of Re neurons in the absence of experimental stimuli were measured during a 60 s long gapfree current clamp recording. Physiological aging had no effect on the V_m of neurons (Fig 4.1A, Young adult, median -66.7 mV, n = 46; Aged, median -66.8 mV, n=53; p = 0.99, Mann-Whitney U test). No effect was observed on the proportion of cells exhibiting spontaneous AP firing (Fig 4.1B, p = 0.44, Chi-squared test) or the frequency of firing in spontaneously active neurons (Fig 4.1C, Young adult, median 2.5 Hz, n = 32; Aged, median 2.5 Hz, n = 42; p = 0.56, Mann-Whitney U test).

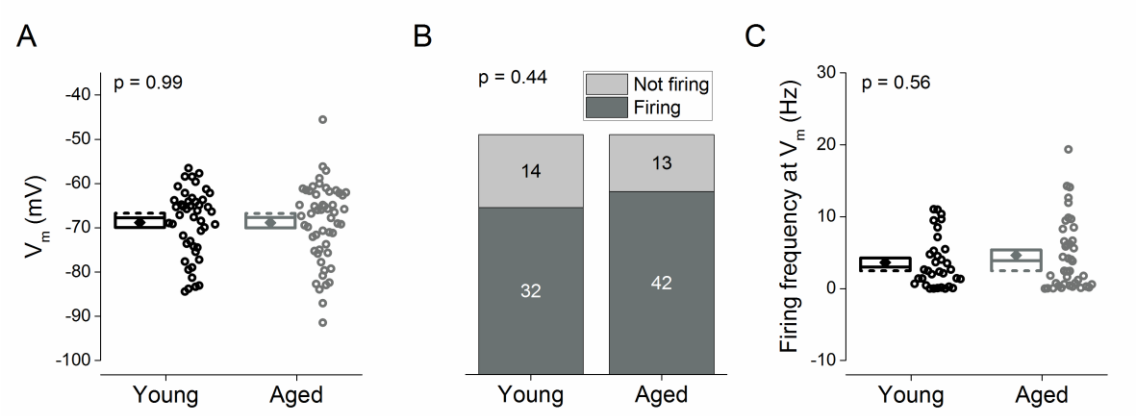

Figure 4.1. Activity at V_m was unaffected by physiological aging. (A) A plot displaying the distribution of V_m observed across groups. Diamond represents mean, dashed line represents median, and box represents sem. p value was calculated using a Mann-Whitney U test. (B) A cumulative column representation of the number of silent and spontaneously firing neurons across age group. p value was calculated using a Chi-squared test. (C) Plot showing, for firing cells, the mean firing frequency across the 60 s recording for each age group. Diamond represents mean, dashed line represents median, and box represents sem. p value was calculated using a Mann-Whitney U test.

The passive properties of the membrane were measured as described in Materials and Methods. Briefly this involved the injection of a 500 ms, -20 pA hyperpolarising current injection. Figure 4.2A shows a representative voltage response to such an injection. Physiological aging had no effect on R_i (Fig 4.2B, Young adult, mean 558 ± 25 MΩ, n = 42; Aged, mean 533 ± 24., n = 49; p = 0.48, unpaired, Student's t-test), τ (Fig 4.2C, Young adult, median 33.5 ms, n = 42; Aged, median 33.5 ms, n = 49; p = 0.73, Mann-Whitney U test) or capacitance (Fig 4.2D, Young adult, median 64.8 pF, n = 42; Aged, median 61.2 pF, n = 49; p = 0.73, Mann-Whitney U test).

The number of neurons displaying rebound firing in response to this hyperpolarising current injection, as shown in Fig 4.2A, was quantified. This pattern of activity results from T-type Ca^{2+} channels opening following release from inactivation as a result of the membrane hyperpolarisation. We first studied the propensity of Re neurons to exhibit this behaviour from -80 mV, the potential from which we measured the passive properties of the neuron. As outlined in section 3, the majority of neurons do not exhibit rebound firing from this prestimulus potential. Thus we also measured this behaviour from -72 mV, a potential at which practically all T-type Ca^{2+} channels are inactivated at rest and thus available to activate following release from inactivation (following a hyperpolarising current step), resulting in greater rates of observed rebound firing. Physiological aging had no effect on the propensity of neurons to exhibit this behaviour from either prestimulus potential (Fig 4.2E, -80 mV, p = 0.65, Chi-squared test; Fig 4.2F, -72 mV, p = 0.42, Chi-squared test).

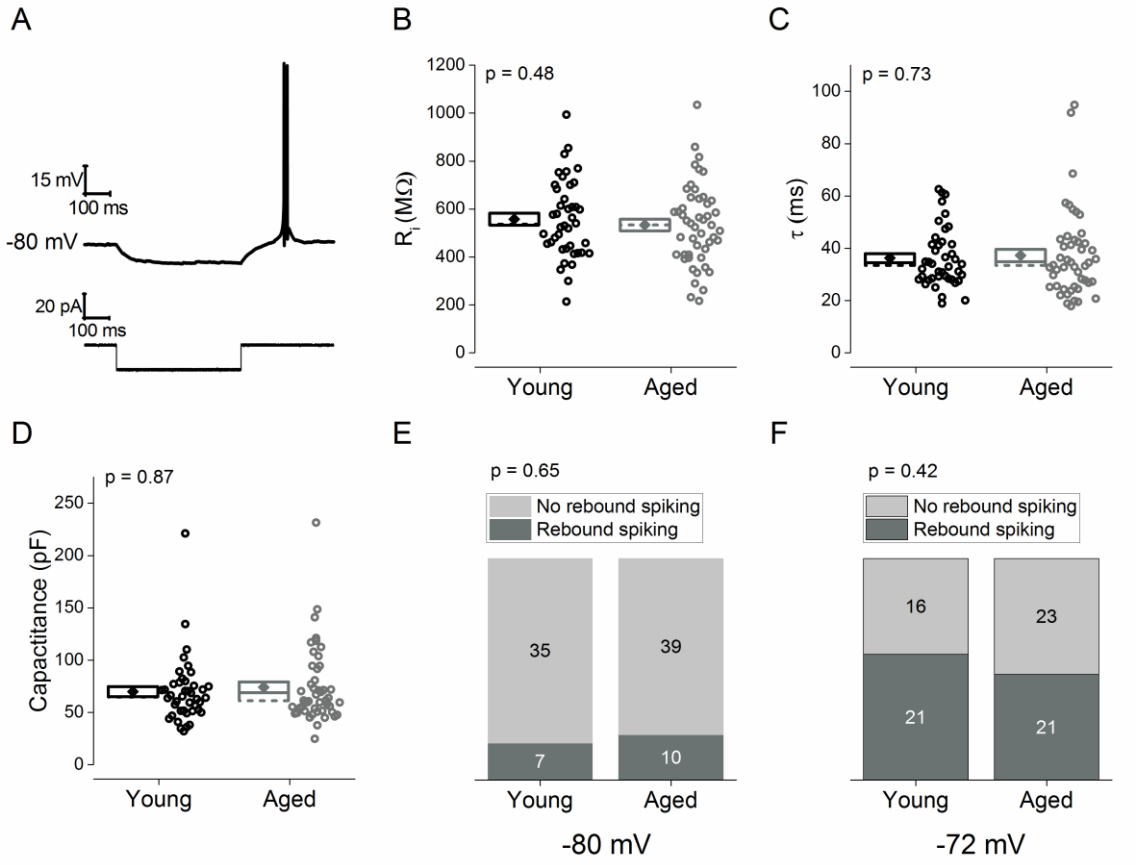

Figure 4.2. Passive membrane properties and rebound firing were unchanged by physiological aging. (A) Sample voltage (top) and current (bottom) trace of a -20 pA, 500 ms hyperpolarising current step from a set membrane potential of -80 mV used to calculate passive membrane properties. Note the rebound firing following cessation of the step. (B-D) Plot showing (B) R_i and (C) τ, calculated from a 500 ms, -20 pA hyperpolarising current injection. (D) Plot showing capacitance calculated as τ/R_i. Diamond represents mean, dashed line represents median, and box represents sem. p values were calculated using an unpaired, student's t-test (R_i), and a Mann-Whitney U test (τ and capacitance). (E+F) A cumulative column representation of the number of neurons which do not exhibit rebound firing and the number of neurons which do exhibit rebound firing across age groups. This was measured from a holding potential of (E) -80 mV and (F) -72 mV. p values were calculated using a Chi-squared test.

4.3.2 Physiological aging has no effect on spike output generated by depolarising current injections.

One change which has been reliably reported across brain regions in response to physiological aging is alterations to the intrinsic excitability of neurons (Randall *et al.*, 2012; Simkin *et al.*, 2015). A variety of depolarising stimuli were applied to probe for alterations to the excitability of Re neurons in response to physiological aging. First we applied an incremental series of 500 ms depolarising current injections (ranging from 10-60 pA) from a prestimulus potential of either -72 mV or -80 mV. A representative voltage response to one such 60 pA current step from -80 mV is displayed in Fig 4.3A. There was no change in excitability from either -72 mV (Fig 4.3B, Young adult, n = 41; Aged, n = 48; F = 0.00, p = 0.99, 2 way RM-ANOVA) or -80 mV (Fig 4.3C, Young adult, n = 41; Aged, n = 49; F = 0.2, p = 0.66, 2 way RM-ANOVA).

Another standard measure of excitability is the rheobase of a neuron, in other words, the minimum amount of current required to generate AP firing. This was measured with a series of depolarising 100 ms current injections, beginning at 2 pA and increasing in 2 pA increments until generation of an AP was observed. An example voltage trace in response to the rheobase current is displayed in Figure 4.3D. Physiological aging had no effect on rheobase from a prestimulus potential of either -72 mV (Fig 4.3E, Young adult, median 28 pA, n = 35; Aged, median 27 pA, n = 40; p = 0.94, Mann-Whitney U test) or -80 mV (Fig 4.2F, Young adult, median 22 pA, n = 36; Aged, median 22 pA, n = 42; p = 0.73, Mann-Whitney U test).

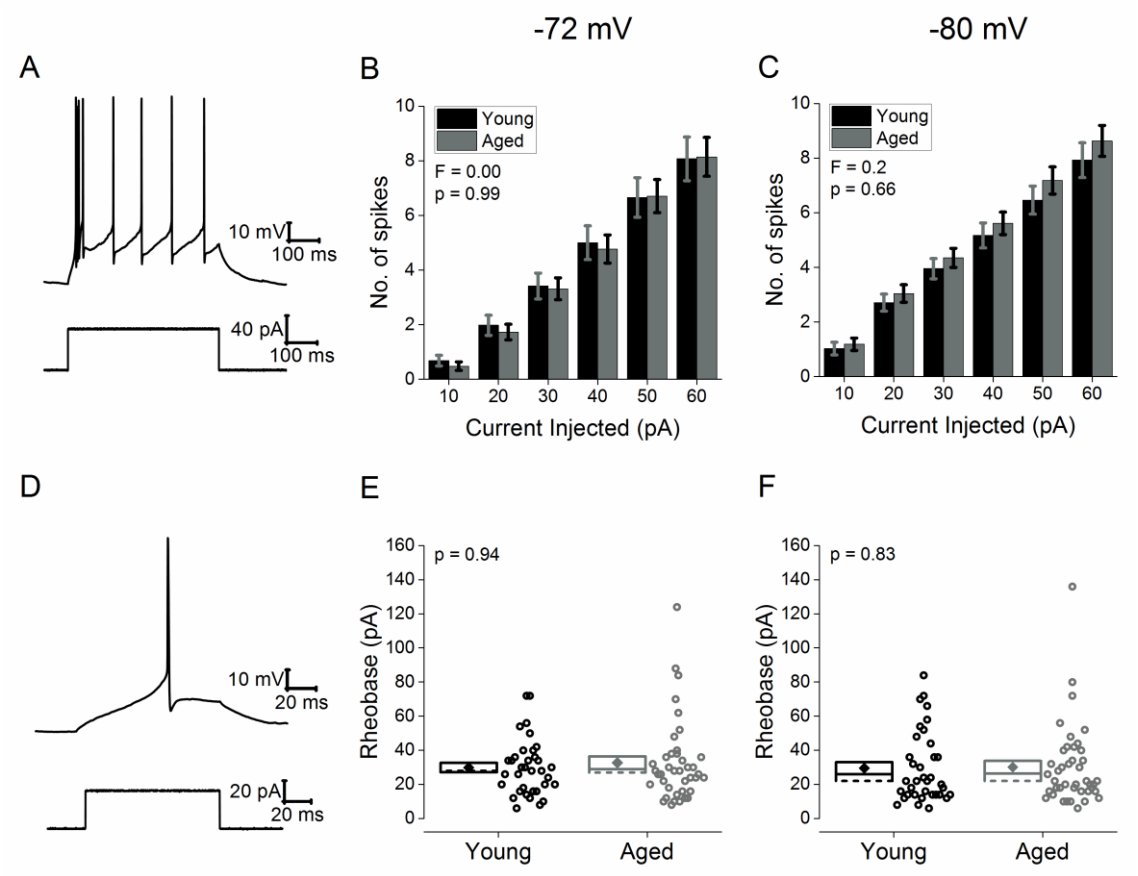

Figure 4.3. Physiological aging had no effect on the excitability of Re neurons in response to square depolarising current injections. (A) Sample voltage response (top) and current trace (bottom) of a 90 pA, 500 ms depolarising current injection from a prestimulus potential of -80 mV. (B+C) The mean number of APs produced in response to a series of 500 ms depolarising current injections from a prestimulus potential of (B) -72 mV and (C) -80 mV. F and p values calculated using a 2 way RM-ANOVA. (D) Sample voltage response (top) and 100 ms rheobase current injection (bottom). (E+F) Plot showing the rheobase of Re neurons at (E) -72 mV and (F) -80 mV. Diamond represents mean, dashed line represents median, and box represents sem. All p values were calculated using a Mann-Whitney U test.

As mentioned above, the excitability profile of Re neurons should be considered in the context of the networks in which it lies. To study how Re neurons respond to more physiological inputs we injected depolarising mock EPSC current injections. First we applied a series of four incrementally increasing αEPSCs (ranging from 75 – 300 pA) with a decay τ of 5 ms. A representative voltage trace in response to these series of injections is highligted in Figure 4.4A. Physiological aging had no effect on the mean number of APs generated over this range of current injections from a prestimulus potential of –72 mV (Fig 4.4B, Young adult, n = 34; Aged, n = 40; F = 1.45, p = 0.24, 2 way RM-ANOVA) or -80 mV (Fig 4.4C, Young adult, n = 35; Aged, n = 42; F = 0.09, p = 0.77, 2 way RM-ANOVA). We also injected a series of three mock EPSCs with a current amplitude of 375 pA but a decay τ increasing in a four fold manner from 5-20 ms. Example voltage traces in response to this series of current injections are displayed in Figure 4.4D. Physiological aging had no effect on the mean number of APs generated over this range of current injections from a prestimulus potential of -72 mV (Fig 4.4E, Young adult, n = 34; Aged, n = 38; F = 0.79, p = 0.38, 2 way RM-ANOVA) or -80 mV (Fig 4.4F, Young adult, n = 34; Aged, n = 41; F < 0.01, p = 0.97, 2 way RM-ANOVA).

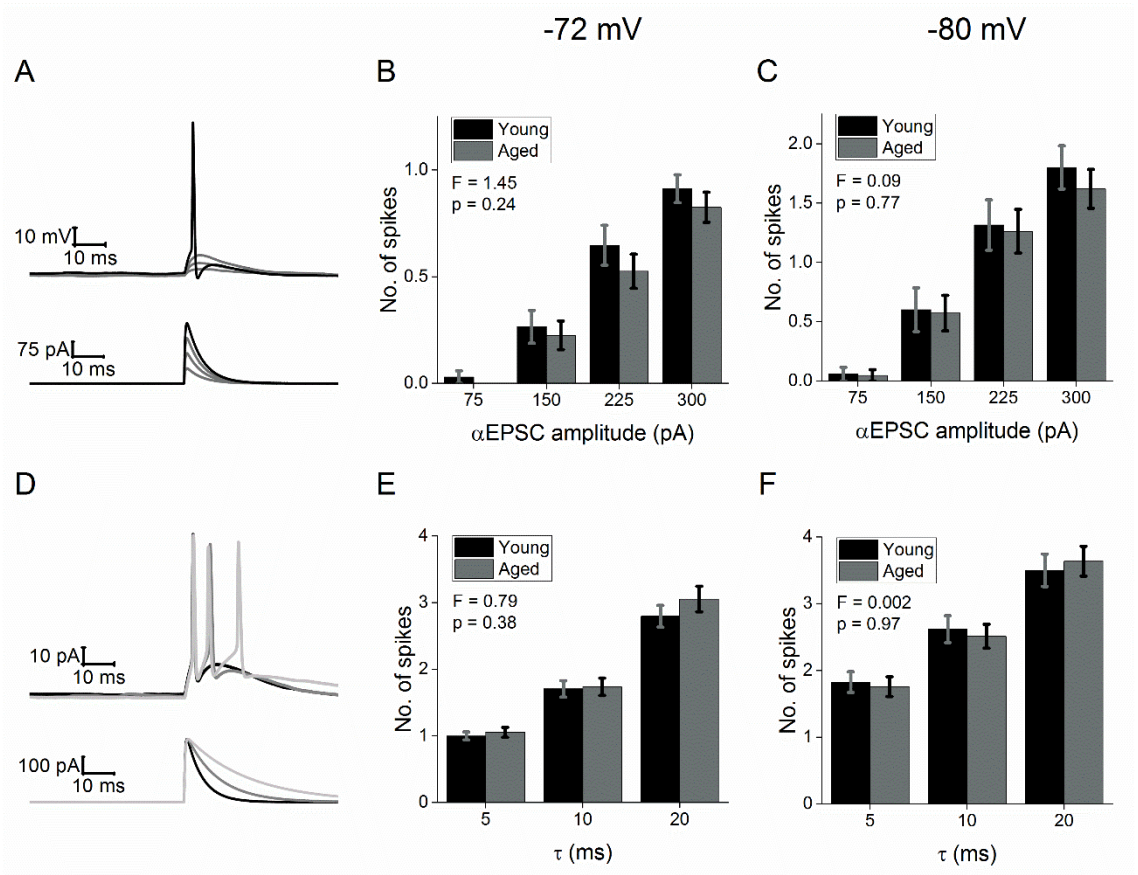

Figure 4.4. Number of APs in response to mock EPSC injections was unchanged by physiological aging. (A) Sample voltage responses (top) and current traces (bottom) of four αEPSC injections of incrementally increasing amplitude (75-300 pA), with a decay τ of 5 ms. (B+C) The mean number of APs produced in response to said series of αEPSC injections from a prestimulus potential of (B) -72 mV and (C) -80 mV. (D) Sample voltage responses (top) and current traces (bottom) of three αEPSC injections with an amplitude of 375 pA, and decay τ increasing in a four-fold manner from 5-20 ms. (E+F) The mean number of APs produced in response to said series of αEPSC injections from a prestimulus potential of (E) -72 mV and (F) -80 mV. All Error bars represent SEM. F and p values calculated using a 2 way RM-ANOVA.

4.3.3 Physiological aging has no effect on the spike frequency adaption or the afterpolarisation following a single spike.

Another frequently reported effect of physiological aging in CA1 pyramidal neurons is a reduction in spike frequency adaption. The presence of a T-type Ca^{2+} conductance greatly increase spike frequency adaption in Re neurons. At -72 mV Re neurons display a fairly regular firing pattern, while at -80 mV T-type Ca^{2+} conductances underlie the high frequency bursting evident at the beginning of the current step (see Figs 3.14 and 3.16). One would expect that any such reduction in T-type Ca^{2+} conductance in Re neurons would lead to a reduction in spike frequency adaption from a prestimulus potential of -80 mV. To measure this we looked at the instantaneous frequencies vs interval number in response to 50 and 60 pA, 500 ms depolarising current steps where at least (85%) of neurons generate at least two APs. We studied this from both -72 mV and -80 mV. Visual inspection of the traces suggests that physiological aging had no effect on the levels of spike frequency adaption from -72 mV (Fig 4.5A+B) or -80 mV (Fig 4.5C+D). Quantifying this is complicated by the cellular variability in the number of APs generated. We compared the first 3 instantaneous frequencies across each group as at both potentials at least 88% of firing neurons generated 4 APs in response to the depolarising stimulus. This confirmed that aging had no effect on spike frequency adaption from -72 mV (Fig 4.5A, 50 pA, Young adult, n = 31; Aged = 35; $F = 0.17$, $p = 0.69$: Fig 4.5B, 60 pA, Young adult, n = 35; Aged = 38; $F < 0.01$, $p = 0.96$) or -80 mV (Fig 4.5C, 50 pA, Young adult, n = 35; Aged = 44; $F = 0.19$, $p = 0.66$: Fig 4.5D, 60 pA, Young adult, n = 37; Aged = 46 ; $F = 0.1$, $p = 0.76$).

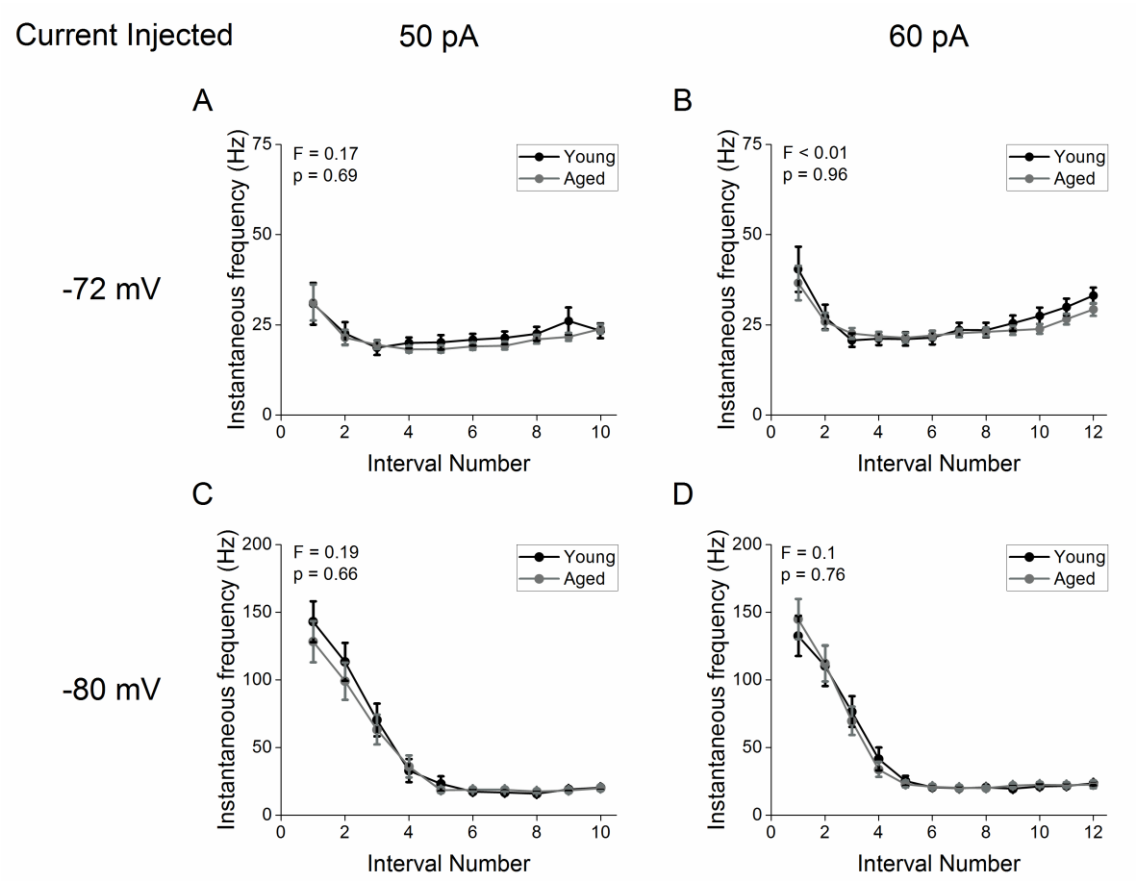

Figure 4.5. AP frequency adaption was unchanged by physiological aging. (A+B) A plot of instantaneous AP frequency vs interval number for a (A) 50 and (B) 60 pA, 500 ms depolarising current step from a prestimulus potential of -72 mV. (C+D) A plot of instantaneous AP frequency vs interval number for a (C) 50 and (D) 60 pA, 500 ms depolarising current step from a prestimulus potential of -80 mV. Error bars represent sem. F and p values calculated using a 2 way RM-ANOVA, calculated by comparing over the first 4 intervals.

The ADP observed following a single spike from a prestimulus potential of -80 mV in Re neurons is also underpinned by T-type Ca^{2+} channels (as shown in Fig 3.16). The absence of a change in high frequency bursting from -80 mV suggests that the reduction in T-type Ca^{2+} channel expression observed in other brain areas (Rice *et al.*, 2014) is not functionally manifested in Re neurons. To confirm this observation we measured the ADP following a single spike from -80 mV. Neurons were divided into one of three categories based on their afterpolarisation following a single AP from -80 mV, namely those expressing a suprathreshold ADP, a subthreshold ADP or expressing no measurable ADP (see Materials and Methods). An example trace of a neuron displaying each type of afterpolarisation is highlighted in Figure 4.6A. Physiological aging had no effect on the proportion of neurons falling into each category (Fig 4.6B, p = 0.56, Chi-squared test). The amplitude of subthreshold ADPs can be quantified directly. Aging also had no effect on the amplitude of this subthreshold ADP peak (Fig 4.6C, Young adult, mean 14.6 ± 1.8 mV, n = 14; Aged, mean 14.2 ± 1.5 mV, n = 14; p = 0.85, unpaired, Student's t-test).

The AHP following a single AP from a prestimulus potential of -72 mV was also examined. Neurons were either categorised as displaying an AHP (AHP ≥ 0), or not displaying an AHP (AHP = 0) as described in Materials and Methods. An example voltage trace of a neuron from each category is displayed in Figure 4.6D. Physiological aging had no effect on the proportion of neurons displaying a measurable AHP (Fig 4.6E, p = 0.71, Chi-squared test) or AHP amplitude in these neurons (Fig 4.6F, Young adult, mean -5.9 ± 0.9 mV, n = 22; Aged, mean -6.7 ± 0.9, n = 20; p = 0.39, unpaired, Student's t-test).

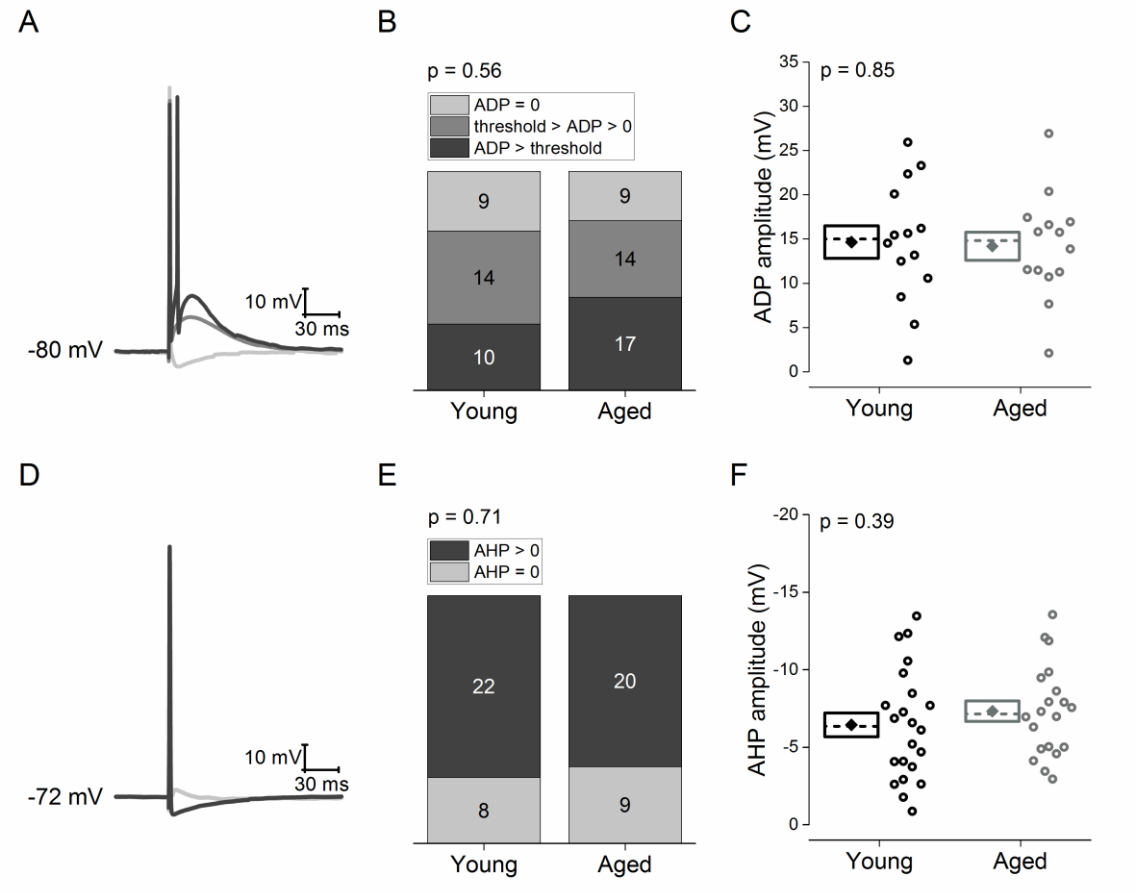

Figure 4.6. Afterpolarisation following a single AP was unchanged by physiological aging. (A) Example voltage traces of a neurons which do not exhibit an ADP (light grey), a neuron exhibiting a subthreshold ADP (grey) and a neuron which exhibits a suprathreshold ADP (dark grey) following elicitation of a single AP from a prestimulus potential of -80 mV. (B) Cumulative column representation of the proportion of neurons in each above category across age group. (C) Plot showing the ADP amplitude in neurons exhibiting a subthreshold ADP. Diamond represents mean, dashed line represents median, and box represents sem. p value was calculated using an unpaired, two tailed student's t-test. (D) Example voltage traces of a neurons which do not exhibit an AHP (light grey), a neuron exhibiting an AHP (dark grey) following elicitation of a single AP from a prestimulus potential of -72 mV. (B) Cumulative column representation of the proportion of neurons in which do and do not exhibit an AHP across age group. (C) Plot showing the AHP amplitude in neurons exhibiting a subthreshold ADP. Diamond represents mean, dashed line represents median, and box represents sem. p value was calculated using an unpaired, two tailed student's t-test.

4.3.4 Physiological aging has no effect on the action potential waveform.

Changes to the AP waveform would have large effects on the behaviour of Re neurons in a network context. Its shape effects the amount of Ca^{2+} which will enter during the AP duration (McCobb & Beam, 1991). Ca^{2+} entry during an AP facilitates many vital cellular processes such as the amount of neurotransmitter released at the synapse and cellular signalling cascades. Meanwhile AP threshold affects the propensity of neurons to generate APs, ie a depolarising shift in AP threshold (as observed in CA1 pyramidal neurons following aging) leads to neuronal hypoexcitability (Randall *et al.*, 2012).

The first AP generated in response to the 60 pA 500 ms depolarising current injection from a prestimulus potential of -80 mV (as seen in Fig 4.3A) was used to measure AP waveform properties as previously described in Materials and Methods. An average AP waveform across groups, and corresponding phase plot, are displayed in Figures 4.7A and 4.7B respectively. Physiological aging had no effect on AP peak (Fig 4.7C, Young adult, mean 16.9 ± 1.0 mV, n = 42; Aged, mean 16.2 ± 1.2 mV, n = 49; p = 0.68, unpaired, Student's t-test), AP width (Fig 4.7D Young adult, mean 0.56 ± 0.01 ms, n = 42; Aged, mean 0.53 ± 0.01 ms, n = 49; p = 0.17, unpaired, Student's t-test), AP threshold (Fig 4.7E, Young adult, mean -53.6 ± 0.5 mV, n = 42; Aged, mean -53.8 ± 0.5 mV, n = 49; p = 0.76, unpaired, Student's t-test), or maximal dV/dt (Fig 4.7F, Young adult, mean 357 ± 13 mV/ms, n = 42; Aged, mean 365 ± 12 mV/ms, n = 49; p = 0.76, unpaired, Student's t-test).

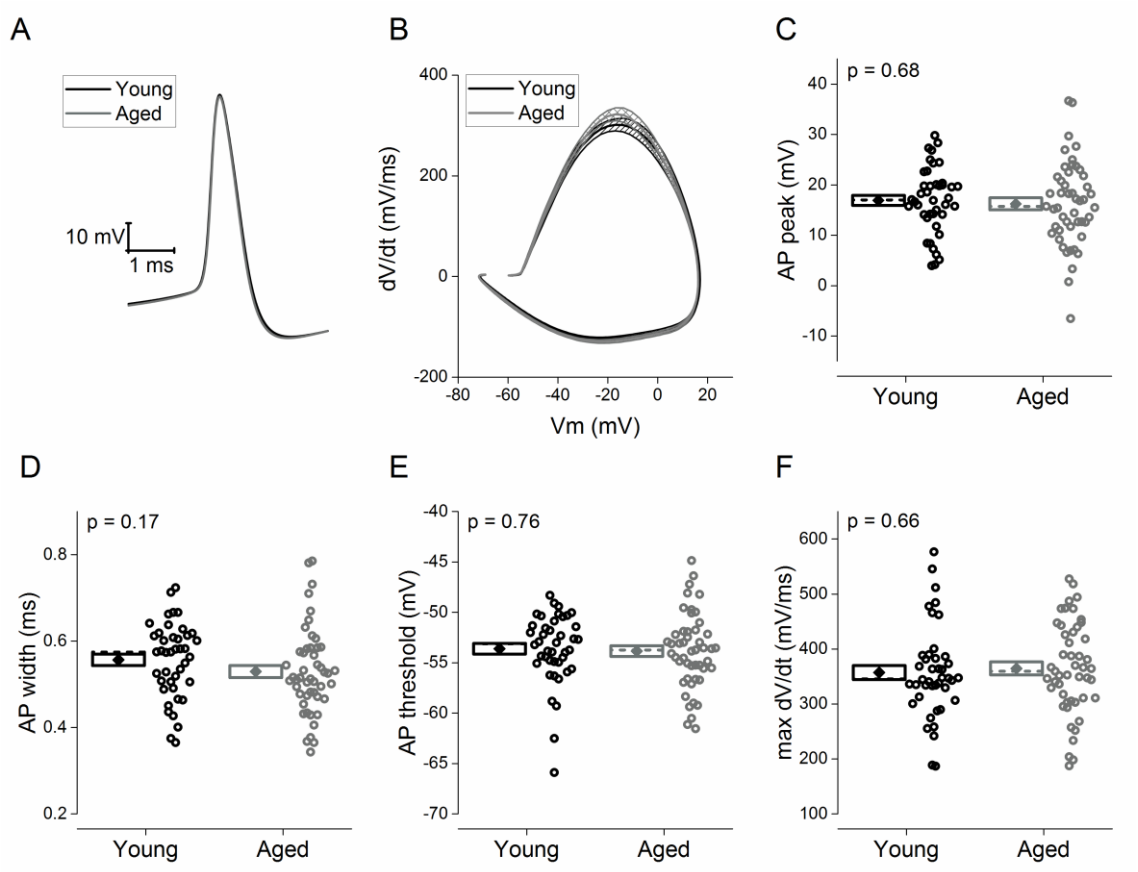

Figure 4.7. AP waveform was unchanged by physiological aging. (A) Average waveform of the first AP generated in response to 60 pA, 500 ms depolarising current injection. (B) Average phase plot of first generated AP, plotting the first derivative of the AP voltage against AP voltage. (C-E) Plot showing the (C) the absolute peak voltage value of the AP, (D) the AP width at half height, (E) AP threshold and (F) the maximal rate of rise. Diamonds represent mean, dashed line represents median, and box represents SEM. All p values were calculated using an unpaired, two tailed student's t-test.

4.4 Discussion

This study represents the first study to examine how physiological aging affects the intrinsic neurophysiological properties of Re neurons. The results described provide evidence that there are no differences in the intrinsic properties of rostral Re neurons between ~5 month old and ~15.5 month old C57-Bl/6J mice.

There was no difference in V_m, proportion of neurons firing spontaneously or the frequency of this firing. On the one hand this is not overly unexpected. The majority of Re neurons display a depolarised V_m and spontaneous firing in the absence of classical amino-acid mediated synaptic drive (see Fig 3.5). Thus one would hypothesise that the proposed reduction in excitatory input from the HPC and mPFC (Mander *et al.*, 2013; Douet & Chang, 2014) would not have any significant effect on the propensity of Re neurons to fire at rest. Conversely one must consider the proposed loss of volume in the medial thalamus and the increased volume of the 3rd ventricle which has been observed with aging (Ota *et al.*, 2007; Hughes *et al.*, 2012). To date, the Re appears to be somewhat unique amongst thalamic nuclei in terms of the propensity of its neurons to fire spontaneously and one might expect that that any significant reduction in volume of the Re would lead to recording from neurons from outside of the Re and associated reductions in the proportion of neurons exhibiting a depolarised V_m and resultant spontaneous AP firing. This discrepancy may be caused by limitations imposed by studies involving human subjects (the majority of studies studying structural changes in the thalamus). The studies suffer from technical difficulties in that the imaging technology is generally insufficient to accurately observe changes at the level of single thalamic nuclei. They also generally relay on cross sectional as opposed to longitudinal design which complicates interpretation as consistent age related volume differences have been observed across sample in cross sectional studies (Walhovd *et al.*, 2011). These structural changes should be further examined in animal models where, following dissection of the brain, laminae between individual thalamic nuclei can be readily visualised. The consistency of observed V_m across age groups does however give some degree of confidence that any atrophy which may occur in the Re is not sufficient to confound this study by leading to misclassification of neurons as being located within the rostral Re.

Passive membrane properties are unchanged by physiological aging. This is largely in line with previous studies from CA1 pyramidal neurons where passive membrane properties have generally been reported to be unchanged in neurons displaying hypoexcitability (Landfield & Pitler, 1984; Kumar & Foster, 2007; Matthews *et al.*, 2009; Gant & Thibault, 2009). However unlike CA1 pyramidal neurons, aging had no effect on the excitability of Re neurons. Previous reports which have demonstrated hypoexcitability in CA1 pyramidal neurons have largely centred on an increase in the amplitude of the post burst AHP (Landfield & Pitler, 1984; Kumar & Foster, 2007; Matthews *et al.*, 2009; Gant & Thibault, 2009) and a depolarising shift in AP threshold (Randall *et al.*, 2012). A prominent post-burst AHP is not observed in Re neurons and thus was not measured in this study while AP threshold was unchanged by aging in these neurons. It is therefore unsurprising that no such change in the total number of APs generated in response to a depolarising input, either square rectangular or mock EPSCs, was observed in Re neurons. There is also no change in the spike frequency adaption. The combination of these factors means that any information which Re neurons receive within the HPC-Re-mPFC circuit should be faithfully transferred regardless of physiological aging. The lack of spike frequency adaption is also suggestive that there is no change to T-type Ca^{2+} channel conductances in these neurons. This along with the similarities in the propensity of Re neurons to rebound fire and the similar size of AP afterpolarisation from -80 mV, suggests that the downregulation in $Ca_v3.1$ mRNA observed in the HPC, enthorhinal cortex and frontal cortex is regionally specific. The expression of Ca_v 3.1 is strong and indiscriminate across thalamic relay nuclei (Talley *et al.*, 1999) and is vital to the normal functioning of thalamic neurons. Given the vast array of sensory and motor information which flows through the thalamus, a sparing of this channels expression in nuclei composing the sensory and motor thalamus is to be expected given the conspicuous absence of the multitude of issues which would arise from such an age-related downregulation. This study suggests that T-type Ca^{2+} channel expression and kinetics also stays constant in nucleus of the limbic thalamus throughout physiological aging. Alterations in the shape of the AP waveform could also affect the ability of Re neurons to faithfully act as a relay within the cognitive network. Physiological aging had no effect on the shape of the AP waveform.

One important thing to consider is whether the ~15 month old “aged” mice (about 50% of the total murine lifespan) used in this study represent an appropriate model of age-related cognitive decline. A recent large scale study (1,739 mice) by Shoji *et al.* (2016) investigated the rate of progressive decline in cognitive function between adolescent (2 - 3 months) and middle aged (8 - 12 months) C57-Bl/6J mice. Significant decline in both spatial and fear memory tests were observed by middle age suggesting that the 15 month old aged mice used in this study should have undergone significant age-related cognitive decline.

In summary this study describes the effects of physiological aging on the intrinsic properties of neurons of the rostral Re. In short, aging had no effect on either the activity at rest or the functional output of the Re in response to a stimulus. This suggests that alterations to the intrinsic properties of Re neurons play no role in the cognitive decline brought about by aging. A wealth of evidence from human imaging studies suggests that the flow of information through the Re may still be compromised as a relay as a result of structural changes within the HPC-Re-mPFC network. Future studies should probe this further with the regional specificity gained from studies in animals allowing the study of the connectivity changes to and from individual thalamic nuclei. Anterograde and retrograde tracing techniques would seem ideal to this end.

5 Alterations in the intrinsic electrophysiological properties of neurons in the rostral nucleus reuniens in a mouse model of amyloidopathy.

5.1 Introduction

The aggregation of Aβ peptides into extracellular amyloid plaques is one of the main pathological hallmarks of AD (Masters *et al.*, 1985). The advent of genetic engineering has facilitated in depth study of this pathology in multiple model organisms, most notably mice. The J20 mouse model is one such widely used model. These animals overexpress a mutated form of human APP ($APP_{swe/ind}$) resulting in range of phenotypes which resemble changes observed in human AD. These include plaque formation (Mucke *et al.*, 2000), synaptic loss (Hong *et al.*, 2016), gliosis (Wright *et al.*, 2013), memory impairments (Palop *et al.*, 2003; Harris *et al.*, 2010; Wright *et al.*, 2013) and an increase in the incidence of spontaneous seizure activity in defined neuronal networks (Palop *et al.*, 2007; Verret *et al.*, 2012).

Very little information is available on the cellular level neurophysiological changes which occur in J20 mice. Verret *et al* (2012) reported a more depolarised RMP in PV positive, fast spiking interneurons in layer II/III of the parietal cortex adding to a significant body of literature examining alterations in the intrinsic properties of neurons in mouse models of amyloidopathy. For example studies have reliably reported a narrower spike width in CA1 pyramidal neurons (Brown *et al.*, 2011*b*; Wykes *et al.*, 2012; Kerrigan *et al.*, 2014; Tamagnini *et al.*, 2015), something which can also be seen in J20 mice (Francesco Tamagnini, unpublished observations). However such studies have exclusively focused on hippocampal and cerebrocortical structures, regions in which a significant plaque load develops (Bugiani *et al.*, 1989). This focus ignores the potential large role alterations in the activity of subcortical structures, such as the limbic thalamus, could play in widespread cognitive deficits observed in AD patients (Aggleton *et al.*, 2016).

Among the multitude of thalamic nuclei, AD pathology exclusively affects the limbic thalamus, including the formation of NFTs and neuropil threads in the Re in the absence of amyloid plaques (Braak & Braak, 1991). Notably however the thalamus shows relatively high levels of APP expression and soluble Aβ in mouse

models of amyloidopathy (Johnson-Wood *et al.*, 1997). Changes in the intrinsic properties of hippocampal CA1 neurons have been discovered prior to the formation of amyloid plaques in a model of amyloidopathy (Wykes *et al.*, 2012; Kerrigan *et al.*, 2014). To investigate whether the intrinsic electrophysiological properties of neurons are altered in a cognitively relevant region in which a robust plaque pathology is absent, the cellular neurophysiological properties of neurons in the rostral Re were examined in 12-14 month old J20 mice. This represents the first study to examine cellular neurophysiological changes in a nucleus of the limbic thalamus in a model of amyloidopathy.

5.2 Methods

All procedures were carried out in accordance with the Animals (Scientific Procedures) Act 1986. Male transgenic (TG) J20 mice (background strain: C57-Bl/6J) and wild-type (WT) littermate controls were bred in house at the University of Exeter. They were subsequently housed on a 12:12 light/dark cycle and granted *ab libitum* access to food and water. This study used mice of approximately 13 months of age (WT, mean 13.1 months, range 12.1-14.2 months, n = 12; TG, mean 13 months, range 12.4-14.3 months, n = 13).

Coronal slices were prepared and neurons were recorded from as described in Materials and Methods. K-gluconate solution #2 (table 2.1) was used as the internal solution throughout current clamp recordings. $CsMeSO_4$ solution #1 was used during direct measurement of T-type Ca^{2+} channel currents.

At the end of a recording session, the single experimental slice was fixed in 4% PFA for >1 hour and subsequently stored in PBS for future immunostaining with an amyloid plaque specific fluorescent tracer Amylo-Glo (Schmued *et al.*, 2012*b*).

Data were analysed using custom written MATLAB scripts and Microsoft Excel. SPSS was used to test for statistical significance. Details can be found in Materials and Methods.

5.3 Results

5.3.1 Visualisation of amyloid plaques in the rostral Re following transgene expression.

To test whether amyloid plaques are present in the Re, 300 µm coronal slices containing the rostral Re were stained with an amyloid specific fluorescent tracer. Amyloid plaques were visualised using UV epifluorescence illumination. Amyloid plaques, which present as fluorescence, were clearly visible in the cortex in J20 mice, confirming previous reports (Mucke *et al.*, 2000). Figure 5.1 (top) highlights such fluorescence in the dorsal regions of the cortex and the rostral tip of the HPC in slices (Bregma, approx. 0.9 mm) obtained from J20 mice, while no such fluorescence observed in WT controls. No fluorescence was observed in the rostral Re in either WT or TG mice (Fig 5.1(bottom)). Thus as observed in human AD patients (Braak & Braak, 1991), J20 mice do not develop amyloid plaques in the Re.

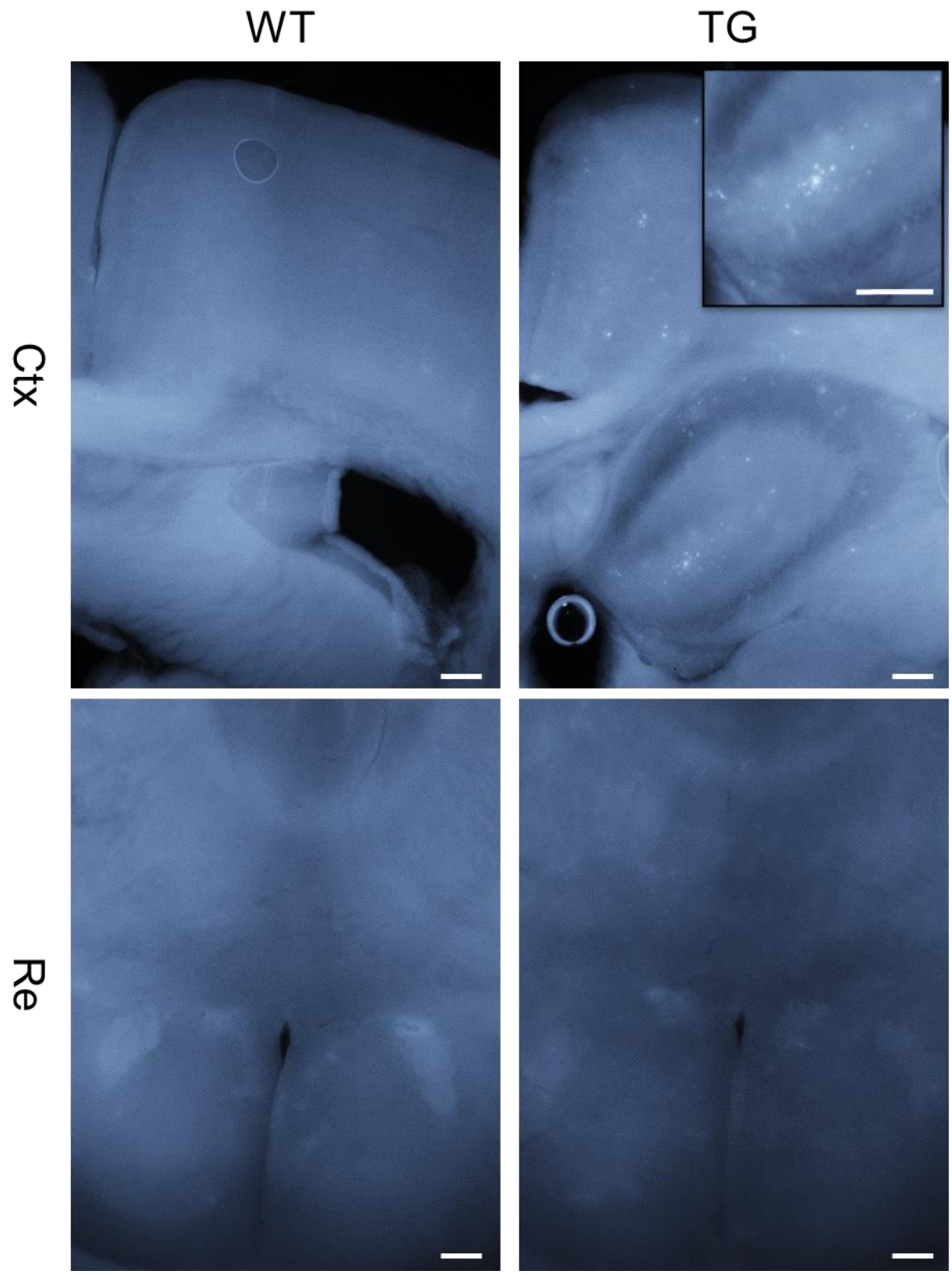

Figure 5.1. Visualisation of amyloid plaques using the fluorescent tracer Amylo-Glo. (Top) Amyloid plaques are present in the cortex (Ctx) and HPC of TG mice (right) but not WT controls (left) at x4 magnification. Highlighted inset is an amyloid plaque in the hippocampus at x10 magnification. (Bottom) Plaques are absent in the Re of both WT and J20 mice at x4 magnification. Scale bar = 0.25 mm.

5.3.2 The effect of transgene expression on V_m and spontaneous firing behaviour.

The proportion of rostral Re neurons exhibiting a relatively hyperpolarised V_m (circa -75 mV) was increased in J20 mice as compared to WT controls (Fig 5.2A, WT, n = 43; TG, n = 49; p = 0.05, Kolmogorov–Smirnov test). As illustrated in Fig 5.2A ~40% of J20 neurons had a V_m of ≤ -75 mV as compared to ~10% of WT neurons. Interestingly this did not correspond to a significant decrease in the number of neurons exhibiting spontaneous AP generation in the absence of experimental stimuli (Fig 5.2B, p = 0.25, Chi-squared test), with the majority of neurons firing at least 1 AP during the 60 s recording duration independent of genotype. The frequency of AP firing was also unchanged (Fig 5.2C, WT, median 3.79 Hz, n = 32; TG, median 5.88 Hz, n = 31; p = 0.7, Mann-Whitney U test). The change in V_m without a consequent change in the proportion of cells exhibiting, or the frequency of spontaneous APs could be a consequence of a change in the V_m of neurons which generate no spontaneous APs. However the V_m of these quiescent neurons was independent of transgene expression (Fig 5.2D, WT, mean -74.4 ± 2.8 mV, n = 11; TG, mean -76.3 ± 2.2 mV, n = 18; p = 0.59, unpaired, two tailed student's t-test).

Re neurons can display different spontaneous firing modes at rest as described in chapter 3. Tonically firing neurons generally generate APs at a rate between 2-20 Hz. A change in the V_m of these neurons could be suggestive of either a change in the AP threshold or the amplitude or timecourse of post AP AHP. The V_m in these neurons is also independent of transgene expression (Fig 5.2E, WT, mean -59.9 ± 1.0 mV, n = 20; TG, mean -57.5 ± 1.1 mV n = 19; p = 0.11, unpaired, two tailed student's t-test). Neurons with a mean frequency of below 2 Hz can show considerable variety in the V_m from which they generate APs. At membrane potentials a few mV hyperpolarised of AP threshold, neurons will reliably generate single "isolated" APs in response to fluctuations in membrane potential while at significantly more hyperpolarised membrane potentials neurons can exhibit high frequency burst firing (see section 3). The V_m of neurons exhibiting <2 Hz AP firing was significantly more hyperpolarised in J20 neurons (Fig 5.2F, WT, mean -65.3 ± 1.3 mV, n = 12; TG, mean -72.3 ± 3.1 mV, n = 12; p = 0.05, unpaired, two tailed student's t-test) explaining the change in the V_m distribution in J20 neurons with a consequent change in firing frequency at V_m.

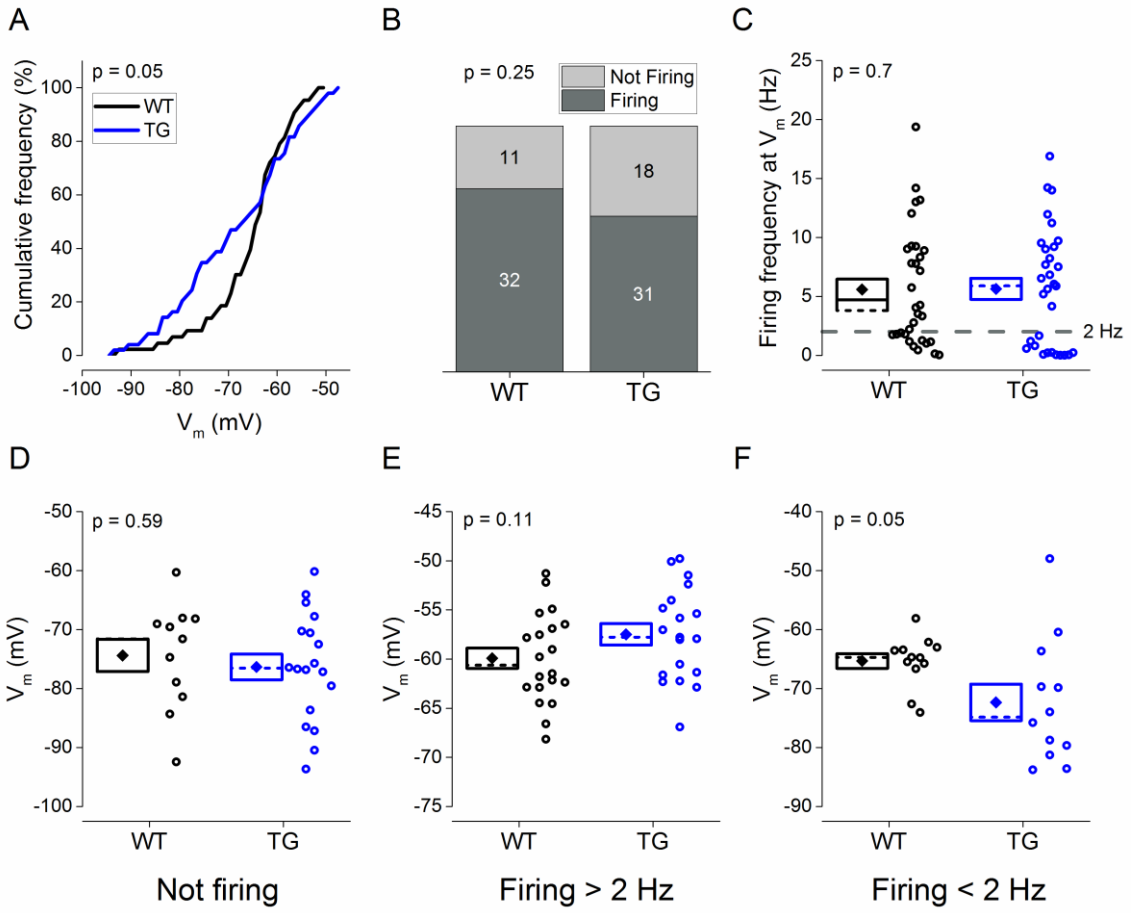

Figure 5.2. Transgene expression increased the frequency of neurons displaying a hyperpolarised V_m. (A) A cumulative histogram displaying the distribution of V_m observed across groups. Black line represents WT neurons; blue line represents TG neurons. p value was calculated using a Kolmogorov–Smirnov test. (B) A cumulative column representation of the number of silent and spontaneously firing neurons across genotype. p value was calculated using a Chi-squared test. (C) Plot showing, for firing cells, the mean firing frequency for each genotype. Diamond represents mean, dashed line represents median, and box represents SEM. p value was calculated using a Mann-Whitney U test. (D-E) Plot showing the V_m of neurons which (D) exhibit no spontaneous APs, (E) exhibit spontaneous AP firing at a frequency > 2 Hz and (F) exhibit spontaneous AP firing at a frequency < 2 Hz. p valves calculated using unpaired student's t-test. Diamond represents mean, dashed line represents median, and box represents SEM. p valves calculated using an unpaired student's t-test.

5.3.3 The effect of transgene expression on proportion of neurons rebound firing and associated passive membrane properties.

The injection of a square hyperpolarising current from a fixed membrane potential can be used to garner useful knowledge on voltage dependant properties of neurons. These include both the propensity of neuron to display rebound firing and its passive membrane properties including R_i and τ. In response to a -30 pA, 500 ms hyperpolarising step (Fig 5.3A), transgene expression resulted in a significant increase in the propensity of neurons to display rebound firing. From a holding potential of -80 mV, ~8% of WT neurons display rebound firing as compared to ~30% of TG neurons (Fig 5.3B, p = 0.01, Chi-squared test). From a holding potential of -72 mV, a potential at which a greater pool of inactivated T-type Ca^{2+} channels exist, ~39% of WT neurons display rebound firing as opposed ~64% of TG neurons (Fig 5.3C, p = 0.03, Chi-squared test). The latency to rebound firing was measured as the time taken from the end of the hyperpolarising current injection to the peak of the 1st rebound spike. This can be compared across genotype from a holding potential of -72 mV as a significant proportion of Re neurons display rebound firing independent of transgene expression. Transgene expression resulted in a significantly shorter duration to the first rebound spike following the cessation of the hyperpolarising current step (Fig 5.3D, WT, median 147.35 ms, n = 15; TG, median 112.53 ms, n = 27; p = 0.02, Mann-Whitney U test).

Passive membrane properties were independent of transgene expression. These were measured from a set membrane potential of -80 mV to prevent cell to cell variability in V_m from confounding measurement of these voltage dependant properties. The median R_i for WT neurons was 426 MΩ as compared to 431 MΩ for TG neurons (Fig 5.4A, p = 0.88, Mann-Whitney U test). The median τ was 29.6 ms for WT neurons as compared to 29.1 ms for TG neurons (Fig 5.4B, p = 0.35, Mann-Whitney U test). Capacitance can be measured as the ratio of these values, namely (τ/R_i). The median capacitance for WT neurons was 64.0 pF as compared to 54.8 pF (Fig 5.4C, p = 0.54).

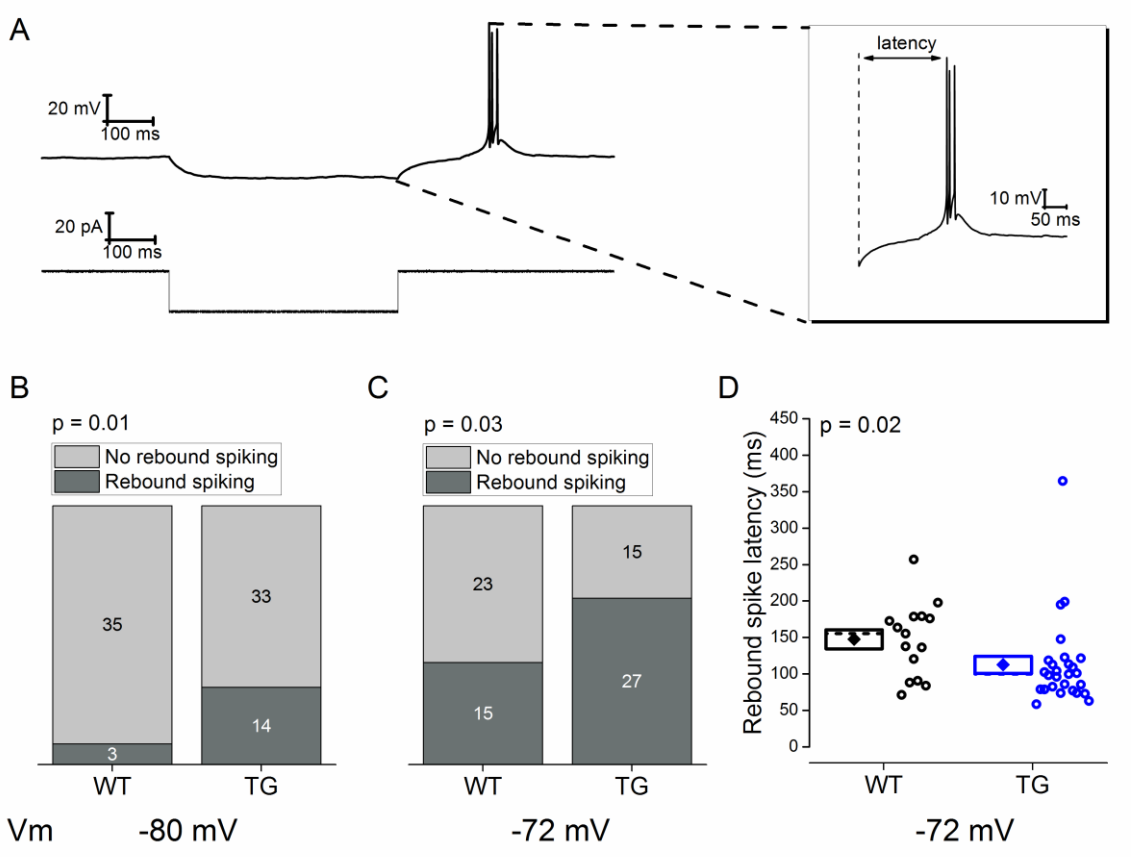

Figure 5.3. Transgene expression resulted in an increase in the proportion of neurons rebound firing and a decrease in the latency to rebound firing. (A) Sample voltage (top) and current (bottom) trace of a -30 pA, 500 ms hyperpolarising current step from a set membrane potential of -72 mV. Rebound firing following cessation of this hyperpolarising step is highlighted inset (right). (B+C) A cumulative column representation of the number of neurons which did not exhibit rebound firing and the number of neurons which did exhibit rebound firing across genotype. This was measured from a holding potential of (B) -80 mV and (C) -72 mV. p values were calculated using a Chi-squared test. (D) Plot showing, for the cells which exhibit rebound spiking from a holding potential of -72 mV, the latency from to the peak of the 1st rebound spike from the cessation of the hyperpolarising current injection. Diamond represents mean, dashed line represents median, and box represents SEM. p value was calculated using a Mann-Whitney U test.

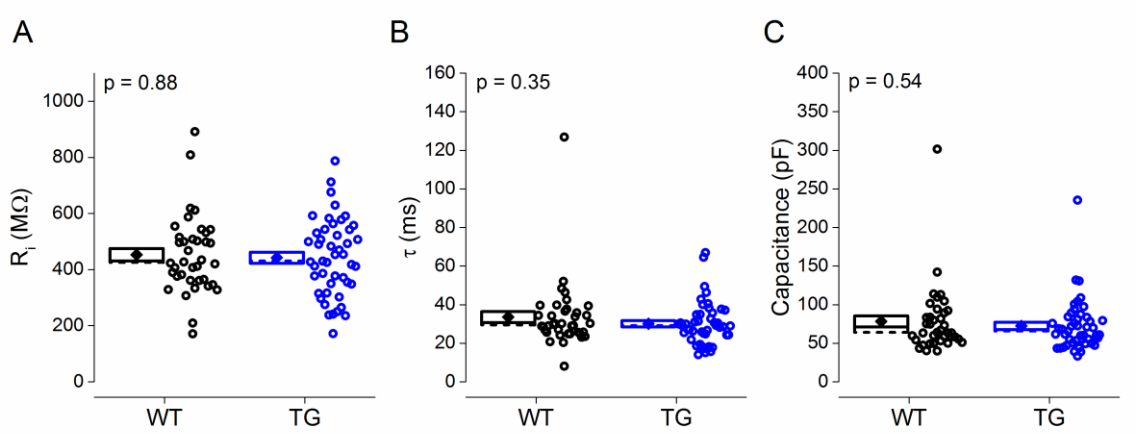

Figure 5.4. Passive membrane properties were independent of transgene expression. (A-B) Plot showing (A) R_i and (B) τ, calculated from a 500 ms, 30 pA hyperpolarising current injection. (C) Plot showing capacitance calculated as $τ/R_i$. Diamond represents mean, dashed line represents median, and box represents SEM. All p values were calculated using a Mann-Whitney U test.

5.3.4 Number of spikes generated following depolarising current injection is independent of transgene expression.

In order to test if the excitability of Re neurons is altered in the Re of J20 mice, we employed a series of six incremental 500 ms depolarising current steps ranging from 15-90 pA from a fixed membrane potential of either -72 or -80 mV. As discussed in chapter 3 the available reservoir of voltage gated ion channels, in particular the T-type Ca^{2+} channel, differs over this 8 mV range resulting in vastly different AP output functions between neurons held at each prestimulus potential (Fig 3.14). A sample voltage trace in response to one such 90 pA depolarising current step from a holding potential of -80 mV is displayed in Figure 5.5A. Note the high frequency, T-type Ca^{2+} channel dependant burst of APs at the beginning of the current injection.

The mean number of APs elicited was not affected by transgene expression at -72 mV (Fig 5.5B, WT, n = 37; TG, n = 44; F = 1.27, p = 0.27, 2 way RM-ANOVA), or -80 mV (Fig 5.5C, WT, n = 38; TG, n = 47; F = 0.55, p = 0.46, 2 way RM-ANOVA). The latency to the first AP was also measured. We defined this as the time taken from the initiation of the current stimulus to the peak of the first AP as demonstrated in Figure 5.5D. This was measured in response to the 4 largest current stimuli (45 – 90 pA) as >88% of neurons fired at least one AP in response to a 45 pA injection across genotype (-72 mV, WT 95%, TG 89%; -80 mV, WT 97%, TG 95%). From a prestimulus membrane potential of -72 mV, transgene expression had no effect on AP latency (Fig 5.5E, WT, n = 35; TG, n = 39; F = 0.88, p = 0.36, 2 way RM-ANOVA), however from a prestimulus potential of -80 mV AP latency was ~32% shorter in cells from J20 mice (Fig 5.5F, WT n = 37; TG, n = 45; F = 6.37, p = 0.02, 2 way RM-ANOVA).

Another standard measure of excitability is the rheobase of a neuron. This is the minimum amount of current required to elicit an AP. To gain an approximation of rheobase, a series of 100 ms incrementally growing 2 pA square current injections were injected. Figure 5.5G shows a voltage response of a neuron in response to the rheobase current injection. Transgene expression had no effect on the rheobase from either -72 mV (Fig 5.5H, WT, median 28 pA, n = 31; TG, median 24 pA, n = 35; p = 0.41, Mann-Whitney U test) or -80 mV (Fig 5.5I, WT, median 29 pA, n = 34; TG, median 28 pA, n = 39; Fig 5.4H, p = 0.42, Mann-Whitney U test).

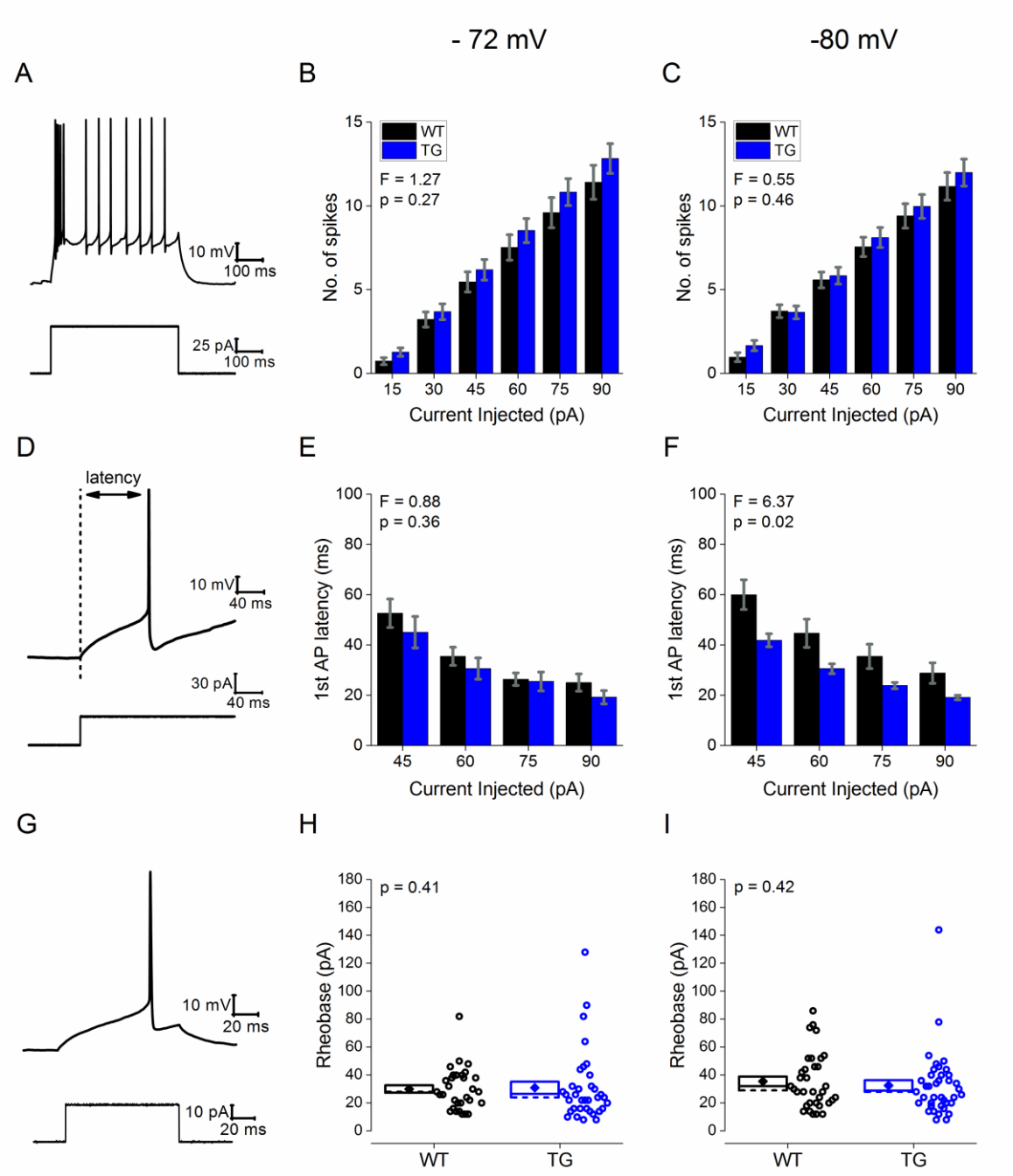

Figure 5.5. The effect of transgene expression on AP production in response to square depolarising current injections. (A) Sample voltage response (top) and current trace (bottom) of a 90 pA, 500 ms depolarising current injection from a prestimulus potential of -80 mV. (B+C) The mean number of APs produced in response to a series of 500 ms depolarising current injections from a prestimulus potential of (B) -72 mV and (C) -80 mV. F and p values calculated using a 2 way RM-ANOVA. (D) Sample voltage response (top) and current trace of a 45 pA depolarising step as in (A). Highlighted is the first 220 ms of the current step highlighting the first AP generated. Latency is calculated as the time from the beginning of the current step to the peak of the AP. (E+F) Mean latency to the first AP generated during the series of 500 ms depolarising current injections at (E) -72 mV and (F) -80 mV. F and p values calculated using a 2 way RM-ANOVA. (G) Sample voltage response (top) and 100 ms rheobase current injection (bottom). (H+I) Plot showing the rheobase of Re neurons at (H) -72 mV

and (I) -80 mV. Diamond represents mean, dashed line represents median, and box represents SEM. All p values were calculated using a Mann-Whitney U test.

These square depolarising current injections, while useful, do not accurately represent how neurons are driven towards AP threshold *in vivo*. To probe the excitability of neurons in response to more physiological inputs, mock EPSCs were injected as previously described in (Brown & Randall, 2009). Figure 5.6A shows a voltage response to a series of 4 αEPSC injections of incrementally increasing amplitude ranging from 75-300 pA. There was no change in the mean number of spikes generated in response to these injections at either -72 mV (Fig 5.6B, WT, n = 31; TG, n = 33; F = 0.53, p = 0.47, 2 way RM-ANOVA), or -80 mV (Fig 5.6C, WT, n = 32; TG, n = 37; F = 2.0, p = 0.17, 2 way RM-ANOVA).

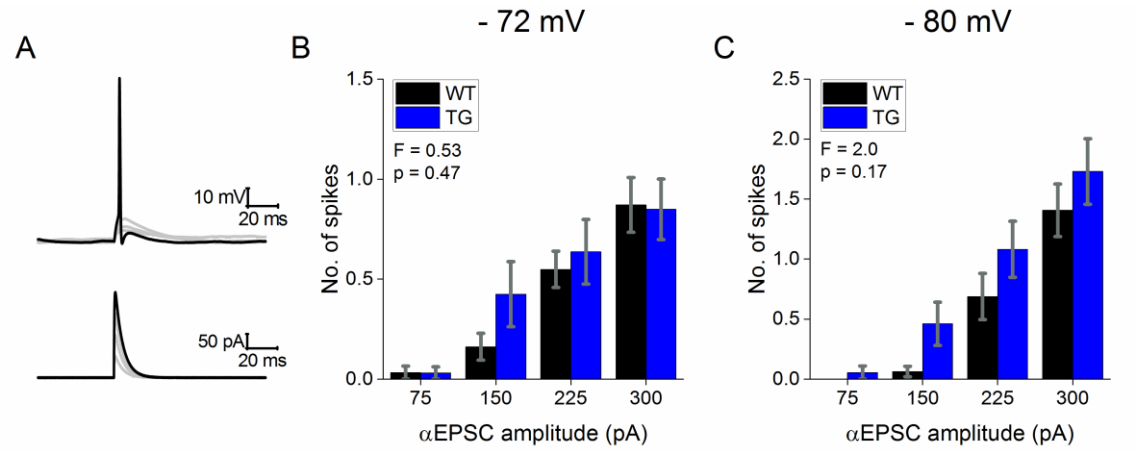

Figure 5.6. Transgene expression had no effect on the number of APs generated in response to αEPSC injections. (A) Sample voltage responses (top) and current traces (bottom) of four αEPSC injections of incrementally increasing amplitude (75-300 pA), with a decay tau of 5 ms. (B+C) The mean number of APs produced in response to said series of αEPSC injections from a prestimulus potential of (B) -72 mV and (C) -80 mV. Error bars represent SEM. F and p values calculated using a 2 way RM-ANOVA.

5.3.5 Action potential waveform is altered in J20 mice

AP waveform properties were measured from the first spike generated in response to the 90 pA, 500 ms current injection. From a prestimulus potential of -80 mV, the average peak aligned AP waveform is displayed for WT and TG neurons in Figure 5.7A. Transgene expression had no effect on AP peak (Fig 5.7B, WT, mean 18.4 ± 1.3 mV, n = 38; TG, mean 17.2 ± 1.1 mV; n = 47; p = 0.49, unpaired, two tailed student's t-test). AP width was significantly shorter in Re neurons in J20 mice (Fig 5.7C, WT, mean 0.68 ± 0.02 ms, n = 38; TG, mean 0.63 ± 0.01 ms, n = 47; p < 0.01, unpaired, two tailed student's t-test). This approx. 8% reduction in AP width is reminiscent of the 10-15% reduction in spike width previously observed in CA1 pyramidal neurons in models of amyloidopathy (Brown *et al.*, 2011*b*; Wykes *et al.*, 2012; Kerrigan *et al.*, 2014; Tamagnini *et al.*, 2015). Transgene expression had no effect on AP threshold (Fig 5.7E, WT, median -52.1 mV, n = 38; TG, median -53.1 mV, n = 47; p = 0.24, Mann-Whitney U test) or the maximal rate of rise observed during the AP window (Fig 5.7F, WT, median 296 mV/ms, n = 38; TG, median 317 mV/ms, n = 47; p = 0.16, Mann-Whitney U test).

From a prestimulus potential of -72 mV all AP properties listed above were independent of transgene expression, however, AP width does trend towards being narrower in J20 neurons (Fig 5.8C, WT, mean 0.72 ± 0.01 ms, n = 37; TG, mean 0.68 ± 0.01 ms, n = 44; p = 0.08, unpaired, two tailed student's t-test). This suggested a voltage dependant decrease in AP width. To test if this was the case a 2 way ANOVA was performed. AP width was significantly altered by transgene expression across voltages (F = 10.01, p = 0.02, 2 way ANOVA) and there was no significant interaction between transgene expression and prestimulus holding potential (F = 0.24, p = 0.63, 2 way ANOVA).

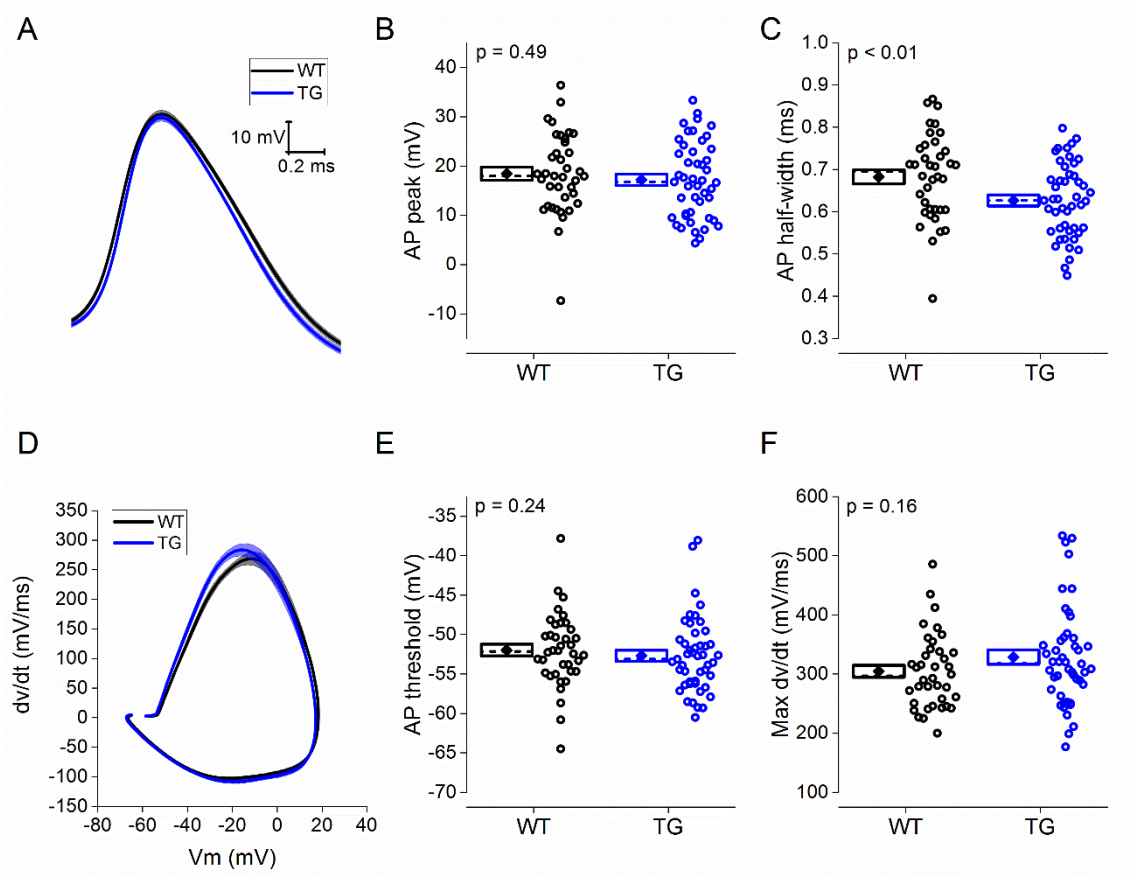

Figure 5.7. Action potential width was decreased in J20 neurons from a prestimulus potential of -80 mV. (A) Average waveform of the first AP generated in response to 90 pA, 500 ms depolarising current injection. (B+C) Plot showing the (B) the absolute peak voltage value of the AP and (C) the AP width at half height. Diamond represents mean, dashed line represents median, and box represents SEM. All p values were calculated using an unpaired, two tailed student's t-test. (D) Average phase plot of first generated AP, plotting the first derivative of the AP voltage against AP voltage. (E+F) Plot showing the (E) AP threshold and (F) the maximal rate of rise. Diamond represents mean, dashed line represents median, and box represents SEM. All p values were calculated using a Mann Whitney U test.

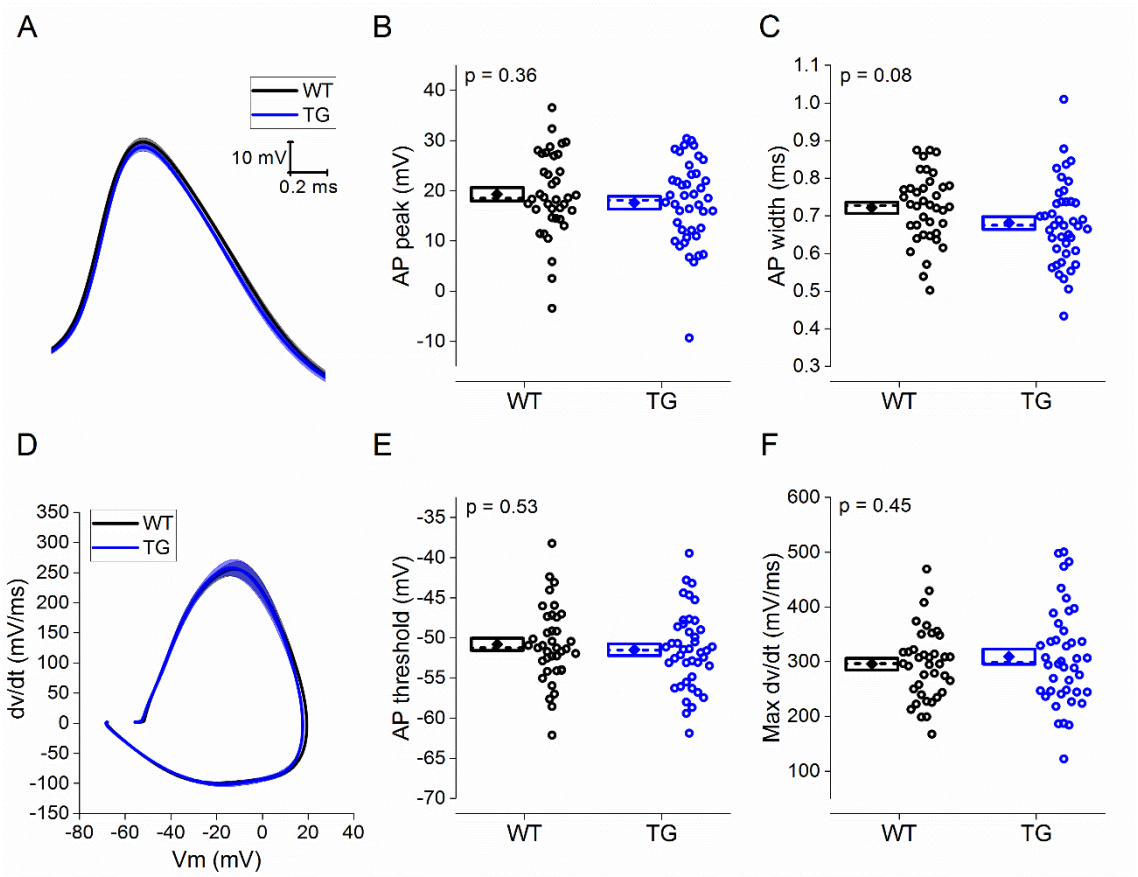

Figure 5.8. Action potential waveform properties were independent of transgene expression from a prestimulus potential of -72 mV. (A) Average waveform of the first AP generated in response to 90 pA, 500 ms depolarising current injection. (B+C) Plot showing the (B) the absolute peak voltage value of the AP and (C) the AP width at half height. Diamond represents mean, dashed line represents median, and box represents SEM. (D) Average phase plot of first generated AP, plotting the first derivative of the AP voltage against AP voltage. (E+F) Plot showing the (E) AP threshold and (F) the maximal rate of rise. Diamond represents mean, dashed line represents median, and box represents SEM. All p values were calculated using an unpaired, two tailed student's t-test.

5.3.6 The effect of transgene expression on T-type Ca^{2+} channel currents

The increased prevalence of rebound firing (Fig 5.3B+C) along with the decrease in latency to the first spike from a prestimulus potential of -80 mV (Fig 5.5F) but not -72 mV (Fig 5.5E) suggests that there may be increase in expression or an alteration in the voltage-dependent kinetics of the T-type Ca^{2+} channel in J20 neurons. One would expect that such a change would be manifested as an observable increase in the ability of neurons to fire at high frequencies from a prestimulus potential of -80 mV but not -72 mV. To this end we examined the firing patterns following our 500 ms depolarising square current injection highlighted in Figure 5.5A. We limited our examination to our two largest depolarising steps at least 88% of neurons fire at least 2 APs (-72 mV, 50 pA, WT, 33/37, 89%, TG, 39/44, 89%; 60 pA, WT, 33/37, 89%, TG, 41/44, 93%: -80 mV, 50 pA, WT, 37/38, 97%, TG, 46/47, 98%; 60 pA, WT, 37/38, 97%, TG, 47/47, 100%). Visual examination of Figure 5.9A-D suggest transgene expression had no effect on the mean instantaneous frequency of AP generation from a prestimulus potential of either -72 or -80 mV in response to 75 pA or 90 pA current injections. The instantaneous frequency between the first and second AP was used as a quantitative measure of high frequency firing. Transgene expression had no effect on the first instantaneous frequency from -72 mV (Fig 5.8A, 50 pA, WT, median 39.4 Hz, n = 33; TG, median 40.6 Hz, n = 39; p = 0.76, Mann-Whitney U test; Fig 5.8B, 60 pA, WT, median 49.1 Hz, n = 33; TG, median 50.9 Hz, n = 41; p = 0.82, Mann-Whitney U test) or -80 mV (Fig 5.8C, 50 pA, WT, median 149.8 Hz, n = 38; TG, median 139.6 Hz, n = 46; p = 0.9, Mann-Whitney U test; Fig 5.8D, 60 pA, WT, median 146.8 Hz, n = 38; TG, median 156.7 Hz, n = 47; p = 0.44, Mann-Whitney U test).

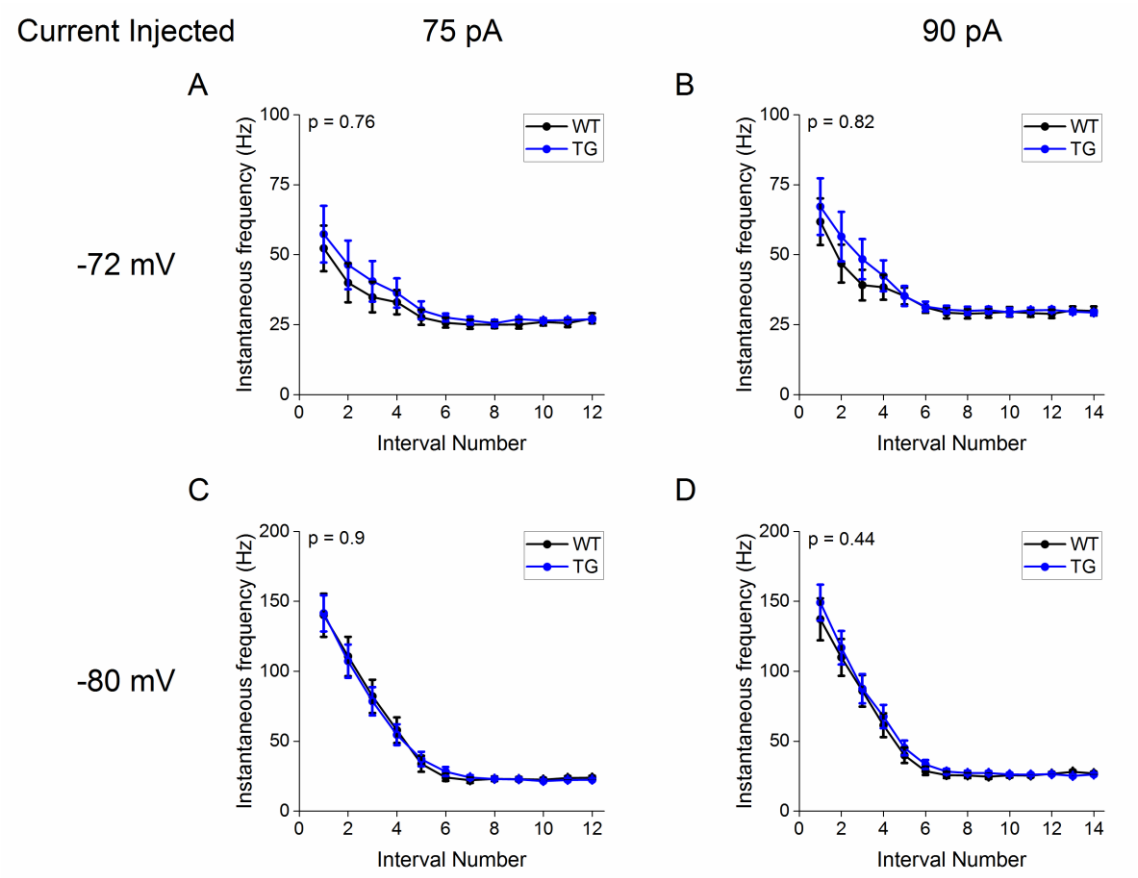

Figure 5.9. Transgene expression had no effect on the output function of generated APs. (A+B) A plot of instantaneous AP frequency vs interval number for a (A) 75 and (B) 90 pA, 500 ms depolarising current step from a prestimulus potential of -72 mV. (C+D) A plot of instantaneous AP frequency vs interval number for a (C) 75 and (D) 90 pA, 500 ms depolarising current step from a prestimulus potential of -80 mV. Error bars represent SEM. F and p values calculated using a 2 way RM-ANOVA, calculated by comparing the instantaneous frequency between the first and second AP.

Another consequence of increased T-type channel conductance would be an increase in the number of cells exhibiting sub and suprathreshold ADPs following generation of a primary AP. The proportion of cells which exhibit these behaviours is unaffected by transgene expression (Fig 5.10A, $p = 0.68$, Chi-squared test). For neurons which display an ADP which is greater than zero but less than AP threshold it is possible to directly measure ADP amplitude. An average trace of these neurons is represented in Figure 5.10B. Transgene expression had no effect on the mean amplitude of the ADP (Fig 5.10C, WT, mean 11.9 ± 2.0 mV, $n = 12$; TG, mean 13.0 ± 1.7, $n = 18$; $p = 0.67$, unpaired, two tailed students t-test). Together these results suggest that the T-type Ca^{2+} channels themselves are not differentially active as a result of transgene expression.

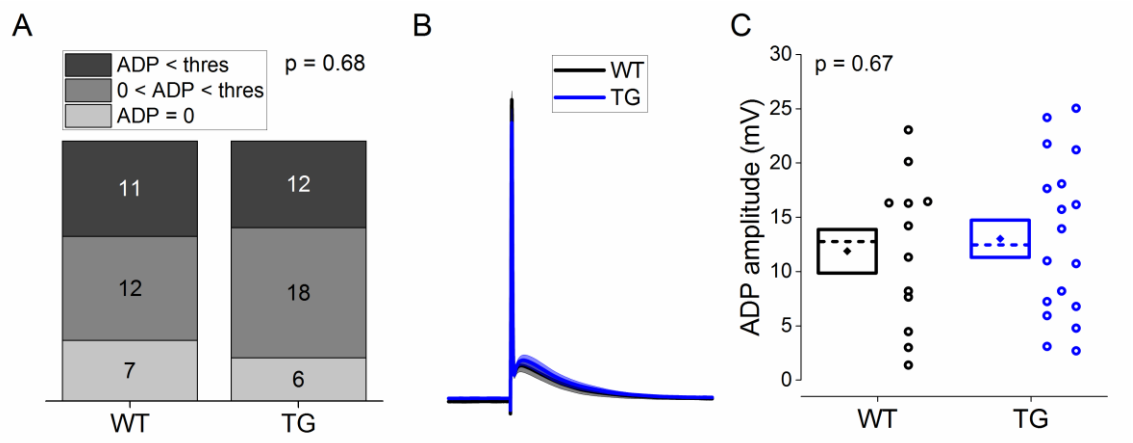

Figure 5.10. Effect of transgene expression on ADP amplitude. (A) Cumulative column representation of the number of neurons which do not exhibit an ADP, the number of neurons exhibiting a subthreshold ADP and the number of neurons which exhibit a suprathreshold ADP across genotype. This was measured from a holding potential of -80 mV. p value was calculated using a Chi-squared test. (B) Average voltage trace in response to a short (1.25 ms), large (2 nA) current injection in cells exhibiting a subthreshold ADP. Line represents mean and shaded area represents SEM. (C) Plot showing the ADP amplitude in neurons exhibiting a subthreshold ADP. Diamond represents mean, dashed line represents median, and box represents SEM. p value was calculated using an unpaired, two tailed student's t-test.

In order to confirm this we directly recorded T-type Ca^{2+} currents using a $CsMeSO_4$ based intracellular solution. To study voltage kinetics of channel activation, a series of voltage steps was applied ranging from -75 mV to -47 mV from a holding potential of -85 mV (see Figure 3.15). In response to larger voltage steps an inward current was observed which was evidently larger and displayed longer activation and inactivation kinetics than the T-type channel currents described in Section 3 (see Figure 5.11A), most likely a result of a large HVA Ca^{2+} channel current. In an attempt to minimise the confounds of measuring the amplitude of T-type Ca^{2+} current, analysis was restricted to those voltage steps ranging from -75 mV to -51 mV, where HVA activation should be minimal.

The steady state inactivation profile of the channel was studied using a depolarising voltage step to -65 mV from a prestep potential incrementally increasing from -105 mV to -66 mV. A representative recording of the evoked currents is displayed in Figure 5.11B. Average I/V plots of maximal inward current and inactivation curves are displayed in Figure 5.11C. Visual examination of the curves indicated that there is no clear hyperpolarising or depolarising shift in either plot. In light of the data presented in Figures 5.11 in conjunction with the similar occurrence of high frequency bursting and comparable observed ADP amplitude, one can say with a degree of confidence that alterations to T-type Ca^{2+} channels do not underlie the alterations in the intrinsic properties of neurons described above.

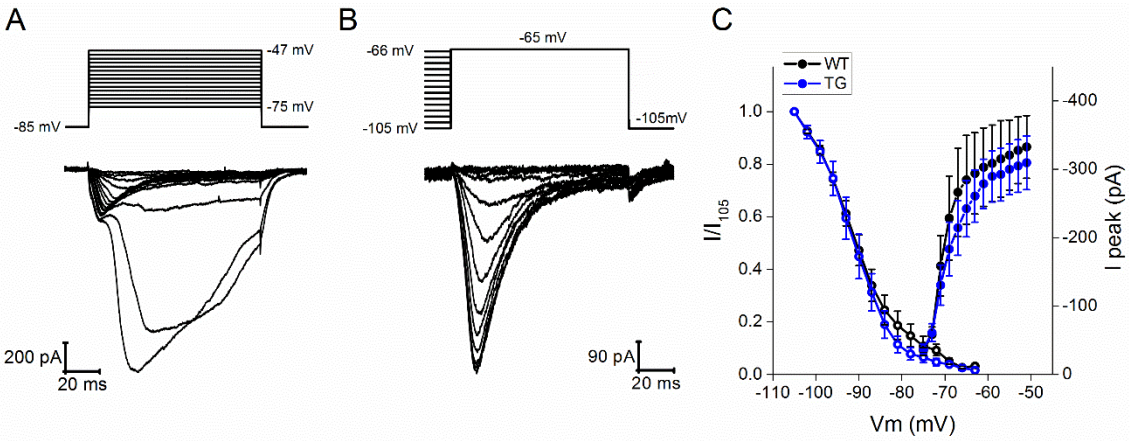

Figure 5.11. The effect of transgene expression on T-type Ca^{2+} channel kinetics. (A) Sample voltage trace and the subsequent current response to a series of 2 mV incremental depolarising voltage steps (from -75 – -47 mV) from a prestimulus potential of -85 mV using a $CsMeSO_4$ based internal solution. (B) Sample voltage trace and the subsequent current response to a series of depolarising voltage steps to -65 mV from an incrementally depolarised prestimulus potential (-105 mV – -66 mV) was used to calculate the steady state inactivation curve of T-type Ca^{2+} channels. (C) Average I-V plot (closed circles) of the peak current observed in response to a series of 2 mV voltage steps. Inactivation curve (open circles) showing the average voltage at which T-type Ca^{2+} channels inactivate.

5.4 Discussion

The results described here provide evidence that the intrinsic properties of neurons in the Re are altered in 12-14 month old J20 mice. The main findings are; 1) a higher proportion of J20 Re neurons displayed a hyperpolarised V_m as compared to WT controls, 2) frequency of rebound firing was increased, 3) there were no changes to passive membrane properties or neuronal excitability, 4) there was a voltage-dependent decrease in the latency to the first AP, and 5) AP width was narrower. All changes in the Re occurred in the absence of the dense pathological plaques commonly associated with AD pathology confirming reports that the intrinsic properties of neurons can be altered in the absence of plaques in mouse models of amyloidopathy (Wykes *et al.*, 2012; Kerrigan *et al.*, 2014). This suggests that soluble forms of Aβ, which are abundant in the thalamus of Aβ overexpressing mice (Johnson-Wood *et al.*, 1997), may be the primary contributor to a proportion of observed alterations to the intrinsic electrophysiological profile of neurons in a model of amyloidopathy.

A greater proportion of Re neurons in J20 mice exhibit a hyperpolarised V_m, although the mechanistic basis of this effect were not studied in detail in this study. One possible candidate mechanism could be the an increase in a hyperpolarising potassium leak current, however given that the passive membrane properties remain unchanged, alterations to a single background conductance seem unlikely. A decrease in a tonic depolarising NMDA mediated current would also be possible. While such a current has yet to be described in Re neurons, the midline thalamus contains NMDA receptors with the NR2D subunit (Beaton *et al.*, 1992), which has a low sensitivity for voltage-dependant magnesium block (Kuner & Schoepfer, 1996). Although the depolarised potential of Re neurons in the presence of NMDA antagonist LY-689560 (Fig 3.5) directly contradicts this hypothesis, the robust delta oscillations produced by the injection of ketamine directly into the Re (Zhang *et al.*, 2012; Duan *et al.*, 2015) points towards the existence of such a current. Simultaneous alterations to two such tonic currents (increased hyperpolarising K^+ leak conductance and reduced depolarising NMDA tone) could feasibly hyperpolarise neurons without a consequent change in passive membrane properties.

While the mechanisms underlying this alteration should undoubtedly be the subject of further investigation, from a functional perspective such an alteration

will have telling consequences on the functional output of Re neurons. As described in chapter 3, neurons sitting at hyperpolarised potentials (circa -80 mV) tend to exhibit high frequency burst firing in response to depolarising current injections. This shift from single spikes to burst firing will have important consequences in context of the cognitive network within which the Re sits. Indeed when delta oscillations are optogenetically induced in the Re, a behaviour caused by large clusters of neurons firing synchronous bursts at delta frequency, working memory deficits are produced (Duan *et al.*, 2015).

Another indication that abnormal burst firing behaviour may be present in Re neurons is the increase in rebound firing observed following hyperpolarising input. The functional consequences of such an alteration would be most evident during SWS where the thalamocortical system exhibits slow wave (<4 Hz) oscillations (Steriade *et al.*, 1993). These oscillations involve large numbers of thalamic relay neurons exhibiting synchronous burst firing and are known to be vital for memory consolidation (Marshall *et al.*, 2006). β-amyloid burden in the mPFC has been shown to disrupt this SWS in humans which correlates to impaired hippocampal dependant memory consolidation (Mander *et al.*, 2015). Concurrently absence seizures, aberrant network activity in which thalamocortical circuits are crucially involved (Snead, 1995), have also been observed in large expanses of the cerebral cortex in J20 mice (Palop & Mucke, 2009) and the presence of such activity has been suggested to underpin cognitive deficits (Sanchez *et al.*, 2012). An increase in burst firing localised to the midline thalamus could provide a cellular correlate of this abnormal network behaviour, as evidenced by the evocation of widespread synchronous cortical activity following low frequency stimulation of the midline thalamus (Dempsey & Morison, 1942). The idea that alterations in the propensity or timing of Re neurons to burst fire could underlie such disruptions is very interesting. If demonstrated, it would raise new possibilities for pharmacological or deep brain stimulation interventions targeting T-type Ca^{2+} channel activity in the midline thalamus as a novel target for targeting memory in AD associated deficits.

Mechanistically the increase in rebound firing and the voltage dependant decrease in the latency to the first AP are indeed, at first glance, suggestive of a direct change to T-type Ca^{2+} channel conductance. However assessment of the proportion of neurons which fire at high frequencies and the size of the ADP

following a single spike, neuronal behaviours which in Re neurons are dependent on T-type Ca^{2+} channel conductance (see section 3), contradict this. These parameters are independent of transgene expression and this lack of change in T-type Ca^{2+} channel conductance was confirmed by direct measurement using a $CsMeSO_4$ based internal solution. The mechanistic basis of these changes is worthy of further investigation, however it was beyond the scope of this study. One possibility is a reduction in the small conductance Ca^{2+} activated potassium (SK) current. These channels have previously been shown to be functionally linked to T-type Ca^{2+} channels in dendrites of the Rt (Cueni *et al.*, 2008) and dopaminergic neurons (Wolfart & Roeper, 2002; Hallworth *et al.*, 2003). A similar mechanism in Re neurons would provide a rapid hyperpolarising current to counterbalance the depolarising Ca^{2+} spike elicited upon Ca^{2+} entry through T-type Ca^{2+} channels. Following activation of T-type Ca^{2+} channels (after release from a hyperpolarising stimulus or following a depolarising current injection from a prestimulus potential of -80 mV but not -72 mV) any alterations to the pathways with which this Ca^{2+} influx leads to the activation of SK current could potentially lead to alterations in rebound firing and the latency to the first AP from a hyperpolarised prestimulus potential. Indeed SK currents have been shown to counteract rebound firing in subthalamic neurons through their coupling to T-type Ca^{2+} channels (Hallworth *et al.*, 2003). One could easily test if SK channel conductance was altered in Re neurons in J20 mice via inclusion of SK channel blocker apamin as a background condition during recordings (although this would depend on the particular SK channel subtype present in the Re).

The ~8% reduction in spike width from -80 mV is reminiscent of what is observed in hippocampal CA1 neurons from the same prestimulus potential in models of amyloidopathy (Brown *et al.*, 2011; Wykes *et al.*, 2012; Kerrigan *et al.*, 2014; Tamagnini *et al.*, 2015). Given the kinetics of the channels involved, Ca^{2+} entry increases in an exponential fashion over the duration of an AP. Mathematical modelling and whole cell experiments have suggested that a similar decrease (10-15%) in CA1 neurons can lead to a 40% reduction in Ca^{2+} entry during an AP (Kerrigan *et al.*, 2014). Given the role of Ca^{2+} ions in vital cellular processes, this decrease in Ca^{2+} entry would undoubtedly have marked effects in normal cellular functioning. One such change is the amount of neurotransmitter being released at the synapse following AP generation.

The underlying mechanisms of this change in AP waveform are unknown, however it has been suggested that an increase in voltage gated potassium channel conductance, specifically Kv 3.1, is the underlying cause in hippocampal CA1 neurons (Wykes *et al.*, 2012). Notably Kv 3.1 is weakly expressed in the Re (Weiser *et al.*, 1994). Further studies should focus on the direct measurement of voltage gated potassium conductances in these neurons utilising nucleated macropatches. The fact that the reduction in AP width is significant from a prestimulus potential of -80 mV while this is not the case from a prestimulus potential of -72 mV raises some interesting questions. Although the change in AP width is not voltage dependant, the size of the effect does seem to be attenuated at more depolarised holding potential (~5.5%). This is the first study which has looked at the AP width in a model of amyloidopathy at a range of prestimulus potentials. It would be interesting to see if similar attenuations were observed at more depolarised holding potentials in CA1 pyramidal neurons, where, a reduction in spike width is a consistant cross model finding in models of amyloidiopathy (Brown *et al.*, 2011; Wykes *et al.*, 2012; Kerrigan *et al.*, 2014; Tamagnini *et al.*, 2015). Such a finding would certainly help ascertain the mechanistic basis of the narrowing of APs. A mechanistic understanding, validated electrophysiologically across multiple brain regions, could allow the prompt answer to questions regarding the regional specificity (or lack thereof) of such alterations. An investigation into brain wide expression of relevant voltage gated ion channels using RNA sequencing could be a high throughput approach to answer such a question.

In summary, J20 mice of 12-14 months old exhibit a variety of alterations to the intrinsic properties of Re neurons independent of Aβ plaque formation. Future studies should seek to investigate the age of onset of the changes described, whether they can be correlated to behavioural deficits, and their mechanistic basis. As described, such studies have the potential to uncover potential new avenues to treat cognitive deficits associated with AD.

6 Alterations in the intrinsic electrophysiological properties of neurons in the rostral nucleus reuniens in a mouse model of frontotemporal dementia

6.1 Introduction

Frontotemporal dementia linked to chromosome 3 (FTD-3) is a rare genetic variant of FTD originally identified in a large Danish family (Gydesen *et al.*, 1987; Brown *et al.*, 1995). Patients present with personality changes, disinhibition of speech, inappropriate emotional responses, hyperorality and dyscalculia (Gydesen *et al.*, 2002) and exhibit progressive decline in measures of verbal memory, working memory and executive function (Stokholm *et al.*, 2013). The primary etiology has been identified as a gain of function missense mutation in the CHMP2B gene which results in truncation of the C-terminus of charged multivesicular protein 2B (CHMP2B) (Skibinski *et al.*, 2005; Isaacs *et al.*, 2011). This protein is a key component of the ESCRT-III complex involved in the endocytosis, subsequent degradation of membrane bound proteins and autophagy (Krasniak & Ahmad, 2016). C-terminal truncation of CHMP2B has adverse effects on endocytic trafficking (Urwin *et al.*, 2010; Clayton *et al.*, 2015) and dendritic spine maturation and functionality (Belly *et al.*, 2010; Chassefeyre *et al.*, 2015).

Mouse models expressing C-terminally truncated $CHMP2B_{intron5}$ at physiological levels reliably report behavioural deficits associated with FTD-3. These include alterations in social novelty behaviour, notably in the absence of an anxiety related phenotype (Gascon *et al.*, 2014; Clayton *et al.*, 2017) and an increase in impulsive behaviour in the context of an open field test (Vernay *et al.*, 2016). To date these models have not been subjected to a comprehensive battery of cognitive tasks, however they do not exhibit cognitive dysfunction on spontaneous alternation or Y-maze spatial novelty preference tests (Clayton *et al.*, 2017).

These mice reliably exhibit widespread pathology across the cerebral cortex and limbic system including neuronal degeneration, p62 positive cytoplasmic inclusions, ubiquitin positive inclusions, and gliosis (Ghazi-Noori *et al.*, 2012; Vernay *et al.*, 2016). Notably these pathologies are prevalent throughout the thalamus (Ghazi-Noori *et al.*, 2012; Clayton *et al.*, 2017). Brain atrophy in the thalamus is observed in FTD (Cardenas *et*

al., 2007) and reduced glucose metabolism and atrophy in the medial thalamus can be used to differentiate FTD from other forms of dementia (Schroeter *et al.*, 2007).

A nucleus of the medial thalamus, the Re has strong excitatory influence on the mPFC (Di Prisco & Vertes, 2006). Lesions to the Re can have significant effects on executive behaviour (Prasad *et al.*, 2017), including impulsive responses (Prasad *et al.*, 2013). Given the changes in executive behaviours and robust thalamic pathology observed in the $CHMP2B_{intron5}$ model described by Ghazi-Noori *et al* (2012), the intrinsic electrophysiological properties of rostral Re neurons were investigated in this model. This represents the first study to examine the cellular electrophysiological properties of a thalamic nucleus in a model of frontotemporal dementia.

6.2 Methods

All procedures were carried out in accordance with the Animals (Scientific Procedures) Act 1986. Male TG $CHMP2B_{intron5}$ mice (background strain: C57-Bl/6J) and WT littermate controls were bred at University College London. They were transported to the University of Exeter and allowed to acclimatise for at least a week in the prior to experimentation. They were housed on a 12:12 light/dark cycle and granted *ab libitum* access to food and water. This study used mice of ~14 months of age (WT, mean: 13.85 months, range: 12.83 – 14.66 months, n = 11; TG, mean: 13.86 months, range: 12.8 – 15.2 months, n = 11).

Coronal slices were prepared and neurons were recorded from as described in Materials and Methods. K-gluconate solution #2 (table 2.1) was used as the internal solution throughout experiments.

Data were analysed using custom written MATLAB scripts and Microsoft Excel. SPSS was used to test for statistical significance. Details can be found in Materials and Methods.

6.3 Results

6.3.1 Activity at rest and passive membrane properties are independent of transgene expression.

To test the basal activity of Re neurons we recorded the membrane voltage for 60 s in the absence of experimental stimuli. The V_m of these neurons was transgene independent (Fig 6.1A, WT, median -63.1 mV, n = 42; TG, median -64.4 mV, n=34; p = 0.75, Mann-Whitney U test). Transgene expression also had no effect on the proportion of neurons which exhibit spontaneous AP firing (Fig 6.1B, p = 0.67, Chi-squared test) or the frequency of this firing (Fig 6.1C, WT, median 4.3 Hz, n = 37; TG, median 5.6 Hz, n = 32; p = 0.6, Mann-Whitney U test).

The high rate of cellular death reported in thalamic neurons in this model suggests that transgene expression affects cellular viability. Such a stressor could lead to robust changes in the passive membrane properties of neurons, for example through affecting the integrity of the phospholipid membrane. The passive membrane properties were measured using a 500 ms, -20 pA hyperpolarising current injection as described in Materials and Methods. Transgene expression had no effect on R_i (Fig 6.2A, WT, mean 532 ± 26 MΩ, n = 41; TG, mean 581 ± 32 MΩ, n = 33; p = 0.23, unpaired, Student's t-test), τ (Fig 6.2B, WT, median 38.8 ms, n = 41; TG, median 33 ms, n = 33; p = 0.39, Mann-Whitney U test).

The capacitance of a neurons is directly proportion to the surface area of the soma as described in section 1.1.2. An estimate of capacitance is measured as the ratio of R_i/τ. Transgene expression resulted in a trend towards a smaller capacitance in Re neurons (Fig 6.2C, WT, median 77.6 pF, n = 41; TG, median 59.4 pF, n = 33; p = 0.1, Mann-Whitney U test).

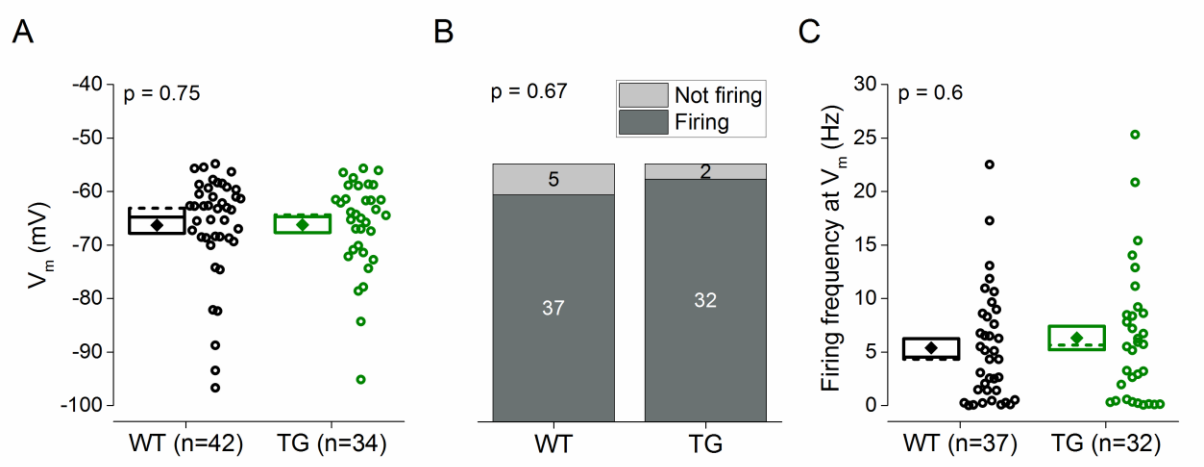

Figure 6.1. Activity at V_m was transgene independent. (A) A plot displaying the distribution of V_m observed across groups. Diamond represents mean, dashed line represents median, and box represents SEM. p value was calculated using a Mann-Whitney U test. (B) A cumulative column representation of the number of silent and spontaneously firing neurons across age group. p value was calculated using a Chi-squared test. (C) Plot showing, for firing cells, the mean firing frequency across the 60 s recording across genotype. Diamond represents mean, dashed line represents median, and box represents SEM. p value was calculated using a Mann-Whitney U test.

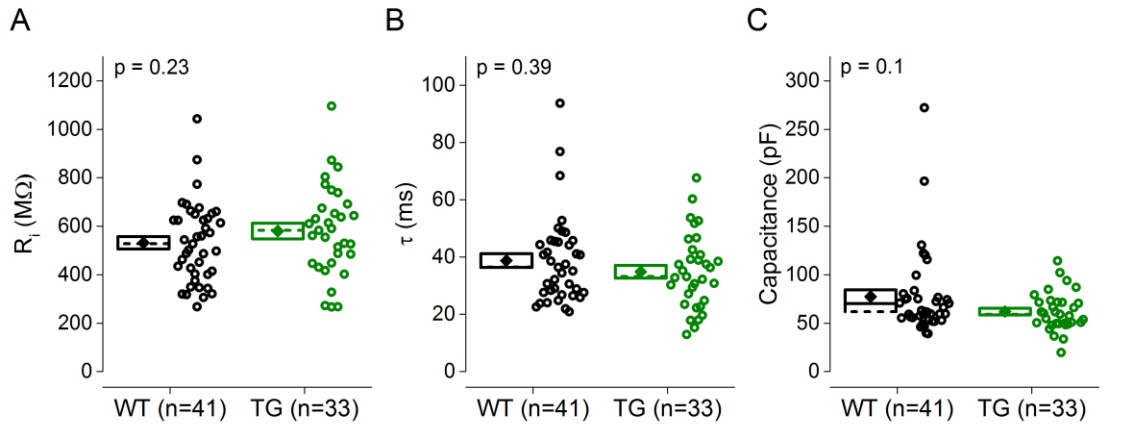

Figure 6.2. Passive membrane properties were transgene independent. (A-C) Plot showing (A) R_i and (B) τ, calculated from a 500 ms, -20 pA hyperpolarising current injection. (C) Plot showing capacitance calculated as τ/R_i. Diamond represents mean, dashed line represents median, and box represents SEM. p values were calculated using an unpaired, student's t-test (R_i), and a Mann-Whitney U test (τ and capacitance).

6.3.2 An increase in the number of spikes generated following prolonged depolarising current injections in Chmp2B$_{intron5}$ mice.

To measure the excitability of neurons a series of 500 ms depolarising current injections ranging from 10-60 pA were applied from a prestimulus potential of -80 mV. A representative voltage trace in response to one such current injection with an amplitude of 60 pA is displayed in Figure 6.3A. Transgene expression lead to a 26% increase in the number of APs generated in response to this series prolonged current injections (Fig 6.3B, $F = 5.02$, $p = 0.03$, 2 way RM-ANOVA).

The rheobase was measured with a series of 100 ms depolarising current steps from a prestimulus potential of -80 mV with an initial amplitude of 2 pA and increasing in 2 pA increments until an AP was generated. A representative voltage response in response to a rheobase current injection is displayed in Figure 6.3C. Transgene expression lead to a trend towards a decrease in the rheobase of TG neurons (Fig 6.3D, WT, median 18 pA; TG, median 14 pA; $p = 0.06$, Mann-Whitney U test).

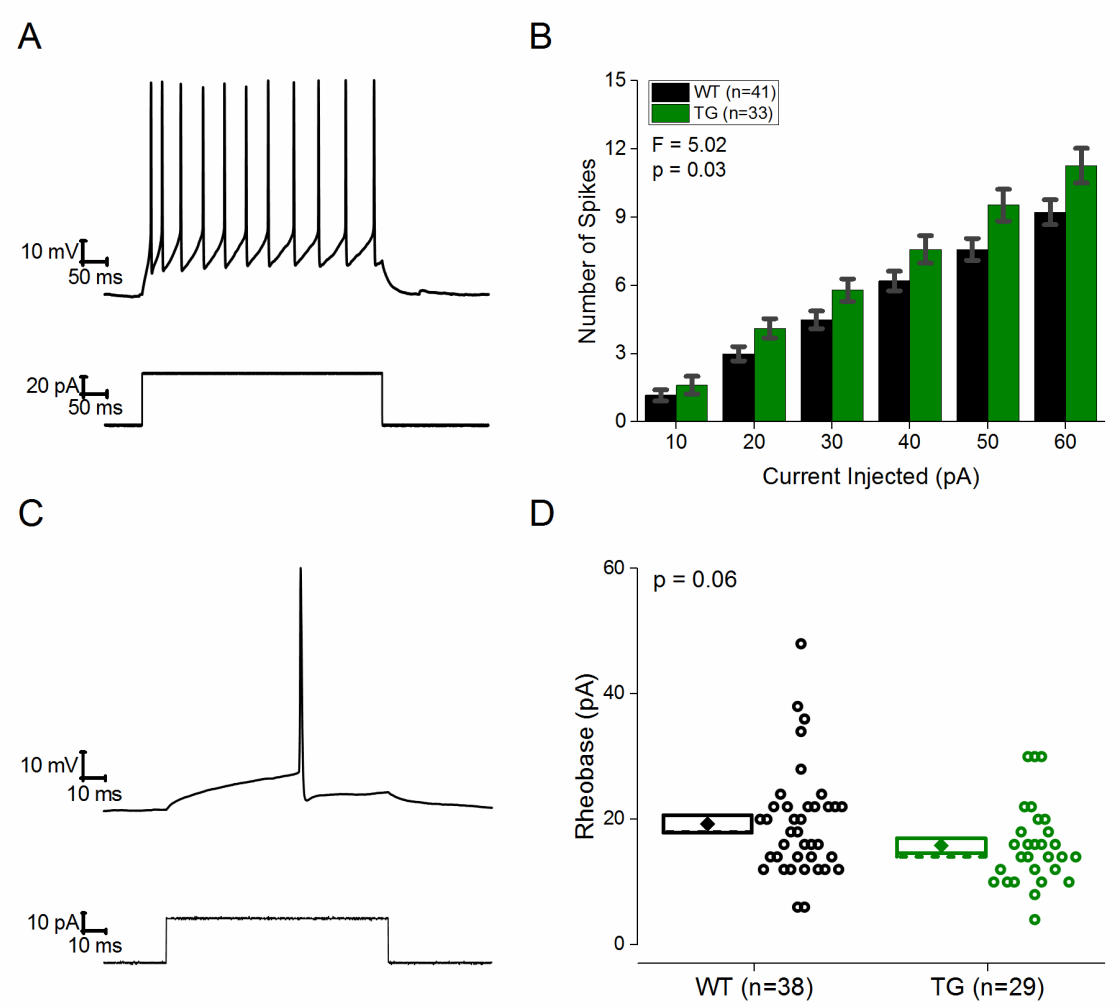

Figure 6.3. An increase in the number of spikes generated following prolonged depolarising current injections in Chmp2B$_{intron5}$ mice. (A) Sample voltage response (top) and current trace (bottom) of a 60 pA, 500 ms depolarising current injection from a prestimulus potential of -80 mV. (B) The mean number of APs produced in response to a series of 500 ms depolarising current injections from a prestimulus potential of -80 mV. F and p values calculated using a 2 way RM-ANOVA. (C) Sample voltage response (top) and 100 ms rheobase current injection (bottom). (D) Plot showing the rheobase of Re neurons at from a prestimulus potential of -80 mV. Diamond represents mean, dashed line represents median, and box represents SEM. All p values were calculated using a Mann-Whitney U test.

Another measure of excitability is the latency to the first AP. This was measured as the time taken following initiation of the current injection to the peak of the first AP generated in response to the series of 500 ms depolarising current injections, as highlighted in Figure 6.4A. To examine whether transgene expression had any significant impact on the latency to the first AP, current injections ranging from 30-60 pA were examined. At least 90% of neurons generate at least 1 AP (WT, 38/41, 93%; TG, 33/34, 97%) in response to current injections >30 pA. Transgene expression reduced the latency to the first AP (Fig 6.4B, $F = 4.04$, $p = 0.05$, 2 way RM-ANOVA). Interestingly the interaction between this reduction and the amplitude of the current stimulus was statistically significant ($F = 3.17$, $p = 0.04$).

The data presented above suggests that transgene expression subtly increases the excitability of Re neurons in response to prolonged current injections. As described in section 3, pooled data of the instantaneous frequencies observed over the course of a prolonged current injection suggest that, on average, Re neurons displays an initial high frequency burst of APs, underpinned by a T-type Ca^{2+} conductance, followed by regular spiking at ~ 20 Hz. The increase in total number of APs generated in response to prolonged current injections could be resultant of an increase in T-type Ca^{2+} conductance, which would lead to an increase in the initial high frequency firing, or an increase in the frequency of "post-burst" tonic firing. We examined the spike frequency adaption in response to 50 pA and 60 pA 500 ms depolarising current injections, inputs at which >97% of neurons generated at least 2 APs in response to (50 pA, WT 97.5%, TG 100%; 60 pA, WT 100%, TG 100%). Visual examination of Figure 6.4C+D suggest that there is no difference in the initial high frequency burst firing however regular firing seem to occur at higher frequencies in $CHMP2B_{intron5}$ mice. To quantify this we compared the instantaneous frequencies of WT and TG neurons that fired at least 9 (50 pA) or 10 (60 pA) APs between the fifth and the eight/ninth interval as appropriate. The fifth interval was chosen as the starting point for comparison as it is the first level where Δ instantaneous frequency is <20% as outlined in table 6.1. Transgene expression increased the firing frequencies within these interval windows in response to both 50 pA (WT, $n = 16$; TG, $n = 19$; $F = 9.6$, $p < 0.01$, 2 way RM-ANOVA) and 60 pA current stimuli (WT, $n = 20$; TG, $n = 20$; $F = 6.2$, $p = 0.02$, 2 way RM-ANOVA).

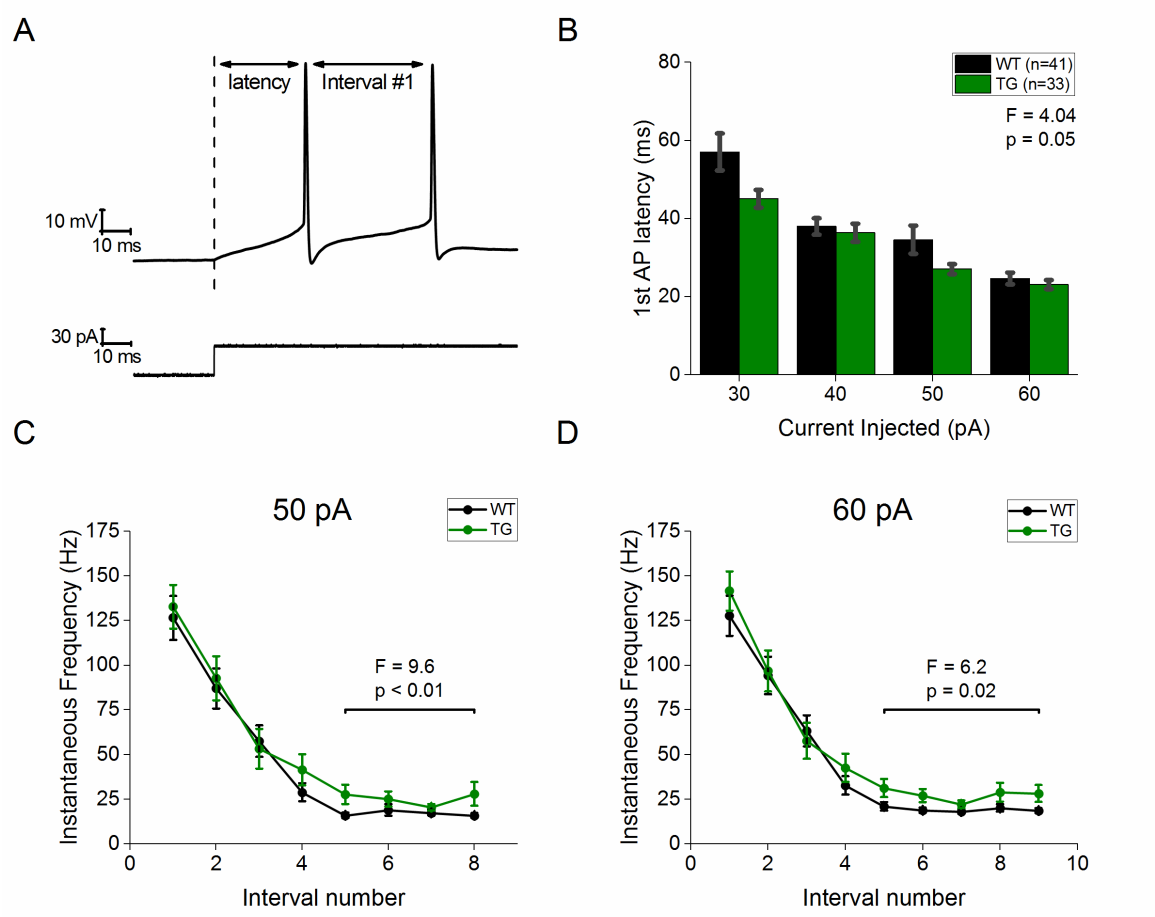

Figure 6.4. Increased excitability in CHMP2B$_{intron5}$ mice manifested as a decrease in latency to the 1st AP and an increase in tonic firing. (A) Sample voltage (top) and current (bottom) trace of the first 100 ms of a 60 pA, 500 ms depolarising current injection. Highlighted is the latency to the first AP and the interval between the first two APs. (B) Mean latency to the first AP generated during the series of 500 ms depolarising current injections from a prestimulus potential of -80 mV. F and p values calculated using a 2 way RM-ANOVA. (C+D) A plot of instantaneous AP frequency vs interval number for a (C) 50 and (D) 60 pA, 500 ms depolarising current step from a prestimulus potential of -80 mV.

Table 6.1. Percentage change in instantaneous frequency across interval number.

Interval		**1 to 2**	**2 to 3**	**3 to 4**	**4 to 5**	**5 to 6**	**6 to 7**	**7 to 8**	**8 to 9**
WT %Δ	50 pA	45.5	51.5	100.2	82.5	16.2	9.5	9.5	
	60 pA	35.6	49.2	93.8	56.9	11.5	4.2	10.2	8.2
TG	50 pA	43.3	74.4	28.4	50.0	10.4	22.9	27.0	

%Δ	60 pA	46.4	68.1	35.7	36.5	15.6	22.4	23.7	2.7

As the increase in excitability in response to prolonged depolarised current injections appears to be a result of an increased regular firing rate irrespective of T-type Ca^{2+} conductance mediated burst firing. Depolarising input which drive neurons towards AP genesis *in vivo* are considerably shorter, and from a pre-stimulus potential of -80 mV often bring the membrane voltage to threshold through activation of T-type Ca^{2+} currents (Fig 3.13). As such this increase in excitability may not be manifested in response to such shorter currents. To test this a series of depolarising αEPSC injections were applied from a pre-stimulus potential of -80 mV. αEPSCs had a decay τ of 5 ms and varied in amplitude from 50-200 pA. Sample voltage traces in response to this series of current injections are displayed in Figure 6.5A. Transgene expression had no effect on the number of APs generated in response to these current injections (Fig 6.5B, WT, n = 36; TG, n = 33; F = 0.48, p = 0.5, 2 way RM-ANOVA).

We also injected a series of three mock EPSCs with a current amplitude of 375 pA but a decay τ increasing in a four fold manner from 5-20 ms. Example voltage traces in response to this series of current injections are displayed in Figure 6.5C. Transgene expression also had no effect on the number of APs generated in response to this series of current injections (Fig 6.5D, WT, n = 38; TG, n = 32; F = 0.14, p = 0.71, 2 way RM-ANOVA).

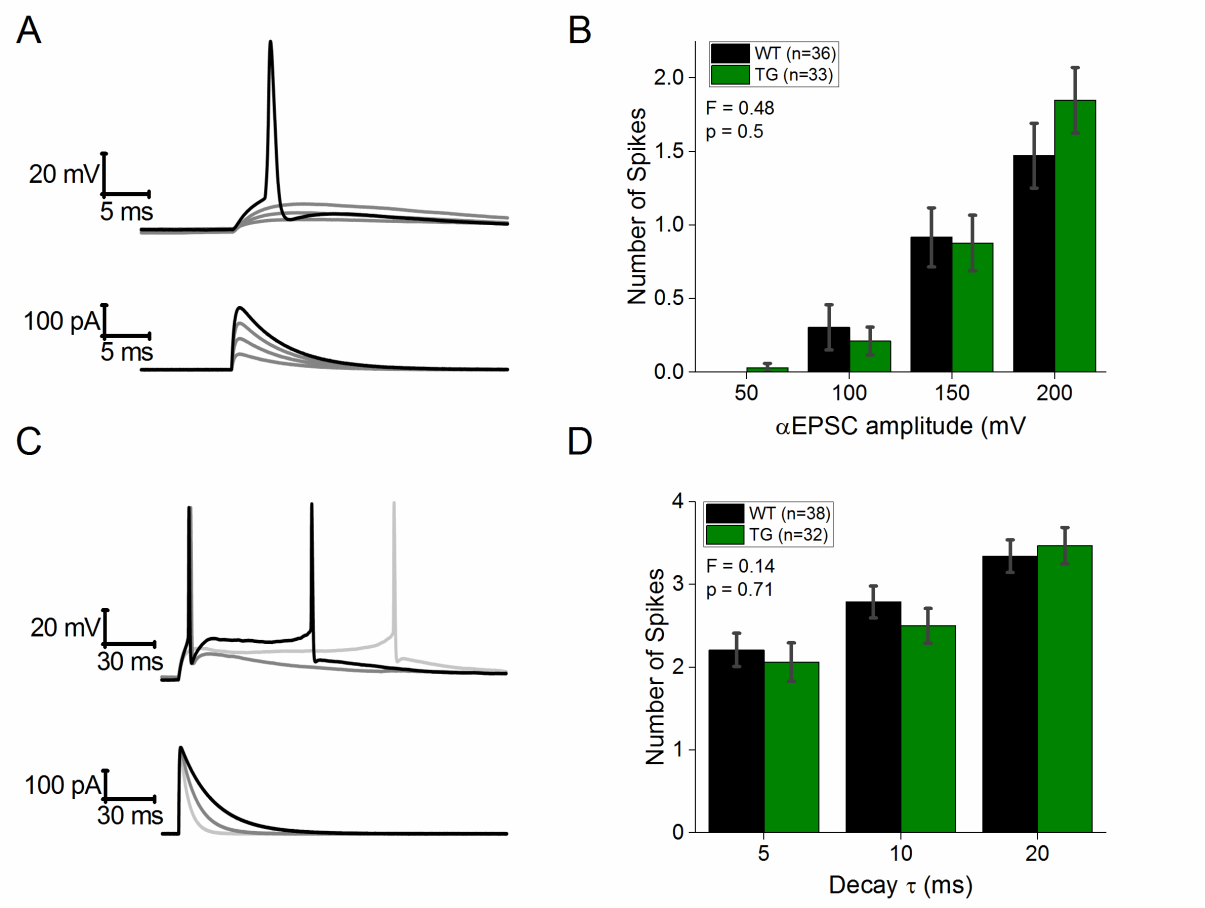

Figure 6.5. Transgene expression had no effect on the number of APs generated in response to mock EPSC current injections. (A) Sample voltage responses (top) and current traces (bottom) of four αEPSC injections of incrementally increasing amplitude (50-200 pA), with a decay τ of 5 ms. (B) The mean number of APs produced in response to said series of αEPSC injections from a prestimulus potential of -80 mV. (C) Sample voltage responses (top) and current traces (bottom) of three αEPSC injections with an amplitude of 250 pA, and decay τ increasing in a four-fold manner from 5-20 ms. (D) The mean number of APs produced in response to said series of αEPSC injections from a prestimulus potential of -80 mV. Error bars represent SEM. F and p values calculated using a 2 way RM-ANOVA.

6.3.3 Action potential waveform is transgene independent.

The AP waveform properties were measured from the first AP generated in response to the 500 ms, 60 pA depolarising input displayed in Figure 6.3A. The average AP waveform across genotype and corresponding phase plots are displayed in Figure 6.6A+B respectively. AP waveform properties were measured as described in Materials and Methods. There was no significant difference in AP width (Fig 6.6D, WT, median 0.73 ms, n = 41; TG, median 0.70 ms, n = 33; p = 0.14, Mann-Whitney U test), AP threshold (Fig 6.6E, WT, median -54.5 mV, n = 41; TG, median -54.2 mV, n = 33; p = 0.94, Mann-Whitney U test) or maximal dV/dt (Fig 6.6F, WT, median 286 mV/ms, n = 41; TG, median 278 mV/ms, n = 33; p = 0.56, Mann-Whitney U test). There was a trend towards a shorter AP peak in TG neurons (Fig 6.6C, WT, median 15.2 mV, n = 41; TG, median 13 mV, n = 33; p = 0.09, Mann-Whitney U test).

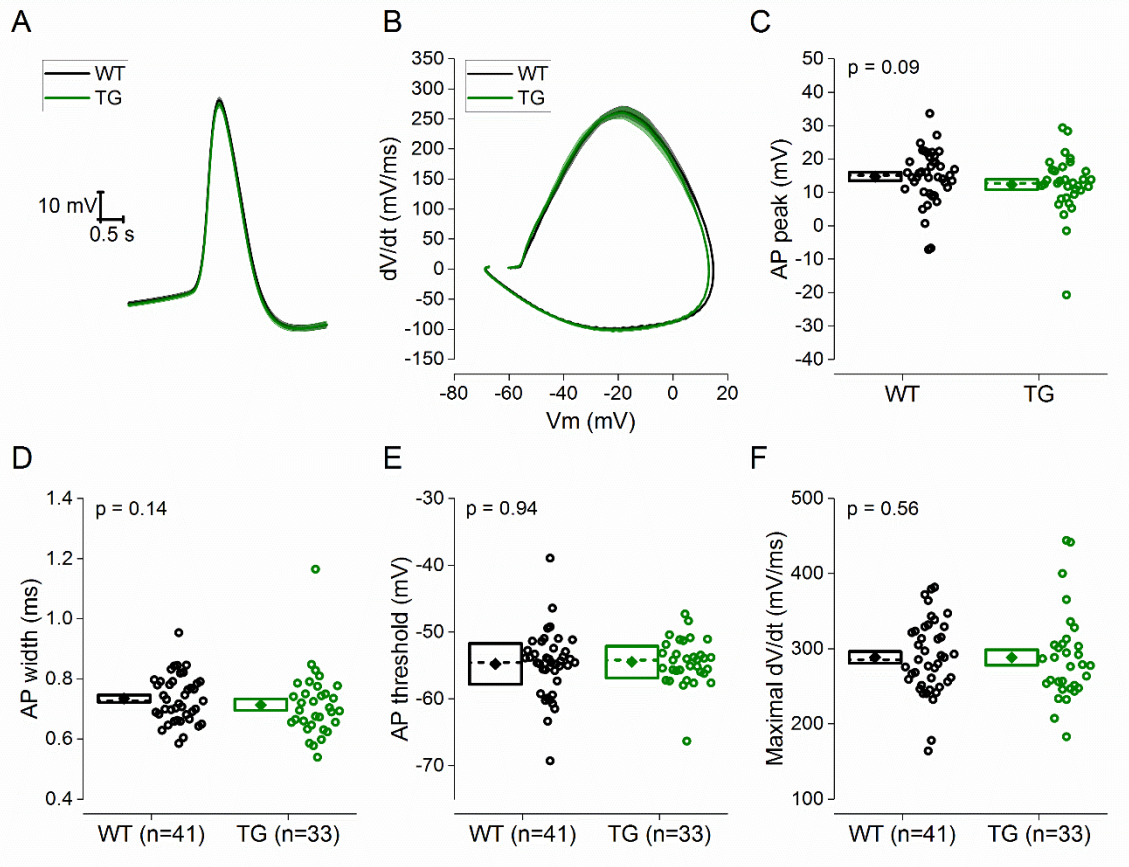

Figure 6.6. AP waveform properties were transgene independent. (A) Average waveform of the first AP generated in response to 60 pA, 500 ms depolarising current injection. (B) Average phase plot of first generated AP, plotting the first derivative of the AP voltage against AP voltage. (C-E) Plot showing the (C) the absolute peak voltage value of the AP, (D) the AP width at half height, (E) AP threshold and (F) the maximal rate of rise. Diamond represents mean, dashed line represents median, and box represents SEM. All p values were calculated using a Mann-Whitney U test.

6.3.4 Single spike afterpotential is transgene independent.

The ADP following a single spike was measured from a pre-stimulus potential of -80 mV. Neurons were divided into one of three categories based on their afterpotential following a single AP from -80 mV, namely those expressing a suprathreshold ADP, a subthreshold ADP or expressing no measurable ADP (see Materials and Methods). Transgene expression had no effect on the proportion of neurons falling into each category (Fig 6.7A, p = 0.88, Chi-squared test). The amplitude of subthreshold ADPs can be quantified directly. An average trace of these neurons for each genotype is displayed in Figure 6.7B. Transgene expression also had no effect on the amplitude of this subthreshold ADP peak (Fig 6.7C, WT, mean 12.9 ± 2.1 mV, n = 14; TG, mean 15.7 ± 1.9 mV, n = 12; p = 0.34, unpaired, Student's t-test).

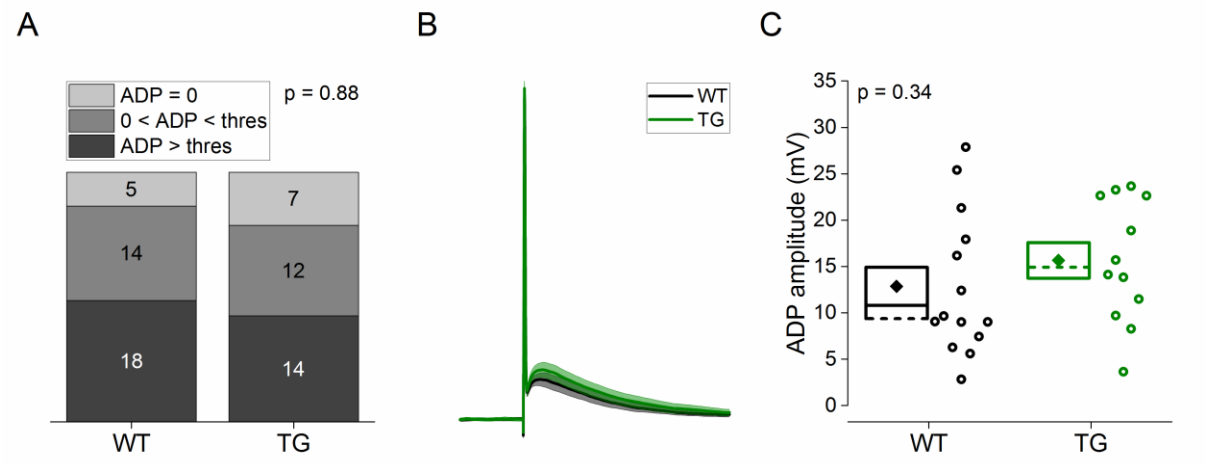

Figure 6.7. ADP following a single spike was transgene independent. (A) Cumulative column representation of the number of neurons which do not exhibit an ADP, the number of neurons exhibiting a subthreshold ADP and the number of neurons which exhibit a suprathreshold ADP across genotype. This was measured from a holding potential of -80 mV. p value was calculated using a Chi-squared test. (B) Average voltage trace in response to a short (1.25 ms), large (2 nA) current injection in cells exhibiting a subthreshold ADP. Line represents mean and shaded area represents SEM. (C) Plot showing the ADP amplitude in neurons exhibiting a subthreshold ADP. Diamond represents mean, dashed line represents median, and box represents SEM. p value was calculated using an unpaired, two tailed student's t-test.

6.4 Discussion

This study represents the first study to describe the intrinsic electrophysiological properties of neurons of the rostral Re in a model of frontotemporal dementia. The main findings were that transgene expression resulted in a subtle increase in the excitability of neurons in response to prolonged depolarising stimuli. The latency of firing of the first AP to a prolonged stimulus was shorter and there was also a trend towards a reduction in the capacitance of neurons and the peak of the AP.

The V_m, the proportion of neurons exhibiting spontaneous APs and the firing properties of these neurons at rest were transgene independent. This suggests that the activity of viable neurons within the Re is not effected by the loss of membrane integrity which would be expected given the widespread thalamic neurodegeneration and gliosis observed in this model (Ghazi-Noori *et al.*, 2012; Clayton *et al.*, 2017).

R_i and τ were unchanged by transgene expression. There was however a trend towards a smaller capacitance in TG neurons. Capacitance, as described above, is proportional to the surface area of a neuron. This suggests that transgene expression and associated inflammatory responses may cause a global shrinking of neuronal surface area. Alternatively as mentioned above expression of $Chmp2B_{intron5}$ causes a reduction in dendritic branching in hippocampal neurons (Belly *et al.*, 2010; Chassefeyre *et al.*, 2015). A reduced capacitance may be indicative of a similar mechanism in Re neurons. A detailed morphological study should be carried out to study whether there are indeed significant morphological alteration in Re neurons. Functionally a reduced membrane capacitance of a neuron would lead to an decrease in the time constant of the voltage deflection charging curve observed in response to a given current stimulus. Some weight is added to the idea that membrane capacitance may be reduced by the response of Re neurons to prolonged current injections, namely a reduction in the latency to the first AP in response to prolonged depolarising current stimuli from a set prestimulus potential of -80 mV is observed in TG neurons.

The subtle increase in the functional output of Re neurons described here is the first report of cellular hyperexcitability in a mouse model of FTD-3. Hyperexcitability has previously been reported in frontal cortex neurons of the TG4510 model of FTD (Crimins *et al.*, 2012). Interestingly ALS, which overlaps clinically, pathologically and

genetically with FTD (Ferrari *et al.*, 2011), also displays a neuronal hyperexcitability phenotype (Wainger *et al.*, 2014).

A reduction in frontocortical microRNA-124 (Mi-124) plays a causative role in the social deficits reported in $CHMP2B_{intron5}$ mice (Gascon *et al.*, 2014). Mi-124 has be shown to be downregulated in neurons following status epilepticus and can alter the excitability of neurons through antagonism of the transcriptional repressor Neuron Restricted Silencer Factor (NRSF) (Brennan *et al.*, 2016). Excess excitation of the Re can facilitate seizures in a hippocampal kindling model of epilepsy (Hirayasu & Wada, 1992) and, through the strong excitatory influence it exerts on the mPFC (Di Prisco & Vertes, 2006), excess excitation of the Re could theoretically facilitate prefronto-cortical seizures. Cortical seizure activity has been observed in mouse models of amyloidopathy and clinical cases of AD where it correlates with pathological symptoms (Palop *et al.*, 2007; Vossel *et al.*, 2013, 2016). Infusion of Mi-124 into the frontal cortex may feasibly be alleviating symptoms through an antagonism of NRSF and subsequent reduction in frontocortical seizure activity. EEG recordings, particularly in frontocortical regions, should be carried out in patients and animal models of FTD-3 to ascertain if seizure activity in the frontal cortex may play a pathological role.

A clear caveat is the specificity of this subtle hyperexcitability to prolonged current injections, largely due to an increase in the rate of tonic firing in these neurons. As such Re neurons do not exhibit hyperexcitability from a prestimulus potential of -80 mV in response to significantly shorter stimuli, such as a mock EPSC injections, which rely on the activation of subthreshold T-type Ca^{2+} conductance to drive V_m towards AP threshold (Figure 3.13). These responses are more physiological and should more accurately describe how Re neurons behave as relays within the context of a neural network. Thus the increase in excitability in response to prolonged period may not substantially change the functional output of Re neurons in response to depolarising stimuli. It may instead represent a non-specific increase in excitability as a consequence of a generalised immune response (Vezzani *et al.*, 2011) which occurs across the multiple brain areas affected by transgene expression (Ghazi-Noori *et al.*, 2012; Clayton *et al.*, 2017).

Levels of spike frequency adaption and measures of burstiness following a primary AP were unaltered. Taken together, the data presented above suggests that the

altered intrinsic electrophysiological properties of Re neurons presented here are not altered in a fashion which is likely to significantly contribute to behavioural deficits. The “increased” excitability is a result of an increase in tonic firing, which likely mirrors the transgene independent spontaneous tonic firing observed in a large proportion of Re neurons. Of course in light of the widespread thalamic cell death observed in this model, the Re may provide less net excitatory input into the mPFC which may contribute somewhat to or exacerbate symptoms. However we are far too early into the study of this disease variant to draw any firm conclusions.

This represents the first study to examine the electrophysiological properties of any brain region in a model of FTD-3. Within the last 10 years there has been an explosion of preclinical models studying the pathology of this FTD variant including a drosophila model (Ahmad *et al.*, 2009), 3 mouse models (Ghazi-Noori *et al.*, 2012; Gascon *et al.*, 2014; Vernay *et al.*, 2016), and a patient-derived induced pluripotent stem cell line (Zhang *et al.*, 2017). These models seek to exploit the advantages garnered from C-terminal truncation of the CHMP2B protein, namely the robust pathology and disease relevant behavioural deficits observed in response to physiological levels of a protein relevant to a familial form of FTD. Future studies will no doubt shed further light on the mechanisms involved in the pathology of this rare variant of FTD which could conceivably be relevant to other variants of FTD.

In conclusion this study highlighted a hyperexcitability phenotype in the neurons of the rostral Re in a mouse model of FTD-3. Although for reasons discussed above this does likely not contribute significantly to the behavioural deficits observed in this model. However this author feels that future electrophysiological studies in this model will significantly contribute to the rich literature on electrophysiological alterations across brain regions in models of FTD variants.

7 General Summary and Discussion

7.1 Electrophysiological properties of Re neurons in young adult mice

The work presented in this thesis includes seminal research into the intrinsic cellular electrophysiological properties of the Re, demonstrating that the Re has a distinct neurophysiological profile relative to other more widely studied thalamic nuclei. These findings have large implications within the field of thalamic neurophysiology where a classical view of a "typical" thalamic relay neuron's neurophysiology has been entrenched within the scientific literature for the past 40 years. This view is based largely on the extrapolation of the findings of a vast literature focussing on a limited selection of the sensory thalamus nuclei (e.g. the lateral geniculate nucleus), to the whole plethora of thalamic nuclei, based largely on the shared developmental history of all thalamic relay nuclei (Jones, 1985). The Re neurons described in this thesis differ from this "typical" thalamic neuron in several functionally important ways, including: 1) a depolarised V_m and propensity of Re neurons to display spontaneous AP firing, 2) an apparent lack of HCN currents, and 3) the diversity in the functional output of neurons following a depolarising stimulus. The passive membrane properties are also different to previous reports of thalamic relay neurons in similar experimental conditions, with the R_i of Re neurons being, on average, about 2-3 times greater. The finding of activity dependant modulation of the firing mode of Re neurons is a completely novel finding in a thalamic relay nucleus and thus one can currently only speculate on the regional specificity or indeed physiological relevance of this phenomena.

Indeed, these potentially unique features of Re neurons will undoubtedly influence our view of how it functions as a relay within the cognitively significant HPC-Re-mPFC circuit. When considered alongside the relatively recent characterisation of thalamic neurons into first and higher order nuclei, which differentially display distinct firing modes (Ramcharan *et al.*, 2005), one must consider the possibility that higher order thalamic nuclei generally display intrinsic properties which are distinct from the "typical" thalamic neuron. Investigating this would involve comparative recordings from several distinct regions of the thalamus in multiple nuclei (containing both first (FO) and higher order nuclei (HO) involved in the same sensory system) in the same animals (i.e. Visual system: lateral geniculate (FO) vs pulvinar (HO); Auditory system: ventral (FO)

vs dorsal (HO) medial geniculate nucleus). Unfortunately in the current scientific funding landscape, such a proposal may not be deemed “sexy” enough to consider devoting funds to. However with initiatives like the Allan brain atlas (http://www.brain-map.org) dedicated to making recordings across vast swathes of the brain, an answer to such a question may be just around the corner.

Of course, a degree of caution is warranted before making definitive statements about the activity of neurons which are part of an intact complex neural network (i.e. the intact mammalian brain) from data obtained from brain slices. It presupposes a level of concordance between *in vitro* and *in vivo* systems which may not be the case. Indeed even the very practice of preparing brain slices will serve to introduce relatively high levels of glutamate into the extracellular space which could confound faithful recordings of intrinsic properties through large influxes of Ca^{2+} into neurons. Concurrently extrapolating findings obtained from the mouse thalamus, (whether *in vitro* or *in vivo*) to the human thalamus could be problematic given the presence of significant populations of interneurons in human thalamic relay nuclei which do not exist in the mouse (Arcelli *et al.*, 1997). This adds an increased level of complexity and computational power to the human thalamus which is impossible to model in rodents.

7.2 Electrophysiological properties of neurons in aged mice.

Performance in cognitive tests declines over the lifespan of both humans and animals. The mechanistic basis of these cognitive deficits are of vital importance to understand in order to facilitate differentiation of these normal changes in cognition from the cognitive deficits observed in age related disorders such as dementia. The study reported in chapter 4 suggests that the intrinsic properties of Re neurons recorded from aged mice (~5 months old) are remarkably similar to those recorded in young adult mice (~16 month old). This suggests that the functional role of Re neurons is critical in normal age related cognitive decline.

While one might question the efficacy of comparing aging in humans (with a lifespan of ~80 years) to mice (with a lifespan of 2-3 years), overall the humble genetically unmodified mouse seems to be a very useful model of human aging. While humans start to develop hallmarks of mammalian aging at around 60 years of age (including: cognitive decline, increased risk of cancer, cataracts, muscle

weakness, immune abnormalities, and impaired fertility to name just a few (Miller, 2004)), these same hallmarks appear in mice within just 2 years, allowing a researcher to study the development of such symptoms at a massively accelerated rate.

7.3 Electrophysiological recording in mouse models of major neurocognitive disorders.

Chapter 5 investigated the electrophysiological properties of Re neurons in a mouse model of amyloidopathy. Understanding the mechanistic basis underpinning the loss of cognitive abilities in models of dementia is of vital scientific importance in order to develop novel therapeutic approaches, however research in models of amyloidopathy has been focused exclusively on regions of the brain where plaques are observed. Work in this thesis demonstrates that the J20 mouse model of amyloidopathy displays numerous alterations to the intrinsic neuronal properties of the non-plaque forming Re including: 1) a higher proportion of neurons exhibiting a hyperpolarised V_m, 2) an increase in the proportion of neurons exhibiting rebound spiking following hyperpolarising current injections, 3) a voltage dependant decrease in the latency to the first AP and 4) a reduction in the AP width. All these alterations should theoretically cause profound alterations in terms of Re relay function and may contribute to the cognitive deficits observed in patients. Attempting to correlate the onset of these alterations with the emergence of cognitive deficits in transgenic mice is of vital importance in order to probe whether such changes in the Re neurophysiology represent fertile ground for the development of new drugs. The midline thalamus incidentally represents quite an attractive pharmacological target due to the existence of a midline thalamic NMDA receptor which has a distinct pharmacological profile (Buller *et al.*, 1994) which could be targeted with designer compounds to modulate midline thalamic activity without many off target effects. Regardless of whether these findings ever result in any sort of clinical relevance, they are undoubtedly novel in a model of amyloidopathy. While changes to intrinsic cellular properties have been described before in CA1 pyramidal neurons prior to plaque formation (Wykes *et al.*, 2012), this is the first report of changes in the intrinsic properties of neurons in a brain region which will never develop plaque pathology. While the research focus on plaque forming regions is

understandable, this chapter suggests that neurophysiological changes in non-plaque forming brain regions in models of amyloidopathy may represent a fertile ground for future research.

Chapter 6 investigated the electrophysiological changes of Re neurons in the CHMP2B model of frontotemporal dementia. Interestingly no alterations to the intrinsic properties of Re neurons was found which was deemed relevant to the behavioural deficits observed in these mice, despite the robust and widespread thalamic neurodegeneration observed in this model.

Undoubtedly issues exist with using mouse models in the study of dementia. For example, while ~95% of AD cases are sporadic, AD mouse models almost exclusively relay on expression of mutated APP (or related genes) found in only a small fraction of total AD cases (familial AD). Thus, there are questions as to their efficacy in modelling sporadic AD. As mentioned (section 1.5.3), another notable problem with models of amyloidopathy is that they do not develop NFT pathology. Finally there are also questions as to the legitimacy of studying the effect of Aβ pathology in a mouse, where the timeframe of exposure is much shorter than AD patients. However in the absence of a viable alternative, and with these limitations firmly in mind, one must persevere.

7.4 Closing remarks

Overall I feel this work contributes significantly to our understanding of both the neurophysiology of the thalamus and the mechanisms underlying AD related cognitive deficits. This thesis is a reminder that, to the frustration of many neuroscientists, the thalamus (and indeed the mammalian brain) is not as straightforward as one may deem convenient. Meanwhile the Re alterations observed in an AD mouse model (which are not present in normal aged mice) suggests that Re dysfunction is a good biomarker for AD related cognitive decline and a potential target for future therapeutic approaches.

References

Aggleton JP (2014). Looking beyond the hippocampus: old and new neurological targets for understanding memory disorders. *Proc Biol Sci*; DOI: 10.1098/rspb.2014.0565.

Aggleton JP, Pralus A, Nelson AJD & Hornberger M (2016). Thalamic pathology and memory loss in early Alzheimer?s disease: moving the focus from the medial temporal lobe to Papez circuit. *Brain* **139,** 1877–1890.

Ahmad ST, Sweeney ST, Lee J-A, Sweeney NT & Gao F-B (2009). Genetic screen identifies serpin5 as a regulator of the toll pathway and CHMP2B toxicity associated with frontotemporal dementia. *Proc Natl Acad Sci* **106,** 12168–12173.

Albrecht D, Royl G & Kaneoke Y (1998). Very slow oscillatory activities in lateral geniculate neurons of freely moving and anesthetized rats. *Neurosci Res* **32,** 209–220.

Alger BE & Nicoll RA (1980). Epileptiform burst afterhyperolarization: calcium-dependent potassium potential in hippocampal CA1 pyramidal cells. *Science* **210,** 1122–1124.

Alonso AC, Zaidi T, Grundke-Iqbal I & Iqbal K (1994). Role of abnormally phosphorylated tau in the breakdown of microtubules in Alzheimer disease. *Proc Natl Acad Sci U S A* **91,** 5562–5566.

Amarillo Y, Zagha E, Mato G, Rudy B & Nadal MS (2014). The interplay of seven subthreshold conductances controls the resting membrane potential and the oscillatory behavior of thalamocortical neurons. *J Neurophysiol* **112,** 393–410.

American Psychiatric Association (2013). *Diagnostic and Statistical Manual of Mental Disorders*, Fifth. American Psychiatric Association, Arlington, VA.

Andorfer C, Acker CM, Kress Y, Hof PR, Duff K & Davies P (2005). Cell-Cycle Reentry and Cell Death in Transgenic Mice Expressing Nonmutant Human Tau Isoforms. *J Neurosci* **25,** 5446–5454.

Andrade R, Foehring RC & Tzingounis A V (2012). The calcium-activated slow AHP: cutting through the Gordian knot. *Front Cell Neurosci* **6,** 47.

Arai R, Jacobowitz DM & Deura S (1994). Distribution of calretinin, calbindin-D28k, and parvalbumin in the rat thalamus. *Brain Res Bull* **33,** 595–614.

Arcelli P, Frassoni C, Regondi MC, De Biasi S & Spreafico R (1997). GABAergic neurons in mammalian thalamus: a marker of thalamic complexity? *Brain Res Bull* **42,** 27–37.

Arriagada P V, Growdon JH, Hedley-Whyte ET & Hyman BT (1992). Neurofibrillary tangles but not senile plaques parallel duration and severity of Alzheimer's disease. *Neurology* **42,** 631–639.

Augustinaite S & Heggelund P (2007). Changes in firing pattern of lateral geniculate neurons caused by membrane potential dependent modulation of retinal input through NMDA receptors. *J Physiol* **582,** 297–315.

Avila J, Lucas JJ, Perez M & Hernandez F (2004). Role of Tau Protein in Both Physiological and Pathological Conditions. *Physiol Rev* **84,** 361–384.

Azouz R, Jensen MS & Yaari Y (1996). Ionic basis of spike after-depolarization and burst generation in adult rat hippocampal CA1 pyramidal cells. *J Physiol* **492 (Pt 1),** 211–223.

Bean BP (2007). The action potential in mammalian central neurons. *Nat Rev Neurosci* **8,** 451–465.

Beaton JA, Stemsrud K & Monaghan DT (1992). Identification of a novel N-methyl-D-aspartate receptor population in the rat medial thalamus. *J Neurochem* **59,** 754–757.

Beckstead RM (1979). An autoradiographic examination of corticocortical and subcortical projections of the mediodorsal-projection (prefrontal) cortex in the rat. *J Comp Neurol* **184,** 43–62.

Belly A, Bodon G, Blot B, Bouron A, Sadoul R & Goldberg Y (2010). CHMP2B mutants linked to frontotemporal dementia impair maturation of dendritic spines. *J Cell Sci* **123,** 2943–2954.

Ben-Ari Y (2002). Excitatory actions of gaba during development: the nature of the nurture. *Nat Rev Neurosci* **3,** 728–739.

Benchenane K, Peyrache A, Khamassi M, Tierney PL, Gioanni Y, Battaglia FP & Wiener SI (2010). Coherent Theta Oscillations and Reorganization of Spike Timing in the Hippocampal- Prefrontal Network upon Learning. *Neuron* **66,** 921–936.

Berendse HW & Groenewegen HJ (1991). Restricted cortical termination fields of the midline and intralaminar thalamic nuclei in the rat. *Neuroscience* **42,** 73–102.

Bertram EH, Mangan PS, Zhang D, Scott CA & Williamson JM (2001). The midline thalamus: alterations and a potential role in limbic epilepsy. *Epilepsia* **42,** 967–978.

Bertram EH & Zhang DX (1999). Thalamic excitation of hippocampal CA1 neurons: a comparison with the effects of CA3 stimulation. *Neuroscience* **92,** 15–26.

Bokor H, Csáki A, Kocsis K & Kiss J (2002). Cellular architecture of the nucleus reuniens thalami and its putative aspartatergic/glutamatergic projection to the hippocampus and medial septum in the rat. *Eur J Neurosci* **16,** 1227–1239.

Bokor H, Frère SGA, Eyre MD, Slézia A, Ulbert I, Lüthi A & Acsády L (2005). Selective GABAergic Control of Higher-Order Thalamic Relays. *Neuron* **45,** 929–940.

Booth CA, Brown JT & Randall AD (2014). Neurophysiological modification of CA1 pyramidal neurons in a transgenic mouse expressing a truncated form of disrupted-in-schizophrenia 1. *Eur J Neurosci* **39,** 1074–1090.

Booth CA, Ridler T, Murray TK, Ward MA, de Groot E, Goodfellow M, Phillips KG, Randall AD & Brown JT (2016*a*). Electrical and Network Neuronal Properties Are Preferentially Disrupted in Dorsal, But Not Ventral, Medial Entorhinal Cortex in a Mouse Model of Tauopathy. *J Neurosci* **36,** 312–324.

Booth CA, Witton J, Nowacki J, Tsaneva-Atanasova K, Jones MW, Randall AD & Brown JT (2016*b*). Altered Intrinsic Pyramidal Neuron Properties and Pathway-Specific Synaptic Dysfunction Underlie Aberrant Hippocampal Network Function in a Mouse Model of Tauopathy. *J Neurosci*.

Bowery NG & Smart TG (2009). GABA and glycine as neurotransmitters: a brief history. *Br J Pharmacol* **147,** S109–S119.

Braak H & Braak E (1991). Alzheimer's disease affects limbic nuclei of the thalamus. *Acta Neuropathol* **81,** 261–268.

Brennan GP, Dey D, Chen Y, Patterson KP, Magnetta EJ, Hall AM, Dube CM, Mei Y-T & Baram TZ (2016). Dual and Opposing Roles of MicroRNA-124 in Epilepsy Are Mediated through Inflammatory and NRSF-Dependent Gene Networks. *Cell Rep* **14,** 2402–2412.

Brown J, Ashworth A, Gydesen S, Sorensen A, Rossor M, Hardy J & Collinge J (1995). Familial non-specific dementia maps to chromosome 3. *Hum Mol Genet* **4,** 1625–1628.

Brown JT, Booth CA & Randall AD (2011*a*). Synaptic activation of mGluR1 generates persistent depression of a fast after-depolarizing potential in CA3 pyramidal neurons. *Eur J Neurosci* **33,** 879–889.

Brown JT, Chin J, Leiser SC, Pangalos MN & Randall AD (2011*b*). Altered intrinsic neuronal excitability and reduced Na+ currents in a mouse model of Alzheimer's disease. *Neurobiol Aging* **32,** 2109.e1-2109.e14.

Brown JT, Gill CH, Farmer CE, Lanneau C, Randall AD, Pangalos MN, Collingridge GL & Davies CH (2003). Mechanisms contributing to the exacerbated epileptiform activity in hippocampal slices of GABAB1 receptor subunit knockout mice. *Epilepsy Res* **57,** 121–136.

Brown JT & Randall AD (2009). Activity-dependent depression of the spike after-depolarization generates long-lasting intrinsic plasticity in hippocampal CA3 pyramidal neurons. *J Physiol* **587,** 1265–1281.

de Bruin JP, Sànchez-Santed F, Heinsbroek RP, Donker A & Postmes P (1994). A behavioural analysis of rats with damage to the medial prefrontal cortex using the Morris water maze: evidence for behavioural flexibility, but not for impaired spatial navigation. *Brain Res* **652,** 323–333.

Brunton J & Charpak S (1998). mu-Opioid peptides inhibit thalamic neurons. *J Neurosci* **18,** 1671–1678.

Bugiani O, Giaccone G, Frangione B, Ghetti B & Tagliavini F (1989). Alzheimer patients: preamyloid deposits are more widely distributed than senile plaques throughout the central nervous system. *Neurosci Lett* **103,** 263–268.

Buller AL, Larson HC, Schneider BE, Beaton JA, Morrisett RA & Monaghan DT (1994). The molecular basis of NMDA receptor subtypes: native receptor diversity is predicted by subunit composition. *J Neurosci* **14,** 5471–5484.

Burrell JR, Kiernan MC, Vucic S & Hodges JR (2011). Motor Neuron dysfunction in frontotemporal dementia. *Brain* **134,** 2582–2594.

Buzsáki G (1991). The thalamic clock: Emergent network properties. *Neuroscience* **41,** 351–364.

Buzsáki G (2002). Theta Oscillations in the Hippocampus. *Neuron* **33,** 325–340.

Cardenas VA, Boxer AL, Chao LL, Gorno-Tempini ML, Miller BL, Weiner MW & Studholme C (2007). Deformation-Based Morphometry Reveals Brain Atrophy in Frontotemporal Dementia. *Arch Neurol* **64,** 873.

Carlesimo GA, Costa A, Serra L, Bozzali M, Fadda L & Caltagirone C (2011). Prospective memory in thalamic amnesia. *Neuropsychologia* **49,** 2199–2208.

Cassel J-C, Pereira de Vasconcelos A, Loureiro M, Cholvin T, Dalrymple-Alford JC & Vertes RP (2013). The reuniens and rhomboid nuclei: Neuroanatomy, electrophysiological characteristics and behavioral implications. *Prog Neurobiol* **111,** 34–52.

Chang Y-M, Rosene DL, Killiany RJ, Mangiamele LA & Luebke JI (2005). Increased Action Potential Firing Rates of Layer 2/3 Pyramidal Cells in the Prefrontal Cortex are Significantly Related to Cognitive Performance in Aged Monkeys. *Cereb Cortex* **15,** 409–418.

Chassefeyre R, Martinez-Hernandez J, Bertaso F, Bouquier N, Blot B, Laporte M, Fraboulet S, Coute Y, Devoy A, Isaacs AM, Pernet-Gallay K, Sadoul R, Fagni L & Goldberg Y (2015). Regulation of Postsynaptic Function by the Dementia-Related ESCRT-III Subunit CHMP2B. *J Neurosci* **35,** 3155–3173.

Chemin J, Monteil A, Perez-Reyes E, Bourinet E, Nargeot J & Lory P (2002). Specific contribution of human T-type calcium channel isotypes (alpha(1G), alpha(1H) and alpha(1I)) to neuronal excitability. *J Physiol* **540,** 3–14.

Chinwalla AT et al. (2002). Initial sequencing and comparative analysis of the mouse genome. *Nature* **420,** 520–562.

Cholvin T, Loureiro M, Cassel R, Cosquer B, Geiger K, De Sa Nogueira D, Raingard H, Robelin L, Kelche C, Pereira de Vasconcelos A & Cassel J-C (2013). The ventral midline thalamus contributes to strategy shifting in a memory task requiring both prefrontal cortical and hippocampal functions. *J Neurosci* **33,** 8772–8783.

Chudasama Y, Passetti F, Rhodes SE V, Lopian D, Desai A & Robbins TW (2003). Dissociable aspects of performance on the 5-choice serial reaction time task following lesions of the dorsal anterior cingulate, infralimbic and

orbitofrontal cortex in the rat: differential effects on selectivity, impulsivity and compulsivity. *Behav Brain Res* **146,** 105–119.

Chudasama Y & Robbins TW (2004). Dopaminergic Modulation of Visual Attention and Working Memory in the Rodent Prefrontal Cortex. *Neuropsychopharmacology* **29,** 1628–1636.

Churchwell JC & Kesner RP (2011). Hippocampal-prefrontal dynamics in spatial working memory: Interactions and independent parallel processing. *Behav Brain Res* **225,** 389–395.

Clayton EL et al. (2017). Early microgliosis precedes neuronal loss and behavioural impairment in mice with a frontotemporal dementia-causing CHMP2B mutation. *Hum Mol Genet*ddx003.

Clayton EL, Mizielinska S, Edgar JR, Nielsen TT, Marshall S, Norona FE, Robbins M, Damirji H, Holm IE, Johannsen P, Nielsen JE, Asante EA, Collinge J, Isaacs AM & Isaacs AM (2015). Frontotemporal dementia caused by CHMP2B mutation is characterised by neuronal lysosomal storage pathology. *Acta Neuropathol* **130,** 511–523.

Clementz BA, Sponheim SR, Iacono WG & Beiser M (1994). Resting EEG in first-episode schizophrenia patients, bipolar psychosis patients, and their first-degree relatives. *Psychophysiology* **31,** 486–494.

Cohen RM, Rezai-Zadeh K, Weitz TM, Rentsendorj A, Gate D, Spivak I, Bholat Y, Vasilevko V, Glabe CG, Breunig JJ, Rakic P, Davtyan H, Agadjanyan MG, Kepe V, Barrio JR, Bannykh S, Szekely CA, Pechnick RN & Town T (2013). A Transgenic Alzheimer Rat with Plaques, Tau Pathology, Behavioral Impairment, Oligomeric A , and Frank Neuronal Loss. *J Neurosci* **33,** 6245–6256.

von Cramon DY, Hebel N & Schuri U (1985). A contribution to the anatomical basis of thalamic amnesia. *Brain* **108 (Pt 4),** 993–1008.

Crimins JL, Rocher AB & Luebke JI (2012). Electrophysiological changes precede morphological changes to frontal cortical pyramidal neurons in the rTg4510 mouse model of progressive tauopathy. *Acta Neuropathol* **124,** 777–795.

Cruts M, Theuns J & Van Broeckhoven C (2012). Locus-specific mutation databases for neurodegenerative brain diseases. *Hum Mutat* **33,** 1340–1344.

Cueni L, Canepari M, Luján R, Emmenegger Y, Watanabe M, Bond CT, Franken P, Adelman JP & Lüthi A (2008). T-type Ca2+ channels, SK2 channels and SERCAs gate sleep-related oscillations in thalamic dendrites. *Nat Neurosci* **11,** 683–692.

Custer SK, Neumann M, Lu H, Wright AC & Taylor JP (2010). Transgenic mice expressing mutant forms VCP/p97 recapitulate the full spectrum of IBMPFD including degeneration in muscle, brain and bone. *Hum Mol Genet* **19,** 1741–1755.

Davoodi FG, Motamedi F, Naghdi N & Akbari E (2009). Effect of reversible inactivation of the reuniens nucleus on spatial learning and memory in rats using Morris water maze task. *Behav Brain Res* **198,** 130–135.

Dawson N, Kurihara M, Thomson DM, Winchester CL, McVie A, Hedde JR, Randall AD, Shen S, Seymour PA, Hughes ZA, Dunlop J, Brown JT, Brandon NJ, Morris BJ & Pratt JA (2015). Altered functional brain network connectivity and glutamate system function in transgenic mice expressing truncated Disrupted-in-Schizophrenia 1. *Transl Psychiatry* **5,** e569.

Dempsey EW & Morison RS (1942). THE PRODUCTION OF RHYTHMICALLY RECURRENT CORTICAL POTENTIALS AFTER LOCALIZED THALAMIC STIMULATION. *Am J Physiol* **135,** 293–300.

Diekelmann S & Born J (2010). The memory function of sleep. *Nat Rev Neurosci* **11,** 114–126.

Disterhoft JF, Moyer JR & Thompson LT (1994). The calcium rationale in aging and Alzheimer's disease. Evidence from an animal model of normal aging. *Ann N Y Acad Sci* **747,** 382–406.

Disterhoft JF & Oh MM (2006). Pharmacological and molecular enhancement of learning in aging and Alzheimer's disease. *J Physiol* **99,** 180–192.

Dolleman-Van der Weel MJ, Lopes da Silva FH & Witter MP (1997). Nucleus Reuniens Thalami Modulates Activity in Hippocampal Field CA1 through Excitatory and Inhibitory Mechanisms. *J Neurosci* **17,** 5640–5650.

Dolleman-van der Weel MJ, Morris RGM & Witter MP (2009). Neurotoxic lesions of the thalamic reuniens or mediodorsal nucleus in rats affect non-mnemonic aspects of watermaze learning. *Brain Struct Funct* **213,** 329–342.

Dolleman-Van der Weel MJ & Witter MP (2000). *Nucleus reuniens thalami innervates γ aminobutyric acid positive cells in hippocampal field CA1 of the rat*.

Domich L, Oakson G & Steriade M (1986). Thalamic burst patterns in the naturally sleeping cat: a comparison between cortically projecting and reticularis neurones. *J Physiol* **379,** 429–449.

Douet V & Chang L (2014). Fornix as an imaging marker for episodic memory deficits in healthy aging and in various neurological disorders. *Front Aging Neurosci* **6,** 343.

Drexel M, Preidt AP, Kirchmair E & Sperk G (2011). Parvalbumin interneurons and calretinin fibers arising from the thalamic nucleus reuniens degenerate in the subiculum after kainic acid-induced seizures. *Neuroscience* **189,** 316–329.

Duan AR, Varela C, Zhang Y, Shen Y, Xiong L, Wilson M & Lisman J (2015). Delta frequency optogenetic stimulation of a thalamic nucleus reuniens is sufficient to produce working memory deficits; relevance to schizophrenia. *Biol Psychiatry* **77,** 1098–1107.

Ego-Stengel V & Wilson MA (2010). Disruption of ripple-associated hippocampal activity during rest impairs spatial learning in the rat. *Hippocampus* **20,** 1–10.

Ellender TJ, Raimondo J V, Irkle A, Lamsa KP & Akerman CJ (2014). Excitatory effects of parvalbumin-expressing interneurons maintain hippocampal epileptiform activity via synchronous afterdischarges. *J Neurosci* **34,** 15208–15222.

Esparza TJ, Zhao H, Cirrito JR, Cairns NJ, Bateman RJ, Holtzman DM & Brody DL (2013). Amyloid-β oligomerization in Alzheimer dementia versus high-pathology controls. *Ann Neurol* **73,** 104–119.

Ferino F, Thierry AM & Glowinski J (1987). Anatomical and electrophysiological evidence for a direct projection from Ammon's horn to the medial prefrontal cortex in the rat. *Exp brain Res* **65,** 421–426.

Ferrari R, Kapogiannis D, Huey ED & Momeni P (2011). FTD and ALS: a tale of two diseases. *Curr Alzheimer Res* **8,** 273–294.

Ferri CP, Prince M, Brayne C, Brodaty H, Fratiglioni L, Ganguli M, Hall K, Hasegawa K, Hendrie H, Huang Y, Jorm A, Mathers C, Menezes PR, Rimmer E, Scazufca M & Alzheimer's Disease International (2005). Global prevalence of dementia: a Delphi consensus study. *Lancet* **366,** 2112–2117.

Floresco SB, Seamans JK & Phillips AG (1997). Selective Roles for Hippocampal, Prefrontal Cortical, and Ventral Striatal Circuits in Radial-Arm Maze Tasks With or Without a Delay. *J Neurosci* **17**, 1880–1990.

Frederickson CJ & Bush AI (2001). Synaptically released zinc: physiological functions and pathological effects. *Biometals* **14,** 353–366.

Gais S, Albouy G, Boly M, Dang-Vu TT, Darsaud A, Desseilles M, Rauchs G, Schabus M, Sterpenich V, Vandewalle G, Maquet P & Peigneux P (2007). Sleep transforms the cerebral trace of declarative memories. *Proc Natl Acad Sci* **104,** 18778–18783.

Gant JC, Sama MM, Landfield PW & Thibault O (2006). Early and Simultaneous Emergence of Multiple Hippocampal Biomarkers of Aging Is Mediated by Ca2+-Induced Ca2+ Release. *J Neurosci* **26,** 3482–3490.

Gant JC & Thibault O (2009). Action potential throughput in aged rat hippocampal neurons: Regulation by selective forms of hyperpolarization. *Neurobiol Aging* **30,** 2053–2064.

Gascon E, Lynch K, Ruan H, Almeida S, Verheyden JM, Seeley WW, Dickson DW, Petrucelli L, Sun D, Jiao J, Zhou H, Jakovcevski M, Akbarian S, Yao W-D & Gao F-B (2014). Alterations in microRNA-124 and AMPA receptors contribute to social behavioral deficits in frontotemporal dementia. *Nat Med* **20,** 1444–1451.

Ghazi-Noori S, Froud KE, Mizielinska S, Powell C, Smidak M, Fernandez de Marco M, O'Malley C, Farmer M, Parkinson N, Fisher EMC, Asante EA, Brandner S, Collinge J & Isaacs AM (2012). Progressive neuronal inclusion

formation and axonal degeneration in CHMP2B mutant transgenic mice. *Brain* **135,** 819–832.

Gibson GE & Peterson C (1987). Calcium and the aging nervous system. *Neurobiol Aging* **8,** 329–343.

Girardeau G, Benchenane K, Wiener SI, Buzsáki G & Zugaro MB (2009). Selective suppression of hippocampal ripples impairs spatial memory. *Nat Neurosci* **12,** 1222–1223.

Goldman-Rakic PS, Cools AR & Srivastava K (1996). The Prefrontal Landscape: Implications of Functional Architecture for Understanding Human Mentation and the Central Executive [and Discussion]. *Philos Trans R Soc B Biol Sci* **351,** 1445–1453.

Goldman JS, Farmer JM, Wood EM, Johnson JK, Boxer A, Neuhaus J, Lomen-Hoerth C, Wilhelmsen KC, Lee VM-Y, Grossman M & Miller BL (2005). Comparison of family histories in FTLD subtypes and related tauopathies. *Neurology* **65,** 1817–1819.

Gómez-Isla T, Hollister R, West H, Mui S, Growdon JH, Petersen RC, Parisi JE & Hyman BT (1997). Neuronal loss correlates with but exceeds neurofibrillary tangles in Alzheimer's disease. *Ann Neurol* **41,** 17–24.

Gorno-Tempini ML et al. (2011). Classification of primary progressive aphasia and its variants. *Neurology* **76,** 1006–1014.

Götz J, Deters N, Doldissen A, Bokhari L, Ke Y, Wiesner A, Schonrock N & Ittner LM (2007). A Decade of Tau Transgenic Animal Models and Beyond. *Brain Pathol* **17,** 91–103.

Graef JD, Huitt TW, Nordskog BK, Hammarback JH & Godwin DW (2011). Disrupted thalamic T-type Ca2+ channel expression and function during ethanol exposure and withdrawal. *J Neurophysiol* **105,** 528–540.

Graef JD, Nordskog BK, Wiggins WF & Godwin DW (2009). An acquired channelopathy involving thalamic T-type Ca2+ channels after status epilepticus. *J Neurosci* **29,** 4430–4441.

Graff-Radford NR, Tranel D, Van Hoesen GW & Brandt JP (1990). Diencephalic amnesia. *Brain* **113 (Pt 1),** 1–25.

Granon S & Poucet B (1995). Medial prefrontal lesions in the rat and spatial navigation: evidence for impaired planning. *Behav Neurosci* **109,** 474–484.

Groenewegen HJ & Berendse HW (1994). The specificity of the "nonspecific" midline and intralaminar thalamic nuclei. *Trends Neurosci* **17,** 52–57.

Gu N, Vervaeke K, Hu H & Storm JF (2005). Kv7/KCNQ/M and HCN/h, but not K Ca 2/SK channels, contribute to the somatic medium after-hyperpolarization and excitability control in CA1 hippocampal pyramidal cells. *J Physiol* **566,** 689–715.

Guillery RW (1995). Anatomical evidence concerning the role of the thalamus in corticocortical communication: a brief review. *J Anat* **187 (Pt 3),** 583–592.

Gunning-Dixon FM, Brickman AM, Cheng JC & Alexopoulos GS (2009). Aging of cerebral white matter: a review of MRI findings. *Int J Geriatr Psychiatry* **24,** 109–117.

Gydesen S, Brown JM, Brun A, Chakrabarti L, Gade A, Johannsen P, Rossor M, Thusgaard T, Grove A, Yancopoulou D, Spillantini MG, Fisher EMC, Collinge J & Sorensen SA (2002). Chromosome 3 linked frontotemporal dementia (FTD-3). *Neurology* **59,** 1585–1594.

Gydesen S, Hagen S, Klinken L, Abelskov J & Sørensen SA (1987). Neuropsychiatric studies in a family with presenile dementia different from Alzheimer and Pick disease. *Acta Psychiatr Scand* **76,** 276–284.

Hallock HL, Wang A & Griffin AL (2016). Ventral Midline Thalamus Is Critical for Hippocampal-Prefrontal Synchrony and Spatial Working Memory. *J Neurosci* **36,** 8372–8389.

Hallock HL, Wang A, Shaw CL & Griffin AL (2013). Transient inactivation of the thalamic nucleus reuniens and rhomboid nucleus produces deficits of a working-memory dependent tactile-visual conditional discrimination task. *Behav Neurosci* **127,** 860–866.

Hallworth NE, Wilson CJ & Bevan MD (2003). Apamin-sensitive small conductance calcium-activated potassium channels, through their selective coupling to voltage-gated calcium channels, are critical determinants of the precision, pace, and pattern of action potential generation in rat subthalamic nucleus neurons in vitro. *J Neurosci* **23,** 7525–7542.

Hamani C, Paulo I de & Mello LEAM (2005). Neo-Timm staining in the thalamus of chronically epileptic rats. *Brazilian J Med Biol Res* **38,** 1677–1682.

Harada A, Oguchi K, Okabe S, Kuno J, Terada S, Ohshima T, Sato-Yoshitake R, Takei Y, Noda T & Hirokawa N (1994). Altered microtubule organization in small-calibre axons of mice lacking tau protein. *Nature* **369,** 488–491.

Harada CN, Natelson Love MC & Triebel KL (2013). Normal cognitive aging. *Clin Geriatr Med* **29,** 737–752.

Harris JA, Devidze N, Halabisky B, Lo I, Thwin MT, Yu G-Q, Bredesen DE, Masliah E & Mucke L (2010). Many Neuronal and Behavioral Impairments in Transgenic Mouse Models of Alzheimer's Disease Are Independent of Caspase Cleavage of the Amyloid Precursor Protein. *J Neurosci* **30,** 372–381.

Hauser WA, Rich SS, Annegers JF & Anderson VE (1990). Seizure recurrence after a 1st unprovoked seizure: an extended follow-up. *Neurology* **40,** 1163–1170.

Hauser WA, Rich SS, Lee JR-J, Annegers JF & Anderson VE (1998). Risk of Recurrent Seizures after Two Unprovoked Seizures. *N Engl J Med* **338,** 429–434.

Hembrook JR & Mair RG (2011). Lesions of reuniens and rhomboid thalamic nuclei impair radial maze win-shift performance. *Hippocampus* **21,** 815–826.

Hembrook JR, Onos KD & Mair RG (2012). Inactivation of ventral midline thalamus produces selective spatial delayed conditional discrimination impairment in the rat. *Hippocampus* **22,** 853–860.

Heneka MT, O'Banion MK, Terwel D & Kummer MP (2010). Neuroinflammatory processes in Alzheimer's disease. *J Neural Transm* **117,** 919–947.

Henseler I, Falkai P & Gruber O (2010). Disturbed functional connectivity within brain networks subserving domain-specific subcomponents of working memory in schizophrenia: Relation to performance and clinical symptoms. *J Psychiatr Res* **44,** 364–372.

Hirayasu Y & Wada JA (1992). N-methyl-D-aspartate injection into the massa intermedia facilitates development of limbic kindling in rats. *Epilepsia* **33,** 965–970.

Hodgkin AL & Huxley AF (1952). A quantitative description of membrane current and its application to conduction and excitation in nerve. *J Physiol* **117,** 500–544.

Hong S, Beja-Glasser VF, Nfonoyim BM, Frouin A, Li S, Ramakrishnan S, Merry KM, Shi Q, Rosenthal A, Barres BA, Lemere , Cynthia A., Selkoe DJ & Stevens B (2016). Complement and microglia mediate early synapse loss in Alzheimer mouse models. *Science* **352,** 712–716.

Hoover WB & Vertes RP (2012). Collateral projections from nucleus reuniens of thalamus to hippocampus and medial prefrontal cortex in the rat: a single and double retrograde fluorescent labeling study. *Brain Struct Funct* **217,** 191–209.

Hughes EJ, Bond J, Svrckova P, Makropoulos A, Ball G, Sharp DJ, Edwards AD, Hajnal J V. & Counsell SJ (2012). Regional changes in thalamic shape and volume with increasing age. *Neuroimage* **63,** 1134–1142.

Hughes SW, Cope DW, Tóth TI, Williams SR & Crunelli V (1999). All thalamocortical neurones possess a T-type Ca2+ "window" current that enables the expression of bistability-mediated activities. *J Physiol*805–815.

Huguenard JR (1996). Low-Threshold Calcium Currents in Central Nervous System Neurons. *Annu Rev Physiol* **58,** 329–348.

Huguenard JR & McCormick DA (2007). Thalamic synchrony and dynamic regulation of global forebrain oscillations. *Trends Neurosci* **30,** 350–356.

Huguenard JR & Prince DA (1992). A novel T-type current underlies prolonged Ca(2+)-dependent burst firing in GABAergic neurons of rat thalamic reticular nucleus. *J Neurosci* **12,** 3804–3817.

Hur EE & Zaborszky L (2005). Vglut2 afferents to the medial prefrontal and primary somatosensory cortices: A combined retrograde tracing in situ hybridization. *J Comp Neurol* **483,** 351–373.

Hurley KM, Herbert H, Moga MM & Saper CB (1991). Efferent projections of the infralimbic cortex of the rat. *J Comp Neurol* **308,** 249–276.

Hutton M et al. (1998). Association of missense and 5'-splice-site mutations in tau with the inherited dementia FTDP-17. *Nature* **393,** 702–705.

Hyman JM, Zilli EA, Paley AM & Hasselmo ME (2010). Working memory performance correlates with prefrontal-hippocampal theta interactions but not with prefrontal neuron firing rates. *Front Integr Neurosci* **4,** 2.

Iqbal K, del C. Alonso A, Chen S, Chohan MO, El-Akkad E, Gong C-X, Khatoon S, Li B, Liu F, Rahman A, Tanimukai H & Grundke-Iqbal I (2005). Tau pathology in Alzheimer disease and other tauopathies. *Biochim Biophys Acta - Mol Basis Dis* **1739,** 198–210.

Isaacs AM, Johannsen P, Holm I, Nielsen JE & FReJA consortium (2011). Frontotemporal dementia caused by CHMP2B mutations. *Curr Alzheimer Res* **8,** 246–251.

Ishikawa A & Nakamura S (2003). Convergence and Interaction of Hippocampal and Amygdalar Projections within the Prefrontal Cortex in the Rat. *J Neurosci* **23,** 9987–9995.

Isomura Y, Sirota A, Özen S, Montgomery S, Mizuseki K, Henze DA & Buzsáki G (2006). Integration and Segregation of Activity in Entorhinal-Hippocampal Subregions by Neocortical Slow Oscillations. *Neuron* **52,** 871–882.

Ito HT, Zhang S-J, Witter MP, Moser EI & Moser M-B (2015). A prefrontal-thalamo-hippocampal circuit for goal-directed spatial navigation. *Nature* **522,** 50–55.

Jahnsen H & Llinás R (1984). Electrophysiological properties of guinea-pig thalamic neurones: an in vitro study. *J Physiol* **349,** 205–226.

Jankowski MM, Islam MN, Wright NF, Vann SD, Erichsen JT, Aggleton JP & O'Mara SM (2014). Nucleus reuniens of the thalamus contains head direction cells. *Elife*; DOI: 10.7554/eLife.03075.

Jankowski MM, Passecker J, Islam MN, Vann S, Erichsen JT, Aggleton JP & O'Mara SM (2015). Evidence for spatially-responsive neurons in the rostral thalamus. *Front Behav Neurosci* **9,** 256.

Javitt DC (2007). Glutamate and Schizophrenia: Phencyclidine, N-Methyl-d-Aspartate Receptors, and Dopamine–Glutamate Interactions. *Intl Rev Neurobiol*, **78,** 69–108.

Jay TM, Burette F & Laroche S (1995). NMDA receptor-dependent long-term potentiation in the hippocampal afferent fibre system to the prefrontal cortex in the rat. *Eur J Neurosci* **7,** 247–250.

Jay TM, Glowinski J & Thierry AM (1989). Selectivity of the hippocampal projection to the prelimbic area of the prefrontal cortex in the rat. *Brain Res* **505,** 337–340.

Jay TM & Witter MP (1991). Distribution of hippocampal CA1 and subicular efferents in the prefrontal cortex of the rat studied by means of anterograde transport ofPhaseolus vulgaris-leucoagglutinin. *J Comp Neurol* **313,** 574–586.

Jensen MS, Azouz R & Yaari Y (1996). Spike after-depolarization and burst generation in adult rat hippocampal CA1 pyramidal cells. *J Physiol*199–210.

Jernigan TL, Archibald SL, Fennema-Notestine C, Gamst AC, Stout JC, Bonner J & Hesselink JR (2001). Effects of age on tissues and regions of the cerebrum and cerebellum. *Neurobiol Aging* **22,** 581–594.

Johnson-Wood K, Lee M, Motter R, Hu K, Gordon G, Barbour R, Khan K, Gordon M, Tan H, Games D, Lieberburg I, Schenk D, Seubert P & McConlogue L (1997). Amyloid precursor protein processing and A beta42 deposition in a transgenic mouse model of Alzheimer disease. *Proc Natl Acad Sci U S A* **94,** 1550–1555.

Jones EG (1985). *The Thalamus*. Springer, New York.

Jones EG (1998). A new view of specific and nonspecific thalamocortical connections. *Adv Neurol* **77,** 49-71-3.

Jones MW & Wilson MA (2005). Theta rhythms coordinate hippocampal-prefrontal interactions in a spatial memory task. *PLoS Biol* **3,** e402.

Kandel ER, Schwartz JH & Jessel TM (2000). *Principles of Neural Science*, 4th edn. McGraw-Hill, New York.

Kerrigan TL, Brown JT & Randall AD (2014). Characterization of altered intrinsic excitability in hippocampal CA1 pyramidal cells of the Aβ-overproducing PDAPP mouse. *Neuropharmacology* **79,** 515–524.

Kesner RP, Hunt ME, Williams JM & Long JM (1996). Prefrontal cortex and working memory for spatial response, spatial location, and visual object information in the rat. *Cereb Cortex* **6,** 311–318.

Khachaturian ZS (1994). Calcium hypothesis of Alzheimer's disease and brain aging. *Ann N Y Acad Sci* **747,** 1–11.

Kolaj M, Zhang L, Ronnekleiv OK & Renaud LP (2012). Midline thalamic paraventricular nucleus neurons display diurnal variation in resting membrane potentials, conductances, and firing patterns in vitro. *J Neurophysiol* **107,** 1835–1844.

Kolmac C & Mitrofanis J (1999). Organization of the basal forebrain projection to the thalamus in rats. *Neurosci Lett* **272,** 151–154.

Krasniak CS & Ahmad ST (2016). The role of CHMP2BIntron5 in autophagy and frontotemporal dementia. *Brain Res* **1649,** 151–157.

Kumar A & Foster T (2007). Environmental enrichment decreases the afterhyperpolarization in senescent rats. *Brain Res* **1130,** 103–107.

Kuner T & Schoepfer R (1996). Multiple structural elements determine subunit specificity of Mg2+ block in NMDA receptor channels. *J Neurosci* **16,** 3549–3558.

LaFerla FM & Oddo S (2005). Alzheimer's disease: Aβ, tau and synaptic dysfunction. *Trends Mol Med* **11,** 170–176.

Landfield PW (1987). “Increased calcium-current” hypothesis of brain aging. *Neurobiol Aging* **8,** 346–347.

Landfield PW & Pitler TA (1984). Prolonged Ca2+-dependent afterhyperpolarizations in hippocampal neurons of aged rats. *Science* **226,** 1089–1092.

Lara-Vásquez A, Espinosa N, Durán E, Stockle M & Fuentealba P (2016). Midline thalamic neurons are differentially engaged during hippocampus network oscillations. *Sci Rep* **6,** 29807.

Lasagna-Reeves CA, Castillo-Carranza DL, Sengupta U, Clos AL, Jackson GR & Kayed R (2011). Tau oligomers impair memory and induce synaptic and mitochondrial dysfunction in wild-type mice. *Mol Neurodegener* **6,** 39.

Lein ES et al. (2007). Genome-wide atlas of gene expression in the adult mouse brain. *Nature* **445,** 168–176.

Lindwall G & Cole RD (1984). Phosphorylation affects the ability of tau protein to promote microtubule assembly. *J Biol Chem* **259,** 5301–5305.

Llinas RR & Steriade M (2006). Bursting of Thalamic Neurons and States of Vigilance. *J Neurophysiol* **95,** 3297–3308.

Loureiro M, Cholvin T, Lopez J, Merienne N, Latreche A, Cosquer B, Geiger K, Kelche C, Cassel J-C & Pereira de Vasconcelos A (2012). The Ventral Midline Thalamus (Reuniens and Rhomboid Nuclei) Contributes to the Persistence of Spatial Memory in Rats. *J Neurosci* **32,** 9947–9959.

Luna-Munguia H, Starski P, Chen W, Gliske S & Stacey WC (2017). Control of in vivo ictogenesis via endogenous synaptic pathways. *Sci Rep* **7,** 1311.

Ly R, Bouvier G, Szapiro G, Prosser HM, Randall AD, Kano M, Sakimura K, Isope P, Barbour B & Feltz A (2016). Contribution of postsynaptic T-type calcium channels to parallel fibre-Purkinje cell synaptic responses. *J Physiol* **594,** 915–936.

Mackenzie IRA et al. (2010). Nomenclature and nosology for neuropathologic subtypes of frontotemporal lobar degeneration: an update. *Acta Neuropathol* **119,** 1–4.

Mair RG, Burk JA & Porter MC (1998). Lesions of the frontal cortex, hippocampus, and intralaminar thalamic nuclei have distinct effects on remembering in rats. *Behav Neurosci* **112,** 772–792.

Mair WGP, Warrington EK & Weiskrantz L (1979). Memory disorder in korsakoff’ s psychosis a neuropathological and neuropsychological investigation of two cases. *Brain* **102,** 749–783.

Mander BA, Marks SM, Vogel JW, Rao V, Lu B, Saletin JM, Ancoli-Israel S, Jagust WJ & Walker MP (2015). β-amyloid disrupts human NREM slow waves and related hippocampus-dependent memory consolidation. *Nat Neurosci* **18,** 1051–1057.

Mander BA, Rao V, Lu B, Saletin JM, Lindquist JR, Ancoli-Israel S, Jagust W & Walker MP (2013). Prefrontal atrophy, disrupted NREM slow waves and impaired hippocampal-dependent memory in aging. *Nat Neurosci* **16,** 357–364.

Marshall L & Born J (2007). The contribution of sleep to hippocampus-dependent memory consolidation. *Trends Cogn Sci* **11,** 442–450.

Marshall L, Helgadóttir H, Mölle M & Born J (2006). Boosting slow oscillations during sleep potentiates memory. *Nature* **444,** 610–613.

Masters CL, Simms G, Weinman NA, Multhaup G, McDonald BL & Beyreuther K (1985). Amyloid plaque core protein in Alzheimer disease and Down syndrome. *Proc Natl Acad Sci U S A* **82,** 4245–4249.

Matthews EA, Linardakis JM & Disterhoft JF (2009). The Fast and Slow Afterhyperpolarizations Are Differentially Modulated in Hippocampal Neurons by Aging and Learning. *J Neurosci* **29,** 4750–4755.

Maylie J, Bond CT, Herson PS, Lee W-S & Adelman JP (2004). Small conductance Ca2+-activated K+ channels and calmodulin. *J Physiol* **554,** 255–261.

McCobb DP & Beam KG (1991). Action potential waveform voltage-clamp commands reveal striking differences in calcium entry via low and high voltage-activated calcium channels. *Neuron* **7,** 119–127.

McCormick DA & Huguenard JR (1992). A model of the electrophysiological properties of thalamocortical relay neurons. *J Neurophysiol* **68,** 1384–1400.

McCormick DA & Pape HC (1990). Properties of a hyperpolarization-activated cation current and its role in rhythmic oscillation in thalamic relay neurones. *J Physiol* **431,** 291–318.

McDonald RJ & White NM (1993). A triple dissociation of memory systems: hippocampus, amygdala, and dorsal striatum. *Behav Neurosci* **107,** 3–22.

McGowan E, Eriksen J & Hutton M (2006). A decade of modeling Alzheimer's disease in transgenic mice. *Trends Genet* **22,** 281–289.

McKenna JT & Vertes RP (2004). Afferent projections to nucleus reuniens of the thalamus. *J Comp Neurol* **480,** 115–142.

McKhann GM, Albert MS, Grossman M, Miller B, Dickson D, Trojanowski JQ & Work Group on Frontotemporal Dementia and Pick's Disease (2001). Clinical and pathological diagnosis of frontotemporal dementia: report of the Work Group on Frontotemporal Dementia and Pick's Disease. *Arch Neurol* **58,** 1803–1809.

Mengual E, Casanovas-Aguilar C, Pérez-Clausell J & Giménez-Amaya JM (2001). Thalamic distribution of zinc-rich terminal fields and neurons of origin in the rat. *Neuroscience* **102,** 863–884.

Meuth SG, Kanyshkova T, Meuth P, Landgraf P, Munsch T, Ludwig A, Hofmann F, Pape H-C & Budde T (2006). Membrane Resting Potential of Thalamocortical

Relay Neurons Is Shaped by the Interaction Among TASK3 and HCN2 Channels. *J Neurophysiol* **96,** 1517–1529.

Miller RA (2004). “Accelerated aging”: a primrose path to insight? *Aging Cell* **3,** 47–51.

Minkeviciene R, Rheims S, Dobszay MB, Zilberter M, Hartikainen J, Fulop L, Penke B, Zilberter Y, Harkany T, Pitkanen A & Tanila H (2009). Amyloid - Induced Neuronal Hyperexcitability Triggers Progressive Epilepsy. *J Neurosci* **29,** 3453–3462.

Miravalle L, Calero M, Takao M, Roher AE, Ghetti B & Vidal R (2005). Amino-Terminally Truncated Aβ Peptide Species Are the Main Component of Cotton Wool Plaques †. *Biochemistry* **44,** 10810–10821.

Miyasaka M & Domino EF (1968). Neural mechanisms of ketamine-induced anesthesia. *Int J Neuropharmacol* **7,** 557–573.

Mölle M, Marshall L, Gais S & Born J (2002). Grouping of spindle activity during slow oscillations in human non-rapid eye movement sleep. *J Neurosci* **22,** 10941–10947.

Moore S, Evans LDB, Andersson T, Portelius E, Smith J, Dias TB, Saurat N, McGlade A, Kirwan P, Blennow K, Hardy J, Zetterberg H & Livesey FJ (2015). APP Metabolism Regulates Tau Proteostasis in Human Cerebral Cortex Neurons. *Cell Rep* **11,** 689–696.

Morsch R, Simon W & Coleman PD (1999). Neurons may live for decades with neurofibrillary tangles. *J Neuropathol Exp Neurol* **58,** 188–197.

Moyer JR, Thompson LT & Disterhoft JF (1996). Trace eyeblink conditioning increases CA1 excitability in a transient and learning-specific manner. *J Neurosci* **16,** 5536–5546.

Mucke L, Masliah E, Yu GQ, Mallory M, Rockenstein EM, Tatsuno G, Hu K, Kholodenko D, Johnson-Wood K & McConlogue L (2000). High-level neuronal expression of abeta 1-42 in wild-type human amyloid protein precursor transgenic mice: synaptotoxicity without plaque formation. *J Neurosci* **20,** 4050–4058.

Muratore CR, Rice HC, Srikanth P, Callahan DG, Shin T, Benjamin LNP, Walsh DM, Selkoe DJ & Young-Pearse TL (2014). The familial Alzheimer’s disease APPV717I mutation alters APP processing and Tau expression in iPSC-derived neurons. *Hum Mol Genet* **23,** 3523–3536.

Nádasdy Z, Hirase H, Czurkó A, Csicsvari J & Buzsáki G (1999). Replay and time compression of recurring spike sequences in the hippocampus. *J Neurosci* **19,** 9497–9507.

Neary D, Snowden JS, Gustafson L, Passant U, Stuss D, Black S, Freedman M, Kertesz A, Robert PH, Albert M, Boone K, Miller BL, Cummings J & Benson DF (1998). Frontotemporal lobar degeneration: a consensus on clinical diagnostic criteria. *Neurology* **51,** 1546–1554.

Neumann M, Rademakers R, Roeber S, Baker M, Kretzschmar HA & Mackenzie IRA (2009). A new subtype of frontotemporal lobar degeneration with FUS pathology. *Brain* **132,** 2922–2931.

Neumann M, Sampathu DM, Kwong LK, Truax AC, Micsenyi MC, Chou TT, Bruce J, Schuck T, Grossman M, Clark CM, McCluskey LF, Miller BL, Masliah E, Mackenzie IR, Feldman H, Feiden W, Kretzschmar HA, Trojanowski JQ & Lee VM-Y (2006). Ubiquitinated TDP-43 in Frontotemporal Lobar Degeneration and Amyotrophic Lateral Sclerosis. *Science (80-)* **314,** 130–133.

Nicolelis MA, Baccala LA, Lin RC & Chapin JK (1995). Sensorimotor encoding by synchronous neural ensemble activity at multiple levels of the somatosensory system. *Science* **268,** 1353–1358.

Niswender CM & Conn PJ (2010). Metabotropic Glutamate Receptors: Physiology, Pharmacology, and Disease. *Annu Rev Pharmacol Toxicol* **50,** 295–322.

North RA & Surprenant A (1985). Inhibitory synaptic potentials resulting from alpha 2-adrenoceptor activation in guinea-pig submucous plexus neurones. *J Physiol* **358,** 17–33.

Nowotny P, Kwon JM, Goate AM, Nowotny P, Kwon JM & Goate AM (2001). Alzheimer Disease. *Encyclopedia of Life Sciences*. John Wiley & Sons, Ltd, Chichester, UK.

Ota M, Obata T, Akine Y, Ito H, Matsumoto R, Ikehira H, Asada T & Suhara T (2007). Laterality and aging of thalamic subregions measured by diffusion tensor imaging. *Neuroreport* **18,** 1071–1075.

Padgett CL & Slesinger PA (2010). GABAB Receptor Coupling to G-proteins and Ion Channels. A*dv pharmacol* **58,** 123–147.

Palop JJ, Chin J, Roberson ED, Wang J, Thwin MT, Bien-Ly N, Yoo J, Ho KO, Yu G-Q, Kreitzer A, Finkbeiner S, Noebels JL & Mucke L (2007). Aberrant Excitatory Neuronal Activity and Compensatory Remodeling of Inhibitory Hippocampal Circuits in Mouse Models of Alzheimer's Disease. *Neuron* **55,** 697–711.

Palop JJ, Jones B, Kekonius L, Chin J, Yu G-Q, Raber J, Masliah E & Mucke L (2003). Neuronal depletion of calcium-dependent proteins in the dentate gyrus is tightly linked to Alzheimer's disease-related cognitive deficits. *Proc. Natl. Acad. Sci. U S A* **100,** 9572–9577

Palop JJ & Mucke L (2009). Epilepsy and cognitive impairments in Alzheimer disease. *Arch Neurol* **66,** 435–440.

Pape H-C (1996). Queer Current and Pacemaker: The Hyperpolarization-Activated Cation Current in Neurons. *Annu Rev Physiol* **58,** 299–327.

Pape H-C, Munsch T & Budde T (2004). Novel vistas of calcium-mediated signalling in the thalamus. *Pflügers Arch Eur J Physiol* **448,** 131–138.

Paxinos G & Franklin KBJ (2001). *Paxinos and Franklin's the Mouse Brain in Stereotaxic Coordinates*.

Pereira de Vasconcelos A & Cassel J-C (2015). The nonspecific thalamus: A place in a wedding bed for making memories last? *Neurosci Biobehav Rev* **54,** 175–196.

Perez-Reyes E (2003). Molecular physiology of low-voltage-activated t-type calcium channels. *Physiol Rev* **83,** 117–161.

Perl DP (2010). Neuropathology of Alzheimer's disease. *Mt Sinai J Med* **77,** 32–42.

Pol-Bodetto S, Jeltsch-David H, Lecourtier L, Rusnac N, Mam-Lam-Fook C, Cosquer B, Geiger K & Cassel J-C (2011). The double-H maze test, a novel, simple, water-escape memory task: Acquisition, recall of recent and remote memory, and effects of systemic muscarinic or NMDA receptor blockade during training. *Behav Brain Res* **218,** 138–151.

Porter MC, Burk JA & Mair RG (2000). A comparison of the effects of hippocampal or prefrontal cortical lesions on three versions of delayed non-matching-to-sample based on positional or spatial cues. *Behav Brain Res* **109,** 69–81.

Prasad JA, Abela AR & Chudasama Y (2017). Midline thalamic reuniens lesions improve executive behaviors. *Neuroscience* **345,** 77–88.

Prasad JA & Chudasama Y (2013). Viral tracing identifies parallel disynaptic pathways to the hippocampus. *J Neurosci* **33,** 8494–8503.

Prasad JA, Macgregor EM & Chudasama Y (2013). Lesions of the thalamic reuniens cause impulsive but not compulsive responses. *Brain Struct Funct* **218,** 85–96.

Di Prisco GV & Vertes RP (2006). Excitatory actions of the ventral midline thalamus (rhomboid/reuniens) on the medial prefrontal cortex in the rat. *Synapse* **60,** 45–55.

Querfurth HW & LaFerla FM (2010). Alzheimer's Disease. *N Engl J Med* **362,** 329–344.

Radhakrishnan V, Tsoukatos J, Davis KD, Tasker RR, Lozano AM & Dostrovsky JO (1999). A comparison of the burst activity of lateral thalamic neurons in chronic pain and non-pain patients. *Pain* **80,** 567–575.

Ramcharan EJ, Gnadt JW & Sherman SM (2005). Higher-order thalamic relays burst more than first-order relays. *Proc Natl Acad Sci U S A* **102,** 12236–12241.

Randall AD, Booth C & Brown JT (2012). Age-related changes to Na+ channel gating contribute to modified intrinsic neuronal excitability. *Neurobiol Aging* **33,** 2715–2720.

Randall AD, Witton J, Booth C, Hynes-Allen A & Brown JT (2010). The functional neurophysiology of the amyloid precursor protein (APP) processing pathway. *Neuropharmacology* **59,** 243–267.

Rasetti R, Sambataro F, Chen Q, Callicott JH, Mattay VS & Weinberger DR (2011). Altered Cortical Network Dynamics. *Arch Gen Psychiatry* **68,** 1207.

Raz N (2004). The aging brain: Structural changes and their implications for cognitive aging. *New Frontiers in Cognitive Aging*, pp. 115–134. Oxford University Press.

Reagh ZM, Murray EA & Yassa MA (2017). Repetition reveals ups and downs of hippocampal, thalamic, and neocortical engagement during mnemonic decisions. *Hippocampus* **27,** 169–183.

Reinagel P, Godwin D, Sherman SM & Koch C (1999). Encoding of Visual Information by LGN Bursts. *J Neurophysiol* **81,** 2558–2569.

Remondes M & Schuman EM (2003). Molecular mechanisms contributing to long-lasting synaptic plasticity at the temporoammonic-CA1 synapse. *Learn Mem* **10,** 247–252.

Rice RA, Berchtold NC, Cotman CW & Green KN (2014). Age-related downregulation of the CaV3.1 T-type calcium channel as a mediator of amyloid beta production. *Neurobiol Aging* **35,** 1002–1011.

Ringholz GM, Appel SH, Bradshaw M, Cooke NA, Mosnik DM & Schulz PE (2005). Prevalence and patterns of cognitive impairment in sporadic ALS. *Neurology* **65,** 586–590.

Roberson ED (2012). Mouse models of frontotemporal dementia. *Ann Neurol* **72,** 837–849.

Roberson ED, Scearce-Levie K, Palop JJ, Yan F, Cheng IH, Wu T, Gerstein H, Yu G-Q & Mucke L (2007). Reducing Endogenous Tau Ameliorates Amyloid -Induced Deficits in an Alzheimer's Disease Mouse Model. *Science (80-)* **316,** 750–754.

Rocher AB, Kinson MS & Luebke JI (2008). Significant structural but not physiological changes in cortical neurons of 12-month-old Tg2576 mice. *Neurobiol Dis* **32,** 309–318.

Room P, Russchen FT, Groenewegen HJ & Lohman AHM (1985). Efferent connections of the prelimbic (area 32) and the infralimbic (area 25) cortices: An anterograde tracing study in the cat. *J Comp Neurol* **242,** 40–55.

Saito T, Suemoto T, Brouwers N, Sleegers K, Funamoto S, Mihira N, Matsuba Y, Yamada K, Nilsson P, Takano J, Nishimura M, Iwata N, Van Broeckhoven C, Ihara Y & Saido TC (2011). Potent amyloidogenicity and pathogenicity of Aβ43. *Nat Neurosci* **14,** 1023–1032.

Samios VN & Inoue T (2014). Interleukin-1β and interleukin-6 affect electrophysiological properties of thalamic relay cells. *Neurosci Res* **87,** 16–25.

Sanchez PE, Zhu L, Verret L, Vossel KA, Orr AG, Cirrito JR, Devidze N, Ho K, Yu G-Q, Palop JJ & Mucke L (2012). Levetiracetam suppresses neuronal network dysfunction and reverses synaptic and cognitive deficits in an Alzheimer's disease model. *Proc Natl Acad Sci* **109,** E2895–E2903.

SantaCruz K, Lewis J, Spires T, Paulson J, Kotilinek L, Ingelsson M, Guimaraes A, DeTure M, Ramsden M, McGowan E, Forster C, Yue M, Orne J, Janus C, Mariash A, Kuskowski M, Hyman B, Hutton M & Ashe KH (2005). Tau Suppression in a Neurodegenerative Mouse Model Improves Memory Function. *Science (80-)* **309,** 476–481.

Santoro B, Chen S, Luthi A, Pavlidis P, Shumyatsky GP, Tibbs GR & Siegelbaum SA (2000). Molecular and functional heterogeneity of hyperpolarization-activated pacemaker channels in the mouse CNS. *J Neurosci* **20,** 5264–5275.

Sargolini F, Fyhn M, Hafting T, McNaughton BL, Witter MP, Moser M-B & Moser EI (2006). Conjunctive representation of position, direction, and velocity in entorhinal cortex. *Science* **312,** 758–762.

Scahill RI, Frost C, Jenkins R, Whitwell JL, Rossor MN & Fox NC (2003). A Longitudinal Study of Brain Volume Changes in Normal Aging Using Serial Registered Magnetic Resonance Imaging. *Arch Neurol* **60,** 989.

Schmued L, Raymick J, Tolleson W, Sarkar S, Zhang Y-H & Bell-Cohn A (2012). Introducing Amylo-Glo, a novel fluorescent amyloid specific histochemical tracer especially suited for multiple labeling and large scale quantification studies. *J Neurosci Methods* **209,** 120–126.

Schroeter ML, Raczka K, Neumann J & Yves von Cramon D (2007). Towards a nosology for frontotemporal lobar degenerations—A meta-analysis involving 267 subjects. *Neuroimage* **36,** 497–510.

Selkoe DJ & Hardy J (2016). The amyloid hypothesis of Alzheimer's disease at 25 years. *EMBO Mol Med* **8,** 595–608.

Sherman SM (2001). Tonic and burst firing: dual modes of thalamocortical relay. *Trends Neurosci* **24,** 122–126.

Sherman SM & Guillery RW (1998). On the actions that one nerve cell can have on another: distinguishing "drivers" from "modulators". *Proc Natl Acad Sci U S A* **95,** 7121–7126.

Sherman SM & Guillery RW (2006). *Exploring the thalamus and its role in cortical function*. The MIT Press, Cambridge, MA.

Shoji H, Takao K, Hattori S & Miyakawa T (2016). Age-related changes in behavior in C57BL/6J mice from young adulthood to middle age. *Mol Brain* **9,** 11.

Shumikhina S & Molotchnikoff S (1999). Pulvinar participates in synchronizing neural assemblies in the visual cortex, in cats. *Neurosci Lett* **272,** 135–139.

Sieben A, Van Langenhove T, Engelborghs S, Martin J-J, Boon P, Cras P, De Deyn P-P, Santens P, Van Broeckhoven C & Cruts M (2012). The genetics and neuropathology of frontotemporal lobar degeneration. *Acta Neuropathol* **124,** 353–372.

Sigurdsson T, Stark KL, Karayiorgou M, Gogos JA & Gordon JA (2010). Impaired hippocampal-prefrontal synchrony in a genetic mouse model of schizophrenia. *Nature* **464,** 763–767.

Silva AJ, Giese KP, Fedorov NB, Frankland PW & Kogan JH (1998). Molecular, Cellular, and Neuroanatomical Substrates of Place Learning. *Neurobiol Learn Mem* **70,** 44–61.

Simkin D, Hattori S, Ybarra N, Musial TF, Buss EW, Richter H, Oh MM, Nicholson DA & Disterhoft JF (2015). Aging-Related Hyperexcitability in CA3 Pyramidal Neurons Is Mediated by Enhanced A-Type K+ Channel Function and Expression. *J Neurosci* **35,** 13206–13218.

Sirota A, Csicsvari J, Buhl D & Buzsaki G (2003). Communication between neocortex and hippocampus during sleep in rodents. *Proc Natl Acad Sci* **100,** 2065–2069.

Skibinski G, Parkinson NJ, Brown JM, Chakrabarti L, Lloyd SL, Hummerich H, Nielsen JE, Hodges JR, Spillantini MG, Thusgaard T, Brandner S, Brun A, Rossor MN, Gade A, Johannsen P, Sørensen SA, Gydesen S, Fisher EM & Collinge J (2005). Mutations in the endosomal ESCRTIII-complex subunit CHMP2B in frontotemporal dementia. *Nat Genet* **37,** 806–808.

Snead OC (1995). Basic mechanisms of generalized absence seizures. *Ann Neurol* **37,** 146–157.

Soares J, Diogo A, Fiorani M, Souza A & Gattass R (2004). Effects of inactivation of the lateral pulvinar on response properties of second visual area cells in Cebus monkeys. *Clin Exp Pharmacol Physiol* **31,** 580–590.

Sowell ER, Peterson BS, Thompson PM, Welcome SE, Henkenius AL & Toga AW (2003). Mapping cortical change across the human life span. *Nat Neurosci* **6,** 309–315.

Spellman T, Rigotti M, Ahmari SE, Fusi S, Gogos JA & Gordon JA (2015). Hippocampal–prefrontal input supports spatial encoding in working memory. *Nature* **522,** 309–314.

Spencer JP, Weil A, Hill K, Hussain I, Richardson JC, Cusdin FS, Chen YH & Randall AD (2006). Transgenic mice over-expressing human β-amyloid have functional nicotinic alpha 7 receptors. *Neuroscience* **137,** 795–805.

Spires TL, Orne JD, SantaCruz K, Pitstick R, Carlson GA, Ashe KH & Hyman BT (2006). Region-specific Dissociation of Neuronal Loss and Neurofibrillary Pathology in a Mouse Model of Tauopathy. *Am J Pathol* **168,** 1598–1607.

Springer SJ, Burkett BJ & Schrader LA (2015). Modulation of BK channels contributes to activity-dependent increase of excitability through MTORC1 activity in CA1 pyramidal cells of mouse hippocampus. *Front Cell Neurosci* **8,** 451.

Steriade M & Deschenes M (1984). The thalamus as a neuronal oscillator. *Brain Res* **320,** 1–63.

Steriade M & Llinás RR (1988). The functional states of the thalamus and the associated neuronal interplay. *Physiol Rev* **68,** 649–742.

Steriade M, McCormick DA & Sejnowski TJ (1993). Thalamocortical oscillations in the sleeping and aroused brain. *Science* **262,** 679–685.

Stokholm J, Teasdale TW, Johannsen P, Nielsen JE, Nielsen TT, Isaacs A, Brown JM, Gade A & Frontotemporal dementia Research in Jutland Association (FReJA) consortium (2013). Cognitive impairment in the preclinical stage of dementia in FTD-3 *CHMP2B* mutation carriers: a longitudinal prospective study. *J Neurol Neurosurg Psychiatry* **84,** 170–176.

Südhof TC (2013). Neurotransmitter Release: The Last Millisecond in the Life of a Synaptic Vesicle. *Neuron* **80,** 675–690.

Svennerholm L, Boström K & Jungbjer B (1997). Changes in weight and compositions of major membrane components of human brain during the span of adult human life of Swedes. *Acta Neuropathol* **94,** 345–352.

Taber KH, Wen C, Khan A & Hurley RA (2004). The limbic thalamus. *J Neuropsychiatry Clin Neurosci* **16,** 127–132.

Takami M, Nagashima Y, Sano Y, Ishihara S, Morishima-Kawashima M, Funamoto S & Ihara Y (2009). -Secretase: Successive Tripeptide and Tetrapeptide Release from the Transmembrane Domain of -Carboxyl Terminal Fragment. *J Neurosci* **29,** 13042–13052.

Takashima A, Petersson KM, Rutters F, Tendolkar I, Jensen O, Zwarts MJ, McNaughton BL & Fernandez G (2006). Declarative memory consolidation in humans: A prospective functional magnetic resonance imaging study. *Proc Natl Acad Sci* **103,** 756–761.

Talley EM, Cribbs LL, Lee JH, Daud A, Perez-Reyes E & Bayliss DA (1999). Differential distribution of three members of a gene family encoding low voltage-activated (T-type) calcium channels. *J Neurosci* **19,** 1895–1911.

Tamagnini F, Novelia J, Kerrigan TL, Brown JT, Tsaneva-Atanasova K & Randall AD (2015). Altered intrinsic excitability of hippocampal CA1 pyramidal neurons in aged PDAPP mice. *Front Cell Neurosci* **9,** 372.

Tamagnini F, Scullion S, Brown JT & Randall AD (2014). Low concentrations of the solvent dimethyl sulphoxide alter intrinsic excitability properties of cortical and hippocampal pyramidal cells. *PLoS One* **9,** e92557.

Taube JS, Muller RU & Ranck JB (1990). Head-direction cells recorded from the postsubiculum in freely moving rats. I. Description and quantitative analysis. *J Neurosci* **10,** 420–435.

Theyel BB, Llano DA & Sherman SM (2010). The corticothalamocortical circuit drives higher-order cortex in the mouse. *Nat Neurosci* **13,** 84–88.

Thibault O, Hadley R & Landfield PW (2001). Elevated postsynaptic [Ca2+]i and L-type calcium channel activity in aged hippocampal neurons: relationship to impaired synaptic plasticity. *J Neurosci* **21,** 9744–9756.

Thibault O & Landfield PW (1996). Increase in single L-type calcium channels in hippocampal neurons during aging. *Science* **272,** 1017–1020.

Torso M, Serra L, Giulietti G, Spanò B, Tuzzi E, Koch G, Caltagirone C, Cercignani M & Bozzali M (2015). Strategic Lesions in the Anterior Thalamic Radiation and Apathy in Early Alzheimer's Disease ed. Ginsberg SD. *PLoS One* **10,** e0124998.

Traboulsie A, Chemin J, Chevalier M, Quignard J-F, Nargeot J & Lory P (2007). Subunit-specific modulation of T-type calcium channels by zinc. *J Physiol* **578,** 159–171.

Traynelis SF, Wollmuth LP, McBain CJ, Menniti FS, Vance KM, Ogden KK, Hansen KB, Yuan H, Myers SJ & Dingledine R (2010). Glutamate Receptor Ion Channels: Structure, Regulation, and Function. *Pharmacol Rev* **62,** 405–496.

Turner JP, Anderson CM, Williams SR & Crunelli V (1997). Morphology and membrane properties of neurones in the cat ventrobasal thalamus in vitro. *J Physiol*707–726.

Urwin H, Authier A, Nielsen JE, Metcalf D, Powell C, Froud K, Malcolm DS, Holm I, Johannsen P, Brown J, Fisher EMC, van der Zee J, Bruyland M, Van Broeckhoven C, Collinge J, Brandner S, Futter C, Isaacs AM & Isaacs AM (2010). Disruption of endocytic trafficking in frontotemporal dementia with CHMP2B mutations. *Hum Mol Genet* **19,** 2228–2238.

Vacher H, Mohapatra DP & Trimmer JS (2008). Localization and targeting of voltage-dependent ion channels in mammalian central neurons. *Physiol Rev* **88,** 1407–1447.

Vale RD (2003). The molecular motor toolbox for intracellular transport. *Cell* **112,** 467–480.

Vanhooren V & Libert C (2013). The mouse as a model organism in aging research: Usefulness, pitfalls and possibilities. *Ageing Res Rev* **12,** 8–21.

Varela C (2014). Thalamic neuromodulation and its implications for executive networks. *Front Neural Circuits* **8,** 69.

Varela C, Kumar S, Yang JY & Wilson MA (2014). Anatomical substrates for direct interactions between hippocampus, medial prefrontal cortex, and the thalamic nucleus reuniens. *Brain Struct Funct* **219,** 911–929.

Varela C & Sherman SM (2007). Differences in Response to Muscarinic Activation Between First and Higher Order Thalamic Relays. *J Neurophysiol* **98,** 3538–3547.

Vernay A, Therreau L, Blot B, Risson V, Dirrig-Grosch S, Waegaert R, Lequeu T, Sellal F, Schaeffer L, Sadoul R, Loeffler J-P & René F (2016). A transgenic mouse expressing CHMP2B intron5 mutant in neurons develops histological and behavioural features of amyotrophic lateral sclerosis and frontotemporal dementia. *Hum Mol Genet* **25,** 3341–3360.

Verret L, Mann EO, Hang GB, Barth AMI, Cobos I, Ho K, Devidze N, Masliah E, Kreitzer AC, Mody I, Mucke L & Palop JJ (2012). Inhibitory Interneuron Deficit Links Altered Network Activity and Cognitive Dysfunction in Alzheimer Model. *Cell* **149,** 708–721.

Vertes RP (2002). Analysis of projections from the medial prefrontal cortex to the thalamus in the rat, with emphasis on nucleus reuniens. *J Comp Neurol* **442,** 163–187.

Vertes RP (2006). Interactions among the medial prefrontal cortex, hippocampus and midline thalamus in emotional and cognitive processing in the rat. *Neuroscience* **142,** 1–20.

Vertes RP, Hoover WB, Szigeti-Buck K & Leranth C (2007). Nucleus reuniens of the midline thalamus: link between the medial prefrontal cortex and the hippocampus. *Brain Res Bull* **71,** 601–609.

Vertes RP, Hoover WB, Do Valle AC, Sherman A & Rodriguez JJ (2006). Efferent projections of reuniens and rhomboid nuclei of the thalamus in the rat. *J Comp Neurol* **499,** 768–796.

Vertes RP, Linley SB & Hoover WB (2015). Limbic circuitry of the midline thalamus. *Neurosci Biobehav Rev*; DOI: 10.1016/j.neubiorev.2015.01.014.

Vezzani A, French J, Bartfai T & Baram TZ (2011). The role of inflammation in epilepsy. *Nat Rev Neurol* **7,** 31–40.

Vossel KA, Beagle AJ, Rabinovici GD, Shu H, Lee SE, Naasan G, Hegde M, Cornes SB, Henry ML, Nelson AB, Seeley WW, Geschwind MD, Gorno-Tempini ML, Shih T, Kirsch HE, Garcia PA, Miller BL & Mucke L (2013). Seizures and Epileptiform Activity in the Early Stages of Alzheimer Disease. *JAMA Neurol* **70,** 1158.

Vossel KA, Ranasinghe KG, Beagle AJ, Mizuiri D, Honma SM, Dowling AF, Darwish SM, Van Berlo V, Barnes DE, Mantle M, Karydas AM, Coppola G, Roberson ED, Miller BL, Garcia PA, Kirsch HE, Mucke L & Nagarajan SS (2016). Incidence and impact of subclinical epileptiform activity in Alzheimer's disease. *Ann Neurol* **80,** 858–870.

Wainger BJ, Kiskinis E, Mellin C, Wiskow O, Han SSW, Sandoe J, Perez NP, Williams LA, Lee S, Boulting G, Berry JD, Brown RH, Cudkowicz ME, Bean BP, Eggan K & Woolf CJ (2014). Intrinsic Membrane Hyperexcitability of Amyotrophic Lateral Sclerosis Patient-Derived Motor Neurons. *Cell Rep* **7,** 1–11.

Walhovd KB, Westlye LT, Amlien I, Espeseth T, Reinvang I, Raz N, Agartz I, Salat DH, Greve DN, Fischl B, Dale AM & Fjell AM (2011). Consistent neuroanatomical age-related volume differences across multiple samples. *Neurobiol Aging* **32,** 916–932.

Walsh DA, Brown JT & Randall AD (2017). *In vitro* characterization of cell-level neurophysiological diversity in the rostral nucleus reuniens of adult mice. *J Physiol* **595,** 3549–3572.

Walsh DM & Selkoe DJ (2004). Deciphering the Molecular Basis of Memory Failure in Alzheimer's Disease. *Neuron* **44,** 181–193.

Warre RC., McNaughton NC. & Randall A. (2002). Differential discrimination of fast and slow synaptic waveforms by two low-voltage-activated calcium channels. *Neuroscience* **110,** 375–388.

Watkins JC & Jane DE (2009). The glutamate story. *Br J Pharmacol* **147,** S100–S108.

Weiser M, Vega-Saenz de Miera E, Kentros C, Moreno H, Franzen L, Hillman D, Baker H & Rudy B (1994). Differential expression of Shaw-related K+ channels in the rat central nervous system. *J Neurosci* **14,** 949–972.

Williams SR, Turner JP, Hughes SW & Crunelli V (1997). On the nature of anomalous rectification in thalamocortical neurones of the cat ventrobasal thalamus in vitro. *J Physiol*727–747.

Wilmot CA, Sullivan AC & Levin BE (1988). Effects of diet and obesity on brain alpha 1- and alpha 2-noradrenergic receptors in the rat. *Brain Res* **453,** 157–166.

Wils H, Kleinberger G, Janssens J, Pereson S, Joris G, Cuijt I, Smits V, Ceuterick-de Groote C, Van Broeckhoven C & Kumar-Singh S (2010). TDP-43 transgenic mice develop spastic paralysis and neuronal inclusions characteristic of ALS and frontotemporal lobar degeneration. *Proc Natl Acad Sci* **107,** 3858–3863.

Wilson MA & McNaughton BL (1994). Reactivation of hippocampal ensemble memories during sleep. *Science* **265,** 676–679.

Witter MP, Ostendorf RH & Groenewegen HJ (1990). Heterogeneity in the Dorsal Subiculum of the Rat. Distinct Neuronal Zones Project to Different Cortical and Subcortical Targets. *Eur J Neurosci* **2,** 718–725.

Wolfart J & Roeper J (2002). Selective coupling of T-type calcium channels to SK potassium channels prevents intrinsic bursting in dopaminergic midbrain neurons. *J Neurosci* **22,** 3404–3413.

Wouterlood FG, Saldana E & Witter MP (1990). Projection from the nucleus reuniens thalami to the hippocampal region: Light and electron microscopic tracing study in the rat with the anterograde tracerPhaseolus vulgaris-leucoagglutinin. *J Comp Neurol* **296,** 179–203.

Wright AL, Zinn R, Hohensinn B, Konen LM, Beynon SB, Tan RP, Clark IA, Abdipranoto A & Vissel B (2013). Neuroinflammation and neuronal loss precede Aβ plaque deposition in the hAPP-J20 mouse model of Alzheimer's disease. *PLoS One* **8,** e59586.

Wright SH (2004). Generation of resting membrane potential. *AJP Adv Physiol Educ* **28,** 139–142.

Wykes R, Kalmbach A, Eliava M & Waters J (2012). Changes in the physiology of CA1 hippocampal pyramidal neurons in preplaque CRND8 mice. *Neurobiol Aging* **33,** 1609–1623.

Xiang Z et al. (2011). The Discovery and Characterization of ML218: A Novel, Centrally Active T-Type Calcium Channel Inhibitor with Robust Effects in STN Neurons and in a Rodent Model of Parkinson's Disease. *ACS Chem Neurosci* **2,** 730–742.

Xu W & Südhof TC (2013). A neural circuit for memory specificity and generalization. *Science* **339,** 1290–1295.

Xu Y-F, Gendron TF, Zhang Y-J, Lin W-L, D'Alton S, Sheng H, Casey MC, Tong J, Knight J, Yu X, Rademakers R, Boylan K, Hutton M, McGowan E, Dickson DW, Lewis J & Petrucelli L (2010). Wild-Type Human TDP-43 Expression Causes TDP-43 Phosphorylation, Mitochondrial Aggregation, Motor Deficits, and Early Mortality in Transgenic Mice. *J Neurosci* **30,** 10851–10859.

Yu FH, Yarov-Yarovoy V, Gutman GA & Catterall WA (2005). Overview of Molecular Relationships in the Voltage-Gated Ion Channel Superfamily. *Pharmacol Rev* **57,** 387–395.

Yue C & Yaari Y (2004). KCNQ/M Channels Control Spike Afterdepolarization and Burst Generation in Hippocampal Neurons. *J Neurosci* **24,** 4614–4624.

Zarei M, Patenaude B, Damoiseaux J, Morgese C, Smith S, Matthews PM, Barkhof F, Rombouts S, Sanz-Arigita E & Jenkinson M (2010). Combining shape and connectivity analysis: An MRI study of thalamic degeneration in Alzheimer's disease. *Neuroimage* **49,** 1–8.

Zhan XJ, Cox CL, Rinzel J & Sherman SM (1999). Current clamp and modeling studies of low-threshold calcium spikes in cells of the cat's lateral geniculate nucleus. *J Neurophysiol* **81,** 2360–2373.

Zhang Y et al. (2017). Patient iPSC-Derived Neurons for Disease Modeling of Frontotemporal Dementia with Mutation in CHMP2B. *Stem Cell Reports* **8,** 648–658.

Zhang Y, Yoshida T, Katz DB & Lisman JE (2012). NMDAR antagonist action in thalamus imposes δ oscillations on the hippocampus. *J Neurophysiol* **107,** 3181–3189.